THE DYNAMIC RESPONSE OF SHORT-SPAN HIGHWAY BRIDGES TO HEAVY VEHICLE LOADS

Mark Finkle Green

Queens' College

A dissertation submitted to the University of Cambridge
for the Degree of Doctor of Philosophy

Department of Engineering
University of Cambridge

November 1990

For Jo Anne

THE DYNAMIC RESPONSE OF SHORT-SPAN HIGHWAY BRIDGES TO HEAVY VEHICLE LOADS

Mark Finkle Green

Summary

This dissertation investigates the dynamics of highway bridges subjected to heavy vehicle loads.

A convolution method based on bridge mode shapes is developed to predict the dynamic response of a bridge to a given set of wheel loads. The convolution integral is solved by transformation to the frequency domain.

In order to validate the bridge response calculation method, an experimental procedure, consisting of impulse tests to determine the bridge modal properties and vehicle tests, is presented. The measured modal properties of the bridges are compared against predictions from beam theory and finite element calculations. Good agreement between theory and measurement is shown. The modal parameters are combined with measured wheel loads in the convolution calculation to predict bridge responses. These predicted responses are compared with the measurements and good agreement is found.

The convolution method is extended by an iterative procedure to include vehicle models and two parametric studies are performed. In the first, the importance of the dynamic interaction between vehicles and bridges is investigated, and guidelines for determining when interaction can be ignored are presented. In the second study, the effects of vehicle suspension design on bridge dynamic response are considered. Vehicles with leaf-spring and air-spring suspensions are considered.

PREFACE AND DECLARATION

This dissertation describes work conducted in the Cambridge University Engineering Department between October 1987 and November 1990.

The project was suggested by Dr. David Cebon who also supervised the work. His comments and advice were always greatly appreciated, and his enthusiasm for the project never waned. I would also like to thank Professor David Newland for his interest in this project, and for acting as my research supervisor in the absence of Dr. Cebon.

The experimental programme would not have been possible without the assistance of the Transport and Road Research Laboratory (TRRL). I am grateful to Dr. Kit Mitchell of the Vehicles and Environment Division (TRRL) for providing vehicles for the tests and to Mr. John Page of the Bridges Division (TRRL) for his assistance with organizing traffic lights. Mr. Vince Kelly and his colleagues at the Berkshire County Council were extremely helpful in organizing the tests, and providing me with construction drawings of the bridges. I must extend my gratitude to Mr. Atul Bhaskar, and my wife, Jo Anne, for their help in conducting the tests. I would also like to thank Mr. John Walden and the staff of the Mechanics Laboratory for all their assistance in preparing for the field tests. Mr. David Cole's help with the analysis of the wheel load data and vehicle simulations is greatly appreciated.

This project has been generously funded by the Association of Commonwealth Universities, the British Council, and the Canadian Women's Club. I am extremely appreciative of their support.

I must extend my thanks to Professor Barrington deV. Batchelor from Queen's University at Kingston whose enthusiasm for research encouraged me to study here.

I would also like to thank my parents for their support and encouragement throughout my studies. I am greatly indebted to my wife, Jo Anne, for her companionship and understanding during this research.

Finally, let me thank all those who have helped me in some way, but who have not been mentioned by name.

Except where specific reference is made to the work of others, this dissertation is the result of my own original work. The work has not previously been submitted in whole, or in part for any degree, diploma, or other qualification. This dissertation is 195 pages in length.

Mark F. Green
Cambridge, November 1990

Contents

1 INTRODUCTION

Bridges serve a vital role in our transportation systems. In a typical journey, a heavy goods vehicle encounters dozens of bridges. During each bridge crossing, it applies dynamic wheel loads which cause the bridge to vibrate. The repeated application of these loads can lead to deterioration and a resulting reduction in the service life of bridges.

In recent years, there has been a tendency towards larger heavy goods vehicles to increase efficiency as well as an increase in heavy vehicle traffic. There is a pressing need to understand the implications of these larger loads on bridge vibrations.

At the same time that dynamic loads on bridges are increasing, new materials and improved design methods have resulted in lighter and more flexible bridges. Because of these engineering advances, highway bridges are increasingly susceptible to vibration. Not only are modern bridges more sensitive to dynamic loads, but they also have natural frequencies in the the same range as those of heavy vehicles. The first resonant frequency of highway bridges is usually below 10Hz and often as low as 2 or 3Hz [8, 11]. Because most heavy vehicles generate their dynamic wheel loads in the 1.5 to 4.5Hz frequency range [17, 19, 26], excitation of one system by the other is significant. To complicate matters further, bridge damping is low (approximately 2 percent of critical in the first bending mode [80, 89]) and does not significantly

reduce the vibrations caused by the bridge-vehicle interaction.

Notwithstanding the importance of vehicle-induced bridge dynamics, major bridge failures are not normally caused by dynamic wheel loads [16]. They cause more subtle problems and contribute to fatigue, surface wear, and cracking of concrete which leads to corrosion problems. Thus dynamic loads continually degrade bridges, and increase the necessity of regular maintenance.

Maintenance costs for highway bridges are extremely high. In the U.K., £20 million [60] are spent each year keeping the network of concrete bridges serviceable. Even this expenditure is not sufficient to account for the new 38 tonne vehicles and the Department of Transport has allocated £2000 million for bridge upgrading over the next 10-15 years. Furthermore, an additional £700 million in strengthening costs is estimated for the transition to 40 tonne vehicles [1]. It is not known what portion of bridge damage is caused by heavy vehicle loads because the dynamic response of bridges to heavy vehicle loads is not adequately understood. Nevertheless, even if only a small percentage arises from bridge vibrations then these dynamics account for major expenditure. This connection between dynamic wheel loads and maintenance costs was highlighted by Husband & Co. [50] in their 1980 report to the Department of Transport concerning the effects of heavy vehicles on bridges.

> "Because of ... variable factors it is not possible to provide an accurate estimation of dynamic effects ... The extent to which heavy vehicles contribute to dynamic effects is mostly related to the running surface of the carriageway. Both an increase in the number of heavy axles and an increase in the weight of heavy axles will increase the rate of wear on road surfacing making maintenance necessary more frequently. If maintenance is not undertaken in time, as the road surface deteriorates the magnitude of dynamic effects will increase and with metal structures, the fatigue life will be shortened."[50]

A better understanding of the dynamics of the bridge-vehicle system is necessary in order to build bridges to resist vibrations, to design better vehicles to reduce

bridge damage, or to regulate vehicle loads and suspensions.

1.1 Background

The first recorded research into bridge vibration appears to be a report published in 1849 by Willis [98], which discussed the causes of the collapse of the Chester Railway Bridge in 1847. This report presented the results of simple laboratory experiments with carriages on light girders, and proposed theoretical equations by ignoring the inertia of the bridge. These equations were later solved by Stokes [86]. Over the next century, investigations into bridge dynamics were mainly concerned with developing analytical solutions for special types of moving loads such as constant forces, sinusoidally varying forces, and linearly increasing forces. Most of these studies were summarized by Inglis [53] in 1934, who also increased the numerical accuracy of the previous solutions.

Digital computers introduced a new era in bridge vibration research because the complexities of bridge and vehicle systems could finally be modelled. Several computational studies have been attempted (see Section 2.1), and extensive testing programmes conducted (see Section 3.1). Even so, a number of fundamental questions still remain unanswered:

(i) Is it possible to model the bridge-vehicle system with sufficient accuracy to predict bridge vibrations?

(ii) How important is the dynamic interaction between bridges and vehicles?

(iii) How do the design parameters of modern vehicles affect bridge response and damage?

(iv) Are current static design methods adequate for the design of bridges for dynamic vehicle loads?

The first question requires examination before any theoretical investigation is

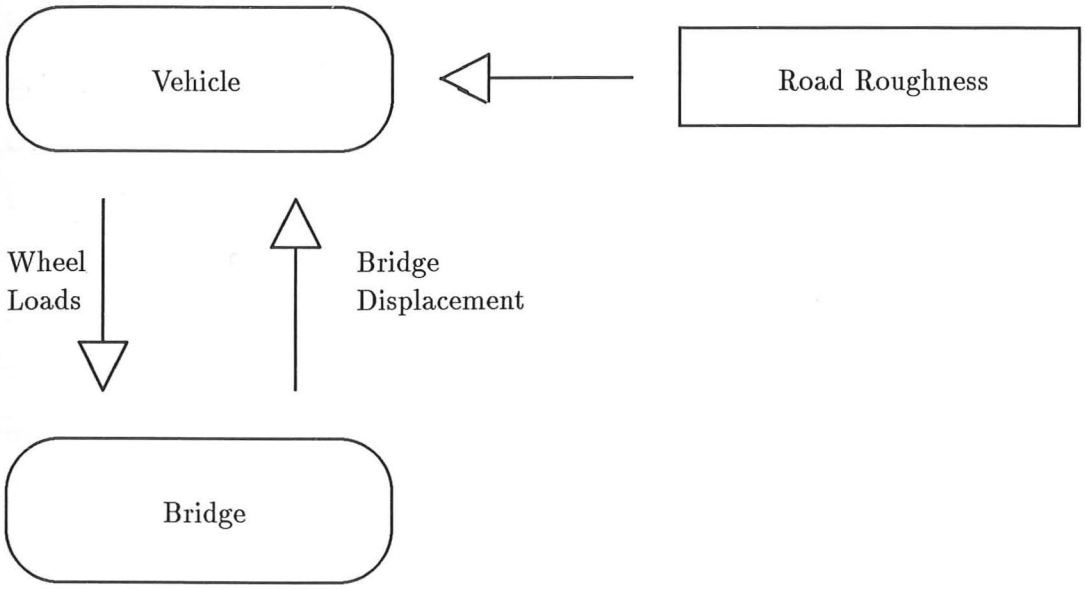

Figure 1.1: Schematic diagram of bridge-vehicle interaction

attempted. The complexity of the problem has been noted by several researchers and was aptly summarized by Wheeler in 1984 [97]:

> "Dynamic response of bridges to vehicles is a highly complex interaction and one that is unlikely to be amenable to theoretical analysis."

This type of thinking has led some researchers to favour large scale experimental tests [7, 8, 14]. Experiments by themselves, however, have disadvantages. Valuable data can be obtained, but it can be difficult to interpret without theoretical models. In addition, the experimental results cannot always be extrapolated to untested bridges. Developing theoretical models that can be experimentally validated is the best compromise.

Regarding the second question, the largest bridge vibrations are known to occur when the bridge and vehicle natural frequencies are close together [7]. Figure 1.1 shows a schematic diagram of bridge-vehicle interaction. The vehicle is excited by road roughness as well as dynamic deflection of the bridge. As a result, the vehicle generates dynamic wheel loads which in turn excite the bridge causing larger dynamic displacements to be fed into the vehicle. This feedback mechanism of interaction forces couples the dynamic response of the bridge to that of the vehicle.

It is not clear, however, under what circumstances large bridge responses are caused mainly by the vehicle being excited by the road (i.e. little interaction), or being excited substantially by the bridge. Guidelines are needed for determining when bridge-vehicle interaction can be ignored.

The importance of vehicle characteristics is the topic of the third question. Vehicles with suspension systems cause lower dynamic bridge responses than unsprung vehicles [8, 94], but no systematic comparison of the dynamic effects of different vehicle suspensions has been found in the literature. Nevertheless, there has been some evidence to suggest that some suspension types tend to cause larger dynamic bridge responses than others [74]. A parametric study concerned with the effects of different types of vehicle suspensions and bridge dynamics is needed.

The final question refers to bridge design practices. Currently, most bridge design codes contain no specific provisions for dynamic analysis. Dynamic effects are considered simply by increasing the static design loads with an empirical dynamic load allowance (or impact factor) that is usually related to span length [4]. This method is easy to apply, but it does not reflect the nature of the dynamic system. This incompatibility has led the ASCE[1] Committee on Loads and Forces on Bridges [4] to raise the following three questions about the AASHTO[2] dynamic load allowances:

1. "Should they be made more conservative?"
2. "Should they be made less conservative?"
3. "Should they be replaced or restructured?"

The ASCE Committee [4] also suggested as a long term goal that "rational procedures for dynamic live load analysis in lieu of the use of specified dynamic allowances" should be identified. This opinion coincides with that of the Ontario Highway Bridge Design Code (OHBDC) [75] which encourages designers to conduct tests or dynamic analyses. Further details of the bridge design specifications for dynamic wheel loads in the U.K., U.S.A., and Ontario are contained in Appendix A.

[1] American Society of Civil Engineers

[2] American Association of State Highway and Transportation Officials

The role of dynamic loads in bridge fatigue has received little attention in the past as only stress cycles caused by moving static loads have been considered [2, 10, 75, 82]. Recently, more emphasis has been placed on the contribution of stress cycles from bridge vibrations [16, 103]. Fatigue is also becoming a concern for concrete structures [16] so more highway bridges are under scrutiny. In order to calculate the dynamic fatigue effects, realistic models of vehicles and bridges are needed [16].

1.2 Conclusions

This dissertation investigates some of the problems outlined in the previous section. The five basic goals of this research are as follows:

(i) to develop a computational method for predicting the dynamic response of bridges to heavy vehicle loads,

(ii) to experimentally validate the method of (i),

(iii) to identify and quantify the importance of the dynamic interaction between vehicles and bridges,

(iv) to study the effects of different vehicle properties on bridge response and damage.

The main body of the work is divided into six chapters with reviews of the pertinent literature contained in the appropriate chapters.

The equations of motion describing the dynamic response of bridges are presented in chapter two along with a new convolution method for solving the equations. The chapter also contains comparisons of the results of the new method with other theoretical solutions.

Chapter three outlines the procedures used for collecting the experimental data necessary to validate the calculation method. The test descriptions are divided into two parts: impulse tests to determine characteristic bridge responses, and vehicle

tests in which the dynamic wheel loads and bridge responses were measured simultaneously. Specifications of the test bridges and vehicles are presented along with details of the instrumentation and data processing equipment.

Data analysis procedures are described in chapter four. Vehicle wheel loads and bridge responses are presented along with the results of the modal analysis. The presentation of the test results leads logically to the topic of chapter five, namely, the model validation. In chapter five, the measured modes are compared against theoretical mode shapes, and the bridge response calculation method is validated experimentally.

In chapter six, the convolution method is extended to include vehicle models and a parametric study of the importance of bridge-vehicle interaction is conducted. Chapter seven presents a parametric study of bridge responses calculated using the validated model. The effects of different vehicle speeds and suspensions are considered. The final chapter summarizes the results of the research and makes recommendations for further research.

MODELLING VEHICLE-INDUCED BRIDGE DYNAMICS

2

Predicting vehicle-induced bridge vibrations involves theoretical modelling of two complicated systems. Models of vehicle dynamics have been validated by various researchers, but although many authors have studied vehicle-induced bridge vibrations, only a few have attempted to validate their models with experiments.

A convolution method for simulating bridge dynamics is presented in this chapter. The time domain convolution integral is solved by transformation to the frequency domain by the Discrete Fourier Transform. The method is well-suited to experimental validation as it can incorporate measured bridge properties, and arbitrary wheel loads. Other advantages are that it is not dependent on any one vehicle or bridge model, is faster than time domain calculations, and can accommodate the dynamic coupling of the bridge and vehicle. Before the convolution method is presented, other bridge models and solution methods will be discussed.

2.1 Dynamics of Bridges and Vehicles

2.1.1 Bridge Models

There are two common theoretical approximations for bridges. The most prevalent is a one-dimensional Euler-Bernoulli beam [6, 25, 28, 42, 43, 45, 51, 52, 54, 56, 66, 72, 74, 83, 84, 87, 94, 99, 100]. By far the most common way of applying this beam approximation is through discretization techniques such as the finite element method [25, 28, 38, 42, 43, 45, 52, 54, 72, 87, 94] but some authors have opted for continuous models [6, 51, 56, 66, 83, 99, 100].

In general, continuous models are used when the vehicle is modelled as a moving constant force or unsprung mass, while finite element calculations have been applied with more complex vehicles. The finite element method allows more complex bridge geometry and loading cases to be considered.

The beam analysis ignores any two dimensional response properties of bridges and thus makes calculations simpler. Nevertheless, there have been some attempts to account for the fact that bridges may exhibit torsional modes of vibration. A simple way of accounting for this two dimensional behaviour is to add torsional degrees of freedom to the beam idealization [42, 43], but the two dimensional problem has most often been approached by approximating the bridge as a plate [40, 42, 43, 55, 57, 71, 94].

Gupta and Traill-Nash [42, 43] compared three models of bridges: a beam idealization, a beam with torsional degrees of freedom, and an orthotropic plate. They concluded that the beam idealization is adequate for preliminary analysis of long, narrow bridges while the orthotropic plate model is a better approximation for other bridges. They also stated that the beam model with torsional degrees of freedom adds complexity to the beam idealization without yielding solutions comparable to those predicted by orthotropic plate analysis [43].

Kulkarni and Ng [57] proposed an interconnected beam idealization of a two dimensional plate structure that involved dividing a plate into a series of beams and

then imposing compatibility conditions between the beams. By analysing individual beams instead of the whole plate, this method reduces the mathematical complexity of the plate model and at the same time models torsional responses [57].

Two other assumptions are usually made for bridge response computations. The first is that the effects of rotary inertia and shear deformation are ignored, and the second that damping is viscous [80]. If the height to span ratio of the bridge is less than $\frac{1}{10}$, then the first assumption is valid [34]. Viscous damping is acceptable because bridge damping is usually light and the response is relatively insensitive to the damping model [36, 94]. Some authors have ignored damping completely to simplify calculations [23, 57, 83, 101].

On the other hand, Eyre and Tilly [33] found that bridge damping varied with the amplitude of vibration. A schematic representation of the damping behaviour they measured is provided in figure 2.1. The damping curve has two plateaus, corresponding to what Eyre and Tilly called 'lower damping' and 'upper damping.' They suggested the lower damping value corresponds to the damping of the superstructure while the higher value incorporates the effects of joints and abutments. Since 'lower damping' usually only occurs with very small oscillations, Eyre and Tilly [33] suggested that the higher damping values be used in practice. Nevertheless, they cautioned that the range of validity of this assumption should be investigated.

A calculation procedure utilizing measured bridge characteristics such as mode shapes would help solve some of the problems associated with completely theoretical models, providing the measurement procedure used loads of representative amplitude. Such a method would not depend, to the same extent, on assumptions about damping, material properties, or torsional behaviour.

2.1.2 Solution Methods

For most analyses of bridge dynamics, the response is calculated as a sum of contributions from individual modes. This process of modal expansion is very popular because of the convenience of uncoupling the modes [9, 23, 35, 48, 57, 71, 92, 99].

In some cases, sufficient accuracy is obtained by considering only the first mode [9, 57, 59, 92, 99]. Veletsos and Huang [94] suggested that the first three modes make the most significant contributions to the response of simply-supported bridges.

Other authors have used influence functions [34, 90] to define an integro-differential equation for bridge dynamics. Fryba [34] compared this integral method with modal expansion and found the former more laborious but faster to converge. In addition he presented a combined method that has some of the advantages of both methods. He suggested modal expansions should be used to compute deflections, but the combined method should be used for obtaining bending moments and shear stresses.

In this study, the bridge response is formulated as a convolution of the vehicle wheel loads with bridge impulse response functions. The latter are expressed as combinations of mode shape values which can be obtained from bridge measurements, continuous models, or finite element calculations.

Regardless of the formulation of the bridge-vehicle model, several different methods of solving the resulting equations of motion exist. Step by step numerical integration techniques are the most widely used and the general procedure, at each time step, is as follows

(i) assume displacements or accelerations based on the results from the previous time step,

(ii) integrate the equations of motion for the bridge and the vehicle to predict the quantities assumed in (i),

(iii) compare the calculations of (ii) with the assumptions of (i),

(iv) repeat (i) to (iii) until the solution converges with the required tolerance.

Different authors have used the Newmark-β method [25, 48, 52, 101], the Wilson-θ method [45], or the Finite Integral Method [72, 87], but the basic concept is the same.

One alternative to numerical integration is the finite difference method, and it has been used with some success [37, 90].

The numerical methods mentioned in this section rely on calculations done completely in the time domain. Solving the equations in the frequency domain and then transforming the solution to the time domain can be much more efficient. This is especially the case if one desires bridge responses to known vehicle loads.

2.2 Calculating Bridge Response to Vehicle Loads

In this work, the bridge and vehicle are modelled separately and then combined through dynamic contact forces and displacements. This requires an iterative solution, but enables the combination of any vehicle model with any chosen bridge model. The rest of this chapter presents general equations of motion for the bridge along with a convolution method for solving them.

2.2.1 Equation of Motion: Bridge

A relatively general formulation of the equation of motion will be considered here. Assuming viscous damping, linear elasticity, small deflections, and neglecting the effects of shear deformation and rotary inertia, the equation of motion for a typical bridge can be written in the following form [70]

$$m(\mathbf{x})\frac{\partial^2 y}{\partial t^2}(\mathbf{x},t) + \mathcal{C}\left\{\frac{\partial y}{\partial t}(\mathbf{x},t)\right\} + \mathcal{L}\{y(\mathbf{x},t)\} = f(\mathbf{x},t) \tag{2.1}$$

where $\mathcal{L}$ is a self-adjoint linear differential operator with respect to the spatial variables (see Appendix B),

$\mathbf{x}$ is a two dimensional position vector,

$m(\mathbf{x})$ is the mass per unit surface area,

$y(\mathbf{x},t)$ is the transverse deflection of the bridge,

$\mathcal{C}$ is a viscous damping operator with respect to the spatial variables,

and $f(\mathbf{x},t)$ is the force exerted by the vehicle on the bridge.

It has been shown [70] that the response of a system governed by equation 2.1,

to an input, $f(\mathbf{x}_f, t)$ is given by the following convolution integral

$$y(\mathbf{x}, t) = \int_{-\infty}^{\infty} h(\mathbf{x}, \mathbf{x}_f, t-\tau) f(\mathbf{x}_f, \tau)\, d\tau \tag{2.2}$$

where $h(\mathbf{x}, \mathbf{x}_f, t)$ is the impulse response function at position $\mathbf{x}$ for an impulse applied at position $\mathbf{x}_f$. Therefore, equation 2.1 may be solved by determining the appropriate impulse response function. In order to relate the impulse response function to mode shapes, the deflection, $y(\mathbf{x}, t)$, is expressed in terms of normal mode functions, $\phi^{(n)}(\mathbf{x})$, as follows

$$y(\mathbf{x}, t) = \sum_{n=1}^{\infty} \phi^{(n)}(\mathbf{x})\, q_n(t) \tag{2.3}$$

where n is the mode number,

and $q_n(t)$ is the response of the n^{th} normal coordinate.

This coordinate transformation allows the modal responses to be uncoupled if the mode shape functions satisfy the following orthogonality relationships [70]

$$\int_R m(\mathbf{x})\phi^{(j)}(\mathbf{x})\phi^{(n)}(\mathbf{x})\, d\mathbf{x} = \delta_{jn} \qquad j, n = 1, 2, 3, \ldots \infty \tag{2.4}$$

$$\int_R \mathcal{L}\left\{\phi^{(j)}(\mathbf{x})\right\} \phi^{(n)}(\mathbf{x})\, d\mathbf{x} = {\omega^{(n)}}^2 \delta_{jn} \qquad j, n = 1, 2, 3, \ldots \infty \tag{2.5}$$

$$\int_R \mathcal{C}\left\{\phi^{(j)}(\mathbf{x})\right\} \phi^{(n)}(\mathbf{x})\, d\mathbf{x} = 2\zeta^{(n)}\omega^{(n)}\delta_{jn} \qquad j, n = 1, 2, 3, \ldots \infty \tag{2.6}$$

where $\omega^{(n)}$ is the n^{th} natural frequency (rad/s),

$\zeta^{(n)}$ is the n^{th} modal damping ratio,

R is the surface area of the bridge,

and δ_{jn} is unity if $j = n$ and zero otherwise.

If the mode shape functions satisfy the undamped free vibration equation corresponding to equation 2.1, then the first two orthogonality conditions will be satisfied (Appendix B). The third orthogonality condition will be satisfied if the damping operator has the following form:

$$\mathcal{C}\left\{\frac{\partial y}{\partial t}(\mathbf{x}, t)\right\} = c_1\, m(\mathbf{x})\, \frac{\partial y}{\partial t}(\mathbf{x}, t) + c_2\, \mathcal{L}\left\{\frac{\partial y}{\partial t}(\mathbf{x}, t)\right\} \tag{2.7}$$

where c_1 and c_2 are arbitrary constants. Viscous damping of this form is known as Rayleigh damping [79]. Newland [70] states Rayleigh damping is "usually satisfactory for lightly-damped structures." As mentioned in section 2.1.1, bridge damping is usually light and the response is insensitive to the damping model [36, 94], and so the Rayleigh damping assumption is reasonable. Rayleigh damping not only allows the modes to be uncoupled, but also ensures that the mode shapes for the damped and undamped cases are identical [70].

Now that the orthogonality relationships are defined, the modal expansion (equation 2.3) can be substituted into the differential equation (equation 2.1). Multiplying by $\phi^{(j)}(\mathbf{x})$, integrating over the surface of the bridge, and applying the orthogonality conditions gives the normal coordinate equation

$$\frac{d^2 q_n}{dt^2}(t) + 2\zeta^{(n)}\omega^{(n)}\frac{dq_n}{dt}(t) + {\omega^{(n)}}^2 q_n(t) = Q_n(t) \tag{2.8}$$

where the generalized force, $Q_n(t)$, is given by

$$Q_n(t) = \int_R \phi^{(n)}(\mathbf{x}) f(\mathbf{x}, t)\, d\mathbf{x}. \tag{2.9}$$

This equation can be used to determine modal impulse response functions, $h^{(n)}(t)$, by setting $Q_n(t) = \delta(t)$ where $\delta(t)$ is the Dirac delta function. The impulse response, $h^{(n)}(t) = q_n(t)$, can be shown to be

$$h^{(n)}(t) = \frac{e^{-\zeta^{(n)}\omega^{(n)}t}\ \sin(\omega_d^{(n)}t)}{\omega_d^{(n)}} \tag{2.10}$$

where $\omega_d^{(n)}$ is the n^{th} damped natural frequency such that

$$\omega_d^{(n)} = \omega^{(n)}\sqrt{1 - {\zeta^{(n)}}^2} \tag{2.11}$$

and $\zeta^{(n)} < 1$.

For the case of a force applied at one position on the bridge (as in equation 2.2), the generalized force of equation 2.8 is equal to the product of the mode shape function and the force at that position $\mathbf{x}_f$

$$Q_n(t) = \phi^{(n)}(\mathbf{x}_f) f(\mathbf{x}_f, t). \tag{2.12}$$

The convolution integral (equation 2.2) can be applied to equation 2.8 to obtain the normal coordinate solution

$$q_n(t) = \int_{-\infty}^{\infty} h^{(n)}(t-\tau)\,\phi^{(n)}(\mathbf{x}_f)\,f(\mathbf{x}_f,\tau)\,d\tau. \tag{2.13}$$

Invoking the modal expansion formula (equation 2.3), gives the bridge response as

$$y(\mathbf{x},t) = \sum_{n=1}^{\infty} \phi^{(n)}(\mathbf{x}) \int_{-\infty}^{\infty} h^{(n)}(t-\tau)\,\phi^{(n)}(\mathbf{x}_f)\,f(\mathbf{x}_f,\tau)\,d\tau. \tag{2.14}$$

Comparing equations 2.2 and 2.14 illustrates that the impulse response function corresponding to equation 2.1 is obtained by an appropriate combination of the mode shape functions,

$$h(\mathbf{x},\mathbf{x}_f,t) = \sum_{n=1}^{\infty} \phi^{(n)}(\mathbf{x})\,\phi^{(n)}(\mathbf{x}_f)\,h^{(n)}(t) \tag{2.15}$$

Up to this point it has been assumed that loads are applied to the bridge at only one position. This is obviously not the case for a moving vehicle, but the ideas that have been developed can be extended to moving loads. For example, consider a vehicle with N_t tyres. The vehicle forcing function can be described in terms of the dynamic wheel loads, $P_l(t)$,

$$f(\mathbf{x}_f,t) = -\sum_{l=1}^{N_t} \delta(\mathbf{x}_f - \mathbf{x}_l(t))\,P_l(t) \tag{2.16}$$

where $\mathbf{x}_l$ is the position of the l^{th} force (see figure 2.2). Each wheel force is still applied at position $\mathbf{x}_f$, but $\mathbf{x}_f$ is now moving with the vehicle. The negative sign is included because displacements and forces are assumed to be positive upwards for both the bridge and vehicle systems. Therefore, wheel loads which act upwards on the vehicle are defined as positive. This means they are negative with respect to the bridge.

Substituting this forcing function (equation 2.16) into equation 2.14, and replacing $\mathbf{x}_f$ with $\mathbf{x}_l$ for $l = 1, 2, ..., N_t$ gives

$$y(\mathbf{x},t) = -\sum_{l=1}^{N_t}\sum_{n=1}^{\infty} \phi^{(n)}(\mathbf{x}) \int_{-\infty}^{\infty} h^{(n)}(t-\tau)\,g^{(n,l)}(\tau)\,d\tau \tag{2.17}$$

$$g^{(n,l)}(\tau) = \phi^{(n)}(\mathbf{x}_l(\tau))P_l(\tau). \tag{2.18}$$

With the general equations of motion in this convolution format, the bridge vibration problem (equation 2.1) can be solved by evaluating the convolution integral. This integral may be evaluated in either the time or frequency domains. For this study, a frequency domain method was chosen and the solution procedure is outlined in the next section.

2.2.2 Solution in the Frequency Domain

The Fourier transform of the response is defined as [69, 70]:

$$Y(\mathbf{x},\omega) = \frac{1}{2\pi}\int_{-\infty}^{\infty} y(\mathbf{x},t)e^{-i\omega t}\,dt \tag{2.19}$$

where $Y(\mathbf{x},\omega)$ is the response transform at position $\mathbf{x}$ and frequency ω, and $i = \sqrt{-1}$.

Substituting the convolution (equation 2.17) into the Fourier integral (equation 2.19) gives

$$Y(\mathbf{x},\omega) = -\sum_{l=1}^{N_t}\sum_{n=1}^{\infty}\phi^{(n)}(\mathbf{x})\,\frac{1}{2\pi}\int_{-\infty}^{\infty}\int_{-\infty}^{\infty} h^{(n)}(t-\tau)g^{(n,l)}(\tau)e^{-i\omega t}\,dt d\tau \tag{2.20}$$

Rearranging variables by letting $\beta = t - \tau$ results in

$$\begin{aligned} Y(\mathbf{x},\omega) &= -\sum_{l=1}^{N_t}\sum_{n=1}^{\infty}\phi^{(n)}(\mathbf{x})\,\frac{1}{2\pi}\int_{-\infty}^{\infty}\int_{-\infty}^{\infty} h^{(n)}(\beta)\,g^{(n,l)}(\tau)\,e^{-i\omega(\beta+\tau)}\,d\beta d\tau \\ &= -\sum_{l=1}^{N_t}\sum_{n=1}^{\infty}\phi^{(n)}(\mathbf{x})\,\frac{1}{2\pi}\int_{-\infty}^{\infty} h^{(n)}(\beta)\,e^{-i\omega\beta}\,d\beta\int_{-\infty}^{\infty} g^{(n,l)}(\tau)\,e^{-i\omega\tau}\,d\tau \\ Y(\mathbf{x},\omega) &= -\sum_{l=1}^{N_t}\sum_{n=1}^{\infty}\phi^{(n)}(\mathbf{x})\,H^{(n)}(\omega)\,G^{(n,l)}(\omega) \end{aligned} \tag{2.21}$$

where $H^{(n)}(\omega)$ is the n^{th} modal frequency response function such that

$$H^{(n)}(\omega) = \frac{1}{({\omega^{(n)}}^2 - \omega^2) + 2i\zeta^{(n)}\omega^{(n)}\omega} \tag{2.22}$$

and $G^{(n,l)}(\omega)$ is the Fourier transform of $g^{(n,l)}(t)$.

Once $Y(\mathbf{x},\omega)$ is computed in the frequency domain, the inverse Fourier transform can be used to recover the time domain solution. The inverse Fourier transform is defined as follows [69, 70]:

$$y(\mathbf{x},t) = \int_{-\infty}^{\infty} Y(\mathbf{x},\omega)e^{i\omega t}\,dt. \tag{2.23}$$

2.2.3 Computer Implementation

To solve these equations by computer, the Discrete Fourier Transform can be used to approximate the continuous Fourier transform. The first step is to compute the transform of $g^{(n,l)}(t)$. The function is sampled to obtain N equally spaced values, $g_r^{(n,l)}$, where

$$g_r^{(n,l)} = g^{(n,l)}(r\Delta) \quad r = 0, 1, 2, ..., N-1 \tag{2.24}$$

and Δ is the time increment. The Discrete Fourier Transform is then applied to the sample as follows [69, 70]

$$G_k^{(n,l)} = \frac{1}{N} \sum_{r=0}^{N-1} g_r^{(n,l)}(\mathbf{x})\, e^{-i(2\pi kr/N)} \tag{2.25}$$

where k = 0,1,2,...,N-1. Discrete versions of $Y(\mathbf{x}, \omega)$ are given by

$$Y_k(\mathbf{x}) = -\sum_{l=1}^{N_t} \sum_{n=1}^{\infty} \phi^{(n)}(\mathbf{x})\, H^{(n)}(k\Delta\omega)\, G_k^{(n,l)} \tag{2.26}$$

where $\Delta\omega$ is the frequency resolution. Finally, the solution is recovered with the Inverse Discrete Fourier Transform given by [69, 70]

$$y_r(\mathbf{x}) = \sum_{r=0}^{N-1} Y_k(\mathbf{x}) e^{i(2\pi kr/N)} \tag{2.27}$$

where $y_r(\mathbf{x}) = y(\mathbf{x}, r\Delta), \quad r = 0, 1, 2, ..., N-1$.

2.2.4 Computational Considerations

In order to implement the discrete transforms in the convolution calculation, the time record must be long enough to obtain the required frequency resolution, $\Delta\omega$, where [69]

$$\Delta\omega = \frac{2\pi}{T} \tag{2.28}$$

and T is the length of the time record such that $T = N\Delta$.

In addition, Δ must be small enough to avoid aliasing of high frequency components into the low frequency range of the transform [69]. Aliasing is prevented

by ensuring that the maximum frequency present in the signal is smaller than the Nyquist frequency:

$$\text{Nyquist frequency} = \frac{1}{2\Delta} \text{ Hz.} \tag{2.29}$$

Finally, allowance must be made for the fact that the convolution defined by the Discrete Fourier Transform is circular. The circularity of the discrete transform means that all the time records in the convolution are assumed to repeat themselves with period T when they are, in fact, not periodic. It has been shown [85] that the differences between circular and linear convolutions can be eliminated by choosing T such that

$$T \geq T_h + T_{vp} \tag{2.30}$$

where T_h and T_{vp} are the lengths of the non-zero portions of the time records of the impulse response function and the vehicle force input, respectively.

To satisfy all these criteria, the time record must be significantly longer than the vehicle crossing time, T_{vp}.

For example, consider a simply supported 40m bridge with a first natural frequency of 3Hz traversed by a 10m long vehicle at 25m/s. If Δ is chosen to be 0.01 seconds, then the Nyquist frequency is 50Hz (314rad/s). With this Nyquist frequency, the first three bridge modes can be included because the third natural frequency is at 27Hz. Vehicle vibration is usually below 20Hz so the 50Hz Nyquist frequency presents no problems. If the damping ratio of the first bridge mode is assumed to be 0.02 then

$$h^{(1)}(t) = \frac{e^{-0.377t}}{18.8} \sin(18.8t). \tag{2.31}$$

The impulse response never completely dies away, but for computational purposes the response can be ignored when the amplitude is below 0.1% of the initial amplitude. With this definition, T_h is equal to 18.3 seconds while T_{vp} is 2.0 seconds. Therefore the time record should be chosen to be greater than 20.3 seconds and with $\Delta = 0.01$ seconds, at least 2030 points are required. For efficiency in computing the

Discrete Fourier Transform, the number of points should be a power of 2 and so 2048 is selected. Finally, the frequency resolution is computed from equation 2.28 as 0.05Hz. This is more than adequate to resolve the frequencies of interest.

To compare the efficiency of frequency and time domain methods, suppose that for the preceding example a time history of total length 4 seconds (400 points) was required. To evaluate the convolution integral in the time domain requires 160000 (400^2) multiplications. On the other hand, the Fast Fourier Transform algorithm requires $\frac{1}{2}N\log_2(N)$ multiplications [69] to compute each transform. The frequency domain method includes two transform calculations and one N point multiplication giving a total of $N + N\log_2(N)$ multiplications. For 2048 points, only 24576 multiplications are required making the frequency domain method about 7 times faster! Even further time savings can be achieved when T_{vp} is approximately the same length as T_h.

2.2.5 Comparison with Known Solutions

Once the convolution calculation was implemented in a computer program, it was possible to verify the method by comparing the results with known solutions for simple cases. A bridge reported in the literature [33, 63, 99] is used as a test case for the remainder of this chapter.

The bridge is idealized as a simply supported beam. The equation of motion for free vibrations of a Bernoulli-Euler beam with viscous damping is

$$m\frac{\partial^2 y}{\partial t^2}(x,t) + \mathcal{C}\left\{\frac{\partial y}{\partial t}(x,t)\right\} + EI\frac{\partial^4 y}{\partial x^4}(x,t) = 0 \qquad (2.32)$$

where m is the mass per unit length of the beam,

$\mathcal{C}$ is the damping operator representing Rayleigh damping,

x is the position along the length of the beam,

E is the Young's modulus of the material,

and I is the second moment of area of the cross-section.

As stated in section 2.2.1, the mode shapes for the damped and undamped cases are the same for Rayleigh damping. The free vibration equation without damping is

$$m\frac{\partial^2 y}{\partial t^2}(x,t) + EI\frac{\partial^4 y}{\partial x^4}(x,t) = 0. \tag{2.33}$$

Using a modal expansion (equation 2.3), and the boundary conditions for a simply-supported beam, the natural frequencies are given by

$$\omega^{(n)} = \left(\frac{n\pi}{L}\right)^2 \sqrt{\frac{EI}{m}} \tag{2.34}$$

and the normalized mode shapes are represented by

$$\phi^{(n)}(x) = \sqrt{\frac{2}{mL}} \sin\left(\frac{n\pi x}{L}\right) \tag{2.35}$$

where L is the length of the beam.

The parameters describing the bridge were based on measurements of the Pirton Lane highway bridge in Gloucester by Wills [99], Leonard [63], and Eyre and Tilly [33]. They reported the bridge length as 40 metres, and the first natural frequency as 3.2Hz with a modal damping ratio of 0.02. The mass per unit length was estimated from drawings in the papers as 12000kg/m. Three modes were used in the analysis, and the natural frequencies of the second and third modes were calculated from equation 2.34. The modal damping ratio was assumed to be constant for the first two modes and the damping ratio for the third was chosen to satisfy equation 2.7.

Mode Number	Natural Frequency (rad/s)	Damping Ratio
1	$\omega^{(1)} = 20.0$	0.02
2	$\omega^{(2)} = 80.0$	0.02
3	$\omega^{(3)} = 180.0$	0.04

Three different types of moving loads were considered: a constant force, a sinusoidally varying force, and a linearly increasing force. On each of figures 2.3 to 2.5, two curves are drawn. One is the solution obtained by the method described in this chapter and designated as the 'calculated' solution. The second curve is produced by using theoretical formulas derived by Fryba [34].

Figure 2.3 shows the effect of speed on the bridge midspan deflection from a constant force. The theoretical curves are only shown for the time the force is on the bridge, and are set to zero otherwise. The deflection increases as the speed of the force increases. Calculated and theoretical curves agree closely.

The beam response to a sinusoidally varying force is presented in figure 2.4, while figure 2.5 contains the response of the beam to a linearly increasing force. In both cases, deflection is plotted at midspan and the velocity is 25m/s. Once again, the calculated solutions compare well with the theoretical solutions.

2.3 Conclusions

A convolution method for calculating the response of a bridge to vehicle loads was developed. The method was implemented on a computer using Fourier transforms to solve the equations of motion for the bridge in the frequency domain. This procedure is considerably more efficient than equivalent time domain methods. Theoretical verification of the method was accomplished by comparing some results with predictions of analytical solutions.

The next three chapters discuss the experimental validation of the convolution method presented in this chapter.

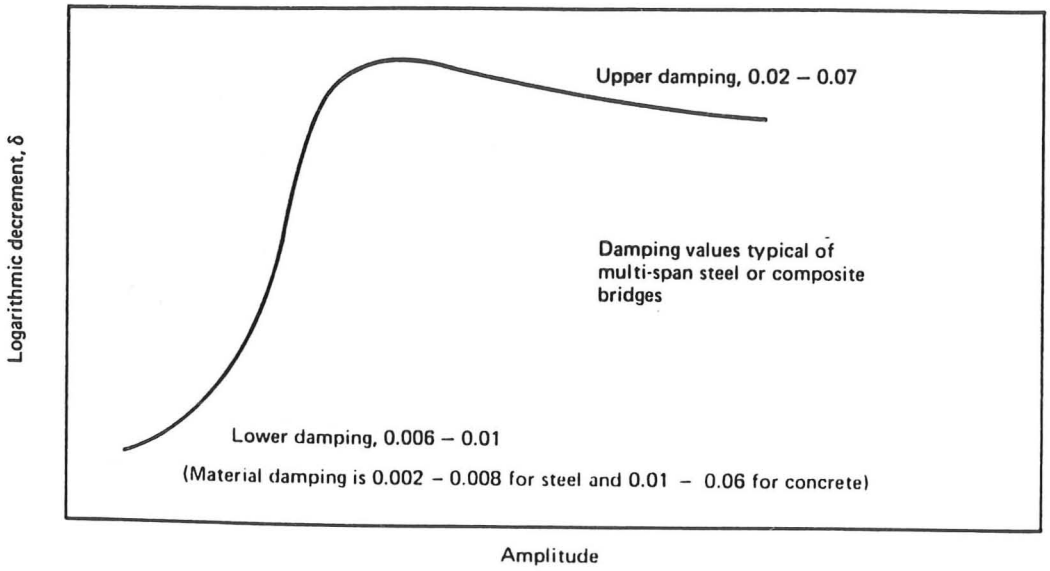

Figure 2.1: Schematic representation of damping behaviour (After Eyre and Tilly [33])

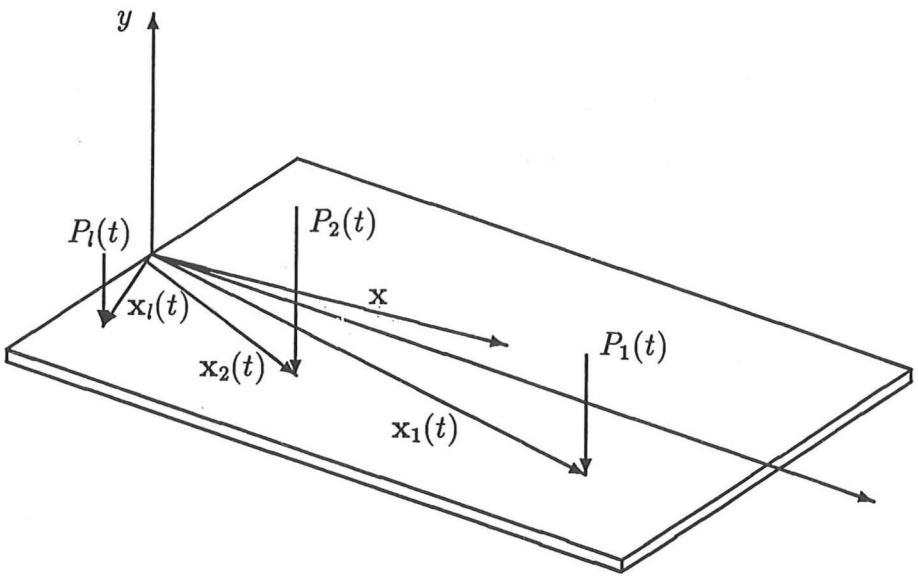

Figure 2.2: Loads moving across a bridge

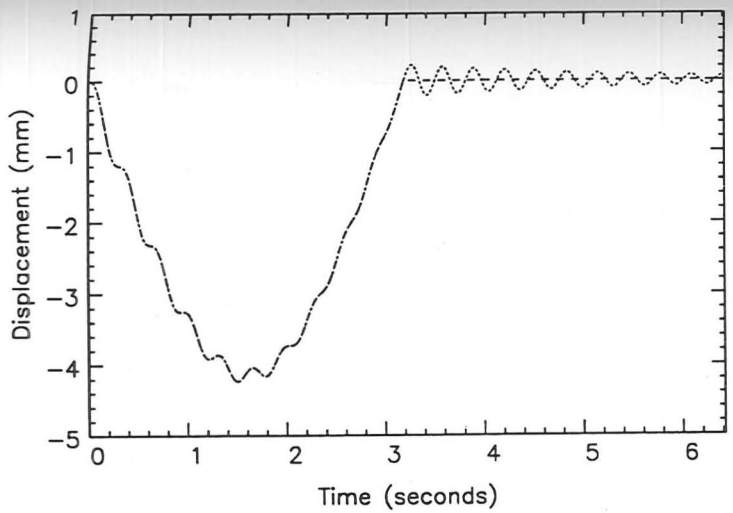

(a) $V = 12.5$ m/s

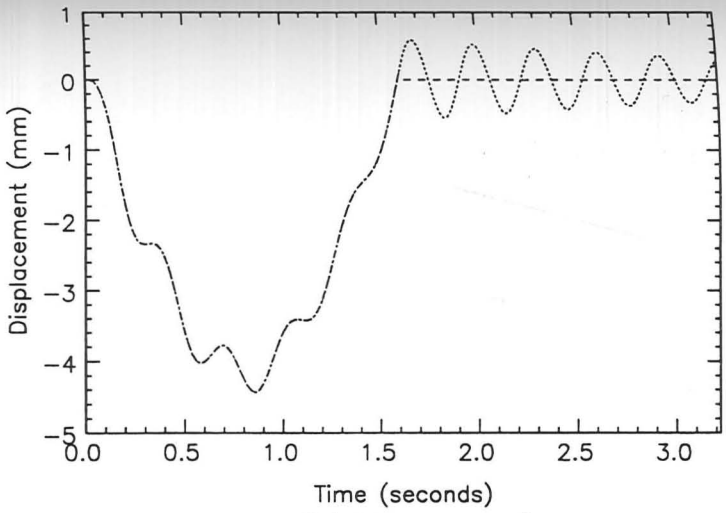

(b) $V = 25.0$ m/s

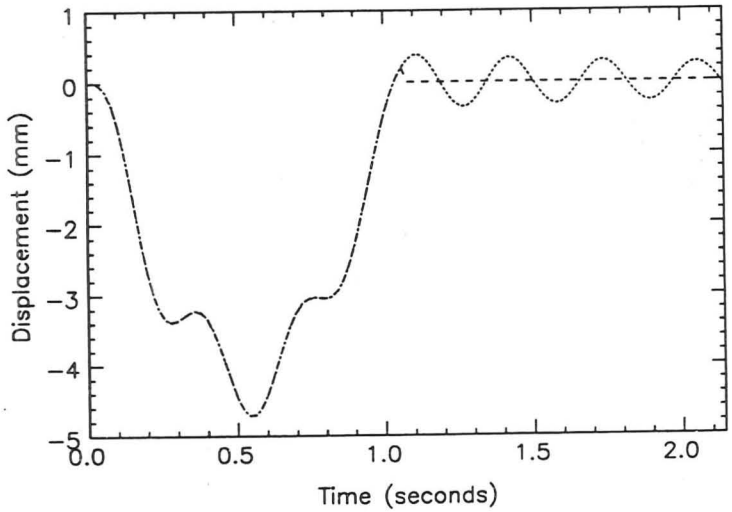

(c) $V = 37.5$ m/s

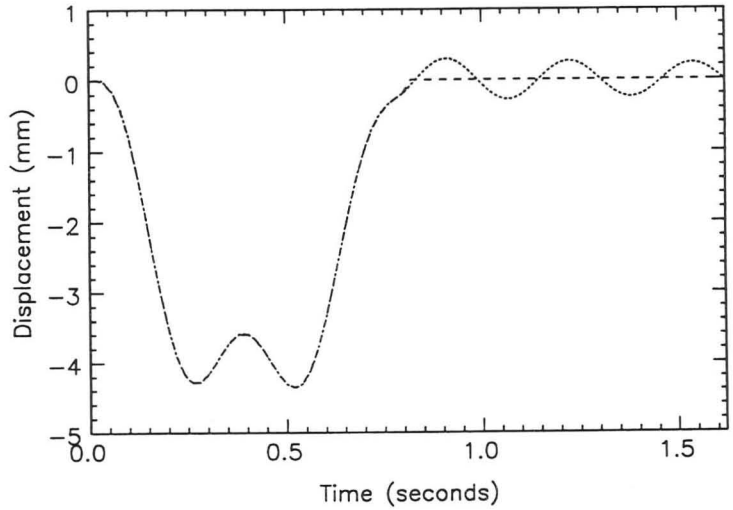

(d) $V = 50.0$ m/s

Figure 2.3: Midspan deflection versus time for different velocities
Single constant force, $P = 392$ kN
Calculated ..... Theory _ _ _ _ _ _ _

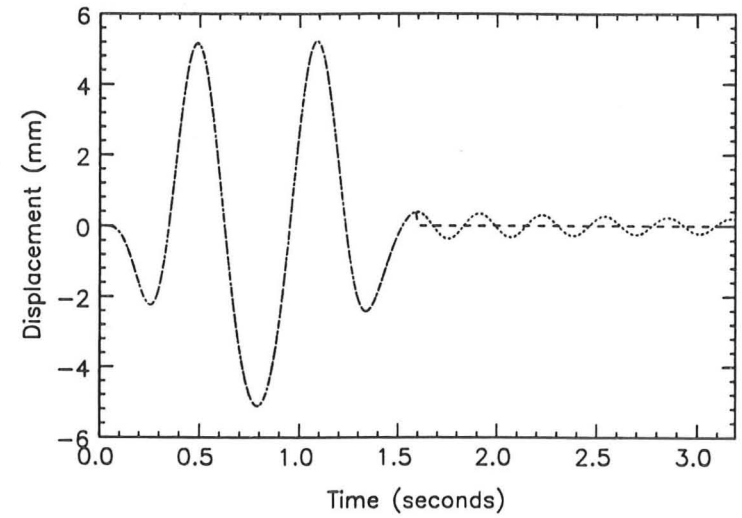

(a) $\Omega = 10$ rad/s

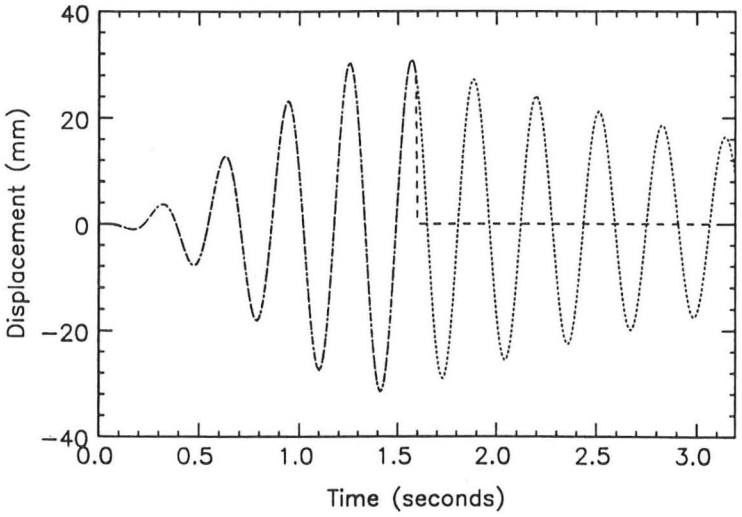

(b) $\Omega = 20$ rad/s

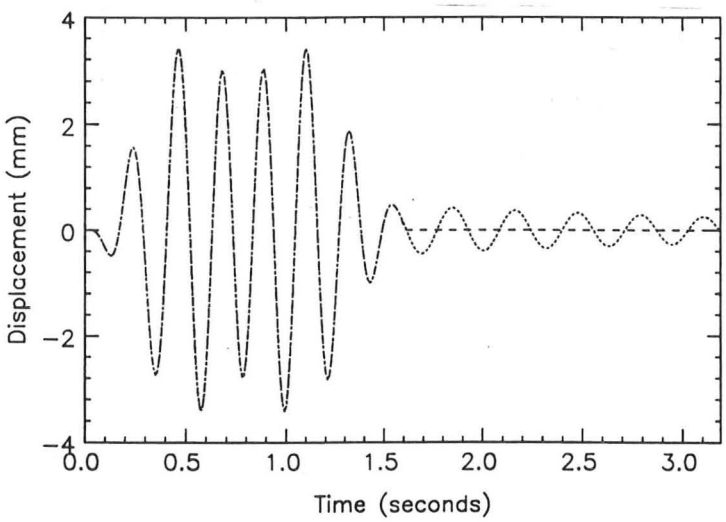

(c) $\Omega = 30$ rad/s

Figure 2.4: Midspan bridge deflection versus time ($V = 25$ m/s)
Single sinusoidal force, $P = 392\sin(\Omega t)$ kN
Calculated ..... Theory _____

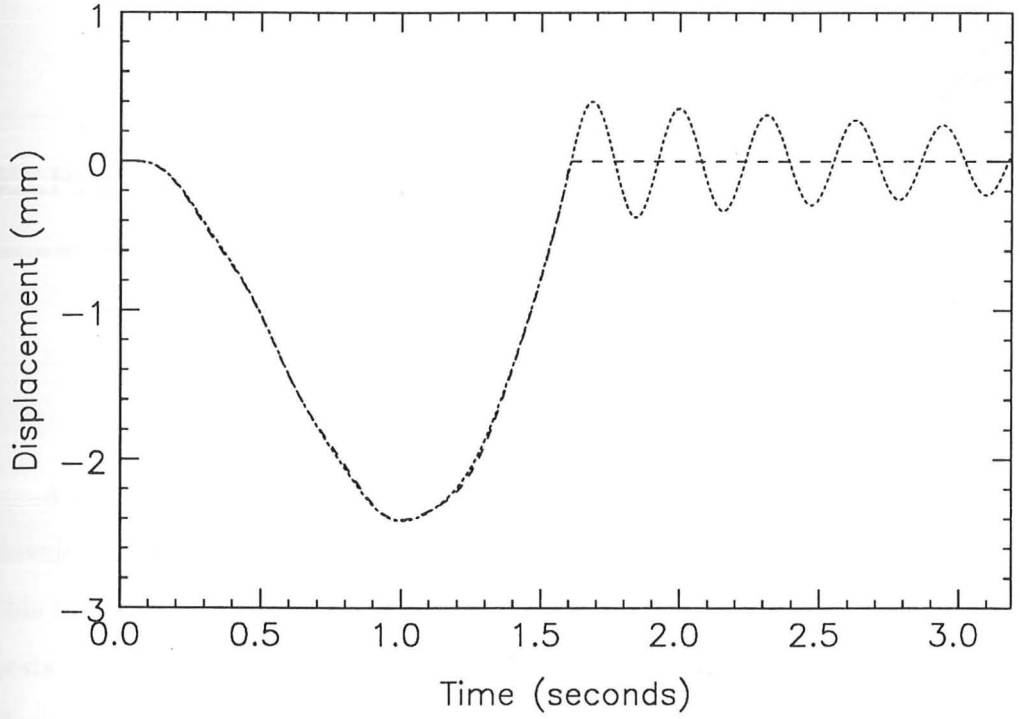

Figure 2.5: Midspan bridge deflection versus time ($V = 25$ m/s)

Single linearly increasing force, $P = \frac{392Vt}{L}$ kN

Calculated ..... Theory _ _ _ _ _ _ _

3

EXPERIMENTAL PROCEDURE

A theoretical method for the prediction of vehicle-induced bridge vibration was developed and compared with other theories in Chapter 2. In order to validate this method, an experimental procedure, combining bridge modal tests with vehicle tests, was adopted. The procedure consisted of four main steps. The first step was the measurement of the bridge transfer functions and mode shapes. Excitation was provided by an instrumented hammer. Step two consisted of single vehicle tests in which vehicle wheel forces and bridge responses were measured simultaneously. In step three, the measured dynamic wheel forces were combined with the bridge modal responses to predict bridge responses. Finally, these predicted responses were compared with the measured bridge responses to validate the model. The experimental procedures for conducting the validation programme are described in this chapter.

3.1 Background

Dynamic testing provides valuable evidence of bridge behaviour. For this reason, many researchers have conducted dynamic experiments on bridges. The dynamic tests have been used to assess bridge deterioration [78, 96], to provide information about 'dynamic increments' [8, 13, 14, 22, 28, 32, 41, 74], to measure modal characteristics [8, 33, 58, 62, 63, 64, 67, 99], to measure dynamic wheel loads [6, 22, 72, 76], or to validate bridge models [6, 72, 87]. Some of the results of these testing programmes will be summarized in this section. Details of standard testing techniques are available in the literature and will not be discussed at great length here. For instance, Prakash Rao, Tamhanker, and Sharma [78] compare different types of static and dynamic tests, and assess the various methods of instrumenting bridges.

3.1.1 Modal Tests

Almost all bridge dynamic testing programmes have been concerned with measuring natural frequencies and damping, but only a few researchers have attempted to measure mode shapes. This section will focus on mode shape measurement, but some damping measurements will also be presented.

During an extensive testing programme in Ontario, Canada, Billing [8] obtained limited mode shape measurements from vehicle-induced bridge responses, but did not confirm them with any theoretical predictions.

On the other hand, Maguire and Severn [64] tested bridge beams during demolition of an old bridge and observed simple beam modes. They measured the first three natural frequencies, but only obtained mode shape values at a limited number of positions.

Shepherd, Brown, and Wood [84] compared measured mode shapes with more complicated theoretical models. They tested a three span truss bridge and modelled it with finite elements. Once again, they measured mode shape values at a limited number of points, and therefore found it difficult to identify the overall form of the modes. Their theoretical analyses facilitated this identification and they obtained

reasonable agreement between their finite element model and the measured mode shapes.

Kumarasena, Scalan, and Morris [58] recently conducted mode shape measurements on a two span suspension bridge to confirm the predictions of a finite element model. Once again, only a small number of measurements were made and therefore the mode shapes were not uniquely determined. Nevertheless, they obtained reasonable agreement between their measurements and finite element predictions. They concluded that for response prediction purposes, measured natural frequencies and damping ratios should be combined with the finite element mode shapes.

Cantieni [15] recently conducted modal tests on a concrete box girder bridge in Switzerland and compared his results with a finite element model of the bridge. He found reasonable agreement between the model and his measurements. Even so, he only measured mode shape values at a few positions over the length of the bridge, and therefore was not able to discern whether discrepancies between measurement and theory were caused by errors in measurement or modelling.

The most comprehensive modal testing of bridges in the U.K. was conducted in the early 1970's by the Transport and Road Research Laboratory (TRRL) [33, 62, 63, 89, 99]. The main objective of these tests was to determine damping behaviour, but mode shapes were also measured.

Wills [99] compared the measured modal properties from the TRRL tests with simple beam and finite element models. Agreement was good for both models, but understandably better for the finite element predictions. The best agreement was obtained for the lowest frequency modes. Natural frequency predictions overestimated the measurements for higher modes. Wills suggested including the effects of rotary inertia and shear deformation to improve the agreement, but did not test his hypothesis. Because extensive mode shape measurements were made, Wills was able to compare the forms of predicted and measured mode shapes rather than simply notice that a few isolated points agreed with theory. He found good agreement in most cases, but some unexplained discrepancies were noticed.

As mentioned earlier, damping measurements were the prime objective of the

TRRL tests. Leonard [63] concluded that no significant relationship existed between damping and temperature while Eyre and Tilly [33] noted a correlation between damping and vibration amplitude (see section 2.1.1). The TRRL damping measurements are presented in the following along with some measurements by researchers in other countries:

Author	Country	Damping ratio (ζ_1)
Eyre and Tilly [33]	U.K.	0.003 - 0.010 (steel)
		0.003 - 0.015 (concrete)
Billing [8]	Ontario,	0.004 - 0.007 (steel)
	Canada	0.008 - 0.038 (concrete)
Green [41]	Ontario	0.006 - 0.024
Cantieni [13]	Switzerland	0.003 - 0.057

All these researchers measured similar bridge damping levels which were rarely larger than 2%.

This review of modal testing indicates that reliable measurement of bridge mode shapes is possible, but has rarely been attempted. Several measurement positions distributed evenly throughout the structure give the best results. Comparison of measurements with beam and finite element predictions provides useful insight into bridge behaviour. Most authors have found good agreement between theory and measurement, thus illustrating the reliability of the testing technique.

3.1.2 Dynamic Wheel Loads

Most bridge testing has concentrated on measuring dynamic bridge responses, but vehicle wheel loads have been measured during a few tests.

Biggs, Suer, and Louw [6] recorded wheel loads during dynamic bridge tests in order to compare measured forces with predictions from a simple vehicle model. They assessed the measurements in a qualitative manner, but did not present any analysis to determine the statistics of the measured loads.

Page [76] conducted a large number of dynamic wheel force measurements on 30 different bridges in the U.K. In order to review his results, the dynamic load

increment, DI_l, will be defined as

$$DI_l = \frac{P - P_{st}}{P_{st}} \tag{3.1}$$

where P_{st} is the static wheel load and P is the dynamic wheel load. Page measured peak dynamic load increments ranging from 0.09 to 0.75, but noticed that all the peak loads occurred near the ends of the bridges. On all but one of the bridges, 90% of the bridge length was subjected to loads with increments below 0.25. The effect of speed on the dynamic load increment was also measured. No significant relationship was noticed for bridges with smooth surfaces, but with rougher surfaces the dynamic load increments increased with speed.

Finally, Cantieni [15] measured wheel loads during bridge tests on the Diebul bridge in Switzerland, but this author has not found any published results of his wheel load analysis.

3.1.3 Dynamic Response Increments

The bridge dynamic response increment, DI_r, is defined analogously to dynamic load increment as

$$DI_r = \frac{y - y_{st}}{y_{st}}. \tag{3.2}$$

where y_{st} is the static bridge response and y is the dynamic response. Many investigators have recorded dynamic response increments and some results of their studies are presented in this section.

Comprehensive research into the dynamics of bridges in Ontario resulted in new design provisions [75] (see Appendix A). Measurements of maximum dynamic response increments were fundamental to this development. Billing [8] reported many of the test results, and they are reproduced in figure 3.1. The most important point to notice is the significant increase in the measured dynamic increments in the 2 to 5Hz frequency band. These increased responses occur because heavy vehicles generate most of their wheel loads in this frequency range. The new Ontario design provisions are also illustrated on the figure. The design provisions account for the

increased response between 2 and 5Hz. As part of the Ontario testing programme, Green [41] analysed the effect of speed on the measured dynamic increments. He noticed an increase in response for faster speeds, especially with rough approaches.

Cantieni [11, 13, 14] computed dynamic increments for bridges in Switzerland and obtained results similar to those in Ontario. He noted a relationship between the dynamic response increment and the bridge fundamental frequency. Some of his results are reproduced in figure 3.2. Cantieni also conducted tests with several vehicles and compared different vehicle configurations. Rigid vehicles with 2, 3, or 4 axles produced larger dynamic increments than articulated vehicles. When more than one vehicle was on the bridge, dynamic increments were reduced. Finally, Cantieni's results showed that dynamic response increments were largest with the roughest bridge surfaces and that this effect was most noticeable at high speeds. This last conclusion correlates well with the observations of Green [41].

A research project to identify vehicles that cause large dynamic increments is currently in progress in Queensland, Australia [22, 21, 72, 73, 74]. Dynamic increments as large as 1.32 with an average of 0.5 were measured on a simply-supported, single span bridge [22, 74] with a fundamental frequency of 10.8Hz. These reported dynamic increments are much larger than those measured in Ontario or by Cantieni. Large increments occurred with both heavy and light vehicles, even though heavy vehicles caused smaller increments on average. The reasons for the large dynamic increments are currently being investigated by the researchers.

3.1.4 Bridge Response Validation

This review has found only a few papers concerned with the validation of vehicle-induced bridge response. Measured modal properties have been compared with theory by several authors (section 3.1.1), but very few authors have compared measured bridge responses with theoretical predictions.

A study by Biggs et al [6] contained the first validation of the bridge-vehicle system. The models were simple. Only simply-supported bridges were considered,

and vehicle models were restricted to one degree of freedom. Both laboratory and field experiments were included in the validation. Comparisons were made between measured bridge responses and those predicted by the simple models. The laboratory results were better than those conducted in the field, but in both cases the quasi-static effects dominated the comparison between theory and measurements. The dynamic components of the predicted and measured responses were often out of phase with each other, although magnitudes were approximately correct. Improvement in the comparison was obtained by using measured wheel loads which indicated that some errors were caused by improper modelling of the vehicle and of the bridge surface roughness. The validation was successful, but the simplicity of the models restricts their applicability to modern vehicles and bridges.

Kulkarni and Ng [57] conducted laboratory experiments to validate their interconnected beam idealization for bridges (see section 2.1.1). They obtained reasonable results, but their errors were relatively large. Theoretical and experimental response curves were often out of phase with each other.

More recent validations with more complicated models were conducted in Australia. Swannel and Miller [87] considered a two axle, four degree of freedom vehicle including non-linear suspension stiffness. They used a lumped mass model for the bridge. Viscous damping was assumed throughout. The surface profile of the bridge was measured, and bridge responses from the passage of a test vehicle were recorded. The recorded responses were compared with the computer simulations. Although reasonable agreement was obtained, quasi-static effects dominated the responses. The comparison between theory and experiment for the superimposed dynamic responses was not good. No explanation was given for the discrepancies except to note that the system is a "complex dynamic response environment where minor changes in parameters (e.g. vehicle vertical motion at bridge entry) can produce important effects"[87].

Finally, Mulcahy, Pulmano, and Traill-Nash [68] obtained a good validation of their bridge and vehicle models with field tests. Nevertheless, their results were again dominated by quasi-static effects and had some sizeable errors at the magnitude of

the superimposed dynamics. Furthermore, they mentioned that tests other than those presented indicated deficiencies in their model validation.

This brief summary of vehicle-bridge validations illustrates there is a need for validated models of bridges and vehicles representative of those currently in use. Correctly validated models should reproduce accurately the dynamic components of vehicle-induced bridge response.

3.2 Site Selection

Several highway bridges were inspected for possible testing. The two most suitable bridges were chosen according to the following criteria :

(i) convenient location for testing by TRRL vehicles

(ii) easy access for instrumentation

(iii) straightness of the bridge and approaches so that the vehicles could attain a wide range of speeds

(iv) the bridge was not skew

(v) low traffic density.

The first bridge was chosen from amongst four prestressed concrete box girder bridges crossing the M4 motorway in Berkshire. All the bridges were similar in design, and on a TRRL bridge testing route. The bridge on Drift Road was chosen because it was the straightest one and had the lightest traffic.

The location of this bridge is shown in figure 3.3 while the cross-section and elevation details are in figure 3.4. Figure 3.6 shows a photograph of the north-western half of the bridge including the instrumented span which was located directly above the eastbound lanes of the motorway. The bridge superstructure is continuous over the three supporting columns. Although the four spans are not all equal, the bridge is symmetric about its middle column.

In order to provide more data and to avoid some of the measurement problems experienced with the Drift Road bridge, it was decided to test another bridge. One problem with the Drift Road bridge was that it was easily excited by the aerodynamic effects of large vehicles passing underneath the bridge, so it was decided to select a bridge that did not cross another road. To provide a contrast to the Drift Road Bridge, an additional requirement was that the second bridge was of a different construction type. The bridge at Lower Earley over the River Lodden was chosen.

The Lower Earley bridge consists of three spans (see figure 3.5), but the inverted T-beams are not continuous over the supports. Even so, there is some continuity because the concrete slab is continuous throughout the length of the bridge and the T-beams are joined at the piers by reinforced concrete diaphragms (see figure 3.7).

3.3 Instrumentation

3.3.1 Transducers

In order to record bridge vibrations due to different types of excitation, appropriate transducers were necessary. The measuring devices had to be easy to install and readily available. A review of bridge testing literature indicated three classes of instrumentation: displacement transducers [8, 32, 83, 84], strain gauges [8, 74, 83], and accelerometers [8, 32, 61, 72].

Strain gauges were rejected for three reasons. Firstly, strain is not a convenient quantity to measure for modal testing because the modal analysis procedure assumes displacement, velocity, or acceleration measurements. Secondly, strain measurements are dependent on local values of mass and stiffness and thus may not represent the behaviour of the whole structure [12]. Finally, strain gauges can be difficult to install in the field [22].

Displacement transducers were considered, but they require an inertial platform which was impractical for these measurements. A laser method for measuring dis-

placement was recently developed by Cantieni [12]. His method avoids the necessity of an inertial platform, but the equipment was not available for these tests.

Piezoelectric accelerometers were seen as a good choice since they are easy to install and remove, operate over a large range of frequencies, and are readily available.

Four B&K type 8318 high sensitivity accelerometers with internal charge amplifiers were used for the tests. The internal amplification reduces signal loss in transmission to the recording apparatus. Figure 3.8 shows one of the accelerometers along with an external line drive supply for powering the charge amplifier.

The accelerometers were mounted on aluminium discs which were glued with strong adhesive to the bridges. For the Drift Road bridge, the accelerometer discs were secured inside the bridge on the bottom of the box girder, while for the Lower Earley bridge the accelerometers were attached upside down on the underside of the bridge.

Ground loops can be a problem when accelerometers or their charge amplifiers are not electrically isolated [49]. Since the accelerometers were mounted on dry parts of the bridge, the concrete was assumed to be an effective electrical isolator and it was not deemed necessary to build an electrical isolation system into the mounts. The accelerometer charge amplifiers were battery powered by external line drive supplies which completed the isolation of the whole system.

Finally, the selection of piezoelectric accelerometers meant it was not possible to measure extremely low frequency vibrations. The internal charge amplifiers have a cut-off frequency at 0.1Hz which means measurements at frequencies below 1Hz are suspect. This did not cause problems with the hammer tests, but the vehicle passage induces a quasi-static deflection that has a period approximately double the time for the vehicle to cross each span. With a 20m bridge span and a 15m vehicle travelling at 5m/s, the passage frequency is 0.14Hz which is at the lower limit of the measuring capabilities of the accelerometers. Fortunately, this is not too much of a problem because the passage frequency is essentially a static effect, which is not vital for this study of the dynamic response of bridges.

3.3.2 Signal Processing

The acceleration signals were filtered and amplified before being captured by the data-logger. To prevent aliasing, Kemo VBF/3 filters were used. These are fourth order Butterworth low pass filters incorporating ac high pass filters ($f_{co} = 0.125$Hz) and selectable gains of 1, 3, or 10.

In some cases, additional amplification was required before digitising and storing the raw data. An eight channel analogue amplifier was developed with variable gains of 1, 3, 10, 30, and 100.

3.3.3 Data Logging and Storage

The analogue signals had to be digitized and stored before any analysis could proceed. Because of the large amount of data to be collected, the data was digitized in the field. With 16 channels, sampling rates up to 133 kHz, and storage for 10^6 data points, the available CED 1401 data logger readily met the requirements. The data logger was driven by an IBM-PC (AT). Figure 3.9 illustrates the general set-up for the tests including the van with the signal processing and data logging facilities. A schematic diagram of the set-up is shown in figure 3.10.

3.3.4 Instrumented Hammer

In order to extract modal information from bridge measurements, it was necessary to obtain a matrix of transfer functions relating excitation at different points on the bridge to responses at other points [30]. Because of the large number of points required, either the excitation source or the accelerometers had to be portable. It was decided to fix the accelerometers in place and develop a portable method of exciting the bridge.

The bridge testing literature was surveyed to assess excitation methods. The possibilities include: the release of an imposed deflection [89], a vehicle driven over a bump [89] (in this case the dynamics of the vehicle confuse the issue), a blow by an impulse hammer or a falling weight [61, 64, 89], or sinusoidal excitation from a

shaker [89]. The first two methods were discarded as inappropriate for this study. Because sinusoidal shakers of suitable size are expensive to acquire and difficult to move, impulse excitation was chosen.

The impulse was applied with an instrumented hammer that was built for a study of ground vibration [49]. It consisted of a 20kg mass at the end of a slender 2m, 3kg arm (figure 3.9). An accelerometer was fixed to the back of the hammer head to measure the acceleration of the head and thus deduce the force applied (see figure 3.11). Unfortunately, the accelerometer also recorded vibration from the hammer arm and this caused the measurements to be erroneous in the region of the natural frequency of the hammer. Figure 3.13 shows a typical impulse and its Fourier spectrum which is defined as the magnitude of the Fourier transform as described by Bendat and Piersol [5]. This Fourier spectrum is more appropriate than power spectral density for analysis of transient data and will be used throughout this dissertation. The initial impulse is followed by hammer arm vibration and eventually a second impulse (about 0.3 seconds after the first impulse). The effects of the second impulse are discussed in detail in Appendix C where the second impulse is shown to cause the Fourier spectrum to vary sinusoidally. The spectrum also shows the hammer arm vibration because the peak near 40Hz corresponds to the natural frequency of the hammer arm. Since the important bridge frequencies were below 30 Hz, hammer vibration was not deemed to be a critical problem. Nevertheless, the hammer was redesigned to incorporate a force transducer (figure 3.12) for the second set of tests. Although this modification virtually eliminated the hammer resonance problem, an acceleration signal was still required to measure the inertia force contribution from the mass of the hammer head outboard of the force transducer. Figure 3.14 shows the contributions of the force transducer output and the outboard mass correction to the total force applied to the bridge. The hammer arm vibration is almost completely removed with no noticeable peak in the frequency domain (figure 3.14b).

For the second set of tests the hammer was dropped on foam rubber to increase the low frequency content of the hammer impulse [30]. A comparison of figures 3.13b

and 3.14b illustrates the redistribution of energy to lower frequencies.

Finally, the possibility that the reaction force at the hammer base contributed to the bridge loading was investigated. Four rubber tubes were used as springs to support the hammer base, and their stiffness was measured by placing different weights on the hammer base and recording the resulting deflections. The hammer was dropped from its full height and the base deflection was measured. By combining the deflection information with the tube stiffness, an estimate of the reaction force was obtained. This force estimate is shown in figure 3.15 (peak for $\approx$ 200N), and when compared with the impulse at the hammer head (peak force $\approx$ 20kN; figures 3.13 and 3.14) the reaction force is insignificant.

3.3.5 Vehicle Instrumentation

The test vehicles were owned, operated, and instrumented by the Transport and Road Research Laboratory (TRRL). Two different methods of logging the data were employed. On the first set of tests the raw analogue signals were recorded on magnetic tape. After the tests, the analogue information was filtered and digitized. By the time the second set of tests were conducted, TRRL had acquired a mobile data-logger and thus the magnetic tape recorder was eliminated.

Each axle of the test vehicles was instrumented with two strain gauges and two accelerometers as shown in figure 3.16. The total wheel force is a combination of the static force, the strain gauge force, and two inertia correction terms. The inertia corrections are obtained from the measured accelerations. The procedure for determining the wheel forces from these measurements has been outlined elsewhere [17, 26], and will not be discussed in detail. Cole [26] has estimated that the maximum error in the measured wheel forces is $\pm$ 6.6%. Average errors should be in the region of 2 or 3%.

3.4 Equipment Calibration

Table 3.1 contains specifications and calibration factors for the instrumentation used for the bridge tests. This section describes the procedures for calibrating the instrumentation.

3.4.1 Accelerometers

Small accelerometers were calibrated by attaching them to a B&K type 4291 accelerometer calibrator. A sinusoidal vibration of 2g peak-peak at 500rad/s is produced by the calibrator.

Since the accelerometers used on the bridge were too heavy to be mounted on the B&K calibrator, they were placed on a shaker table alongside a previously calibrated accelerometer. The calibrated accelerometer was used to determine the calibration constant for the larger accelerometers.

3.4.2 Force Transducer

A check was made to ensure the factory calibration of the hammer force transducer was reasonable. The force transducer was attached to a shaker table, and various masses were securely fastened to the top of the transducer. A calibrated accelerometer was fixed to the top of the attached mass, and the shaker table was driven at different amplitudes over a frequency range of 1 to 100Hz. The recordings were used to estimate the calibration constant as well as the outboard mass of the force transducer. Within the accuracy of the method, the measured calibration constant was found to be equal to the factory calibration, and the outboard mass was estimated as half the total mass of the force transducer.

3.4.3 Amplifiers

The charge amplifiers were calibrated by passing a voltage signal through a capacitor connected to the amplifier input. By comparing the input charge with the output voltage, the calibration constant was obtained.

The procedure for the calibration of the voltage amplifier was similar except the capacitor was not necessary.

3.5 Impulse Test Procedures

The primary purpose of the impulse tests was to determine the bridge modal properties. The repeatability and linearity of the measurements were also assessed. Two sets of tests were performed on the Drift Road bridge, but only one on the Lower Earley bridge. The first tests at Drift Road were conducted during November 1988, while the second tests and the Lower Earley tests were done during September and October 1989.

3.5.1 Data Logging Configuration

The sampling rate was governed by the requirements of the impulse hammer. Both bridges have first natural frequencies below 10Hz and vehicle excitation is not expected to exceed 20Hz [17, 26], so measurement of frequencies up to 100Hz was more than adequate. The impulse hammer, however, applies significant energy at higher frequencies (see figures 3.13 and 3.14).

A sampling frequency of 500Hz was selected and the filter cut-off frequency was set to 150Hz. With the Nyquist frequency at 250Hz (equation 2.29), there was no chance of aliasing because only frequencies above 350Hz would alias into the range between 0 and 150Hz.

Figure 3.17 shows the effect of the transient response of the filter on the impulse. The solid curve was filtered at 150Hz while the dotted one was obtained with a filter cut-off of 1000Hz. With the lower filter cut-off frequency, an overshoot is

evident immediately after the impact. Nevertheless, the frequency components of the Discrete Fourier Transform (DFT) below the cut-off frequency are the same whether or not the overshoot is present. Figure 3.17b presents the Fourier spectra of both impulses. The solid and dotted curves are almost identical.

For the first set of tests on the Drift Road bridge, the record length was set at 1024 points. When the responses were analysed in the laboratory it became evident that the sample length was too short. The low frequency modes had not died away completely. This was not evident during the tests because the high frequencies dominated the response and died away before the end of the sample time. A windowing analysis procedure to account for the truncation of the response is presented in section 4.2.3. In order to avoid any truncation on the second set of tests, a 4096 point record of length 8.2 seconds was chosen.

The four accelerometers were mounted on the bridges as shown in figures 3.18 and 3.19. Each accelerometer position was numbered as shown in the two figures and in table 3.2.

3.5.2 Repeatability and Linearity

Repeatability was measured by dropping the hammer from the same height 5 times. Linearity was determined in a similar manner except that the hammer was dropped from three different heights. In order to compare the responses from impulses of varying magnitude, normalized impulse response functions were calculated. The calculation procedure is as follows:

(i) remove any dc offset from both the impulse and the response,

(ii) calculate the DFT of both the impulse and the response,

(iii) compute the transfer function by dividing the response transform by the impulse transform,

(iv) apply a filter in the frequency domain to remove components of the transfer function above the anti-aliasing filter cut-off frequency,

(v) perform the inverse DFT on the transfer function to obtain a normalized impulse response function.

In figure 3.20, three normalized impulse responses from both bridges are presented. For each bridge the curves were obtained from measurements made with the hammer dropped from its full height. The hammer and the accelerometer were both positioned at the midspan of the instrumented spans. The fact that all three curves on each figure are nearly coincident illustrates that both bridges exhibit repeatable behaviour.

Normalized impulse responses from hammer drops of three different magnitudes were compared to assess the linearity of the system. Figure 3.21 shows the normalized impulse responses for three different hammer heights on both bridges. The hammer was dropped from three heights: 2.0m, 1.6m, and 1.0m. Both bridges exhibit linear behaviour over this range.

3.5.3 Modal Tests

In order to determine the mode shapes of the bridges, many impulse tests were conducted. Two parallel lines, representing the wheel tracks of the test vehicles, were marked on each bridge. The hammer was dropped at several points along each track. The matrix of tests for each bridge is shown in figures 3.18 and 3.19. For the Drift Road bridge, hammer tests were conducted at 25 positions while for the Lower Earley bridge the hammer was dropped at 56 different positions. At each position the hammer was dropped 5 times.

Figure 3.18 shows that the tests on the Drift Road bridge concentrated on span 2 which was directly above the London bound traffic of the M4 (see also figure 3.6). Most of the tests were conducted on the wheel track near the bridge centre-line. Ten hammer positions on one half of the span and two positions on the other half were chosen. To estimate mode shapes along both wheel paths, three sets of impulse tests were conducted on the outside wheel track. Finally, the adjacent span was tested at 10 different positions to determine the continuity of the mode shapes between the

two spans. The other two spans were not tested because the mode shapes could be determined from symmetry.

A more comprehensive testing programme was conducted on the Lower Earley bridge. The northern span was selected as the primary one for the tests and 15 positions were chosen along each wheel path. Tests were also carried out on both of the other two spans as shown in figure 3.19. Additional hammer tests were conducted along both wheel tracks on the southbound lane of the bridge.

3.6 Vehicle Test Procedures

The second phase of the experiments involved measuring the bridge dynamic response to the passage of a single instrumented vehicle. It was possible, on both occasions, to perform all of the vehicle tests in one day. The Drift Road bridge was tested on 24 November 1988, and the Lower Earley bridge was tested on 5 October 1989. Photographs of the test vehicles are presented in figures 3.22 and 3.23. The test vehicle for the Drift Road bridge was a four-axle articulated vehicle with a semi-trailer. The tractor had a leaf spring suspension while the trailer had an independent air suspension. For the Lower Earley tests, the vehicle was similar except the air suspension was on the tractor and the leaf springs on the trailer. Each vehicle was loaded with concrete blocks to a static weight of approximately 32 tonnes. Table 3.3 shows the axle weights and spacings for the two test vehicles.

The bridge instrumentation was set up in the modal testing configuration except that triggering signals were needed to synchronize the bridge response with the dynamic wheel loads (see figure 3.10). At each end of the bridge, a reflector and light beam set was erected. When the vehicle passed the light beam, a reflector on the vehicle caused a pulse to be sent to the roadside data logger. At the same time, a light beam on the vehicle hit the roadside reflector sending a signal to the vehicle instrumentation.

The test vehicle was driven over the bridge in both directions at vehicle speeds

of 15, 30, 50, and 55km/h. Extra runs at 65km/h were conducted on the Lower Earley bridge. Two runs were made at each speed in each direction.

The next chapter describes the analysis of the data recorded during the tests and presents some of the experimental results.

Table 3.1: Specification of equipment used for bridge testing

Transducers

type	sensitivity	application
B&K 8318 (high sensitivity accelerometer)	316 μA/ms^{-2}	bridge vibration
DJB 302 A/03/W (accelerometer)	0.88 pC/ms^{-2}	impulse hammer
Kistler 971A (force transducer)	3.96 pC/N	impulse hammer

Amplifiers

type	gain	application
B&K 2813 (line drive supply)	1 mV/μA	line drive supply for B&K 8318 accelerometers
B&K 2511 (vibration meter)	1-10,000 mV/pC	charge amplifier for hammer accelerometer
Force transducer charge amplifier	0.01 mV/pC	charge amplifier for force transducer
Hammer accelerometer charge amplifier	1.0 mV/pC	charge amplifier for hammer accelerometer
8 channel voltage amplifier	1, 3, 10, 30, 100	amplification of vibration signals

Filters

type	gain	corner frequency	application
Kemo VBF/3 (n=4 Butterworth)	1, 3, 10	0.125Hz (high pass) 0.1Hz - 10kHz (low pass)	anti-aliasing filter and signal amplifier

Table 3.2: Accelerometer Positions

Position Number	Location
1	midspan, centre-line
2	1/3 point of span, centre-line
3	1/4 point of span, centre-line
4	midspan, offset

Table 3.3: Vehicle axle weights and spacings

Bridge	Axle	Axle position (m)	Static axle weight (tonnes)
Drift Road	Steer	0.00	6.48
	Drive	3.50	9.05
	Front Trailer	11.22	7.94
	Rear Trailer	13.06	8.78
			Total: 32.25
Lower Earley	Steer	0.00	6.40
	Drive	3.28	9.32
	Front Trailer	10.18	8.31
	Rear Trailer	12.20	7.65
			Total: 31.68

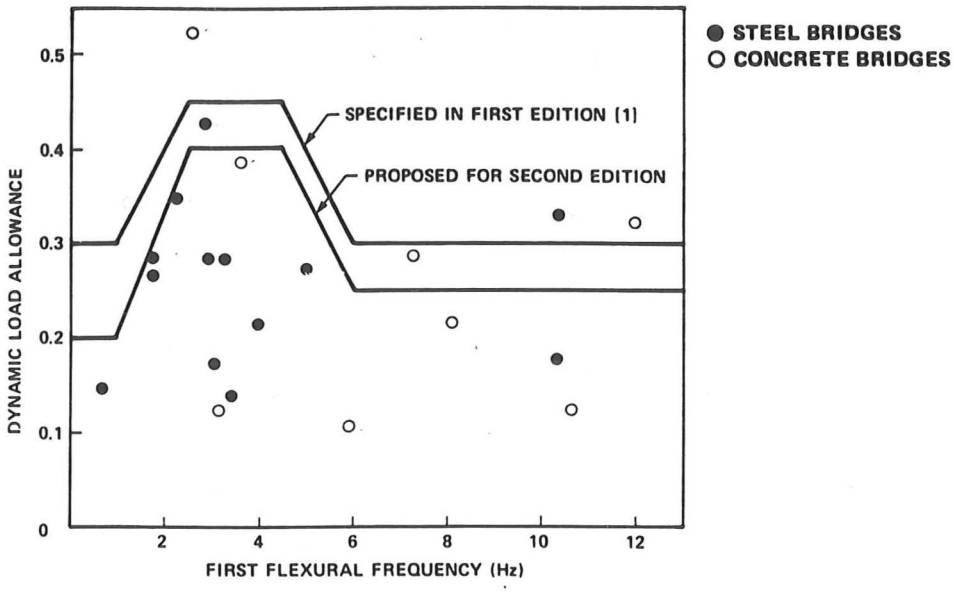

Figure 3.1: Dynamic response increments measured in Ontario including the Ontario Bridge Design Code dynamic load allowance (After Billing [8])

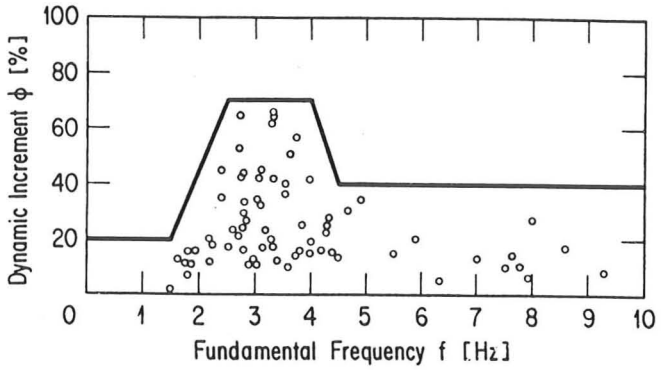

Figure 3.2: Dynamic response increments measured in Switzerland (After Cantieni [11])

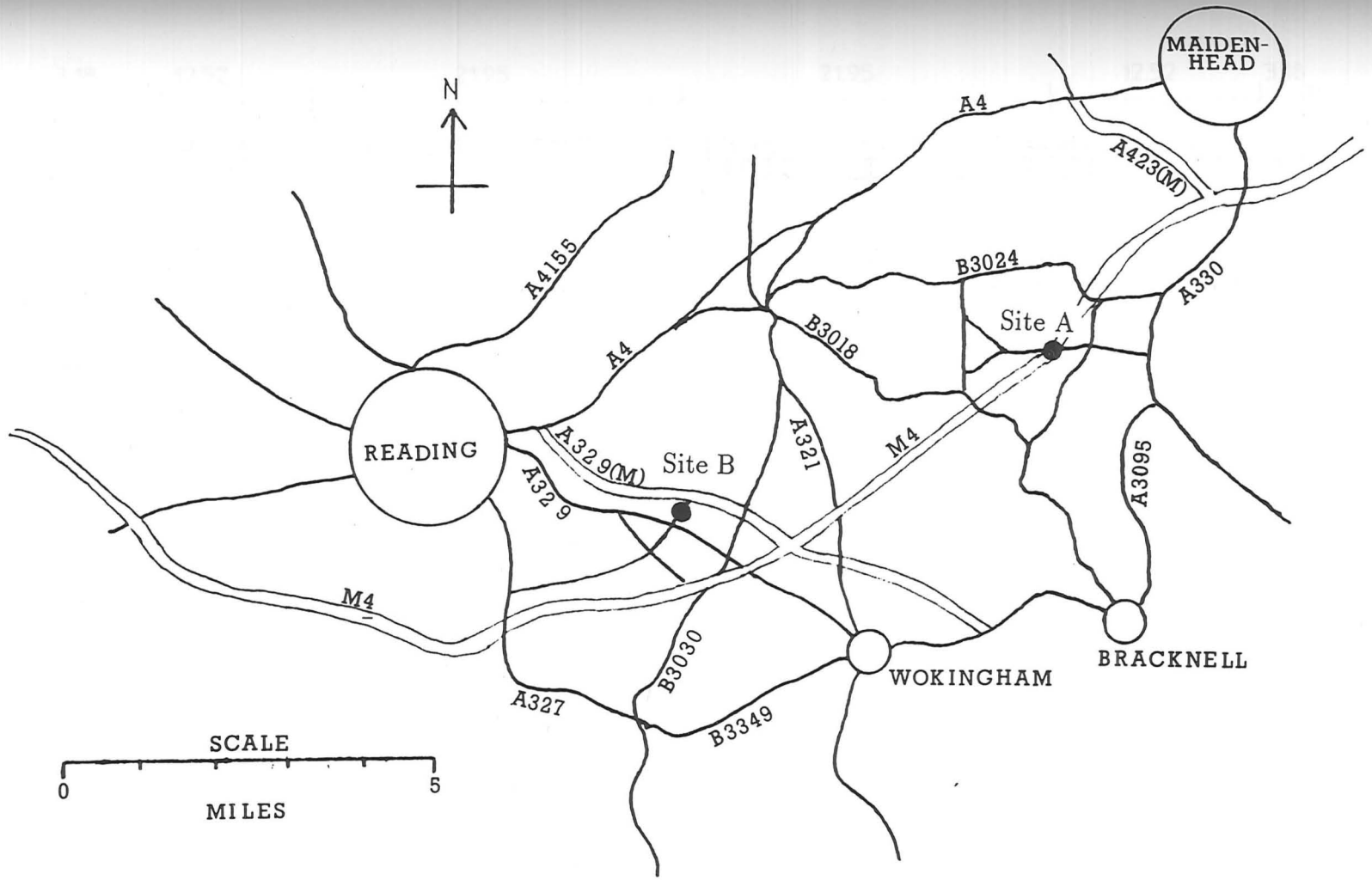

Figure 3.3: Map of Reading area showing the location of test bridges
Site A - Drift Road bridge
Site B - Lower Earley bridge

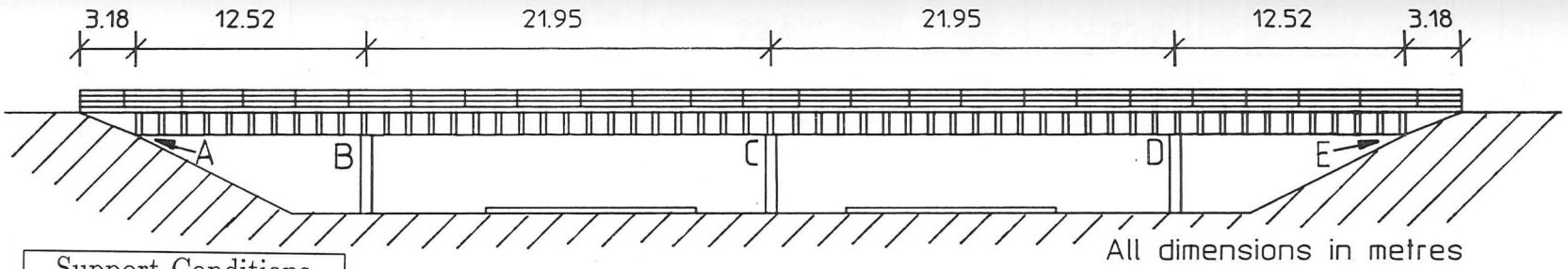

Support Conditions	
A	Elastomer bearing
B	Sliding bearing
C	Built-in support
D	Sliding bearing
E	Elastomer bearing

(a) Elevation

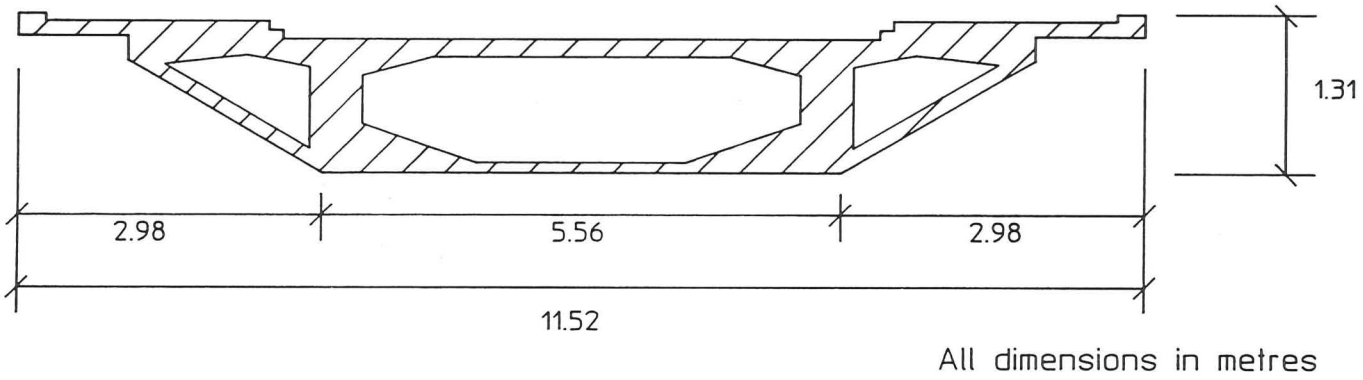

(b) Cross-section

Figure 3.4: Details of the Drift Road bridge

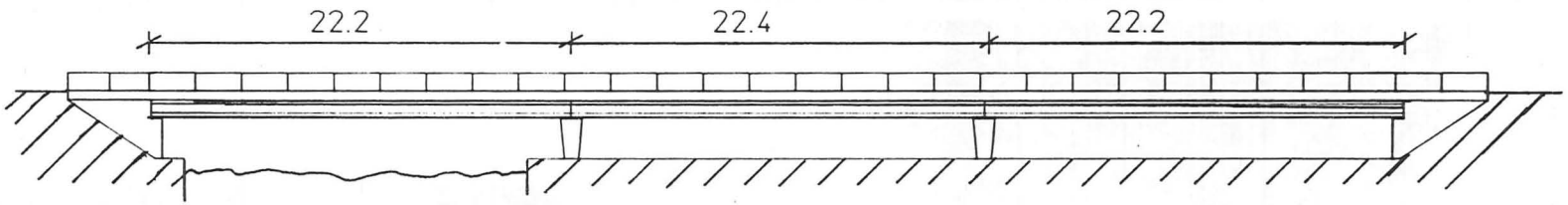

(a) Elevation

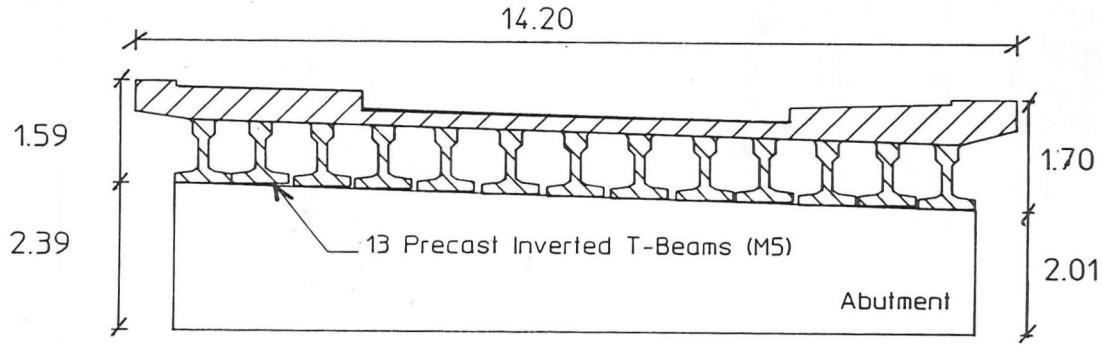

(b) Cross-section

Figure 3.5: Details of the Lower Earley bridge

Figure 3.6: Drift Road bridge showing the test span

Figure 3.7: Lower Earley bridge - detail at pier

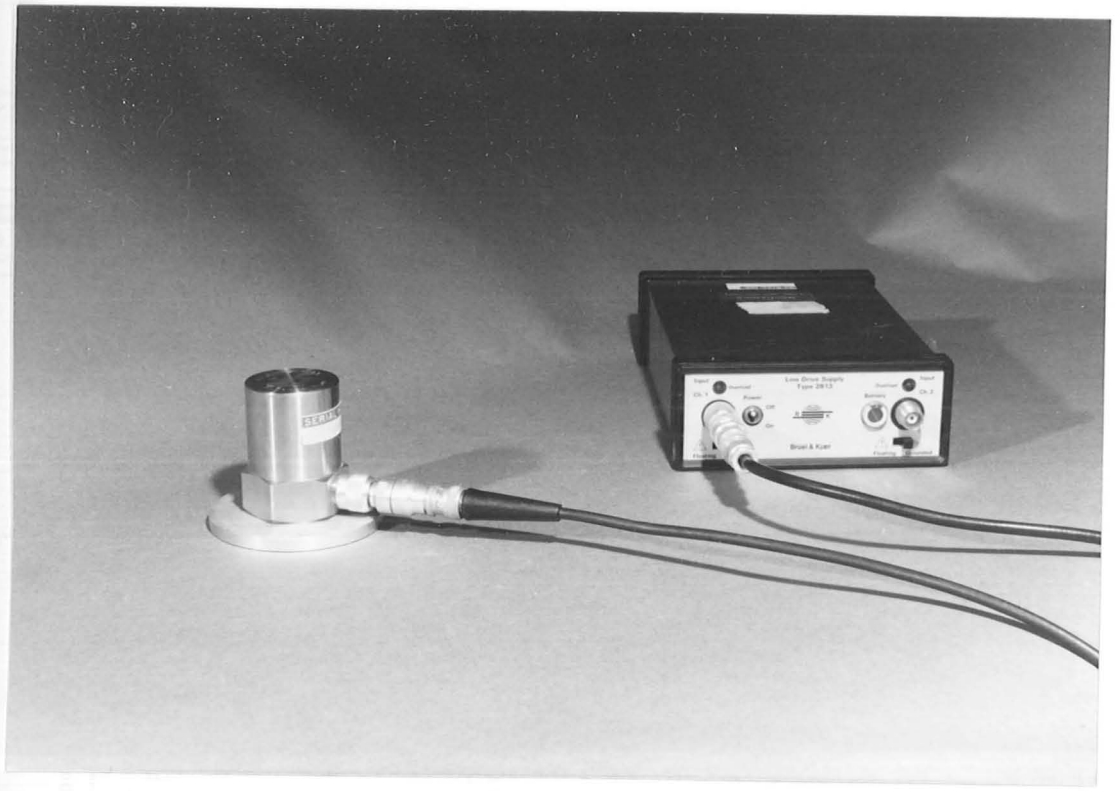

Figure 3.8: Accelerometer for measuring bridge vibration, and external line drive supply

Figure 3.9: General set-up for impulse tests

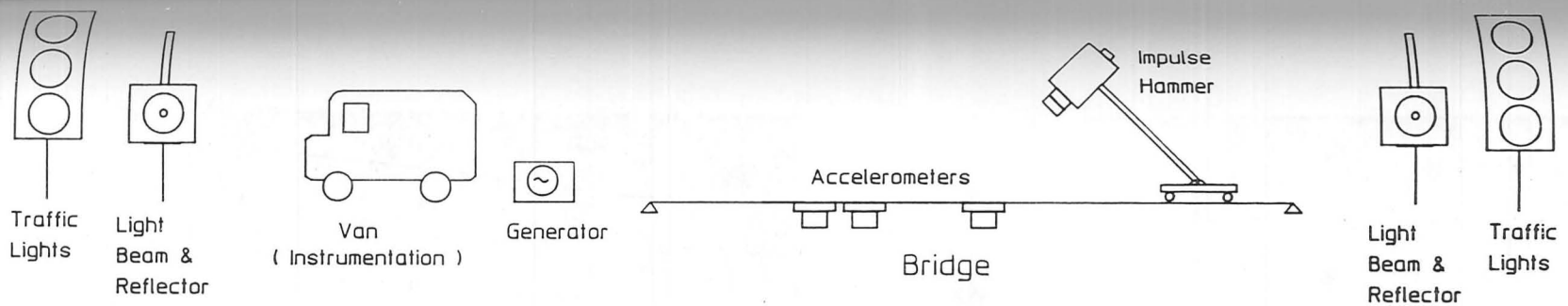

(a) General set-up

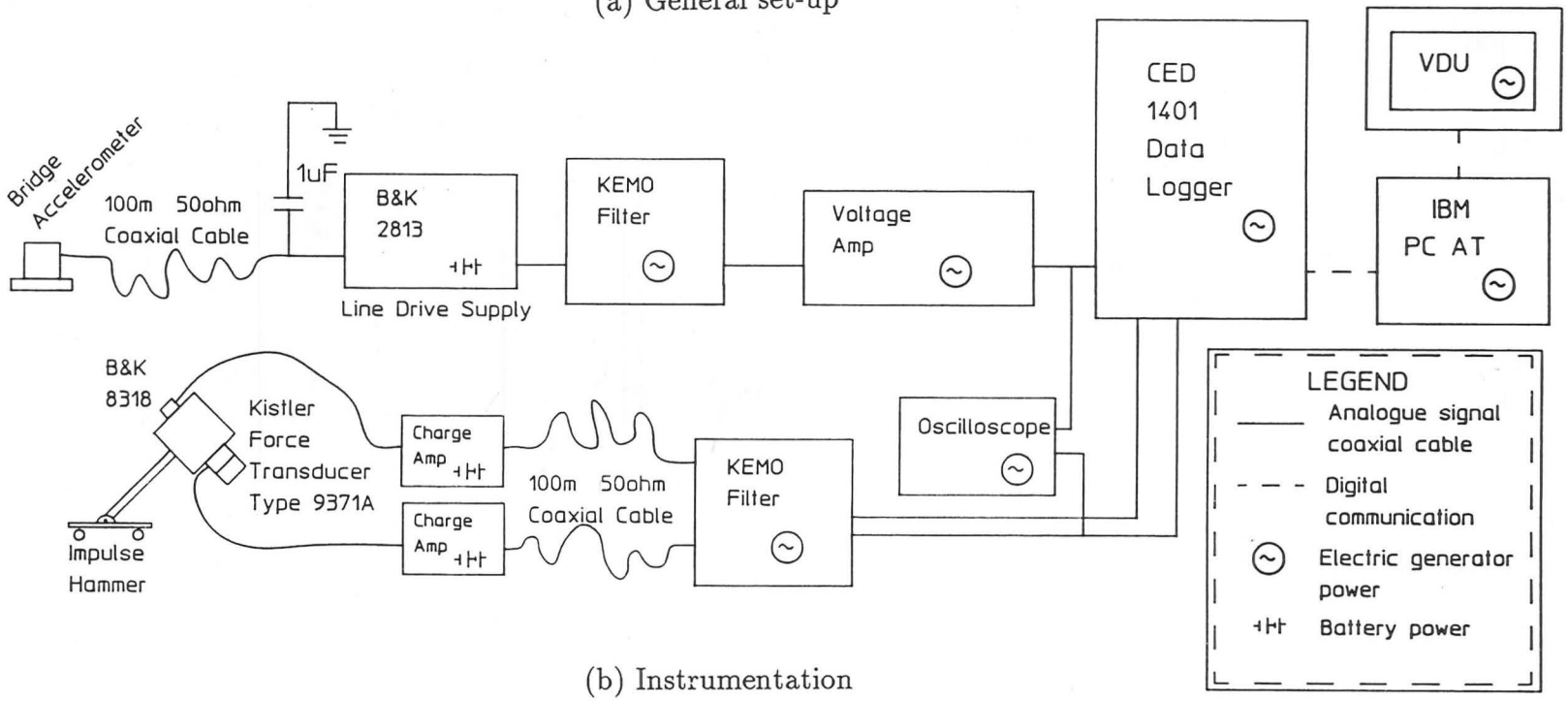

(b) Instrumentation

Figure 3.10: Schematic diagram of equipment for measuring bridge vibrations during impulse and vehicle tests

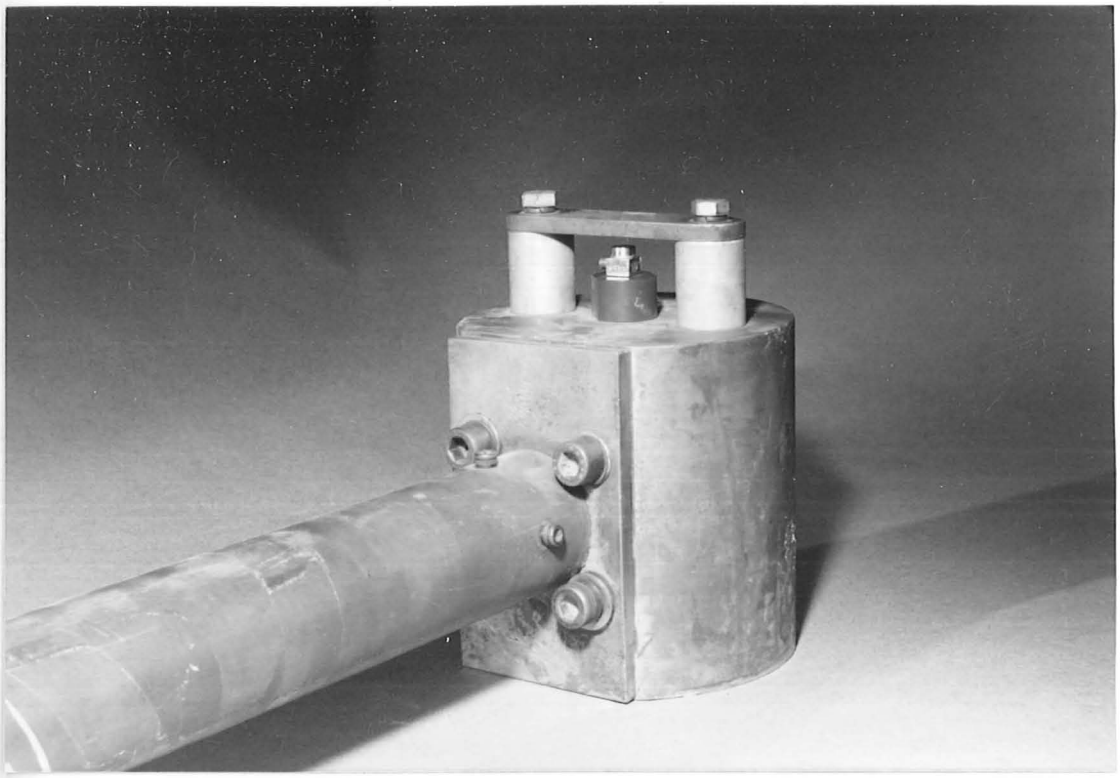

Figure 3.11: Original hammer head with accelerometer

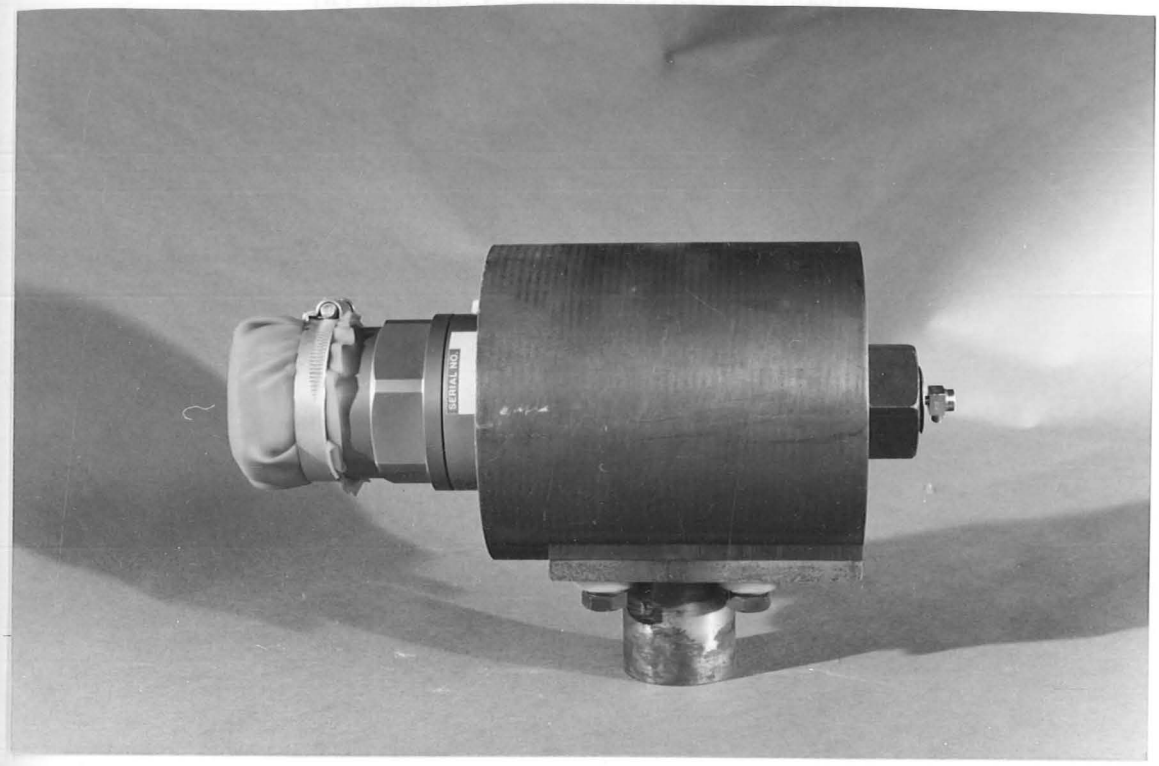

Figure 3.12: Modified hammer head with force transducer and accelerometer

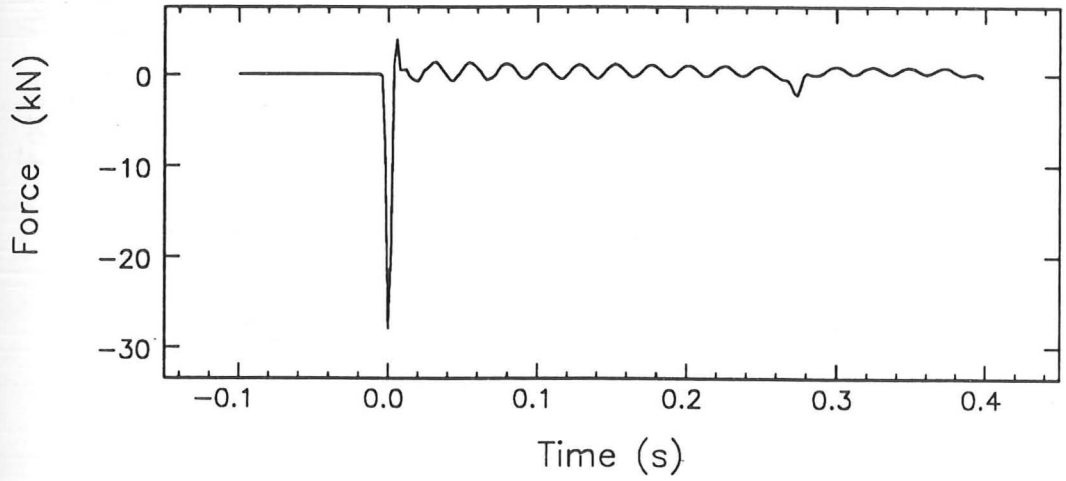

(a) Impulse with hammer arm vibration

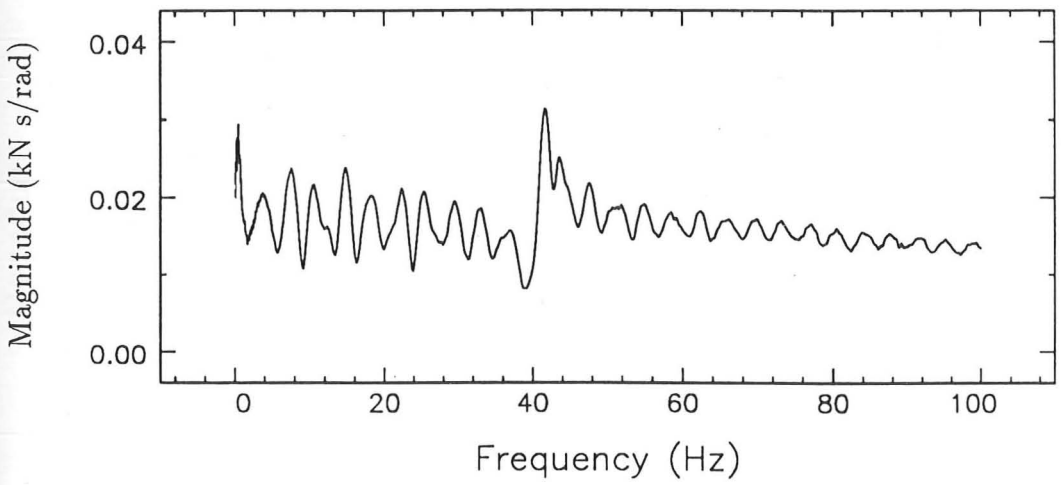

(b) Fourier spectrum of impulse

Figure 3.13: A typical impulse - Initial hammer configuration

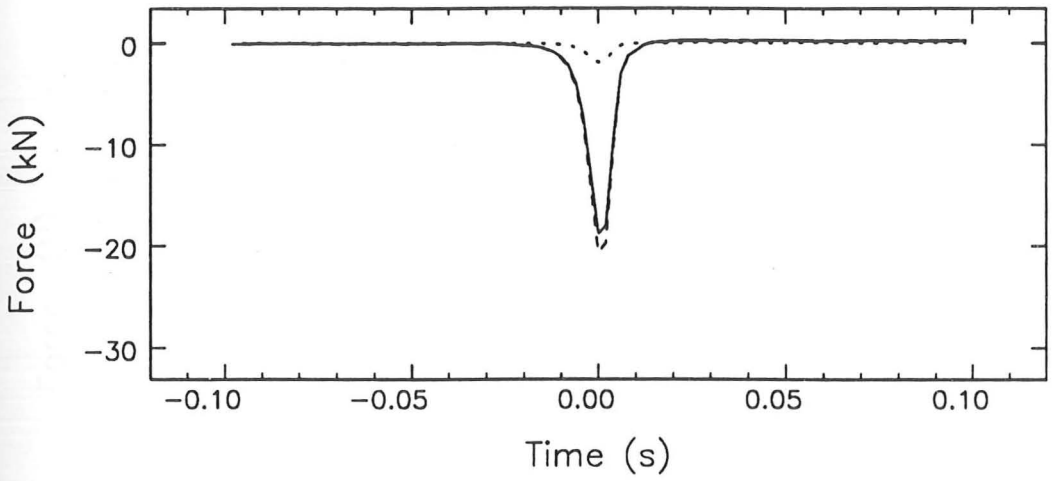

(a) Components of impulse
Force transducer output _____
Outboard mass contribution . . . . . .
Impulse applied to bridge _ _ _ _ _ _ _

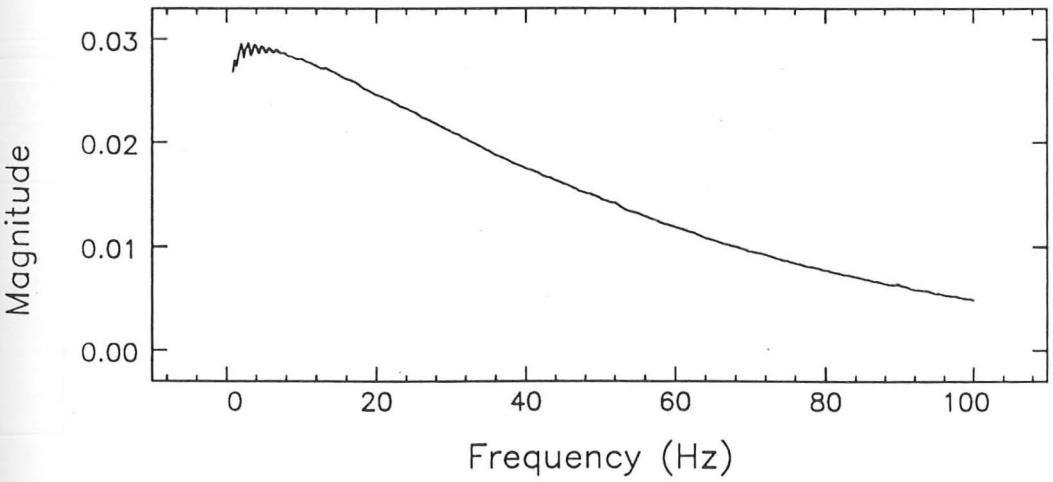

(b) Fourier spectrum of impulse applied to bridge

Figure 3.14: A typical impulse - Modified hammer configuration

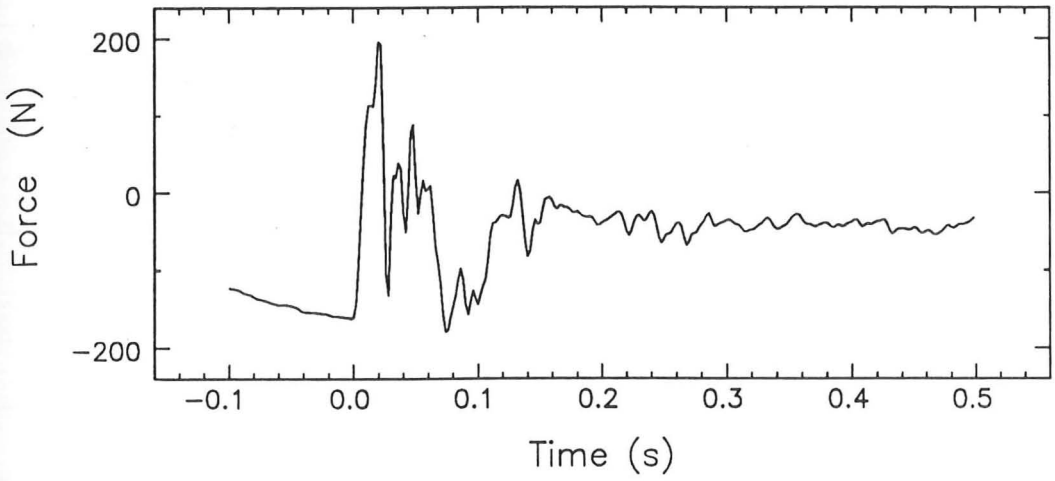

Figure 3.15: Reaction force at hammer base

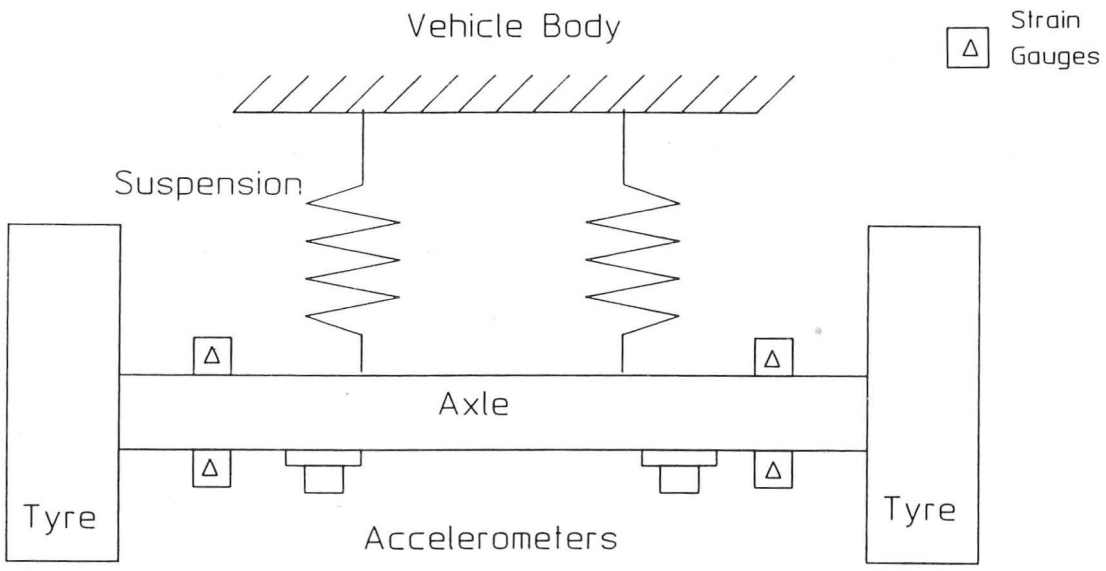

Figure 3.16: Schematic diagram of vehicle instrumentation

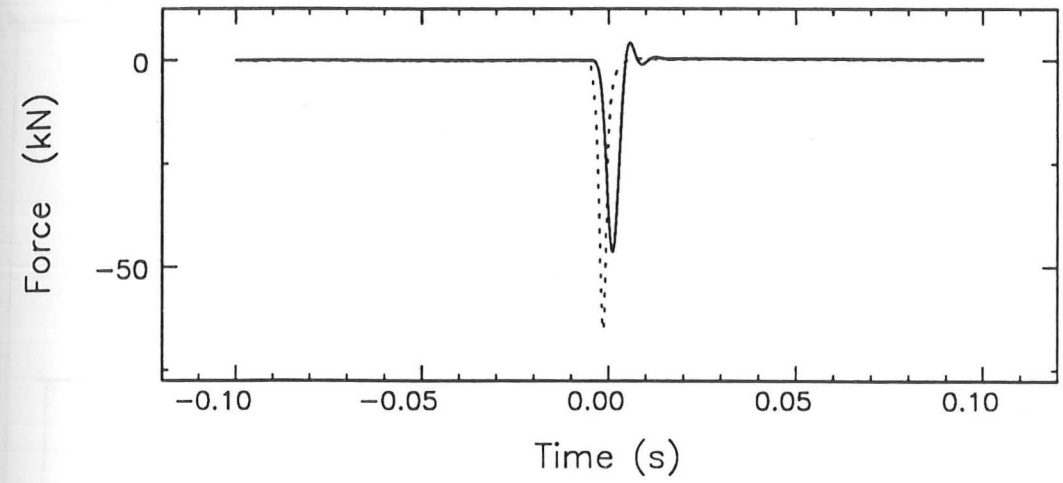

(a) Impulses

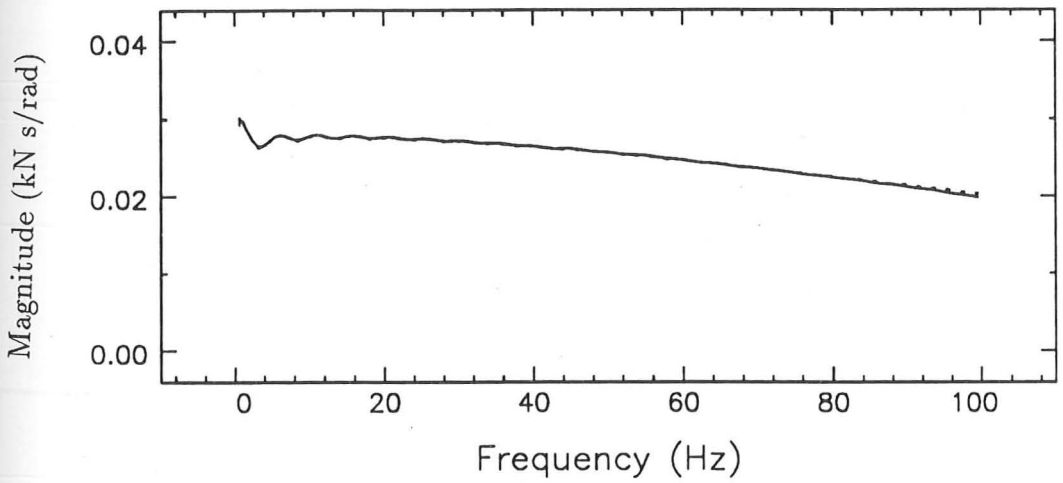

(b) Fourier spectra of impulses

Figure 3.17: Effect of filtering an impulse
f_{co} = 150Hz _____
f_{co} = 1000Hz . . . . . .

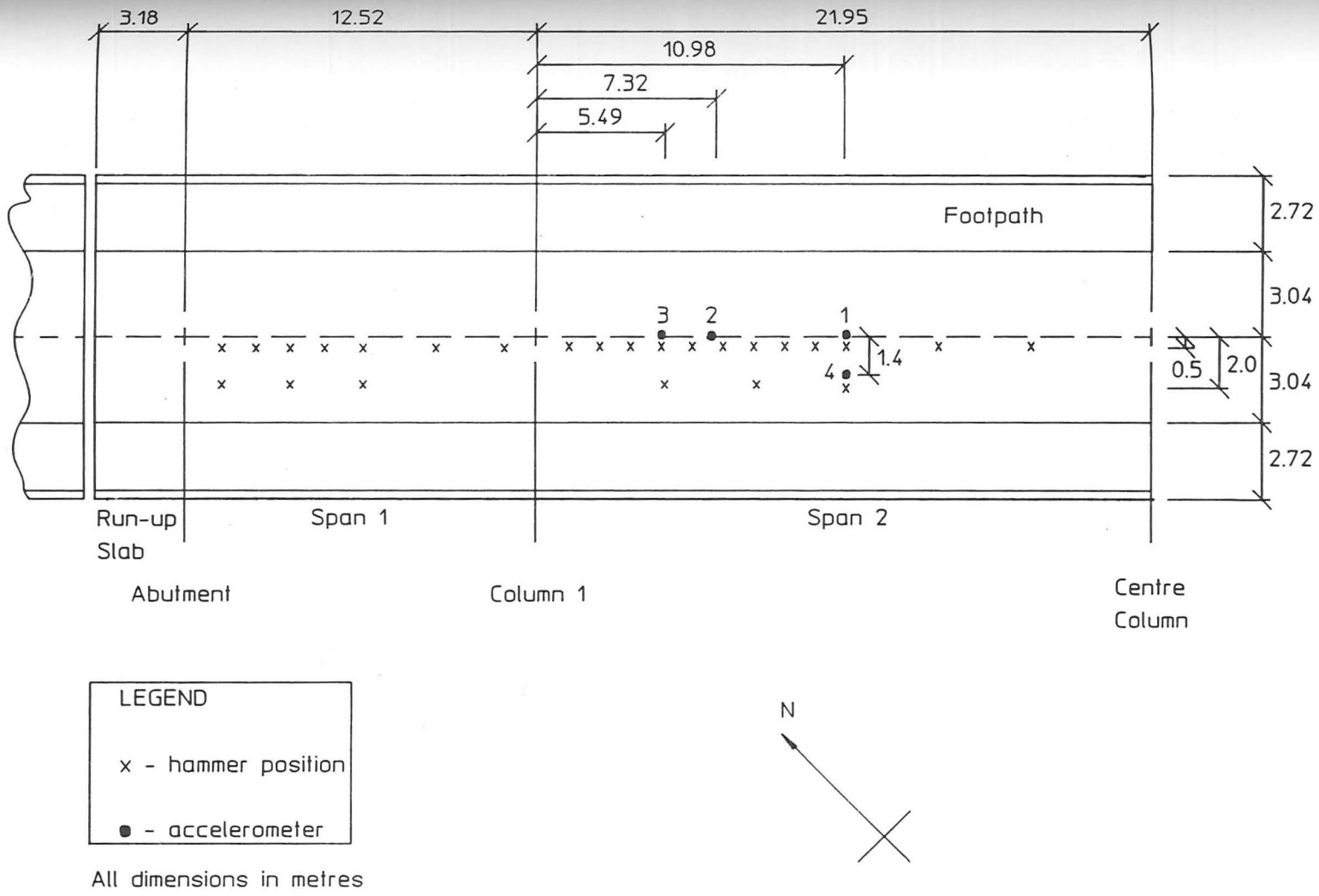

Figure 3.18: Plan of north-west half of Drift Road bridge

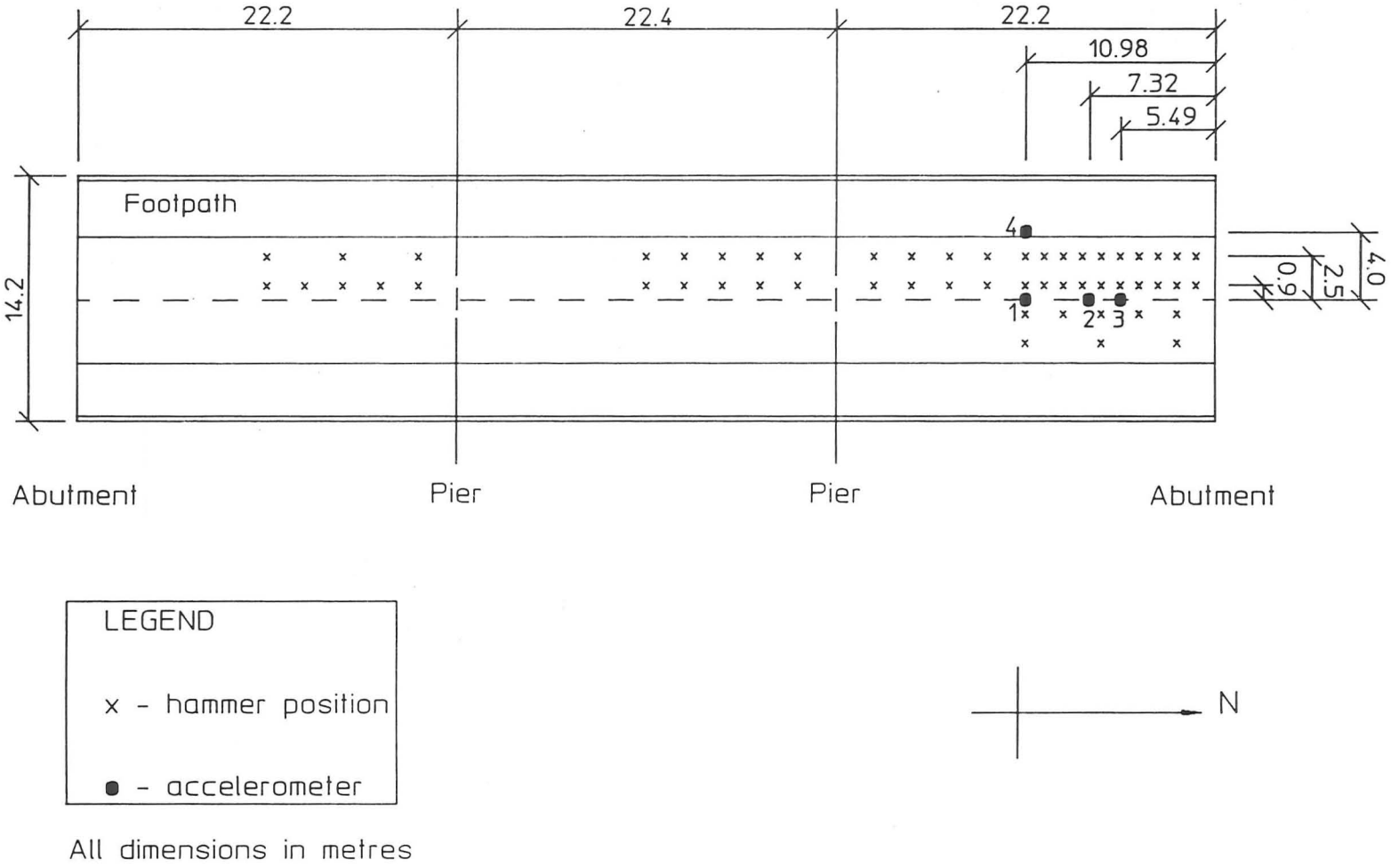

Figure 3.19: Plan of Lower Earley bridge

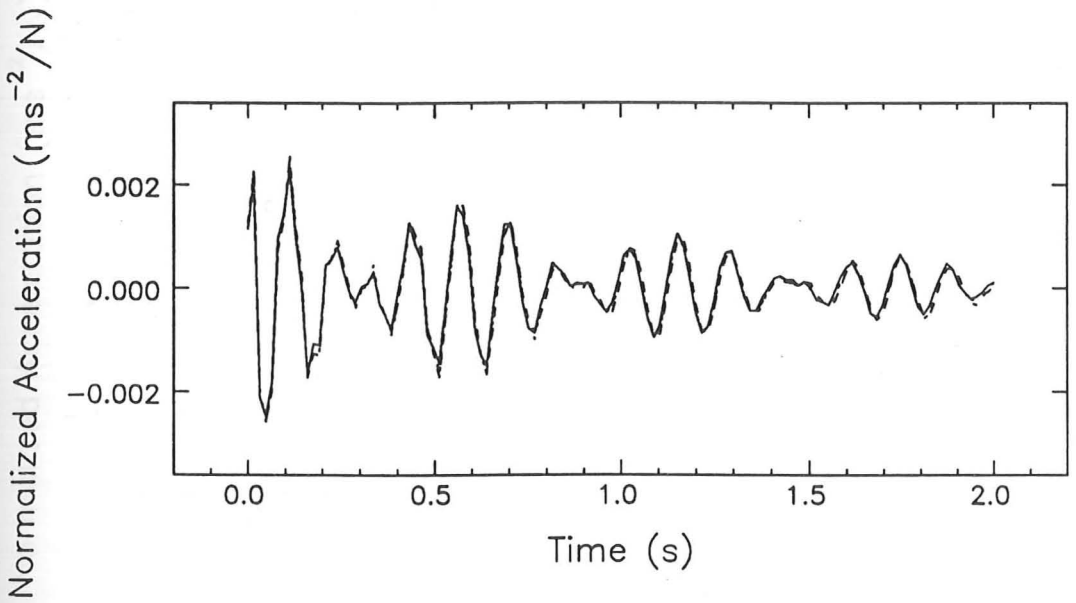

(a) Drift Road bridge

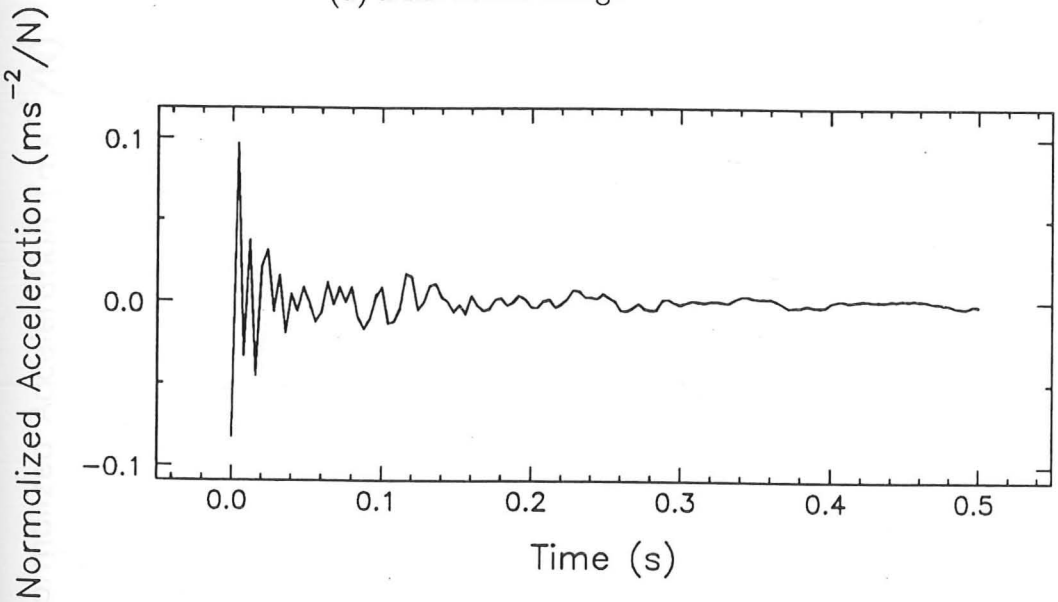

(b) Lower Earley bridge

Figure 3.20: Normalized impulse responses for three hammer drops from the same height
Drop Number 1 ————————
Drop Number 2 ----------
Drop Number 3 - - - - - - - - - -

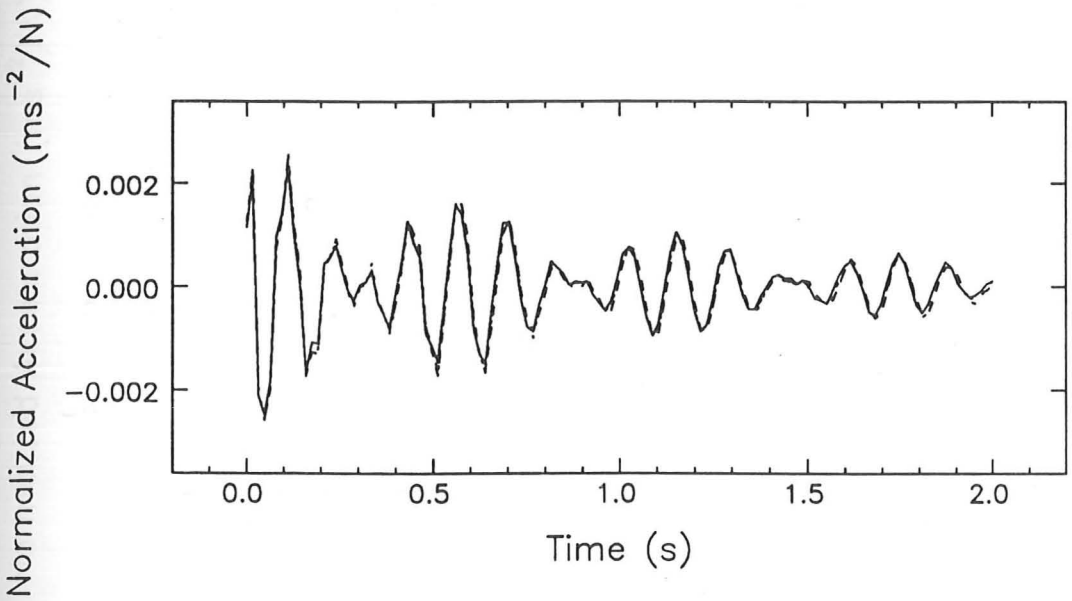

(a) Drift Road bridge

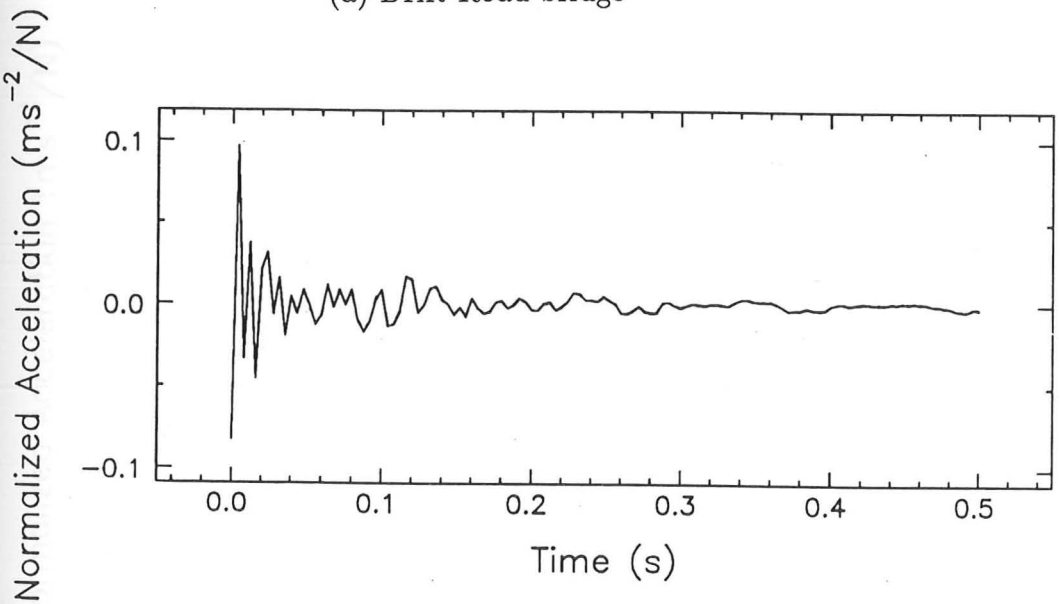

(b) Lower Earley bridge

Figure 3.20: Normalized impulse responses for three hammer drops from the same height
Drop Number 1 ——————
Drop Number 2 - - - - - - - - - - - - - -
Drop Number 3 . . . . . .

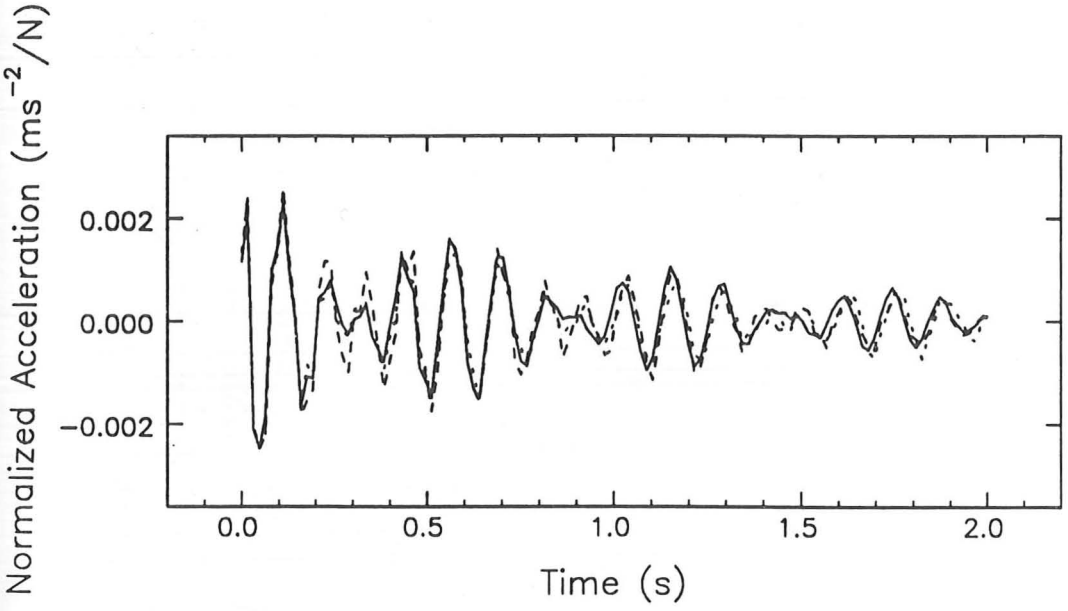

(a) Drift Road bridge

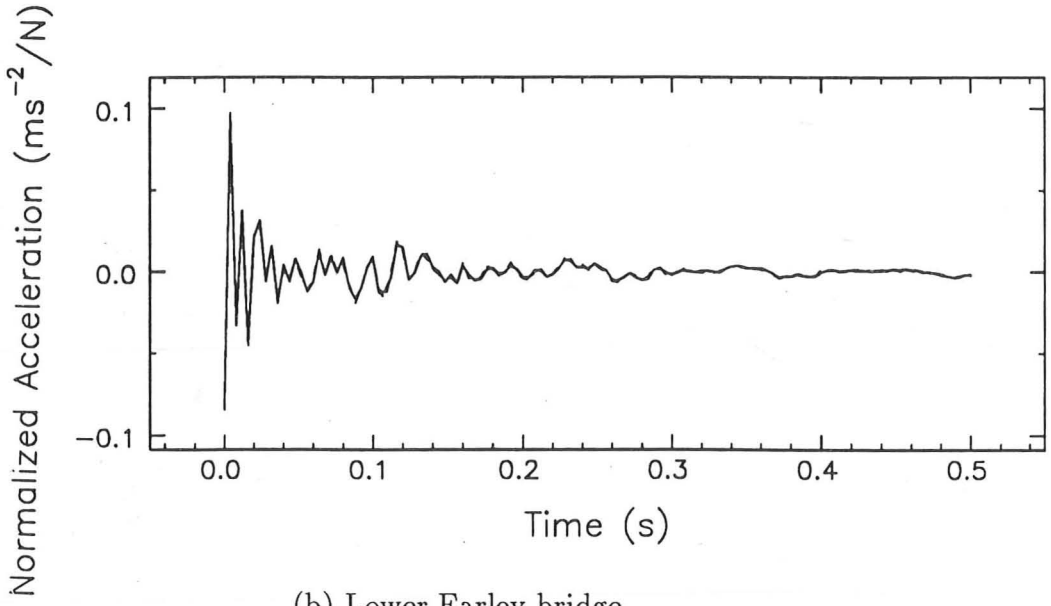

(b) Lower Earley bridge

Figure 3.21: Normalized impulse responses for three hammer drops from different heights
Height 2.0m _____
Height 1.6m - - - - - - - - - - - - - -
Height 1.0m . . . . . .

Figure 3.22: Test vehicle for Drift Road bridge

Figure 3.23: Test vehicle for Lower Earley bridge

4 DATA ANALYSIS

This chapter is concerned with analysis of the data collected by the procedures of chapter 3. Data from both the vehicle tests and the impulse tests is presented.

The dynamic wheel loads and the resulting bridge responses are examined in both the time and frequency domains. In addition, some statistics of the measured dynamic wheel loads are presented.

The analysis procedures for determining the bridge modal parameters from the impulse tests are also discussed.

4.1 Vehicle Tests

Vehicle tests were conducted to measure the vibrational response of the test bridges to a single pass of an instrumented heavy goods vehicle. In order to compare the measured bridge responses with those predicted from the convolution calculation procedure presented in chapter 2, the wheel loads were also measured. In this section, analysis of the vehicle test data is presented and comments are made about important characteristics of both the vehicle wheel loads and the vehicle-induced dynamic bridge response.

4.1.1 Analysis of the Dynamic Wheel Load Data

The dynamic wheel loads were determined for each vehicle test run. For the purposes of illustration, one vehicle run per bridge has been selected for presentation in this dissertation.

Figure 4.1 contains wheels loads for a south-east to north-west run at 50km/h on the Drift Road bridge. At time zero the front axle of the vehicle encounters the first span of the bridge while the trailing axle leaves the bridge 6.1 seconds later. The large dynamic tyre forces at both ends of the bridge are caused by discontinuities in the surface profile at the expansion joints. The expansion joints are located just before the run-on slab (see figure 3.18) and this explains why the vehicle is bouncing before it enters the first span. Expansion joints and other large irregularities in the bridge road surface are the main cause of high dynamic wheel loads on bridges [14, 76]. Figure 4.1(a & b) illustrates that the loads can be almost double the static values. For this vehicle, the largest variations in the tyre forces occur on the front two axles which have steel leaf-spring suspensions. The trailer axles are connected to an independent air suspension and this results in lower dynamic wheel loads, although figure 4.1(c & d) shows that relatively more high frequency (wheel-hop) motion is present than for the leaf-spring suspensions. This behaviour is typical of air suspensions [65].

A set of wheel loads for a south to north run over the Lower Earley bridge is presented in figure 4.2. The vehicle speed is 65km/h and the front axle enters the bridge at time zero. The trailing axle leaves the bridge 5.6 seconds later. This vehicle has air-springs on the tractor axles and leaf-springs on the trailer. The front two axles generate lower dynamic wheel loads, but at higher frequencies. In general, the wheel loads are smaller for the Lower Earley tests and the expansion joint at the bridge entrance does not excite the vehicle to same degree as on the Drift Road bridge. This indicates a smoother riding surface on the bridge as well as better quality expansion joints. Unfortunately, no surface profile data was measured, so a quantitative assessment of the bridge roughness is not possible.

As a further study, the wheel load data was formulated in terms of dynamic load

increments (defined in section 3.1.2). This study is interested in determining not only the maximum dynamic load increments, but also the standard deviation of the increments. Other authors have referred to this standard deviation as the dynamic load coefficient [65, 88]. Figures 4.3 to 4.6 contain the dynamic load increments calculated from both bridge tests plotted against speed. In general, dynamic load increments increase with speed.

The maximum values for the Drift Road bridge are plotted in figure 4.3 while the standard deviations are in figure 4.4. For the steel suspensions (steer and drive axles), the increase with speed seems to be almost linear, but the air suspensions do not follow any obvious type of behaviour. The maximum dynamic load increment for the steel suspension is approximately 1.0 which corresponds to doubling the static wheel load. The standard deviations vary between 10 and 20% for the air suspensions and up to 40% for the steel suspensions.

Figures 4.5 and 4.6 show maximum values and standard deviations of dynamic increment for the Lower Earley bridge. In this case the maximum increments are only about 0.5 which indicates smaller dynamic loads than were applied to the Drift Road bridge. The maximum load increments are almost independent of speed, and especially so for the two steel suspensions (trailer axles). Nevertheless, the standard deviation of the load increments increases slightly with speed.

The frequency content of the wheel loads was analysed by calculating the Fourier spectrum [5] of the various wheel load traces. As described in section 3.3.4, the Fourier spectrum is a more appropriate measure than spectral density for transient signals. Figures 4.7 and 4.8 illustrate the frequency content of the wheel loads measured on the Drift Road and Lower Earley bridges respectively. As is evident from these figures, most of the energy in the wheel loads is concentrated in the 1-4Hz range although wheel-hop causes a second peak between 10 and 15Hz. This is typical of heavy goods vehicles as has been shown by other authors [17, 19, 26, 65].

4.1.2 Bridge Response from Vehicle Tests

Measured bridge responses from typical vehicle tests on both bridges are shown in figures 4.9 and 4.10. The displacement time histories were obtained by integrating the acceleration signals twice. As mentioned in section 3.3.1, the quasi-static responses were not measured accurately by the accelerometers, and so a high-pass filter with a cut-off frequency of 1.0Hz was applied to the signals to avoid drifting during the integration. For both bridges the dominant frequencies are below 10Hz.

In order to determine the frequency content of the measured bridge responses, Fourier spectra were computed for the various vehicle tests. Typical spectra for both bridges are shown in figures 4.11 and 4.12. Most of the energy is concentrated in the region below 15Hz. This is expected because the dynamic wheel loads only have significant amplitude below 15Hz.

4.2 Impulse Tests

The main reason for the impulse tests was to determine the mode shapes and damping values of the bridge. The modal parameter extraction was done primarily in the frequency domain, but some preliminary analysis was conducted in the time domain and is discussed in this section.

4.2.1 Impulse Tests at Drift Road: Time Domain

Typical impulses and the resulting bridge responses, measured at four different positions, are shown in figures 4.13 and 4.14. Results from the first set of tests are presented in figure 4.13, while the second test results are in figure 4.14 . In both cases the hammer was located at the middle of the measurement span.

One point to note about the hammer impulse in figure 4.13 is that there are two distinct impacts. The second impulse (at approximately 0.3 seconds) induces additional response from the bridge, but this does not adversely affect the analysis of the data. A detailed discussion of the effect of the double impulse is included in

Appendix C. In the second set of tests the hammer was allowed to drop only once.

Two effects that are immediately visible in the responses of figure 4.13 are the dominance of frequencies between 50 and 60Hz, and the beating in the response. The beating indicates that there are at least two closely spaced frequencies while the predominance of the higher frequencies occurs because some bridge modes in the 50-60Hz region are easily excited by the impulse. A qualitative comparison of these impulse responses with the vehicle induced responses of figure 4.9 shows that these higher frequencies are not significant for vehicle-induced bridge vibration.

For the second set of tests at Drift Road, changes were made to reduce the presence of these higher frequencies in the impulse responses. Since the important frequencies were known to be below 20Hz, the acceleration signals were filtered at 25Hz in order to reduce the effect of the responses at higher frequencies. In addition, the hammer was dropped on soft foam to concentrate the energy in the lower frequencies (see section 3.3.4). Finally, the sample length was extended to 8 seconds. By comparing figures 4.13 and 4.14, the effects of these changes are evident. The responses from the later tests are dominated by frequencies below 20Hz.

4.2.2 Impulse Tests at Lower Earley: Time Domain

A typical impulse and the resulting responses are shown in figure 4.15. For the Lower Earley tests the hammer was not allowed to drop a second time.

The responses in this case are noticeably different from those measured at Drift Road. The prominent frequencies are below 20Hz and the modal density is greater than at Drift Road. Most of the response dies away after only a few seconds, and so the record length (8 seconds) is more than adequate.

4.2.3 Transfer functions

The first stage in the extraction of the modal parameters from the impulse tests was the calculation of transfer functions (or frequency response functions). The tests at each hammer position produced four averaged transfer functions; one for

each accelerometer position. The procedure for calculating transfer functions was standardized and is summarized as follows:

(i) remove any dc offset from both the impulse and the response,

(ii) determine the position of the maximum value of the impulse and adjust the time scale so that the maximum value of the impulse occurs at time 0 (see figures 4.13, 4.14, and 4.15),

(iii) apply an exponential window to the time series to reduce noise at the end of the responses and to avoid truncation errors:

$$w(t) = \begin{cases} 1 & t < 0 \\ e^{-Kt} & t \geq 0, \quad K \geq 0 \end{cases} \tag{4.1}$$

K was taken as 1.0 for the Drift Road bridge and 0.5 for the Lower Earley bridge,

(iv) extend the record length by adding zeros,

(v) calculate the DFT of both the impulse and the response,

(vi) compute the transfer function by dividing the response transform by the impulse transform,

(vii) repeat the procedure outlined in (i) to (vi) for five different hammer drops at the same position and then average the resulting transfer functions.

Averaged transfer functions for the Drift Road bridge are shown in figure 4.16. Four plots are shown; one corresponding to each accelerometer position. For all four transfer functions the hammer was located at the quarter point of the instrumented span. The transfer function is only shown for frequencies up to 25Hz, because the vehicle-induced bridge response is concentrated at frequencies below 20Hz. The solid lines on the plots are the measured transfer functions.

In the region below 20Hz, three flexural modes and two torsional modes are evident. The first peak, at 6.8Hz, corresponds to the fundamental flexural frequency of the bridge while the peak at 8.7Hz is the second flexural mode. The third mode (19.3Hz) is only evident on the transfer functions corresponding to accelerometers number 2 (1/3 point) and 3(1/4 point).

The transfer function for the offset accelerometer shows two small peaks at 11.2Hz and 12.3Hz that are not present on the other two transfer functions. These peaks correspond to torsional modes.

The three flexural peaks are narrow and quite sharp which indicate that the modes are lightly damped.

Figure 4.17 shows transfer functions calculated from impulses applied at the middle of the instrumented span of the Lower Earley bridge. These transfer functions are markedly different from those measured at the Drift Road site; more modes are present, and the response is not dominated by any one mode nor pair of modes. In the region below 20Hz, there are 4 obvious peaks at 5.7, 9.7, 11.3, and 18.0Hz. An examination of the transfer function corresponding to the off-centre accelerometer indicates modes not evident in the other accelerometer traces. The extra peaks occur at 6.9, 7.4, and 13.3Hz.

4.3 Modal Analysis

After the transfer functions were calculated, it was possible to identify the natural frequencies of the bridges and to make qualitative judgements about damping levels. In order to quantify these estimates, some form of numerical modal analysis is necessary. Modal analysis also provides a measurement of the modal constant which contains information about the relative magnitudes and phases of vibration in each individual mode.

Modal analysis is essentially a curve-fitting procedure to relate a measured frequency response function with a theoretical model. The theoretical models are usu-

ally based on the assumption of a single degree of freedom system, but some methods have been developed that are suitable for general multiple degree of freedom analysis [30]. The single degree of freedom system assumption is usually justified by noting that near resonance the frequency response function is dominated by only one mode. Methods assuming a single degree of freedom system therefore work best when the natural frequencies are well separated [30].

The second major assumption of the modal analysis procedure concerns the type of damping. Either structural or viscous damping is usually assumed. As was mentioned in chapter 2, the viscous damping assumption was used in this analysis. For viscous damping, the mobility (or velocity) transfer function, calculated with an exponential window (equation 4.1) applied to the impulse responses, is

$$\Upsilon_{jk}(\omega) = \sum_{n=1}^{\infty} \frac{i\omega A_{jk}^{(n)}}{{\omega^{(n)}}^2 - \omega^2 + 2i(\zeta^{(n)}\omega^{(n)} + K)\omega} \tag{4.2}$$

where $\Upsilon_{jk}(\omega)$ is the mobility transfer function measured at position k from an input at position j, and $A_{jk}^{(n)}$ is the n^{th} modal constant.

The modal analysis procedure outlined in this chapter consists of attempting to estimate values of $\omega^{(n)}$, $\zeta^{(n)}$, and $A_{jk}^{(n)}$.

4.3.1 Modal Parameter Extraction: Theory

Several methods are available [30, 77], and are described in detail by Ewins [30]. The circle fit method was chosen.

In order to perform the circle fit, the real and imaginary parts of the transfer function are plotted against each other in the Argand plane. According to theory the data will trace a circular arc near resonance, so a circle is fit to points near resonance (figure 4.18) and a measure of the error is obtained. The location of the natural frequency is determined by finding the position at which the sweep of the circle is at a maximum (figure 4.18). Damping estimates are then obtained by considering points on either side of the resonant frequency. Let ω_a and ω_b represent positions on the modal circle above and below the natural frequency, respectively, and θ_a and θ_b the corresponding subtended angles as shown in figure 4.18. The damping ratio

is given by [30]

$$\zeta^{(n)} = \frac{\omega_a^2 - \omega_b^2}{2\omega^{(n)}[\omega_a tan(\frac{\theta_a}{2}) + \omega_b tan(\frac{\theta_b}{2})]} - \frac{K}{\omega^{(n)}}. \tag{4.3}$$

Using this formula for the damping ratio, each point above the natural frequency is combined with each point below to give several damping estimates. The mean and variance of the estimates are calculated. This yields an average damping ratio with a bound on the estimation error.

Finally the magnitude and phase of the modal constant are calculated from the size of the circle and the orientation of the natural frequency on the circle. The modal constant, $A_{jk}^{(n)}$, is given by [30]

$$A_{jk}^{(n)} = \left|A_{jk}^{(n)}\right| e^{i\theta_{jk}^{(n)}} \tag{4.4}$$

with

$$\left|A_{jk}^{(n)}\right| = \frac{D_{jk}^{(n)}}{2(\zeta^{(n)}\omega^{(n)} + K)} \tag{4.5}$$

where $D_{jk}^{(n)}$ is the circle diameter and $\theta_{jk}^{(n)}$ is the angle of inclination of the modal circle as shown on figure 4.18. If this angle is zero for all positions on the structure, then the modes are real.

Since single degree of freedom analyses are not always appropriate, several curve fitting techniques have been developed to deal with multiple degree of freedom systems [30]. One of the simpler methods is an extension of the single degree of freedom circle fit method. The first stage in the extended analysis is to perform the single degree of freedom circle fit to obtain reasonable estimates of the modal parameters. These estimated parameters are then used to adjust the measured mobility near resonance to account for the presence of the other modes. The adjusted values then conform more closely to those of a single degree of freedom system and the circle fit procedure can be more effective. This modified circle fit method was employed in this study when the modes were closely spaced. Details of other multiple degree of freedom modal analysis procedures are readily available elsewhere [30, 31].

The circle fit method was chosen for application to the data presented in this dissertation because of the method's versatility and ease of extension to include multiple degree of freedom systems.

4.3.2 Transfer Function Regeneration: Theory

After extracting the modal parameters, a theoretical transfer function can be regenerated and compared with the corresponding measurement. Since it is almost impossible to measure all of the modes that contribute to response in any given region, initial attempts at regeneration often have disappointing results [30]. The correlation between measurement and regeneration can be improved, however, by the inclusion of two additional terms to account for frequencies above and below the analysed frequency range. If all of the modes between m_1 and m_2 have been measured then

$$\Upsilon_{jk}^{(r)}(\omega) = \sum_{n=m_1}^{m_2} \frac{i\omega A_{jk}^{(n)}}{{\omega^{(n)}}^2 - \omega^2 + 2i(\zeta^{(n)}\omega^{(n)} + K)\omega} \tag{4.6}$$

where $\Upsilon_{jk}^{(r)}(\omega)$ is the regenerated mobility curve. The theoretical curve is given by equation 4.2 and so the regeneration error, $E_{jk}^{(r)}(\omega)$, is

$$\begin{aligned} E_{jk}^{(r)}(\omega) &= \Upsilon_{jk}(\omega) - \Upsilon_{jk}^{(r)}(\omega) \\ &= \sum_{n=1}^{m_1} \frac{i\omega A_{jk}^{(n)}}{{\omega^{(n)}}^2 - \omega^2 + 2i(\zeta^{(n)}\omega^{(n)} + K)\omega} \\ &\quad + \sum_{n=m_2+1}^{\infty} \frac{i\omega A_{jk}^{(n)}}{{\omega^{(n)}}^2 - \omega^2 + 2i(\zeta^{(n)}\omega^{(n)} + K)\omega}. \end{aligned} \tag{4.7}$$

Since the regenerated model is valid only in the analysed frequency range, approximations can be made to estimate the error term within the analysed frequency range. The first error term of equation 4.7 can be approximated as mass dominated and the second term as stiffness dominated. The error term then has the following approximate form [30]

$$E_{jk}^{(r)} \approx \frac{1}{i\omega M_{jk}^{(r)}} + \frac{i\omega}{K_{jk}^{(r)}} \tag{4.8}$$

where $M_{jk}^{(r)}$ is the mass residual and $K_{jk}^{(r)}$ is the stiffness residual.

Following procedures described by Ewins [30], stiffness residuals were calculated by considering points on the transfer function outside the analysed frequency range. The mass residuals were not computed because all the low frequency modes were measured. The inclusion of the stiffness residuals in the theoretical regeneration of the transfer function did not significantly improve the correlation between the regenerated and measured transfer functions. Therefore, stiffness residuals were not included in the regeneration plots presented in this dissertation.

4.3.3 Mode Shape Determination: Theory

The procedures outlined in the preceding two sections illustrate methods for obtaining modal constants from transfer functions. The measured modal constants have the following form:

$$A_{jk}^{(n)} = \phi^{(n)}(\mathbf{x}_j)\ \phi^{(n)}(\mathbf{x}_k) \tag{4.9}$$

where $\mathbf{x}_j$ and $\mathbf{x}_k$ define the positions of the input and response, respectively.

In order to explain the procedure for extracting the values of $\phi^{(n)}$ from the modal constants, consider N_h transfer functions relating N_h different hammer positions to the response measured at one position, $\mathbf{x}_k$. Applying the circle fit procedure to the transfer functions results in the following set of modal constants

$$A_{1k}^{(n)},\ A_{2k}^{(n)},\ A_{3k}^{(n)}, \ldots,\ A_{N_h k}^{(n)}. \tag{4.10}$$

If we also have a point measurement (response and input at the same position), then enough information exists to scale the mode shape properly. For a point measurement, equation 4.9 reduces to

$$\phi^{(n)}(\mathbf{x}_p) = \sqrt{A_{pp}^{(n)}} \tag{4.11}$$

where $\mathbf{x}_p$ defines the position of the point measurement and $A_{pp}^{(n)}$ is the modal constant obtained from the point mobility. Once the magnitude from the point

measurement is determined, the other mode shape values can be scaled by using equation 4.9.

In practice, each modal constant is based on a slightly different estimate of the natural frequency and the corresponding damping ratio. Therefore, before the mode shape calculation is performed, average values of the natural frequency and damping ratio must be computed.

$$\tilde{\omega}^{(n)} = \frac{1}{N_h N_{in}} \sum_{k=1}^{N_{in}} \sum_{j=1}^{N_h} \omega_{jk}^{(n)} \tag{4.12}$$

$$\tilde{\zeta}^{(n)} = \frac{1}{N_h N_{in}} \sum_{k=1}^{N_{in}} \sum_{j=1}^{N_h} \zeta_{jk}^{(n)} \tag{4.13}$$

where N_{in} is the number of instrument positions and $\tilde{}$ indicates averaged values.

The revision of the estimates for natural frequency and damping ratio means that the modal constants must be adjusted accordingly. It was stated that the modal constant calculated using the circle fit procedure is given by

$$\left|A_{jk}^{(n)}\right| = \frac{D_{jk}^{(n)}}{2(\zeta_{jk}^{(n)}\omega_{jk}^{(n)} + K)}. \tag{4.14}$$

If the adjusted values $\tilde{\omega}^{(n)}$, $\tilde{\zeta}^{(n)}$ are now used then

$$\left|\tilde{A}_{jk}^{(n)}\right| = \frac{D^{(n)}}{2(\tilde{\zeta}_n\tilde{\omega}_n + K)} = \left|A_{jk}^{(n)}\right| \frac{\zeta_{jk}^{(n)}\omega_{jk}^{(n)} + K}{\tilde{\zeta}_n\tilde{\omega}_n + K}. \tag{4.15}$$

The adjusted values of the modal constants, $\tilde{A}_{jk}^{(n)}$, can be used to calculate the mode shape values.

4.3.4 Modal Analysis: Drift Road

The circle fitting procedure outlined in section 4.3.1 was applied to the transfer functions calculated at the various hammer positions. Three flexural modes and two torsional modes were studied and figure 4.19 shows example circle fits for each mode calculated when the hammer was at the quarter point of the instrumented span. The fitting procedure gave good results. Notice the calculated position of the

natural frequency on the modal circle. The deviation of the radial line corresponding to the natural frequency position from the horizontal axis indicates the phase of the modal constant as described in section 4.3.1. In these examples, the phase angles are approximately zero. This was the case for all of the modes and positions analysed and therefore all modes were considered to have real parts only.

Each modal circle produced a number of estimates of the damping ratio, but the scatter was reasonably small (less than 5%) and usually dependent on the quality of fit of the modal circle.

After the modes in the 0-20Hz range were estimated, the transfer functions were regenerated based on the measured modal parameters. A comparison of measured transfer functions with the regenerated ones is shown in figure 4.16. The agreement is good and so the modal parameters have been measured accurately. The fits are especially good in the region below 15Hz which is where most of the vehicle energy is concentrated. The effect of the mass and stiffness residuals have not been included in figure 4.16 because the fits are sufficiently accurate without them.

Modal parameters for all of the measured transfer functions were estimated, and average damping ratios and natural frequencies were calculated. The average values are as shown in table 4.1.

These averaged values were used to modify the modal constants as described in section 4.3.3. The modified constants were then substituted into equations 4.9 to 4.11 to determine the mode shapes. Figure 4.20 shows the measurements for the first three flexural mode shapes. Only half the bridge is shown and the vertical lines indicate the positions of the columns. Hammer positions along both wheel tracks are represented by points on the diagram and it is evident that the modal shape values do not vary between the tracks. This indicates that these modes are purely flexural.

On the other hand, figure 4.21 shows the mode shapes corresponding to the other two natural frequencies. The measurements from the two wheel tracks give different mode shape values which indicates that the modes exhibit torsional behaviour.

A comparison of the measured mode shapes with curves from a theoretical anal-

ysis is presented in section 5.1.

4.3.5 Modal Analysis: Lower Earley

A total of eight modes was identified for modal analysis; six of them were present on all of the transfer functions but two were only identified on the transfer functions corresponding to the off-centre accelerometer. All of the modal circles described in the following were from measurements made with the hammer at the middle of the instrumented span.

Figure 4.22 illustrates the circle fitting procedure on all eight modes. The natural frequencies corresponding to the modal circles are indicated on the diagrams. In this example, most of the modes conform well to the circle fit, but mode number five displays larger errors than the others. An inspection of the transfer function (figure 4.17) reveals that mode five (11.3Hz) is quite close to mode four (9.7Hz) which has a much larger magnitude. Therefore, this mode is strongly affected by its neighbouring mode. Similar problems were encountered with other modes at different positions, but it was generally possible to obtain some good measurements for all the modes.

Finally, mode number four deserves closer inspection. The circle fit is satisfactory, but the bottom of the circle formed by the data points has a slight indentation. This effect is caused by the presence of another mode extremely close to the main mode that was not resolved by the modal analysis. This did not present a serious problem for measurements on the instrumented span, because the larger mode dominated and the two modes were accurately represented as one mode. Nevertheless, on the other two spans the smaller mode was not dominated to the same degree and it was difficult to obtain estimates of the modal parameters. This difficulty was taken into account when curves were fit to the mode shape values for response prediction purposes and appropriate approximations were made (see section 5.1.3).

On all of the modal circles the position of the natural frequency is indicated, and it is evident that the lines from the natural frequency position to the circle centres do

not deviate significantly from the horizontal. Modes one, two, three, and five show the largest deviations, but errors in the estimation of the natural frequency could be responsible. In all four cases, changing the natural frequency estimate by one frequency increment would result in the natural frequency radial line being parallel to the horizontal axis. Since the horizontal orientation of this radial line indicates a real mode, it was assumed that all of the modes were real.

The best fit modal circles were used to produce average values of the natural frequencies and damping ratios (see table 4.2).

Figure 4.17 illustrates the regeneration of the transfer function from the modal parameters measured at midspan. Below 20 Hz, the fit is very good except for the region between 12 and 17Hz. The errors are slightly larger in this region, but should not be significant for predicting vehicle-induced bridge response because most of the bridge response is below 10Hz.

Following the procedure outlined in section 4.3.3, the mode shapes corresponding to each measured natural frequency were calculated and are shown in figure 4.23. Measurements from both wheel tracks are included. Vertical lines on the plots separate the three spans. Most of the modes indicate significant differences between measurements in the two wheel tracks, so the modes cannot be assumed to be purely flexural. The measurements were most accurate on the instrumented span (left side of the plots). When the hammer was on the other two spans, the symmetric and anti-symmetric modes cancel each other and reduce the amplitude of the measured vibration. This decreases the signal to noise ratio and makes accurate measurements more difficult.

A comparison of these mode shapes with theory and finite element approximations is presented in the next chapter.

Table 4.1: Natural frequencies and damping ratios
Drift Road bridge

Mode	Natural Frequency (f_m in Hz)	Damping ratio
1	6.8	0.019
2	8.6	0.021
3	11.2	0.033
4	12.3	0.019
5	18.0	0.034

Table 4.2: Natural frequencies and damping ratios
Lower Earley bridge

Mode	Natural Frequency (f_m in Hz)	Damping ratio
1	5.7	0.045
2	6.9	0.088
3	7.4	0.086
4	9.7	0.026
5	11.3	0.014
6	13.3	0.026
7	18.0	0.038
8	24.4	0.019

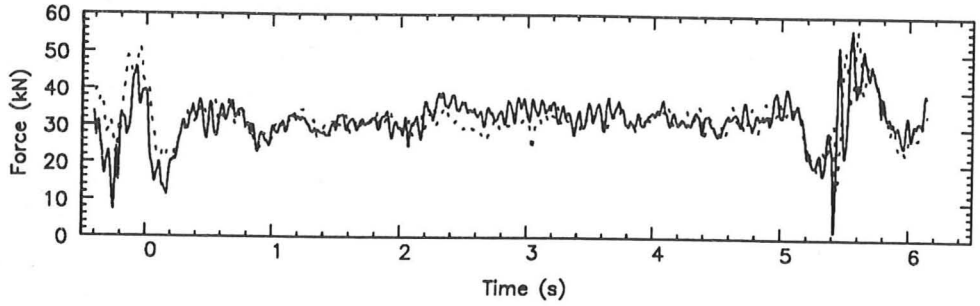

(a) Steer axle

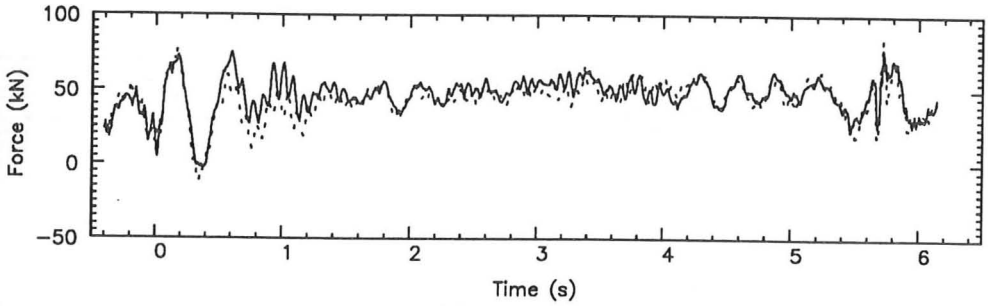

(b) Drive axle

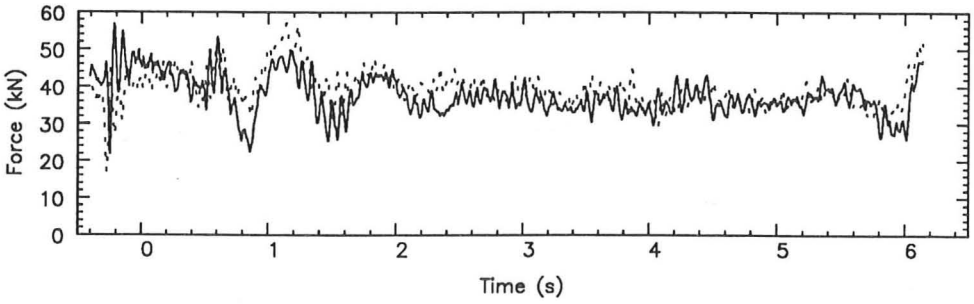

(c) Front trailer axle

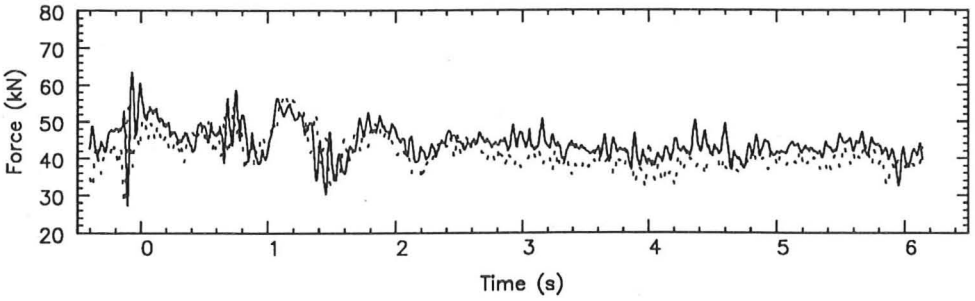

(d) Rear trailer axle

Figure 4.1: Drift Road bridge - Tyre forces
Direction: South-east to north-west, Speed: 50 km/h
Vehicle suspensions: leaf-springs on tractor, air-springs on trailer
Vehicle enters the bridge at time zero
Curbside wheel _____
Centre-line wheel - - - - - - - - - -

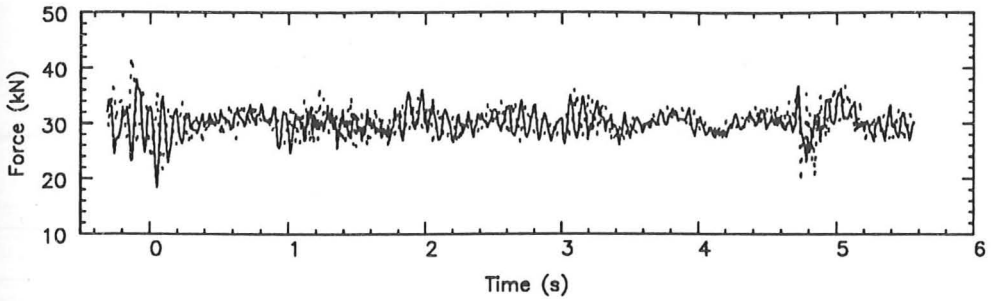

(a) Steer axle

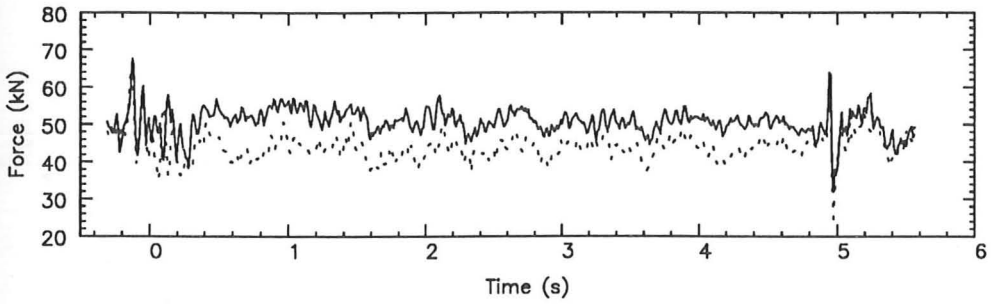

(b) Drive axle

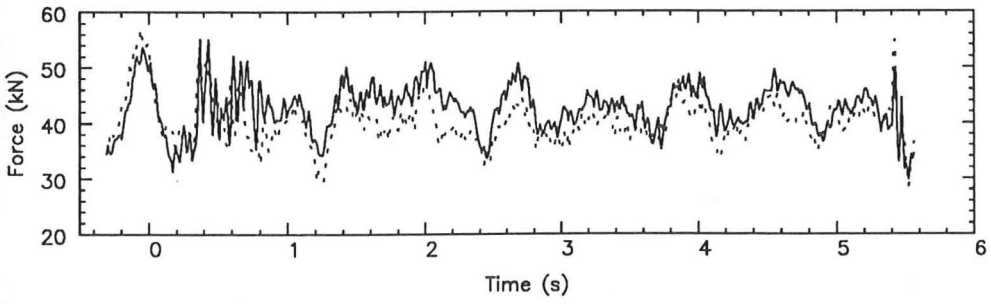

(c) Front trailer axle

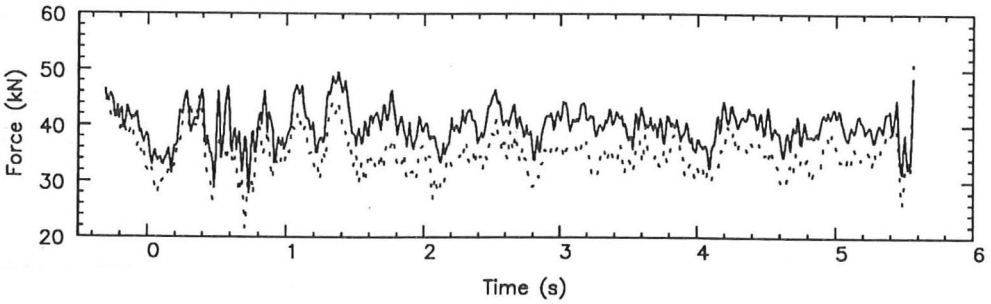

(d) Rear trailer axle

Figure 4.2: Lower Earley bridge - Tyre forces
Direction: South to north, Speed: 65 km/h
Vehicle suspensions: air-springs on tractor, leaf-springs on trailer
Vehicle enters the bridge at time zero
Curbside wheel ———————
Centre-line wheel - - - - - - - - - -

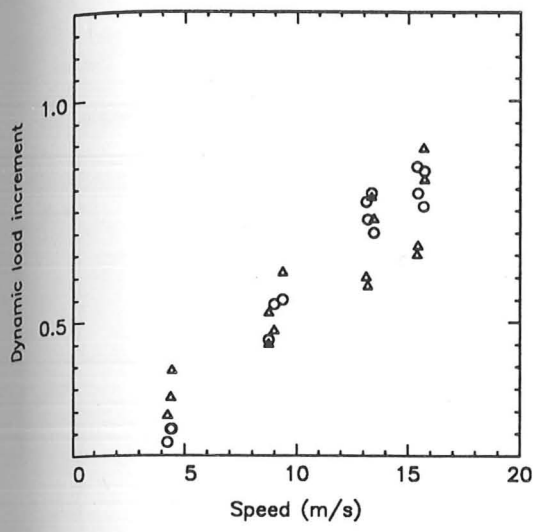

(a) Steer axle

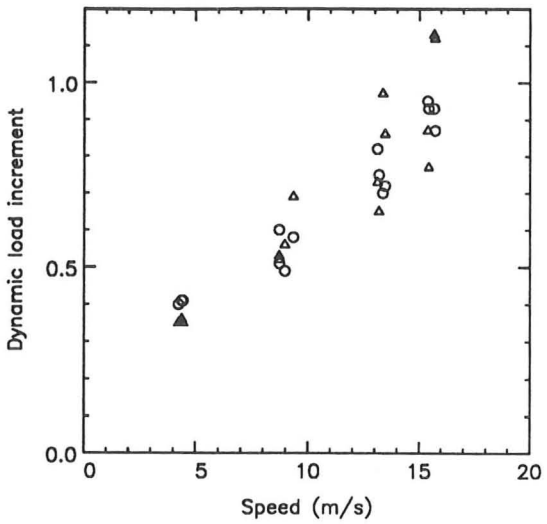

(b) Drive axle

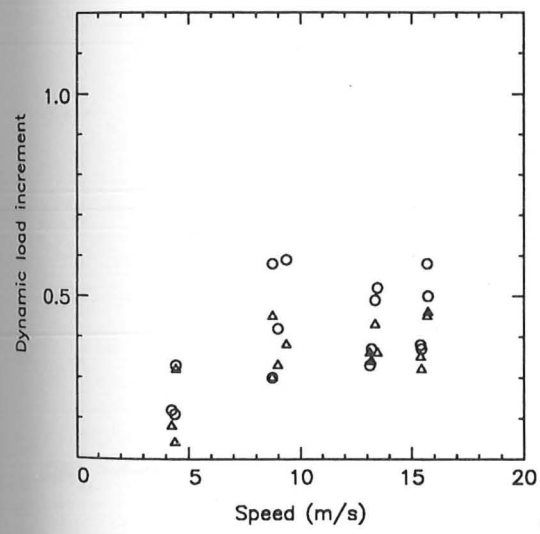

(c) Front trailer axle

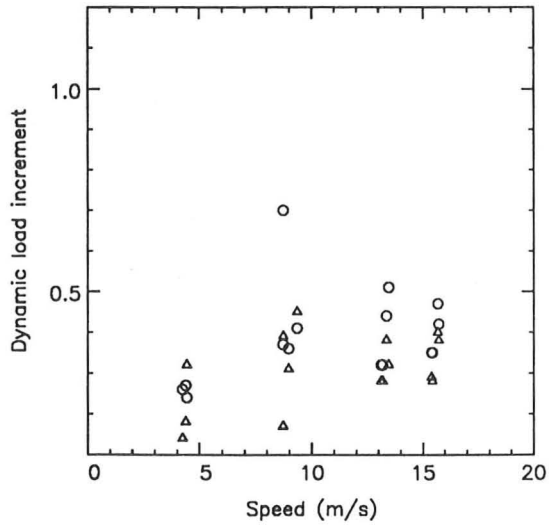

(d) Rear trailer axle

Figure 4.3: Drift Road bridge - Maximum dynamic load increments
Vehicle suspensions: leaf-springs on tractor, air-springs on trailer
Curbside wheel o Centre-line wheel △

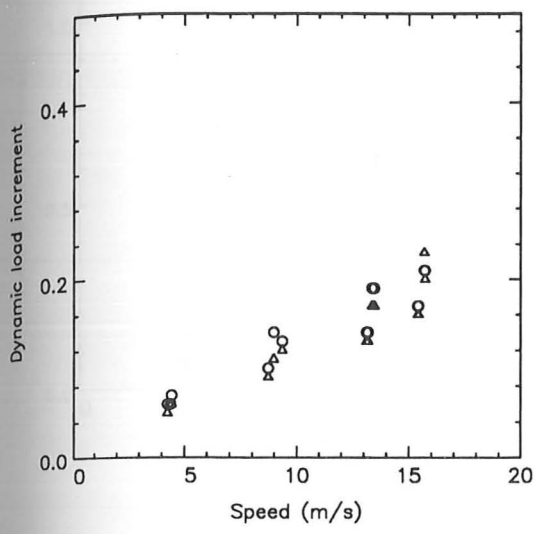

(a) Steer axle

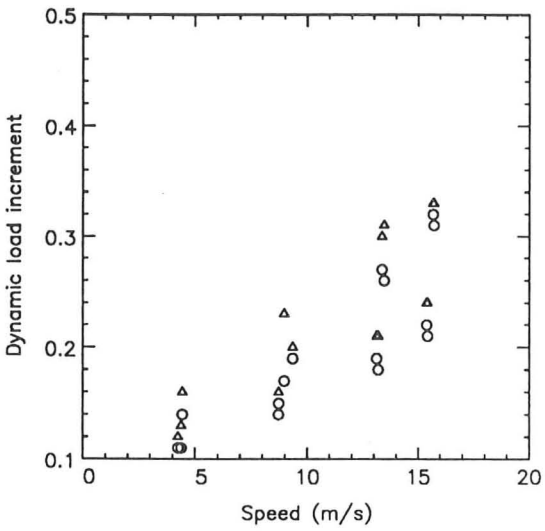

(b) Drive axle

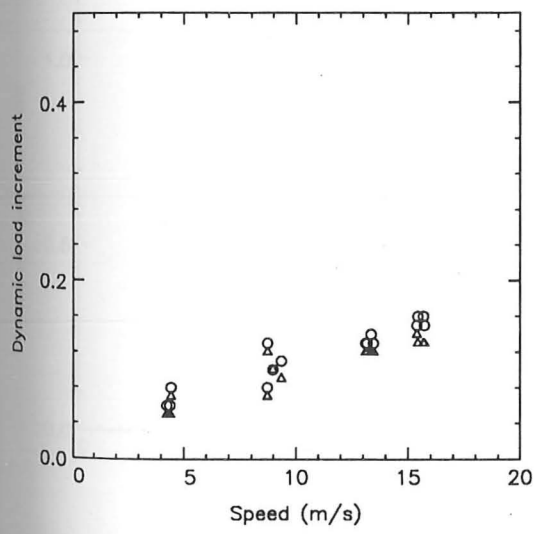

(c) Front trailer axle

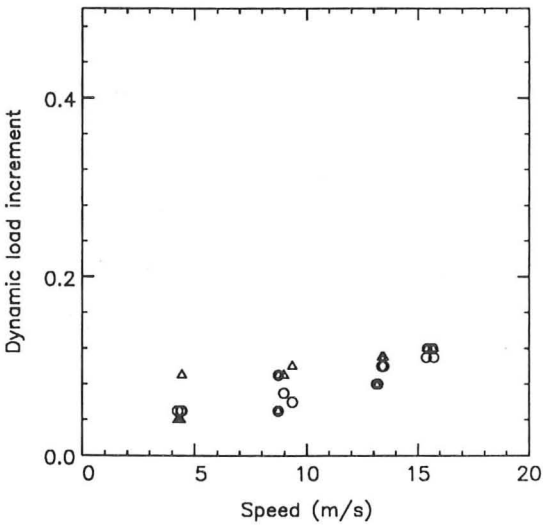

(d) Rear trailer axle

Figure 4.4: Drift Road bridge - Standard deviation of dynamic load increments
Vehicle suspensions: leaf-springs on tractor, air-springs on trailer
Curbside wheel o Centre-line wheel △

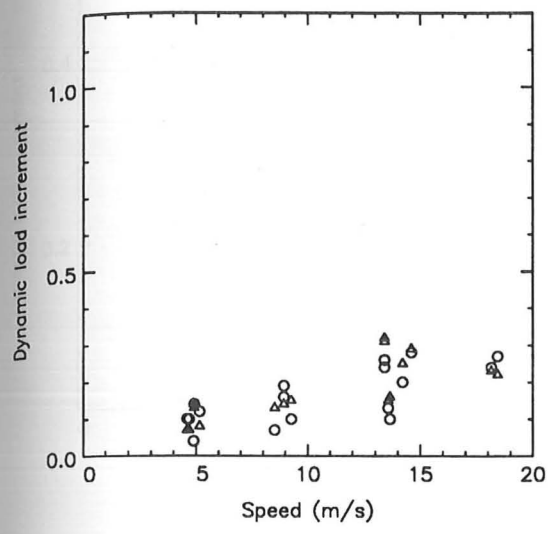

(a) Steer axle

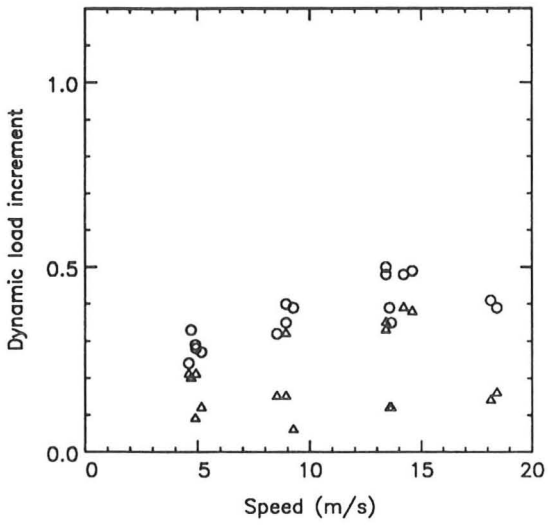

(b) Drive axle

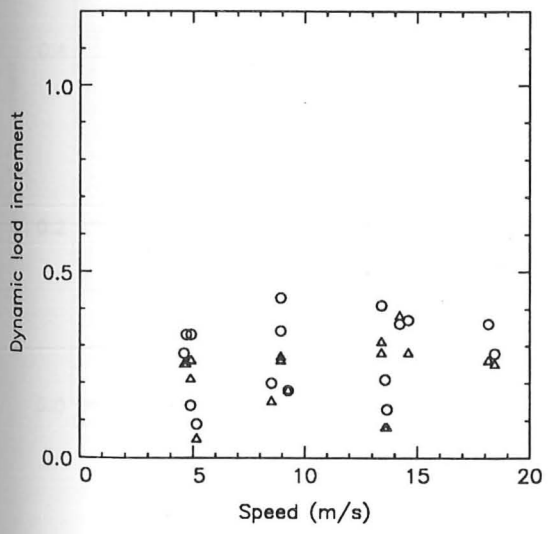

(c) Front trailer axle

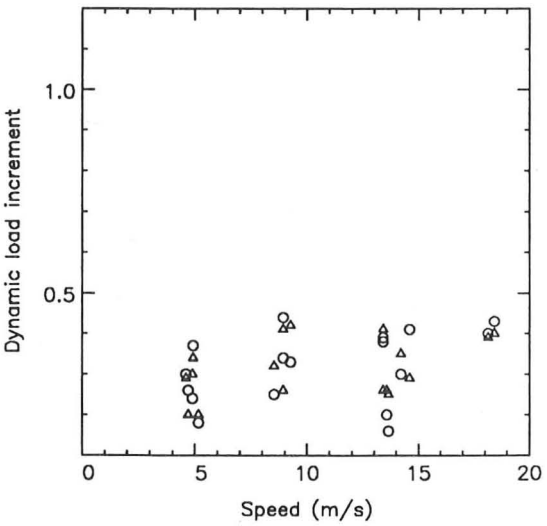

(d) Rear trailer axle

Figure 4.5: Lower Earley bridge - Maximum dynamic load increments
Vehicle suspensions: air-springs on tractor, leaf-springs on trailer
Curbside wheel o Centre-line wheel △

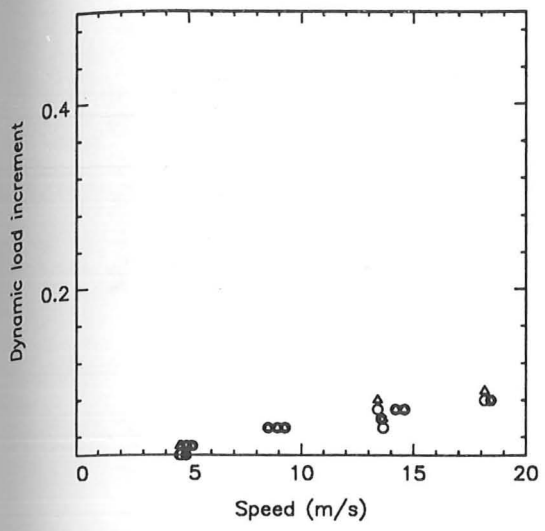

(a) Steer axle

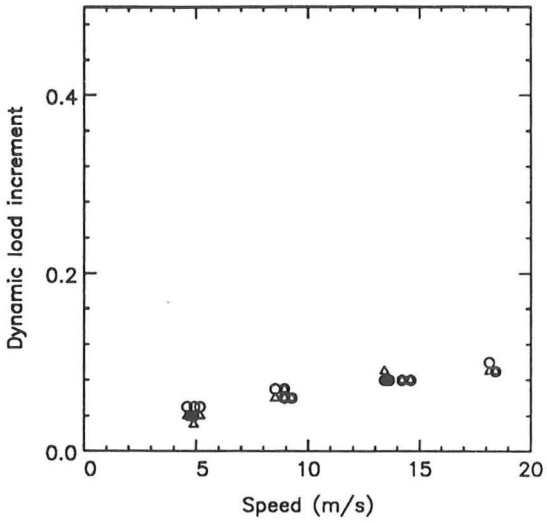

(b) Drive axle

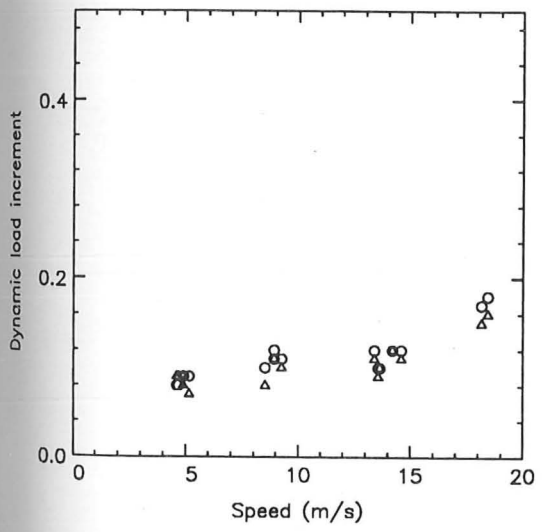

(c) Front trailer axle

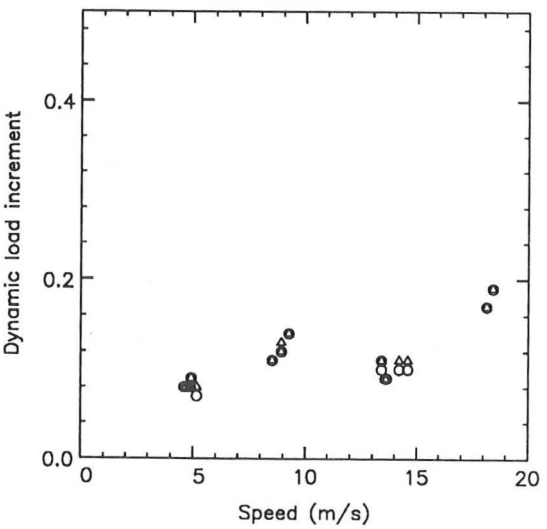

(d) Rear trailer axle

Figure 4.6: Lower Earley bridge
Standard deviation of dynamic load increments
Vehicle suspensions: air-springs on tractor, leaf-springs on trailer
Curbside wheel o Centre-line wheel △

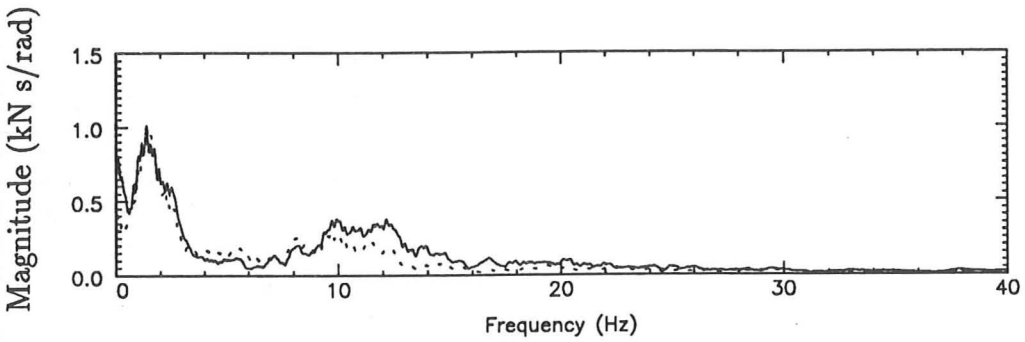

(a) Steer axle

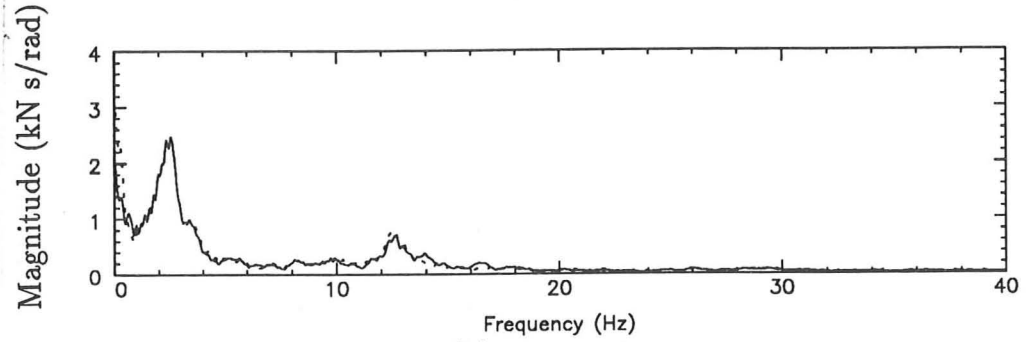

(b) Drive axle

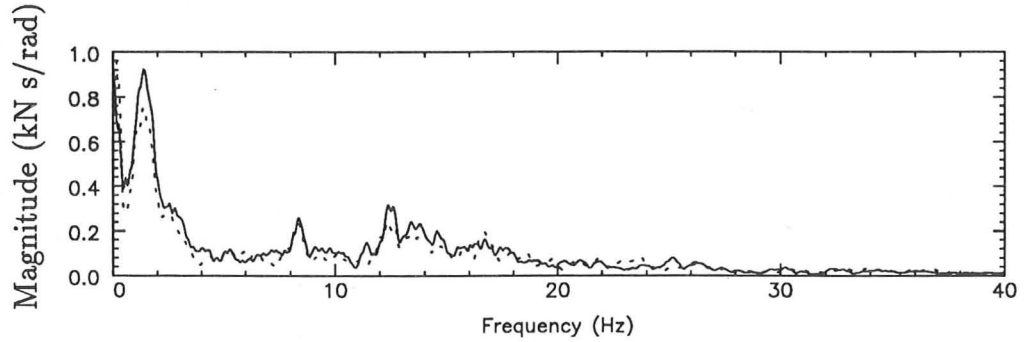

(c) Front trailer axle

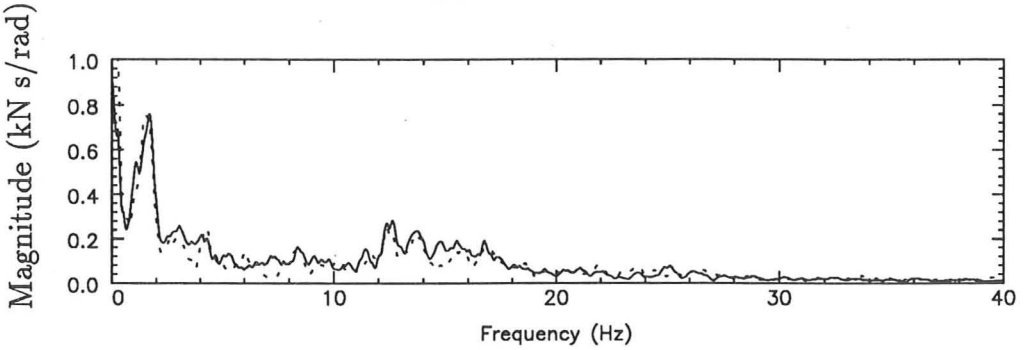

(d) Rear trailer axle

Figure 4.7: Drift Road bridge - Fourier spectra of tyre forces
Direction: South-east to north-west, Speed: 50 km/h
Vehicle suspensions: leaf-springs on tractor, air-springs on trailer
Curbside wheel _____
Centre-line wheel . . . . . .

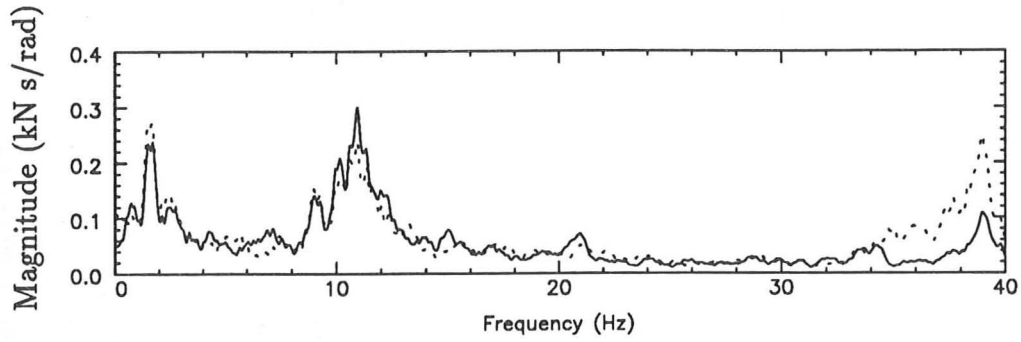

(a) Steer axle

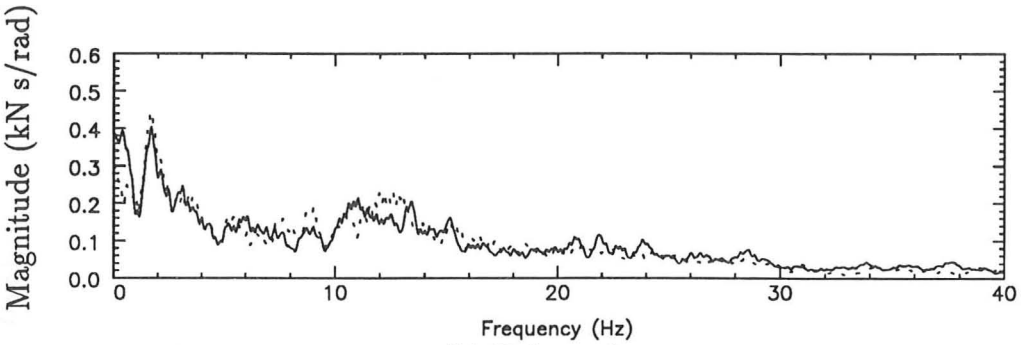

(b) Drive axle

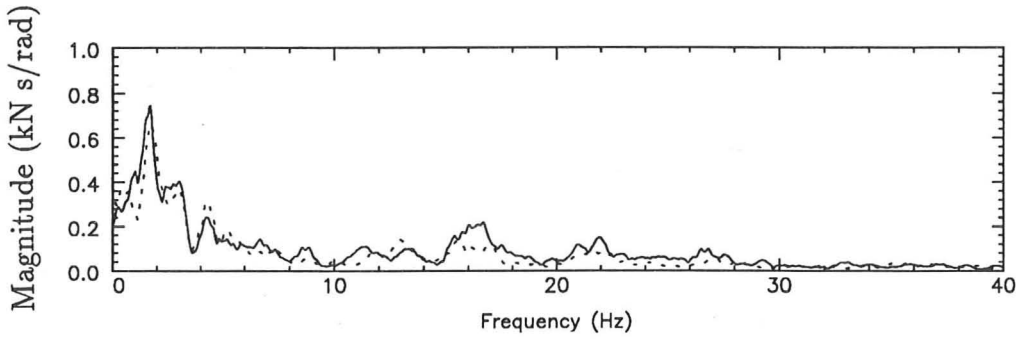

(c) Front trailer axle

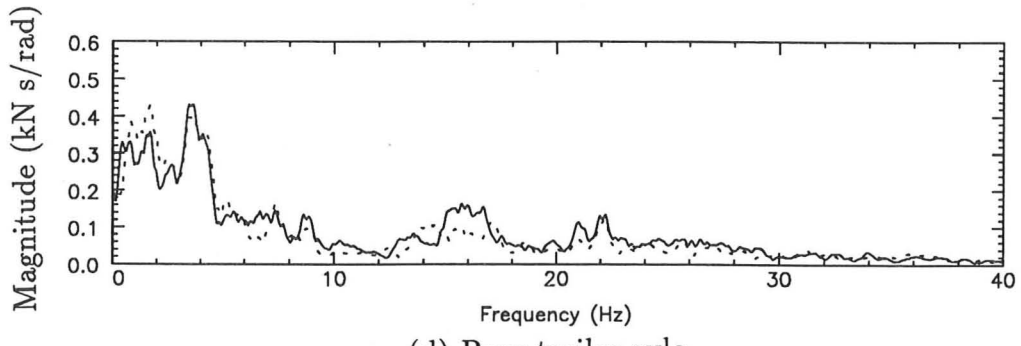

(d) Rear trailer axle

Figure 4.8: Lower Earley bridge - Fourier spectra of tyre forces
Vehicle suspensions: air-springs on tractor, leaf-springs on trailer
Curbside wheel ————
Centre-line wheel - - - - - - - - -

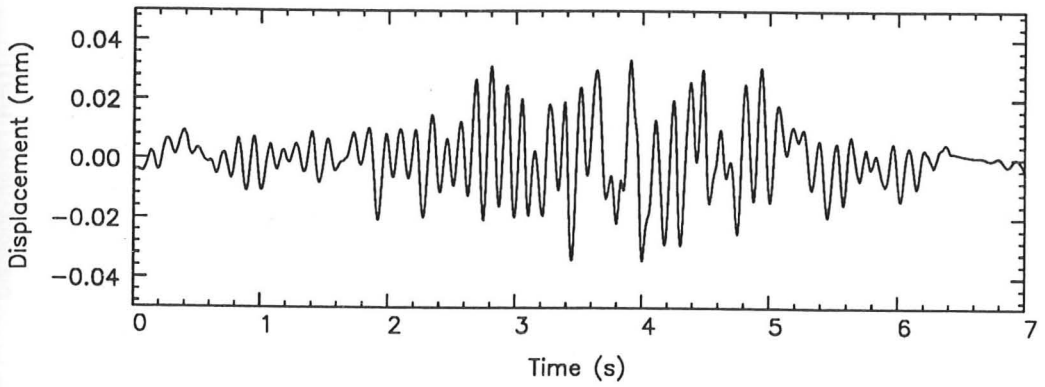

(a) Measurement position 1 (midspan)

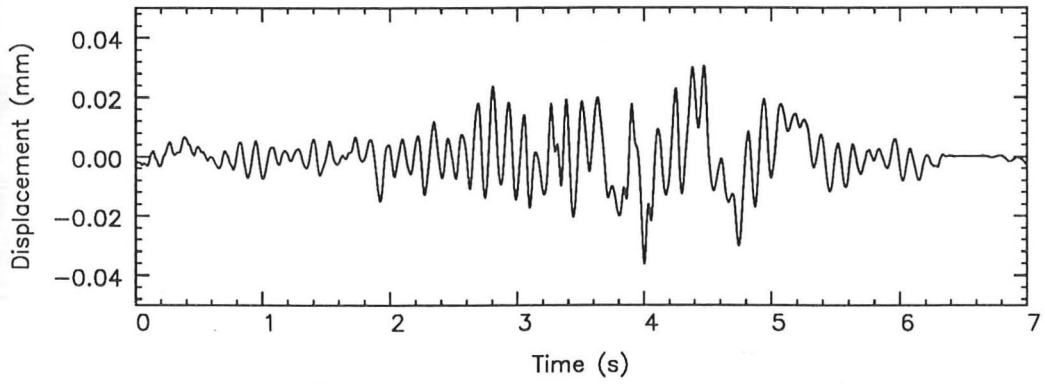

(b) Measurement position 3 (1/4 span)

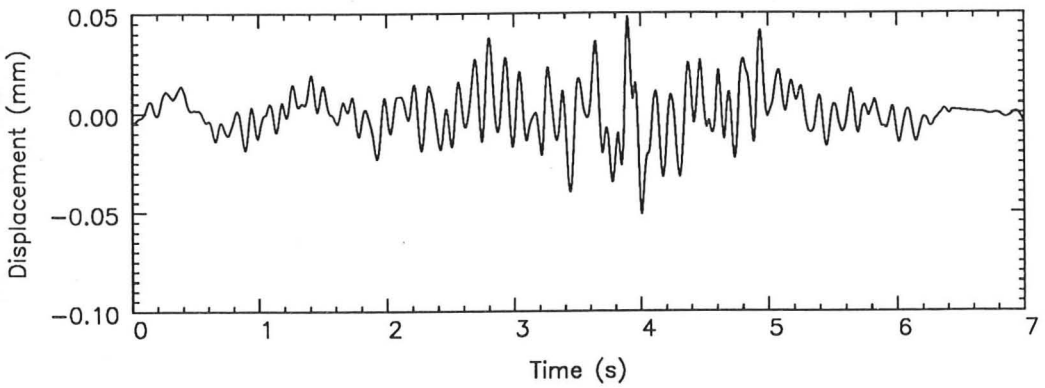

(c) Measurement position 4 (midspan, offset)

Figure 4.9: Drift Road bridge - Measured bridge responses
Direction: South-east to north-west, Speed: 50 km/h
Vehicle enters the bridge at time zero.

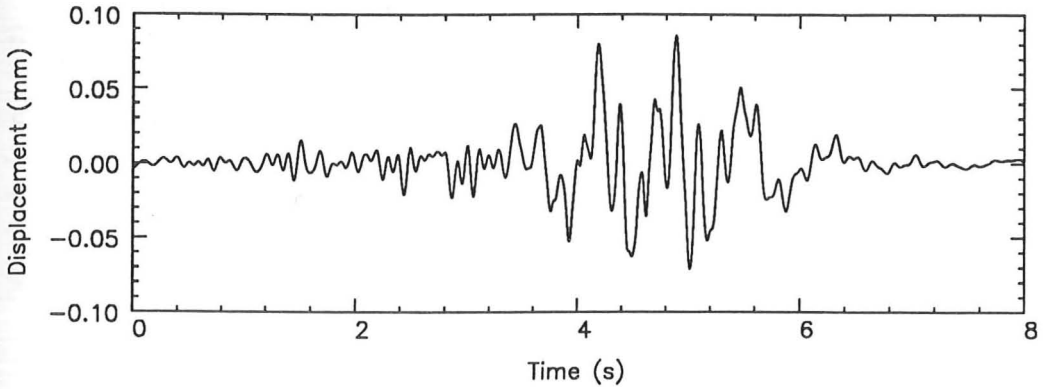

(a) Measurement position 1 (midspan)

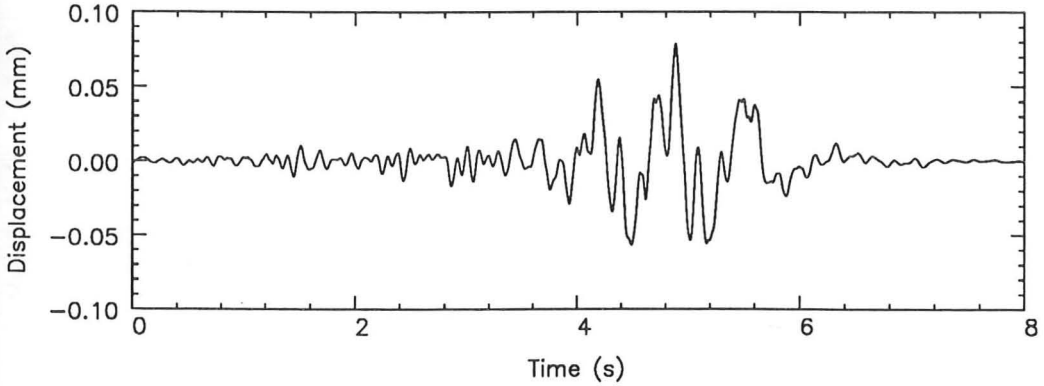

(b) Measurement position 3 (1/4 span)

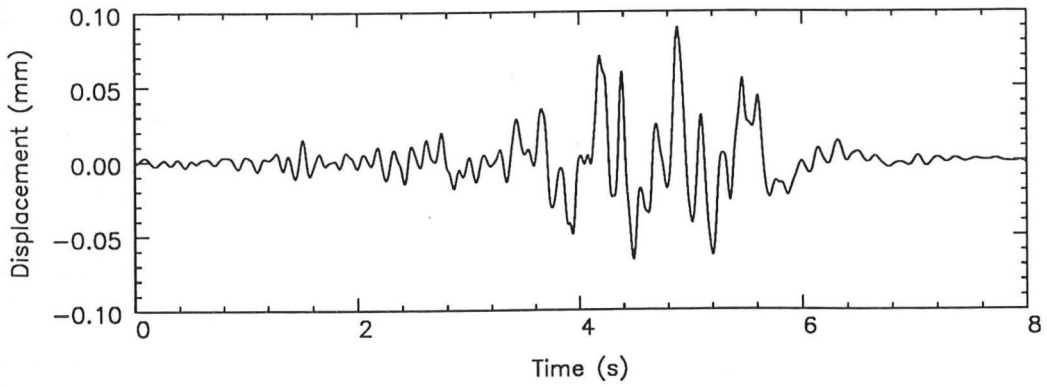

(c) Measurement position 4 (midspan, offset)

Figure 4.10: Lower Earley bridge - Measured bridge responses
Direction: South to north, Speed: 65 km/h
Vehicle enters the bridge at time zero.

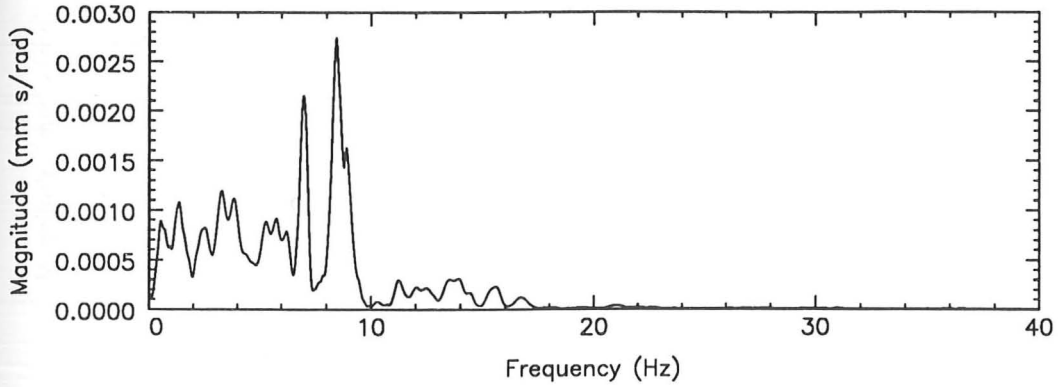

(a) Measurement position 1 (midspan)

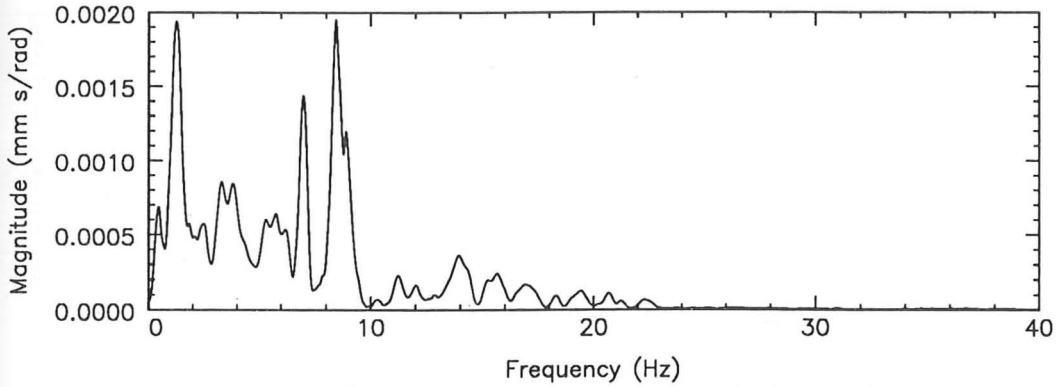

(b) Measurement position 3 (1/4 span)

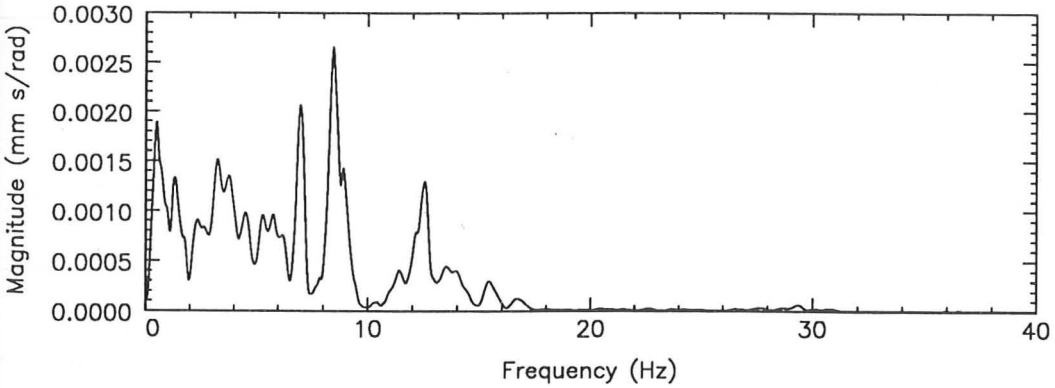

(c) Measurement position 4 (midspan, offset)

Figure 4.11: Drift Road bridge - Fourier spectra of bridge responses
Direction: South-east to north-west, Speed: 50 km/h

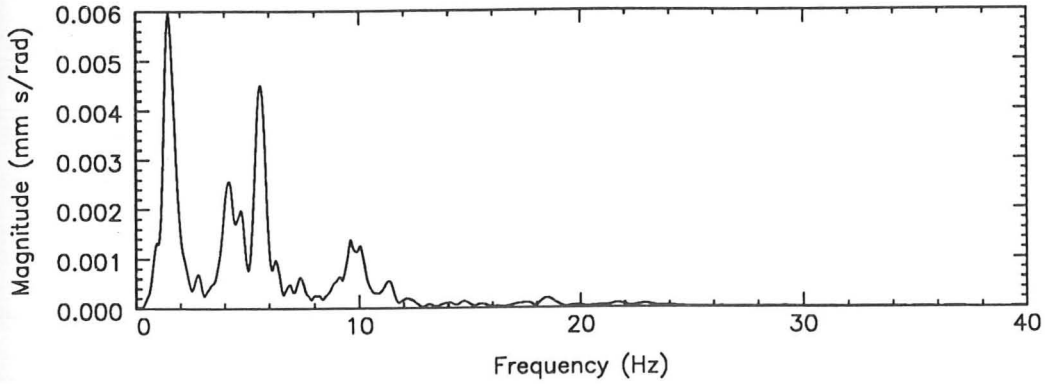

(a) Measurement position 1 (midspan)

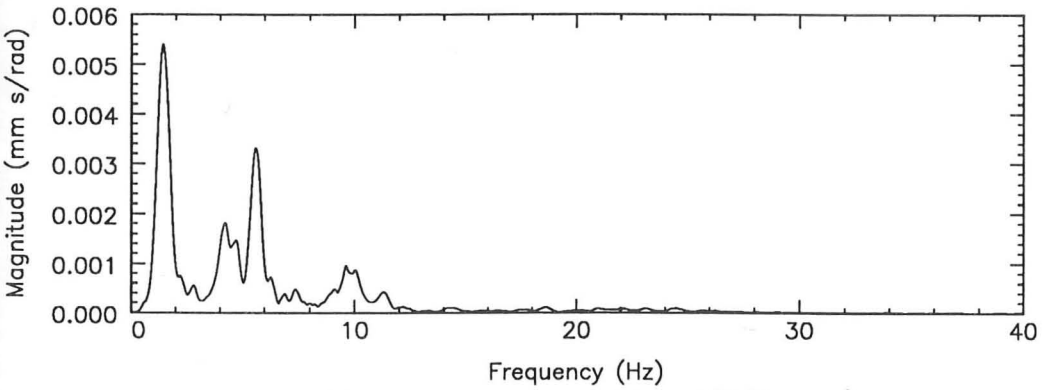

(b) Measurement position 3 (1/4 span)

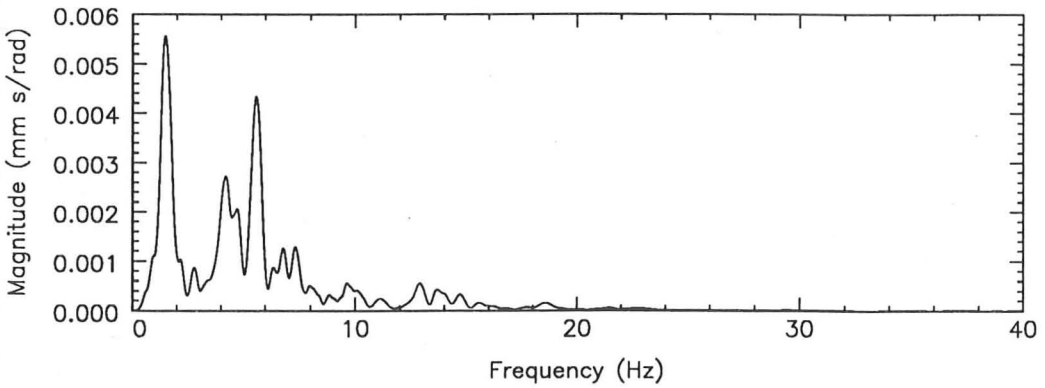

(c) Measurement position 4 (midspan, offset)

Figure 4.12: Lower Earley bridge - Fourier spectra of bridge responses
Direction: South to north, Speed: 65 km/h

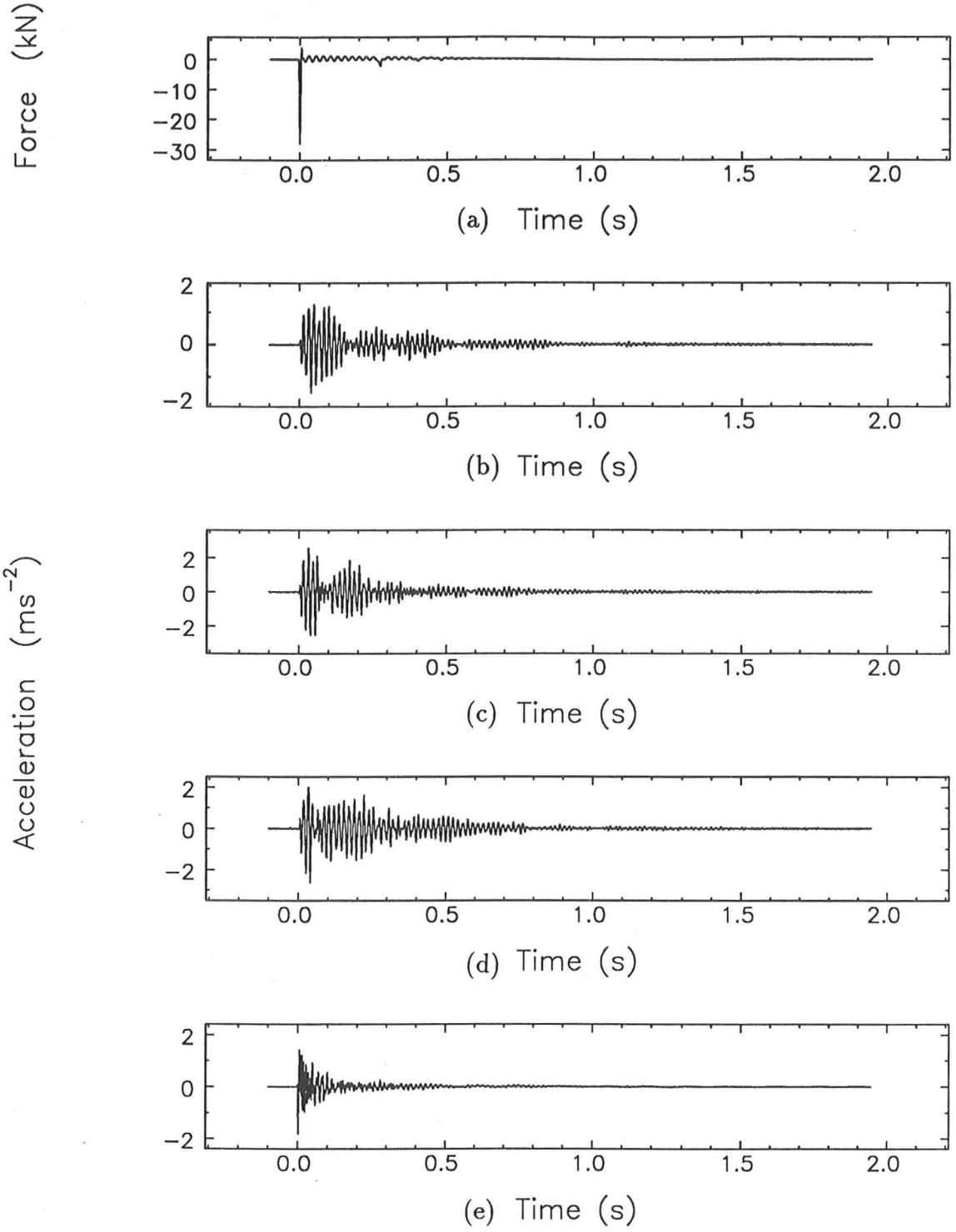

Figure 4.13: Drift Road bridge - Typical impulse responses (first tests)
Hammer at 1/4 point of instrumented span
(a) Hammer impulse
(b) Measurement position 1 (midspan)
(c) Measurement position 2 (1/3 span)
(d) Measurement position 3 (1/4 span)
(e) Measurement position 4 (midspan, offset)

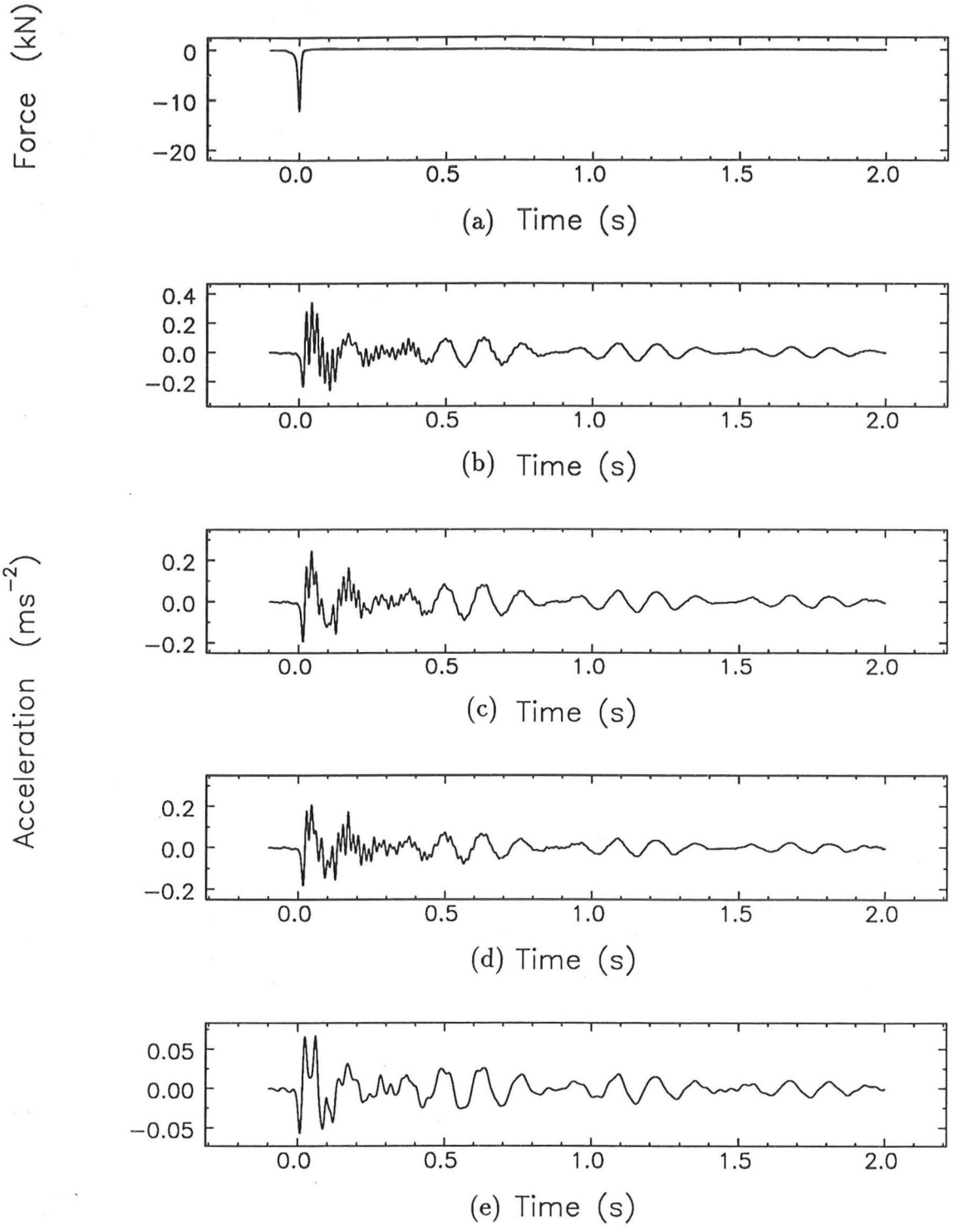

Figure 4.14: Drift Road bridge - Typical impulse responses (second tests)
Hammer at 1/4 point of instrumented span
(a) Hammer impulse
(b) Measurement position 1 (midspan)
(c) Measurement position 2 (1/3 span)
(d) Measurement position 3 (1/4 span)
(e) Measurement position 4 (midspan, offset)

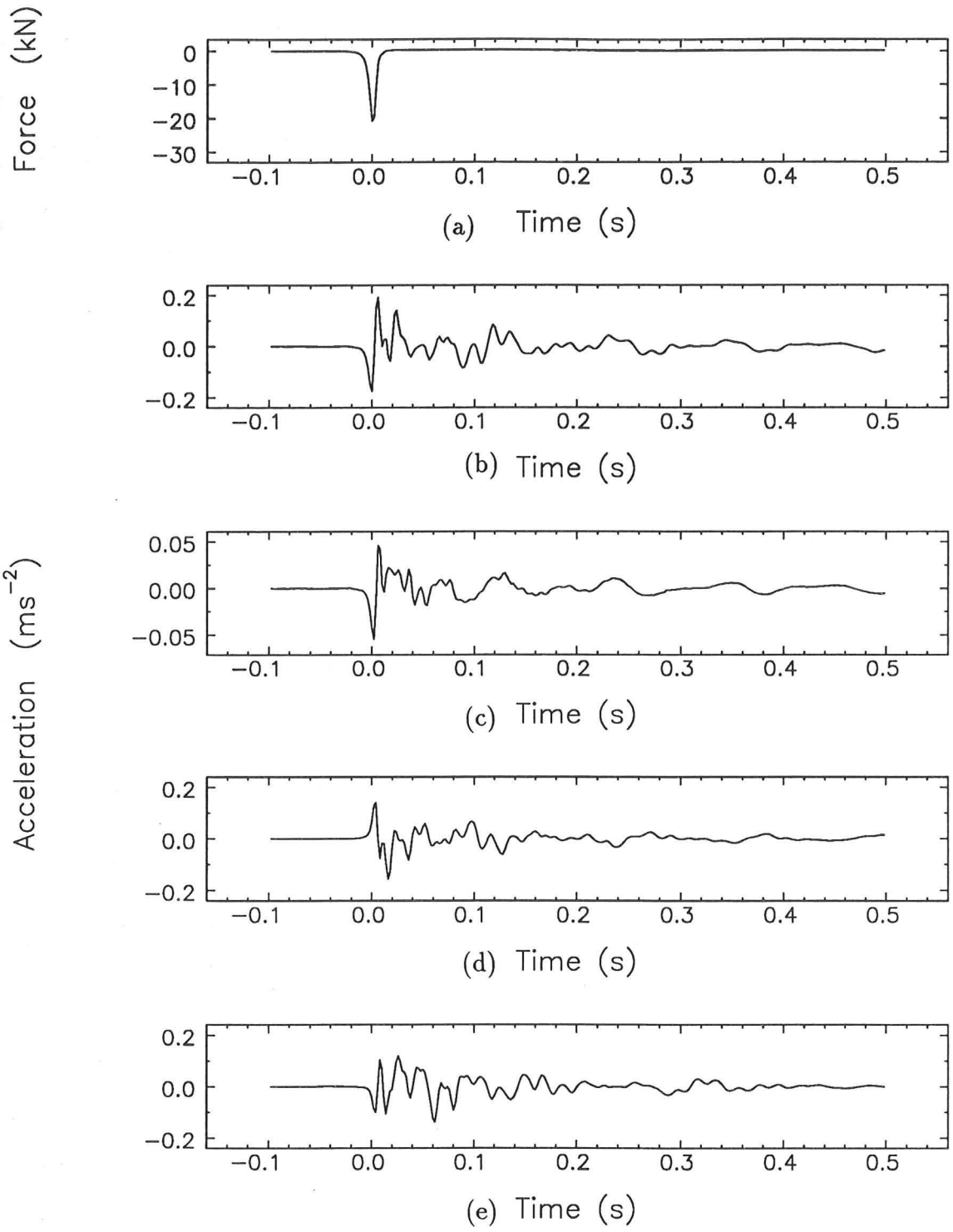

Figure 4.15: Lower Earley bridge - Typical impulse responses
Hammer at middle of instrumented span
(a) Hammer impulse
(b) Measurement position 1 (midspan)
(c) Measurement position 2 (1/3 span)
(d) Measurement position 3 (1/4 span)
(e) Measurement position 4 (midspan, offset)

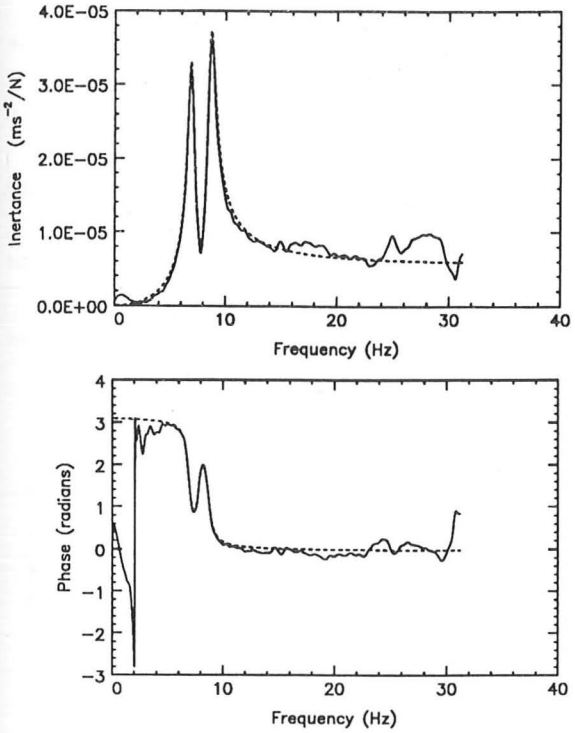

(a) Measurement position 1 (midspan)

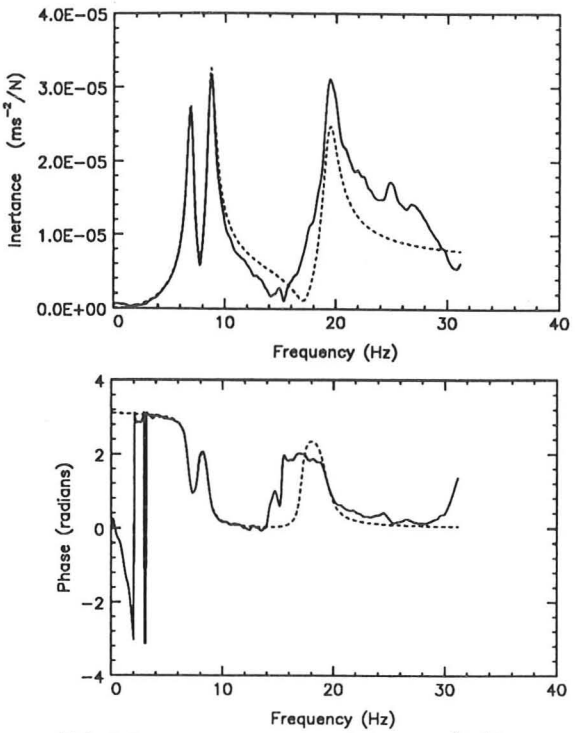

(b) Measurement position 2 (1/3 span)

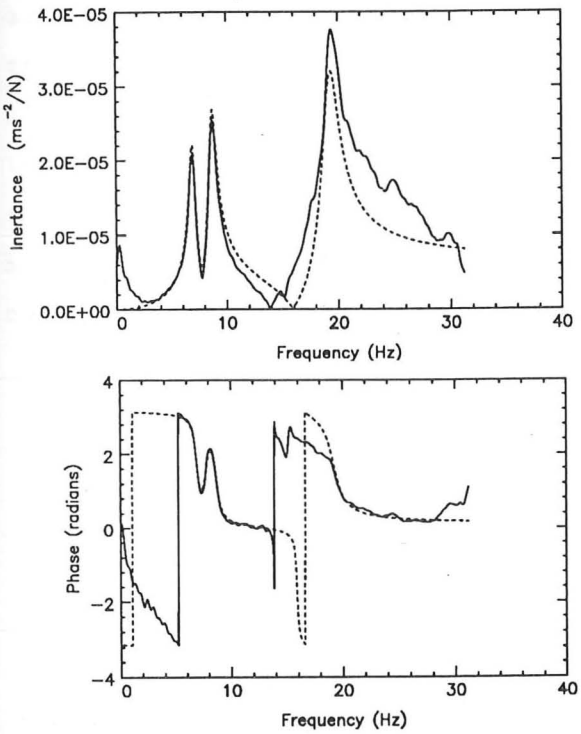

(c) Measurement position 3 (1/4 span)

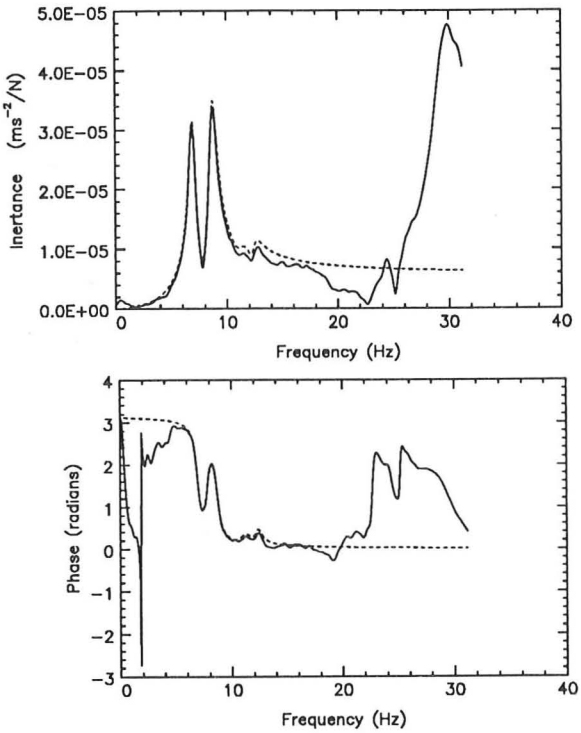

(d) Measurement position 4 (midspan, offset)

Figure 4.16: Drift Road bridge - Typical transfer functions
Hammer at 1/4 point of instrumented span
Measured _____ Regenerated ----------

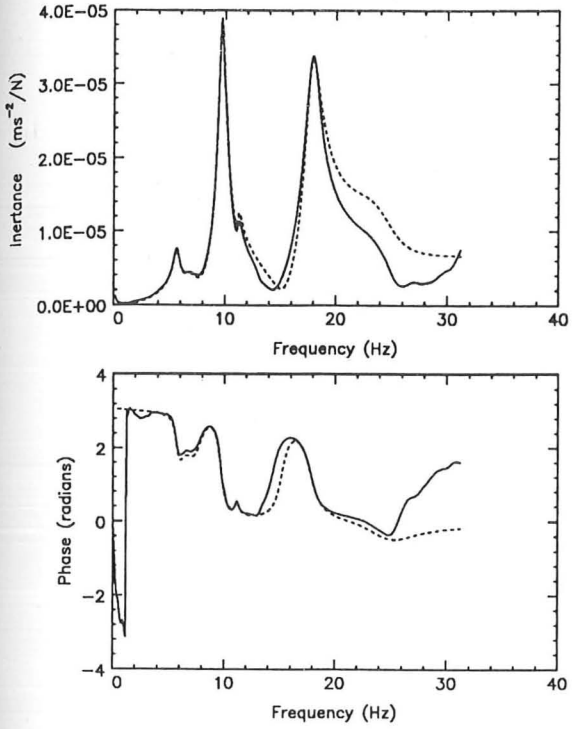

(a) Measurement position 1 (midspan)

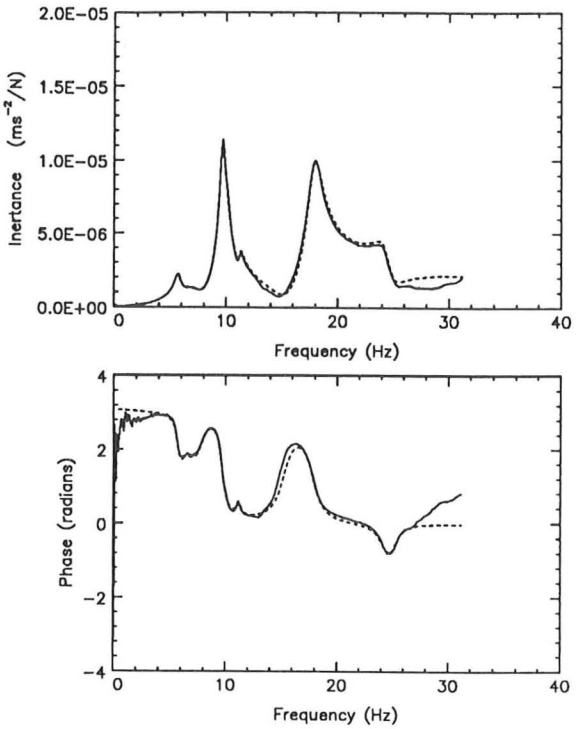

(b) Measurement position 2 (1/3 span)

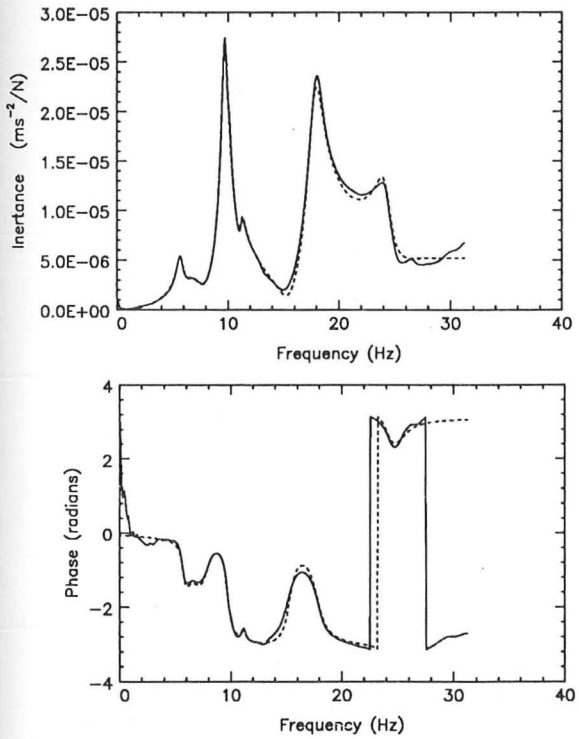

(c) Measurement position 3 (1/4 span)

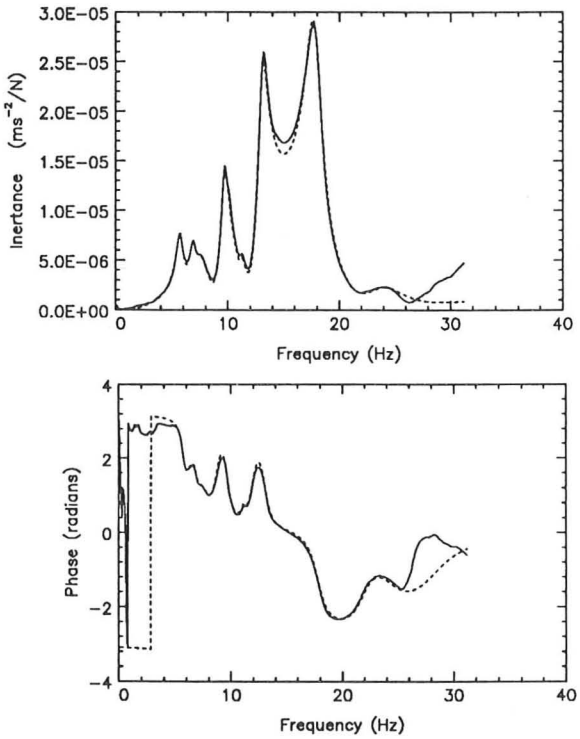

(d) Measurement position 4 (midspan, offset)

Figure 4.17: Lower Earley bridge - Typical transfer functions
Hammer at middle of instrumented span
Measured _____ Regenerated ----------

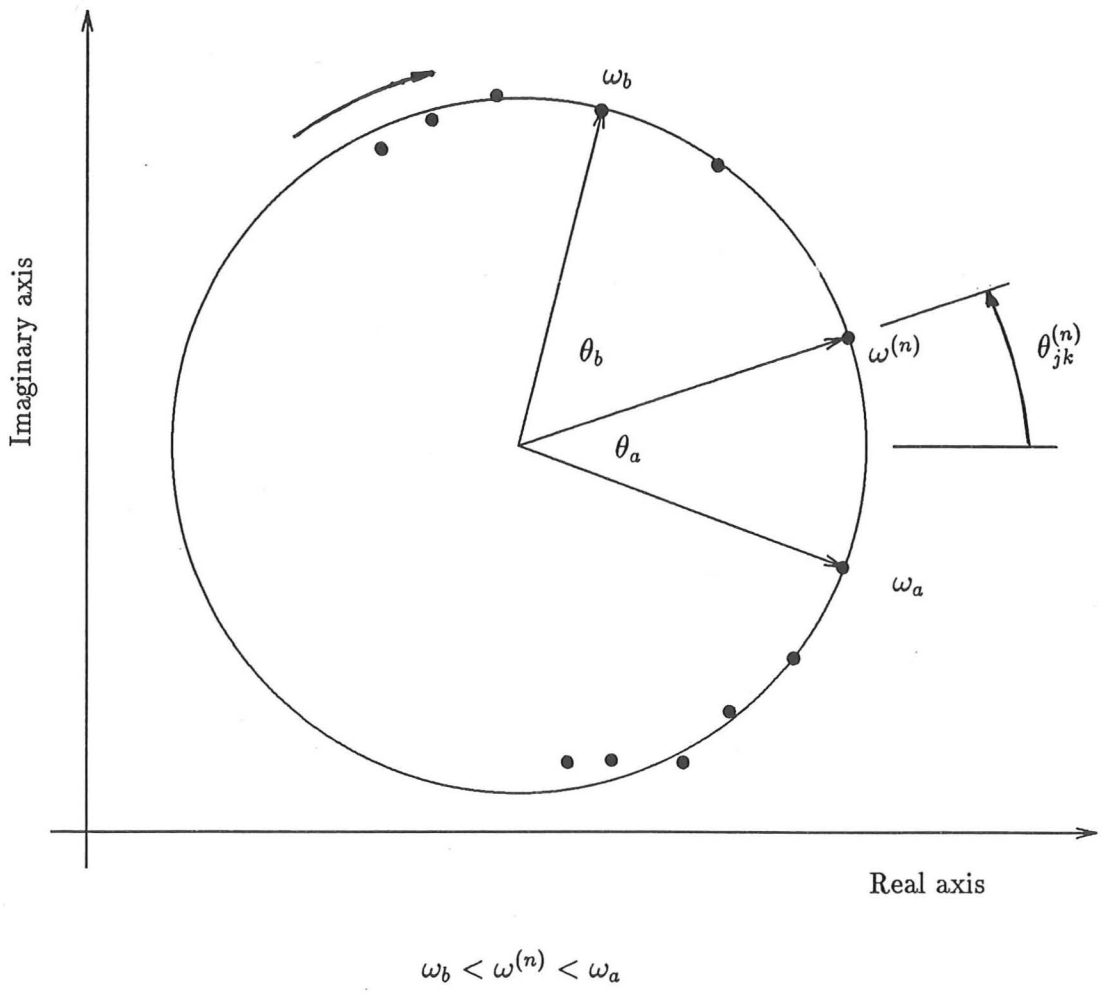

Figure 4.18: Circle fitting procedure for modal analysis

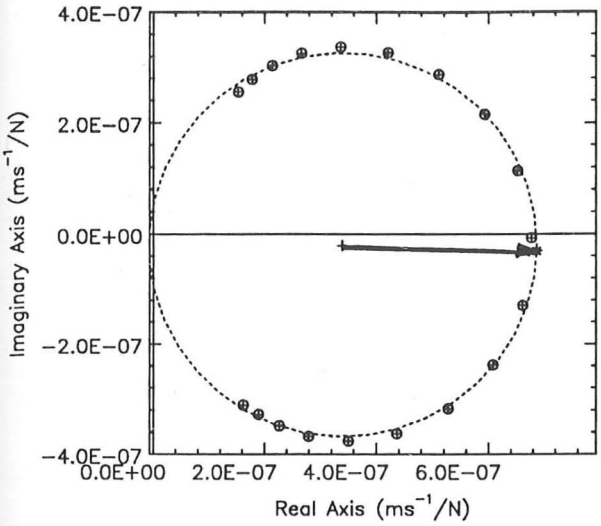

(a) Mode 1 : f_m = 6.8 Hz

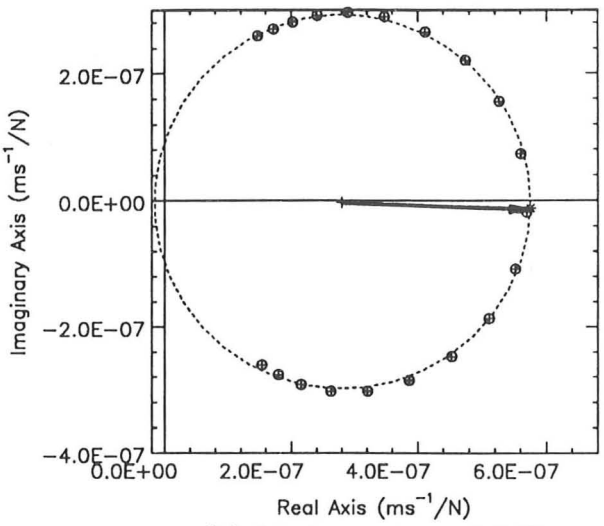

(b) Mode 2 : f_m = 8.6 Hz

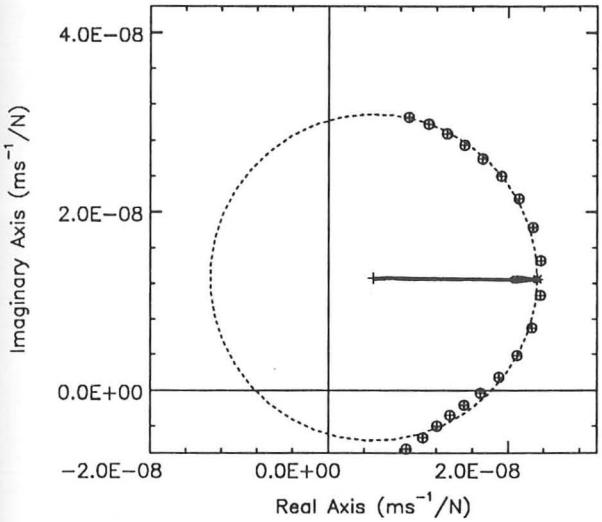

(c) Mode 3 : f_m = 11.2 Hz

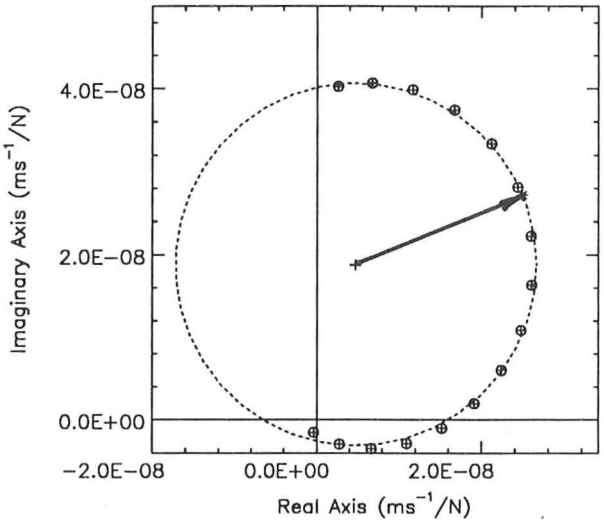

(d) Mode 4 : f_m = 12.3 Hz

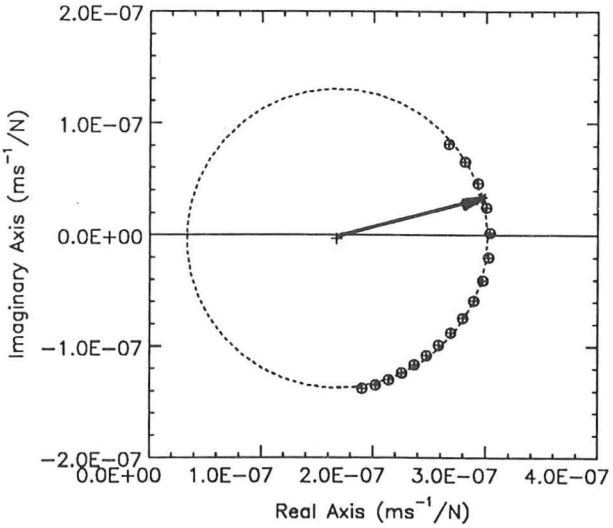

(e) Mode 5 : f_m = 19.3 Hz

Figure 4.19: Drift Road bridge - Typical circle fits
Hammer at quarter point of instrumented span
Radial lines indicate the estimated positions of the natural frequencies

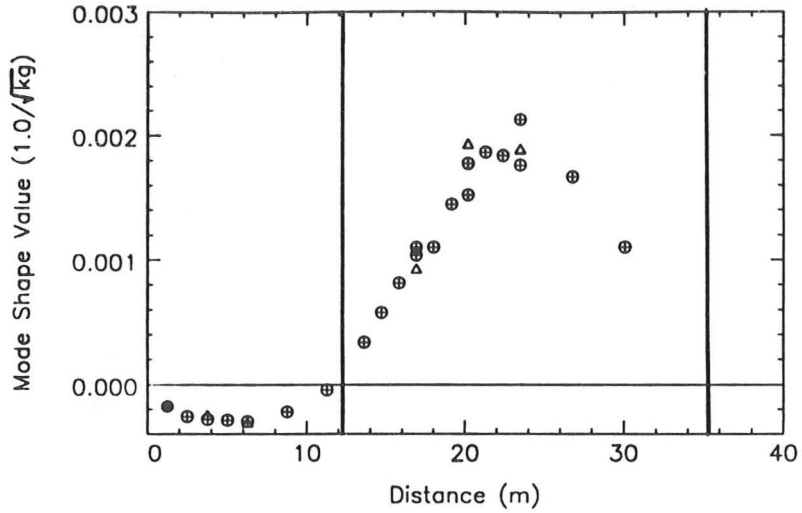

(a) Mode 1 : $f_m = 6.8$ Hz

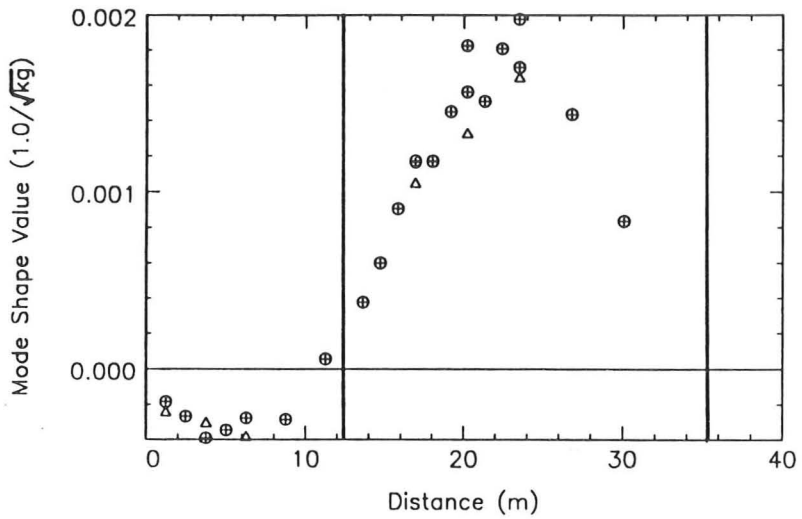

(b) Mode 2 : $f_m = 8.6$ Hz

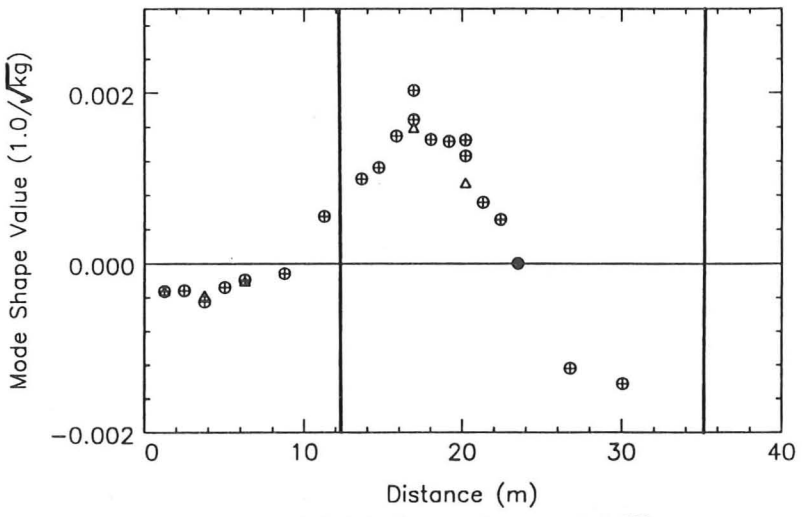

(c) Mode 5 : $f_m = 19.3$ Hz

Figure 4.20: Drift Road bridge - First three flexural mode shapes
Vertical lines indicate the column positions
Centre-line wheel track ⊕
Curbside wheel track △

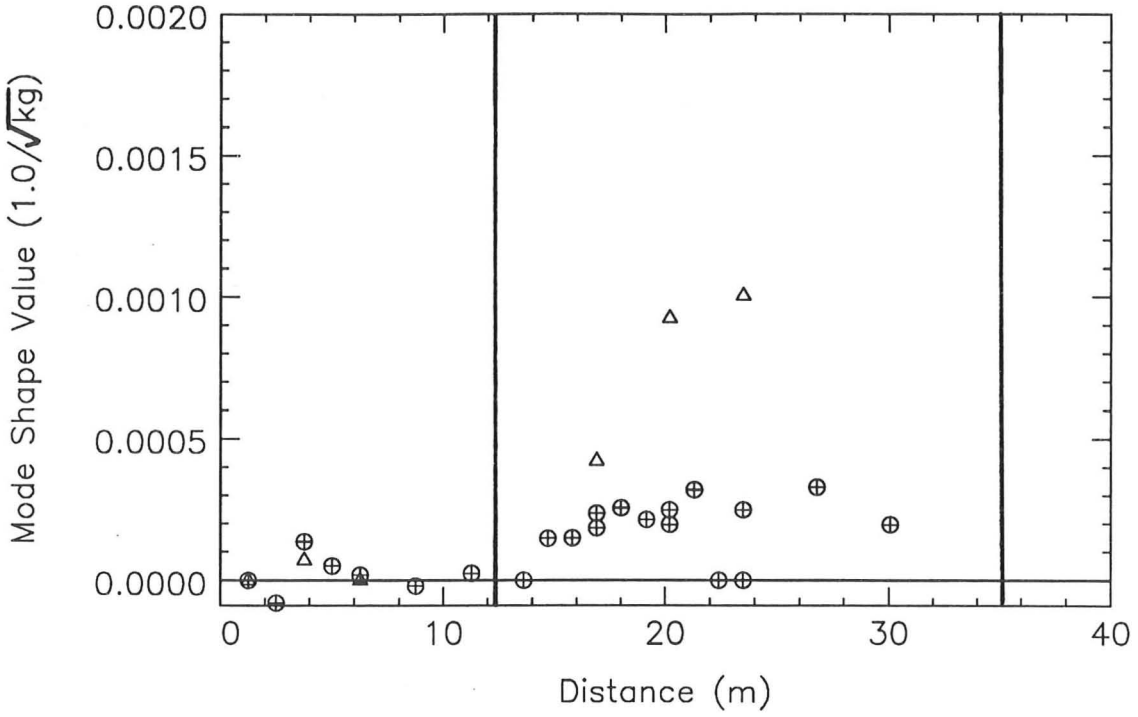

(a) Mode 3 : $f_m = 11.2$ Hz

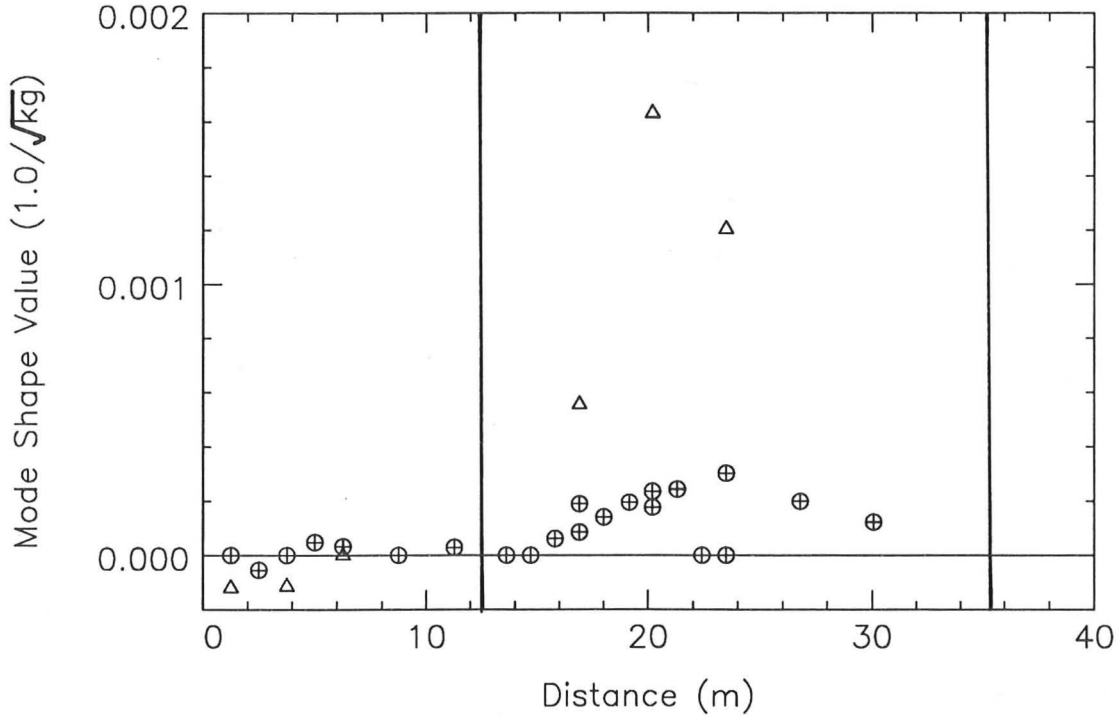

(b) Mode 4 : $f_m = 12.3$ Hz

Figure 4.21: Drift Road bridge - First two torsional mode shapes
Vertical lines indicate the column positions
Centre-line wheel track ⊕
Curbside wheel track △

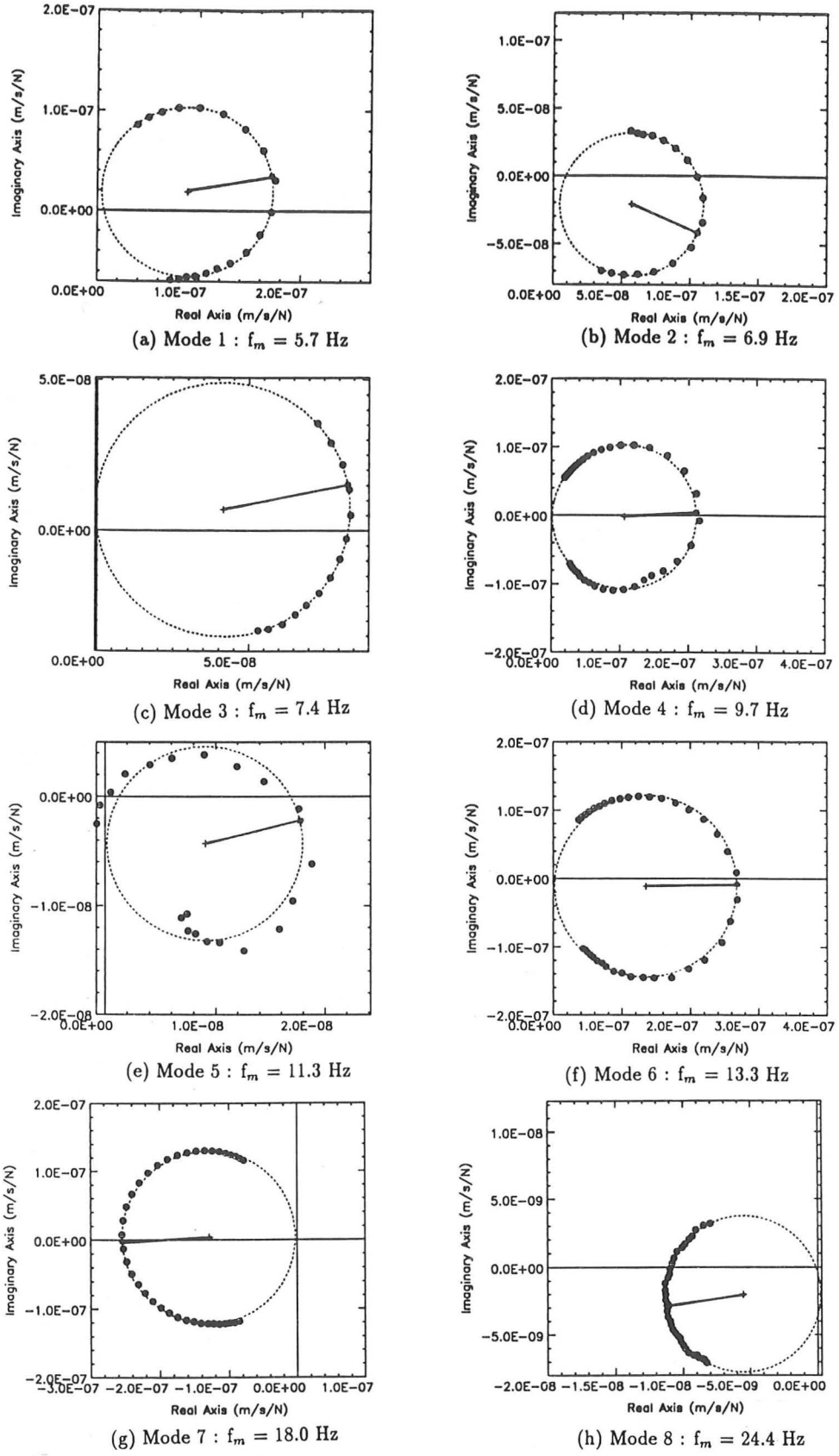

(a) Mode 1 : f_m = 5.7 Hz

(b) Mode 2 : f_m = 6.9 Hz

(c) Mode 3 : f_m = 7.4 Hz

(d) Mode 4 : f_m = 9.7 Hz

(e) Mode 5 : f_m = 11.3 Hz

(f) Mode 6 : f_m = 13.3 Hz

(g) Mode 7 : f_m = 18.0 Hz

(h) Mode 8 : f_m = 24.4 Hz

Figure 4.22: Lower Earley bridge - Typical circle fits
Hammer at middle of instrumented span
Radial lines indicate the estimated positions of the natural frequencies

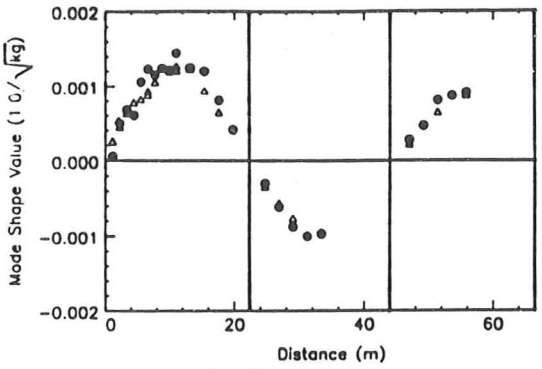

(a) Mode 1 : f_m = 5.7 Hz

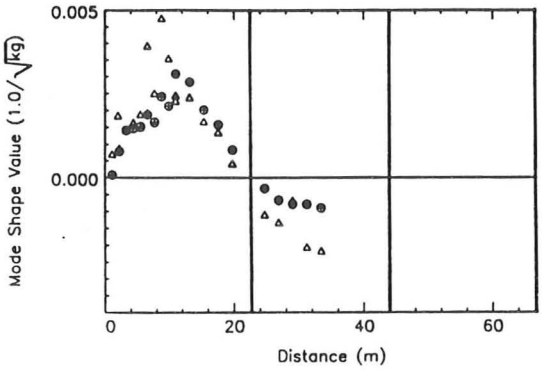

(b) Mode 2 : f_m = 6.9 Hz

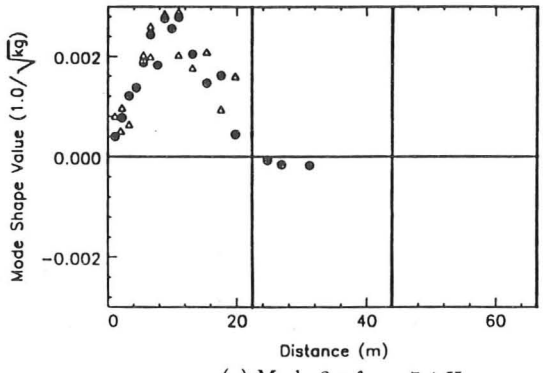

(c) Mode 3 : f_m = 7.4 Hz

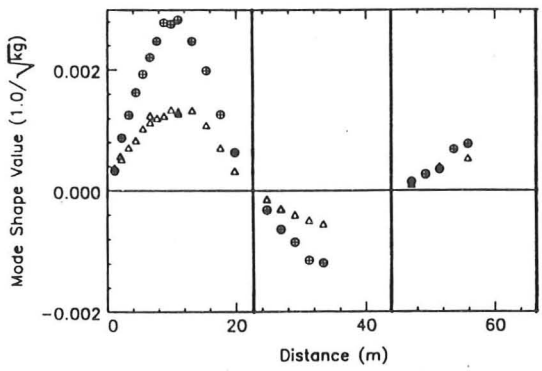

(d) Mode 4 : f_m = 9.7 Hz

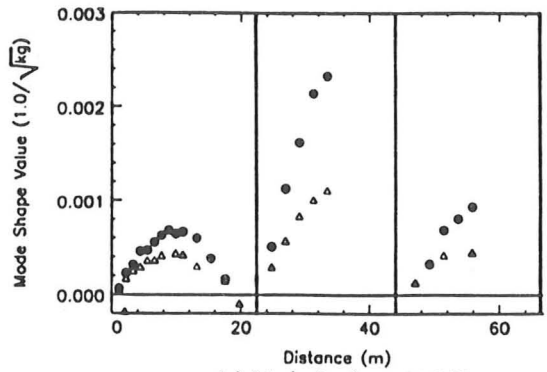

(e) Mode 5 : f_m = 11.3 Hz

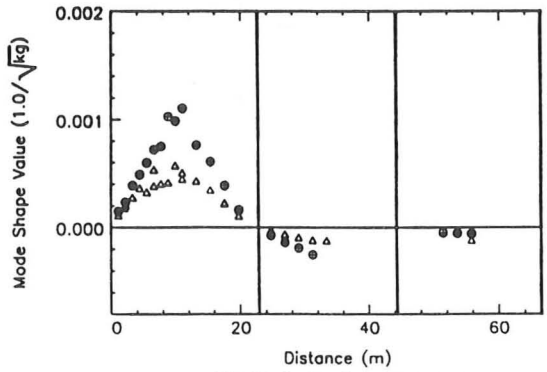

(f) Mode 6 : f_m = 13.3 Hz

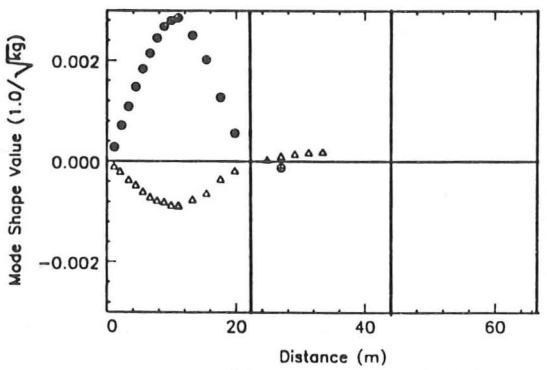

(g) Mode 7 : f_m = 18.0 Hz

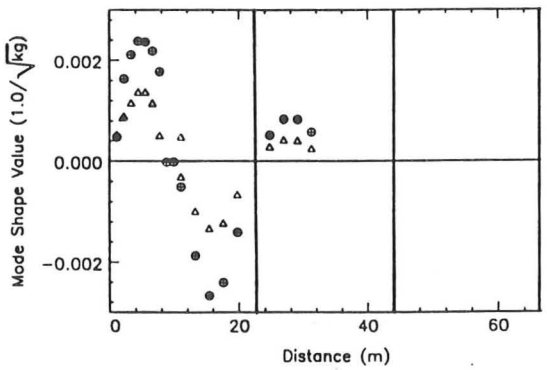

(h) Mode 8 : f_m = 24.4 Hz

Figure 4.23: Lower Earley bridge - Measured mode shapes
Vertical lines indicate the column positions
Centre-line wheel track ⊕
Curbside wheel track △

5 VALIDATION OF THEORY

The final stage of the experimental validation is comparison of the measured results with theoretical predictions. This chapter will conduct that comparison to validate the convolution method presented in chapter 2.

Mode shapes predicted by analytical and finite element models of the two test bridges are compared with the measured mode shapes. The validation of the vehicle-induced bridge response calculation method is presented in section 5.2.

5.1 Prediction and Comparison of Modal Parameters

Two different theoretical models were used to predict the vibrational behaviour of the test bridges. They were modelled as beams on rigid supports, and more accurately using finite elements to include flexible supports and plate action.

The mass and stiffness properties were obtained from the construction drawings, supplied by the Berkshire County Council. Because both bridges were constructed of prestressed concrete, it was assumed that the concrete was always in compression. Therefore the calculated stiffness properties relate to the gross section instead of an equivalent cracked section. The Young's modulus of concrete was estimated from

values suggested in British Standard 5400 [10].

Table 5.1 contains the estimates of the mass, stiffness, and strength parameters for both bridges. Small variations of cross-sectional properties along the length of the bridges were not deemed important as it has been shown that these variations do not significantly affect the vibrational characteristics of bridges [28].

5.1.1 Beam Model

The differential equation for transverse vibrations of an undamped Euler-Bernoulli beam of uniform cross-section is

$$m\frac{\partial^2 y}{\partial t^2}(x,t) + EI\frac{\partial^4 y}{\partial x^4}(x,t) = 0 \tag{5.1}$$

where m is the mass per unit length,

E is the Young's modulus,

and I is the second moment of area of the cross-section.

Following the method outlined in chapter 2, the solution to equation 5.1 can be written in terms of the mode shapes, $\phi^{(n)}(x)$,

$$y(x,t) = \sum_{n=1}^{\infty} \phi^{(n)}(x) q_n(t) \tag{5.2}$$

where n is the mode number,

and $q_n(t)$ are the normal coordinates.

Substituting equation 5.2 into equation 5.1 and separating variables results in the following modal differential equation

$$\frac{d^4\phi^{(n)}}{dx^4} - k_n^4 \phi^{(n)} = 0 \tag{5.3}$$

which has solutions of the form

$$\phi^{(n)}(x) = C_1^{(n)} \cos(k_n x) + C_2^{(n)} \cosh(k_n x) + C_3^{(n)} \sin(k_n x) + C_4^{(n)} \sinh(k_n x) \tag{5.4}$$

where $C_1^{(n)}$, $C_2^{(n)}$, $C_3^{(n)}$, $C_4^{(n)}$, and k_n are constants dependent upon the boundary conditions. Once these constants are determined, the natural frequencies can be calculated from

$$\omega^{(n)} = k_n^2 \sqrt{\frac{EI}{m}}. \tag{5.5}$$

5.1.2 Drift Road Bridge

Figure 5.1 illustrates a beam idealization of the Drift Road bridge. The ends of the bridge were restrained by the run-up slab (see figure 3.18) and this was modelled by assuming fixed ends. The bridge is symmetric about the centre support and can be analysed by considering half of the bridge with two different centre support conditions: one simply supported (to model the asymmetric modes), and the other fully restrained (to model the symmetric modes). At all of the supports, bridge displacement was assumed to be zero. For fixed ends the additional constraint was zero slope while for the simple support the bending moment was assumed to be zero. At the intermediate support, the slopes and bending moments are assumed to be continuous.

The first three natural frequencies were computed and compared with the experimental measurements (table 5.2). Reasonable agreement was achieved, but the beam theory predicted the first two natural frequencies to be farther apart than the measured values. This was not surprising since the beam analysis took no account of the effects of the centre column which was constructed as an integral part of the bridge superstructure.

Figure 5.2 shows the first three flexural modes. The experimental data is plotted for comparison. All of the modes were mass normalized by applying the orthogonality relationships of section 2.2.1 for consistency. The mode shapes correlate well with experiment, especially the measurements on the longer span. These results are more accurate because the largest amplitude vibrations are expected to occur on the longer span. Therefore, the impulse responses measured on the longer span have a higher signal to noise ratio, and should be more accurate. There are larger

discrepancies evident on the shorter span and particularly so with the third mode. These errors occur because of the difficulty in obtaining accurate measurements on the shorter span.

A simple estimation for the torsional vibrations was obtained by considering the bridge as a bar with two perpendicular axes of symmetry. For torsional response, $\psi(x,t)$, is defined as the angle of rotation about the centroidal axis of the bridge. The relevant differential equation is :

$$\rho I_p \frac{\partial^2 \psi}{\partial t^2}(x,t) = GJ \frac{\partial^2 \psi}{\partial x^2}(x,t) \tag{5.6}$$

where G is the shear modulus of elasticity,

ρ is the mass density,

I_p is polar moment of area of the cross section,

and J is the torsional constant of the cross section.

A modal expansion (equation 5.2) was assumed, resulting in the following modal differential equation

$$\frac{d^2\phi^{(n)}}{dx^2} + k_n^2 \phi^{(n)} = 0 \tag{5.7}$$

with the torsional modes given by

$$\phi^{(n)}(x) = C_1^{(n)} cos(k_n x) + C_2^{(n)} sin(k_n x) \tag{5.8}$$

Because of symmetry, only half of the bridge was analysed. It was assumed that there was no rotation at the supports because the bridge was constructed with torsional stiffeners at each support and the columns themselves restrict rotation. With no rotation at the supports, the spans act independently and so only the longer span was considered because it has the lowest frequencies. Applying these assumptions to equation 5.8 results in C_1 becoming zero and the first two modes having the following form

$$\phi^{(1,2)}(x) = C_2 sin(\frac{\pi x}{L}) \tag{5.9}$$

where L is the length of the longer span. One mode is symmetric while the other is anti-symmetric but otherwise they are identical. All other torsional natural frequencies were found to be outside the frequency range of interest.

In figure 5.3 the torsional mode shapes are compared with the measured data by plotting the angle of torsional rotation. The comparison is reasonable although the predicted modes are slightly larger in amplitude than the measured values.

In order to improve on the accuracy of the beam analysis, a finite element model was developed. The bridge was divided into seven components: four spans and three columns. Each component was then discretized into twenty beam elements. The beam elements had torsional stiffness which allowed approximations of the torsional natural frequencies.

The natural frequencies computed by the finite element analysis are presented in table 5.2. There is some improvement in the accuracy which results from the inclusion of the columns in the finite element solution. In particular, the first and second flexural modes are slightly closer together. Errors in the estimation of the natural frequencies were caused by inadequate modelling of the support conditions at the abutments and errors in estimating the stiffness properties of the bridge. The finite element predictions of the flexural modes are contained in figure 5.2 while the torsional modes are compared with experiment in figure 5.3. The torsional modes are illustrated by plotting the angle of torsional rotation. The mode shapes obtained from the two different models are quite similar, although in the second flexural mode and the first torsional mode there is some movement at the centre support that is not modelled by the beam solutions. The finite element solution predicts that the symmetric torsional mode has the lower natural frequency.

5.1.3 Lower Earley Bridge

The Lower Earley bridge was initially modelled as a three span continuous beam on simple supports (figure 5.4). Because of symmetry, it was analysed by dividing the bridge at the middle of the centre span. The anti-symmetric modes were obtained

by considering a simple support at the free end of the beam, while a vertical roller support at the free end simulated the symmetric modes.

The four lowest natural frequencies were computed from the beam idealization and the results were compared with measurements (table 5.3). Figure 5.5 compares the results of the mode shape predictions with measurements. The agreement is good for the four predicted modes.

Since the beam theory did not predict all the measured modes and there was doubt as to whether or not the supports at the piers acted as simple supports, a finite element calculation was attempted. Figure 5.6a illustrates the support arrangements at the piers. The precast beams are supported on two sets of bearing pads and connected with a reinforced concrete diaphragm. In order to model these bearing pads, the first finite element model consisted of beam elements supported by two springs (figure 5.6b) with stiffness k_b (table 5.1) . The resultant mode shapes were identical to those obtained from simple beam theory. The natural frequencies are shown in table 5.3, but no significant improvement over the beam estimates was noticed.

A two-dimensional model was necessary to predict the other modes. The bridge was modelled as an orthotropic plate on flexible supports at the piers using four-noded quadrilateral plate elements. Figure 5.6b defines the direction of the x-axis to be parallel to the bridge centre-line. For the two-dimensional bridge model, the z-axis is perpendicular to the plane of the paper. Referring to figure 3.5 and noting that there is significant clearance between the bases of the inverted T-beams, it is apparent that the bridge had quite different bending stiffnesses in the x and z directions. In the orthotropic plate model, the bending stiffness in the x-direction was determined by considering both the slab and the beams, whereas the stiffness in the z-direction was determined from the slab alone. The x-y shear modulus and hence the torsional rigidity of the plate elements was corrected to account for the shape of the cross-section [102]. Each bridge span was divided into a 10x5 mesh with 10 elements in x-axis direction. Typical results from the plate analysis are presented in table 5.3 and figure 5.7 shows the first three predicted modes of vibration. From

an examination of these plate solutions (figure 5.7), it was evident that along any line in the x-axis direction the mode shapes had forms similar to those predicted by the beam model. On the basis of this finite element analysis, it was thought reasonable to assume that all of the first eight modes of the bridge had, longitudinally, one of the four simple beam mode shapes (figure 5.8). For each measured mode, it was fairly easy to choose a beam mode shape; the relative magnitudes along the centre-line and curbside tracks were calculated by least-squares fits with the measured magnitudes along these tracks. For measured mode number 4, it was not clear which beam mode best fit the data. As was mentioned in the data analysis chapter (section 4.3.5), there were two modes extremely close together that were not resolved by the modal analysis. For hammer tests on the instrumented span, the responses of the lower frequency mode dominated and so a smooth sinusoidal curve was fitted through these points to approximate the two modes by a single mode. The measurements on the other two spans were unreliable because the two modes were not always in phase and a single mode approximation was not deemed to be appropriate. Therefore, the measurements on the other two spans were neglected. The fit to mode number 4 does not correctly model the mode shape, but it will be shown to be a good engineering approximation for predicting the response of the bridge to heavy vehicle loads.

5.2 Comparison of Predicted and Measured Bridge Responses

In order to validate the bridge response calculation method, the measured modal parameters were combined with the dynamic wheel loads in the convolution integral of section 2.2.1. Using the frequency domain method of section 2.2.2 to evaluate the convolution integral, bridge responses for each passage of the test vehicle were predicted. These predicted responses were then compared with the measured responses to verify the calculation method.

The mode shapes used in the convolution procedure were those presented in figures 5.2, 5.3 and 5.8.

One difficulty in the comparison of measurement and theory was that it was difficult to measure the bridge response at low frequencies (see section 3.3.1). This meant that the quasi-static displacement of the bridge was not measured. Since

the predicted response includes the quasi-static bridge response, it was necessary to remove this effect before an effective comparison could be made. This was accomplished with the application of a high pass digital filter with a cut off frequency of 1.0Hz. The filter had attenuation properties similar to those of a eighth order Butterworth filter [39], and was designed in accordance with the recommendations of Stockham [85].

5.2.1 Drift Road Bridge

Typical validation results for the Drift Road bridge are presented in figures 5.9 to 5.11. The time scales on all the figures are adjusted so that the front axle of the vehicle enters the bridge at time zero.

For figure 5.9, the vehicle speed is 50km/h and the direction of travel is towards the north-west. The responses measured by accelerometers 1, 3, and 4 (see section 3.5.1) are shown. The response at position 3 (1/4 span) includes the effects of mode 5 while the two torsional modes are only present in the response at position 4 (midspan, offset). Because all three responses are similar, we deduce that the displacement response is dominated by the first two modes. There is favourable comparison, both in amplitude and form, between measurements and predictions. The traces are generally in phase with each other, but the predicted responses are consistently larger than the measured responses. The amplitude difference is particularly evident in the section of the record before 2.6 seconds. Between 2.6 seconds and 5.2 seconds the test vehicle was directly over the instrumented span and so it is not surprising that the best agreement occurs in this time interval. The amplitude differences are unlikely to be caused by inaccurate mode shapes because of the good agreement between measured and predicted mode shapes for the first two modes. A better explanation is that the out of phase modal responses do not cancel each other to the same degree in the predictions as in the measurements. These phasing errors could be caused by incorrect synchronising of the vehicle position with the bridge response due to slight speed variations or errors in the triggering signals.

Figure 5.10 illustrates the predicted and measured midspan displacement responses for a test run at 50km/h with the vehicle travelling in the opposite direction. Once again, the agreement is reasonable but the predicted response is still larger than the measurement. There are also some peaks in the early stages of the predicted response that are not present in the measured response. These peaks occur because the mode shape values were inaccurate on the first span of the bridge (figure 5.2).

Figure 5.11 illustrates the comparison between prediction and measurement in the frequency domain by plotting the Fourier spectrum of the responses. The agreement is satisfactory and the main differences are in amplitude. Most of the important frequencies are correctly predicted except for the first mode of the bridge at 6.8Hz. There is a single distinct peak on the measured response, but this is not reflected by the prediction.

Neither response is dominated by individual modes and there is no low frequency peak corresponding to the bounce frequency of the vehicle. Most of the bridge response is in the frequency region between 5 and 10Hz. A re-examination of the Fourier spectrum of the wheel loads (see figure 4.7) shows the vehicle wheel loads have little energy in this region. The magnitude of the dynamic response is therefore critically dependent on the accuracy of the dynamic wheel loads in a frequency region where they are difficult to measure precisely.

One important factor to bear in mind when interpreting the results for this bridge is that the original acceleration measurements were contaminated by noise. Aerodynamic excitation caused by heavy vehicles passing underneath the bridge resulted in significant ambient vibration of the bridge. Although most of this vibration was at relatively high frequencies, some of it was evident at frequencies below 20 Hz. This noise problem almost certainly contributes to the discrepancies between the predicted and measured responses.

Finally, some of the errors may be attributed to insufficient data from the modal analysis. In section 4.3.4, it was shown that the regenerated transfer functions differed from the measured ones in the frequency region above 10Hz. These errors

were caused by inaccurate measurement of the torsional modes and the third flexural mode, as well as the absence of high frequency modes. The modal analysis errors were relatively small, but their effects may be magnified by errors from phasing, wheel load estimation, and noise.

5.2.2 Lower Earley Bridge

The validation procedure was significantly more successful on the Lower Earley bridge. Typical results are presented in figures 5.12 to 5.14.

For figure 5.12, the vehicle is travelling north at 50km/h and the bridge response is shown for accelerometer positions 1, 3, and 4 (see figure 3.19). The agreement between prediction and experiment is excellent. The curves do not match well in the first two seconds, but during this time interval the vehicle is on the first span and has not reached the instrumented span. After the first two seconds, the predicted response exceeds the measured response at a few points, but otherwise the curves are very close for all three measurement positions. The largest discrepancies occur on the offset accelerometer (4), but most of the errors are in the initial two seconds. This indicates the modes exhibiting torsional behaviour do not cancel each other the way they should. More mode shapes are necessary to correctly model the response at this measurement position, but this would require additional field tests with more off-centre accelerometers.

Figure 5.13 presents a typical result with the vehicle travelling in the other direction (north to south). The speed is 65km/h and the response is shown at the midspan of the instrumented span. The agreement is excellent.

Fourier spectra of the predictions and measurements of figure 5.12 are shown in figure 5.14. As expected, the agreement between the two curves is excellent and all of the important features of the measured curves are represented in the predicted curves.

On the measured response there are two closely spaced peaks near 10Hz, but only one peak is predicted. This difference is the result of the approximation of the

two modes by one as mentioned in section 5.1.3. The two modes were represented by the approximation of figure 5.8. Since the predicted and measured curves match closely except for the fine detail of the double peak, the approximation is acceptable for predicting the bridge response to heavy vehicle loads.

In contrast to the Drift Road bridge (figure 5.11), figure 5.14 shows the Lower Earley bridge response to be dominated by a few distinct frequencies. The body bounce modes of the vehicle induce a large response at about 1.5Hz, while the bridge modes at 5.7Hz and near 10Hz are important. Examining the Fourier spectra of the vehicle wheel loads (see figure 4.8) reveals that the wheel loads have considerable energy near each of these peaks. The low frequency peak is evident for all axles, while the steer axle and rear trailer axles contribute significant amounts of energy near 10Hz and 4Hz respectively. The bridge responses are dominant in frequency regions where the wheel loads should be more accurate, and therefore we expect the predictions for this bridge to be better than those for the Drift Road bridge.

5.3 Conclusions

The results of the validation procedure were very good and indicate that the frequency domain convolution method is accurate for predicting the response of highway bridges to heavy vehicle loads.

Simple beam and plate models gave reasonable predictions of bridge vibration modes, however, it was not as easy to predict natural frequencies. No attempt was made to estimate damping values. The modes of vibration were best predicted on the Drift Road bridge because its box girder construction meant that it behaved like a beam. The composite slab and girder construction of the Lower Earley bridge presented more problems in modelling, but in the end, mode shapes similar to those from an equivalent beam approximation were shown to accurately represent the measured bridge response to a heavy vehicle.

The predicted and measured bridge responses from the passage of a heavy vehicle

compared well on both bridges. The agreement was better on the Lower Earley bridge than on the Drift Road bridge, but noise and other measurement problems on the latter account for most of the errors.

The convolution method presented in chapter two has been validated both by experiments and by comparisons with other theories for simple cases.

In the next chapter, the validated bridge response calculation method will be extended to include vehicle models and the importance of bridge-vehicle interaction will be investigated.

Table 5.1: Bridge model properties

	Drift Road	Lower Earley
E (GPa)	32.2	34.0
I (m^4)	0.78	1.82
m (tonne/m)	10.9	20.4
G (GPa)	13.4	14.2
J (m^4)	2.2	0.05
I_p (m^4)	38.62	-
k_b (N/m)	-	25.0 x 10^9
ρ (tonne/m^3)	2.4	2.4

Table 5.2: Drift Road bridge - Natural frequencies (Hz)

Mode	Type	Measured	Beam theory	Finite element
1	Flexural	6.8	6.5	6.9
2	Flexural	8.6	9.4	9.3
3	Torsional	11.2	12.8	11.5
4	Torsional	12.3	12.8	12.8
5	Flexural	19.3	20.8	21.2

Table 5.3: Lower Earley bridge - Natural frequencies (Hz)

Mode	Measured	Beam theory	Finite element	
			Beam	Plate
1	5.7	5.5	6.0	5.8
2	6.9	7.1	7.2	7.1
3	7.4	-	-	7.3
4	9.7	-	-	9.2
5	11.3	10.3	10.3	10.0
6	13.3	-	-	12.2
7	18.0	-	-	17.4
8	24.4	22.1	22.4	22.3

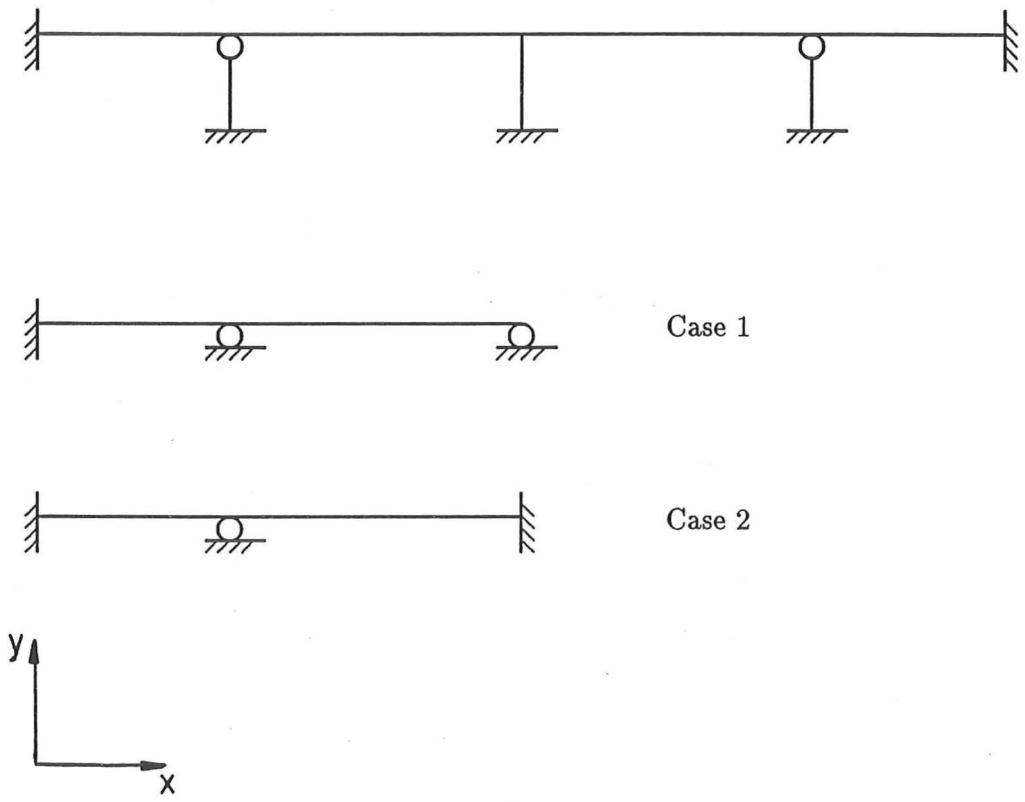

Figure 5.1: Drift Road bridge - Beam approximations

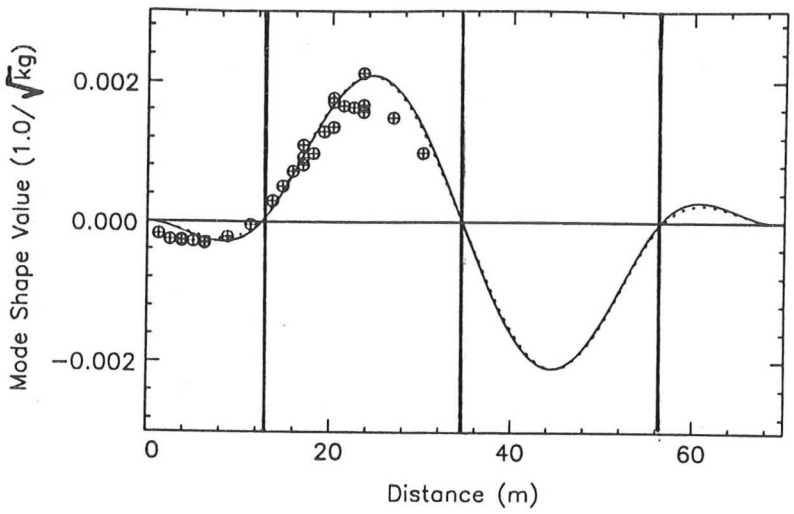

(a) Mode 1 : $f_m = 6.8$ Hz

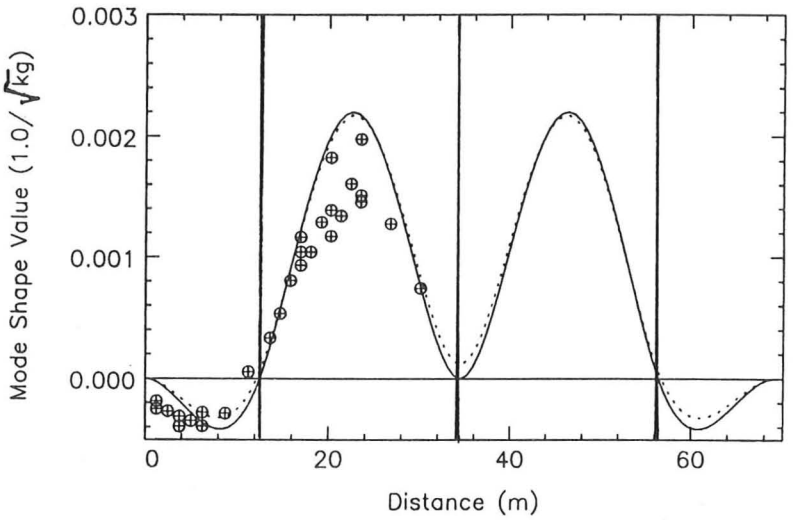

(b) Mode 2 : $f_m = 8.6$ Hz

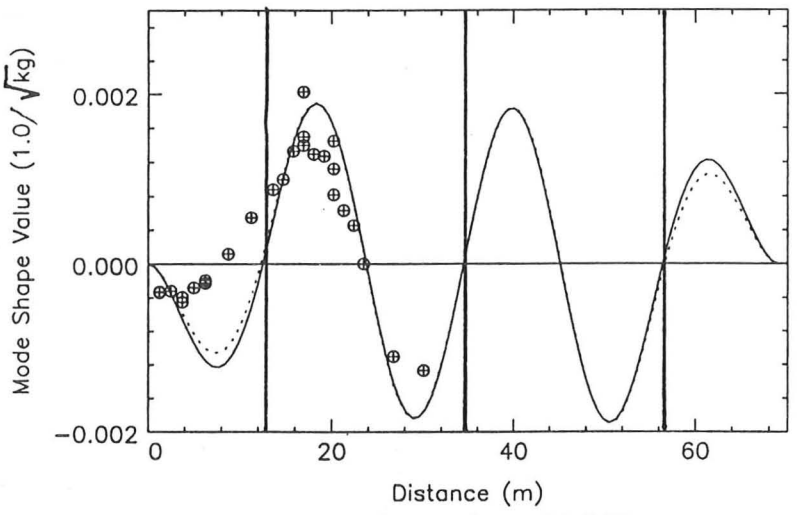

(c) Mode 5 : $f_m = 19.3$ Hz

Figure 5.2: Drift Road bridge - First three flexural mode shapes
Vertical lines indicate the positions of the columns
Measured ⊕
Beam theory _____ (used in convolution procedure)
Finite element . . . . . .

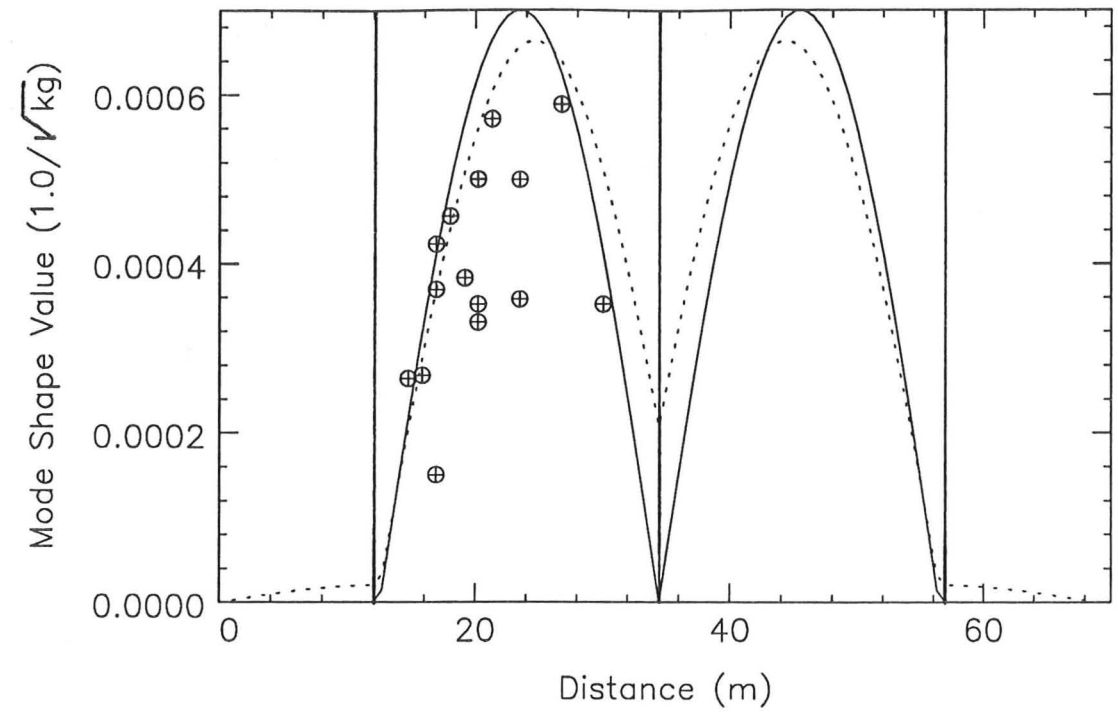

(a) Mode 3 : $f_m = 11.2$ Hz

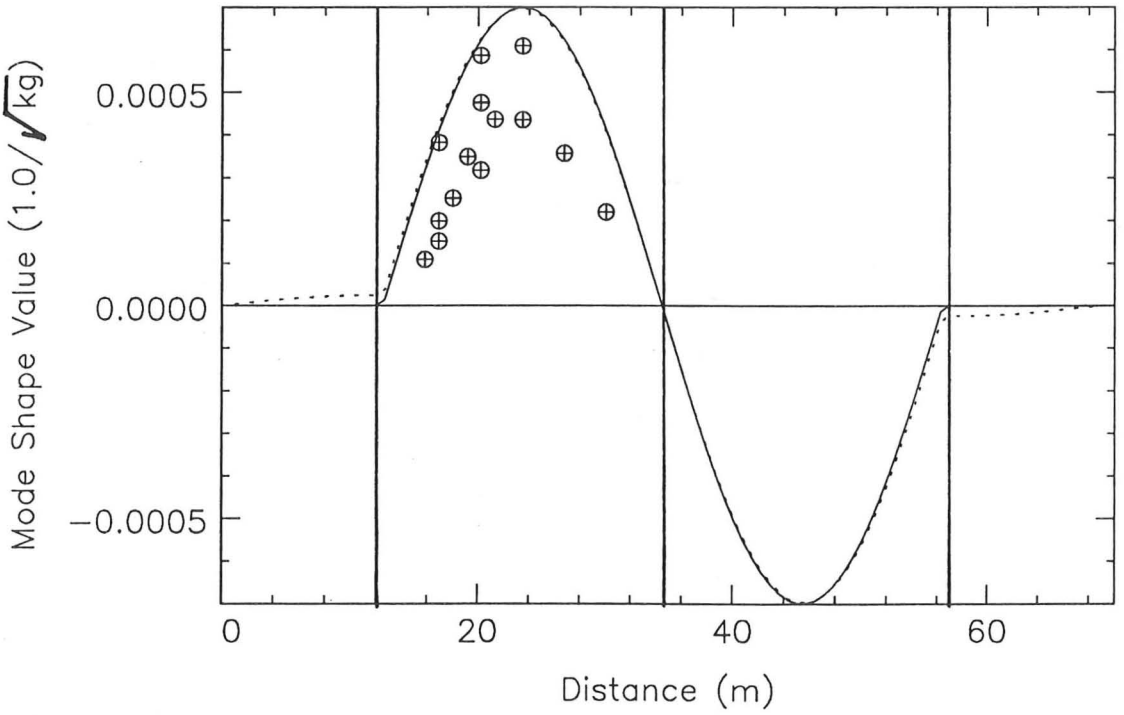

(b) Mode 4 : $f_m = 12.3$ Hz

Figure 5.3: Drift Road bridge - First two torsional mode shapes
Vertical lines indicate the positions of the columns
Measured ⊕
Beam theory _____ (used in convolution procedure)
Finite element - - - - - - - - - -

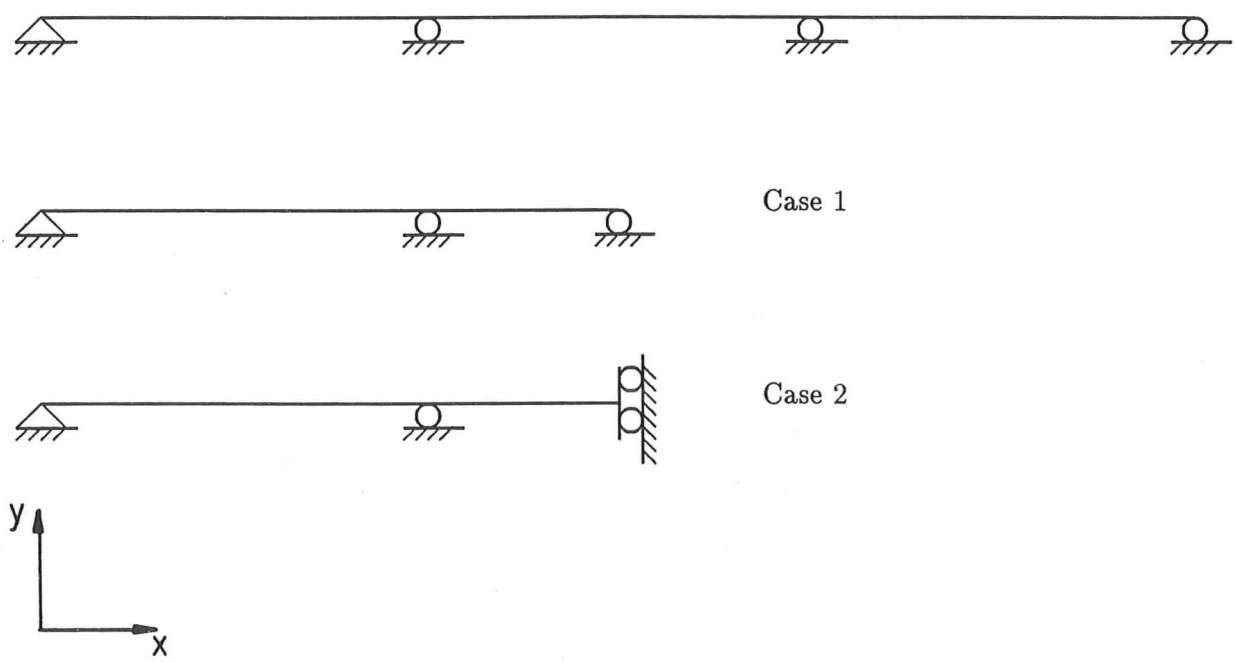

Figure 5.4: Lower Earley bridge - Beam approximations

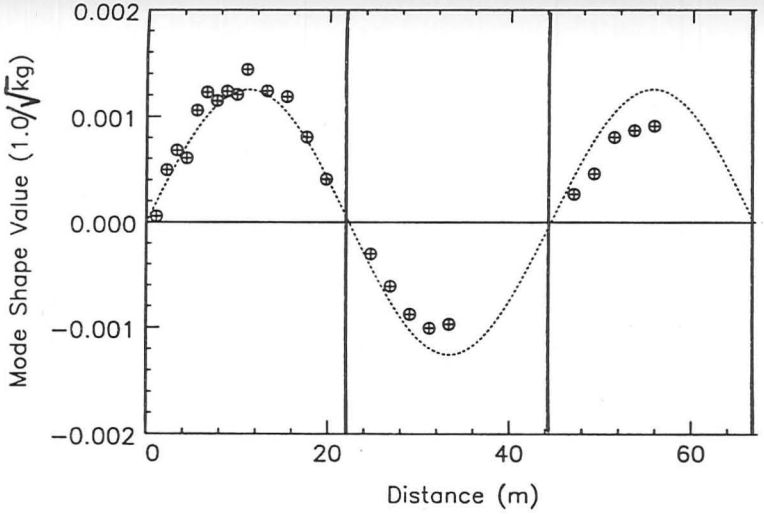

(a) Mode 1 : $f_m = 5.7$ Hz

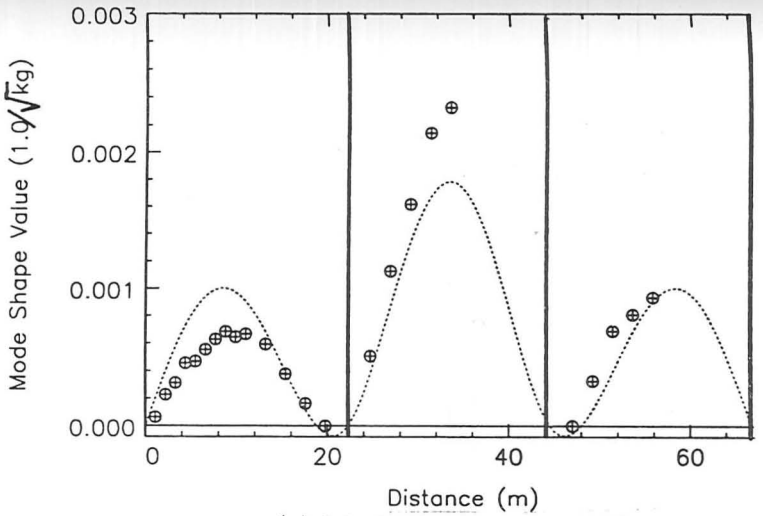

(c) Mode 5 : $f_m = 11.3$ Hz

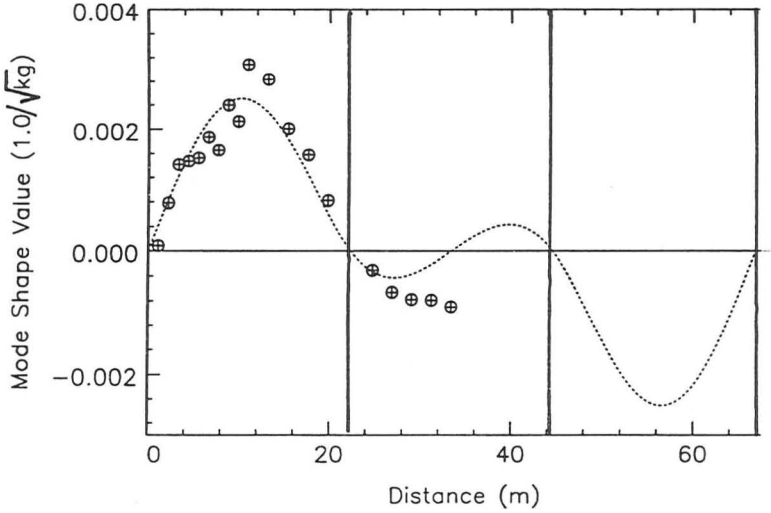

(b) Mode 2 : $f_m = 6.9$ Hz

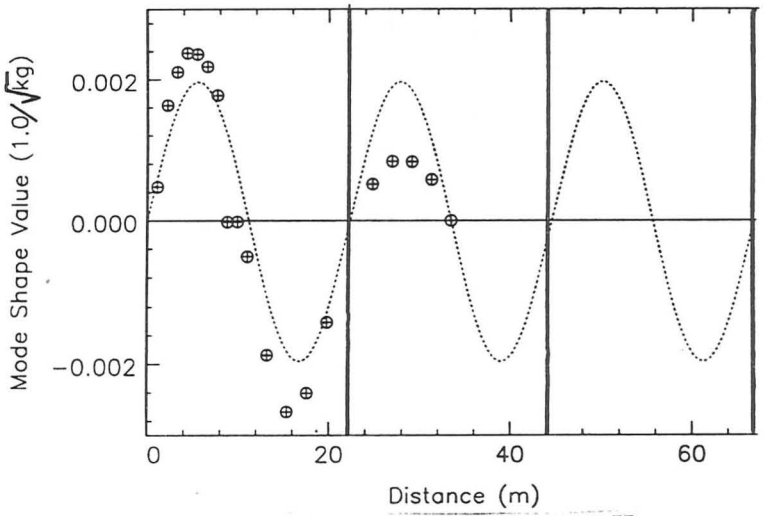

(d) Mode 8 : $f_m = 24.4$ Hz

Figure 5.5: Lower Earley bridge - First four beam mode shapes
Vertical lines indicate the positions of the supports
Measured ⊕
Beam theory ----------

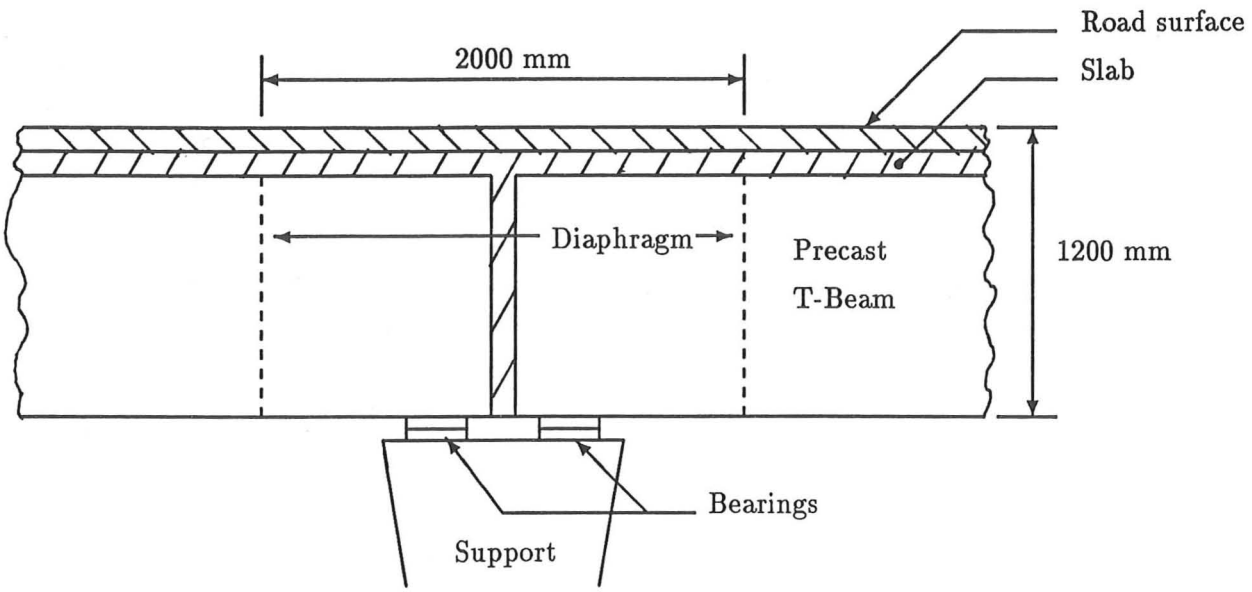

(a) Actual arrangement

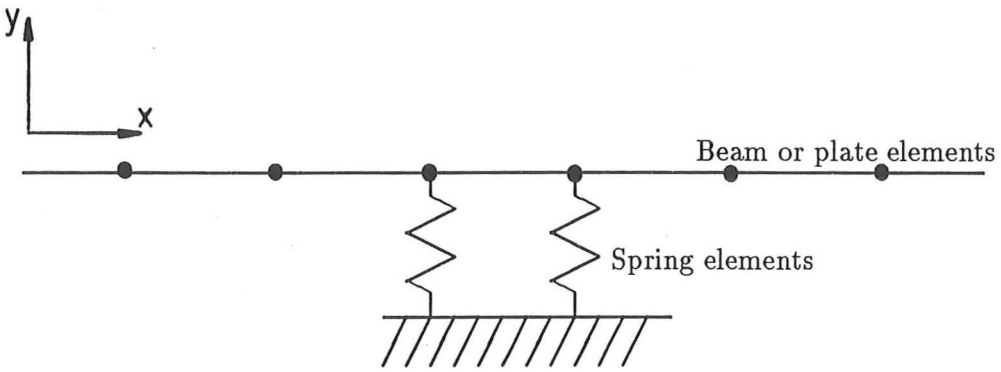

(b) Finite element approximation

Figure 5.6: Lower Earley bridge - Details of support at piers

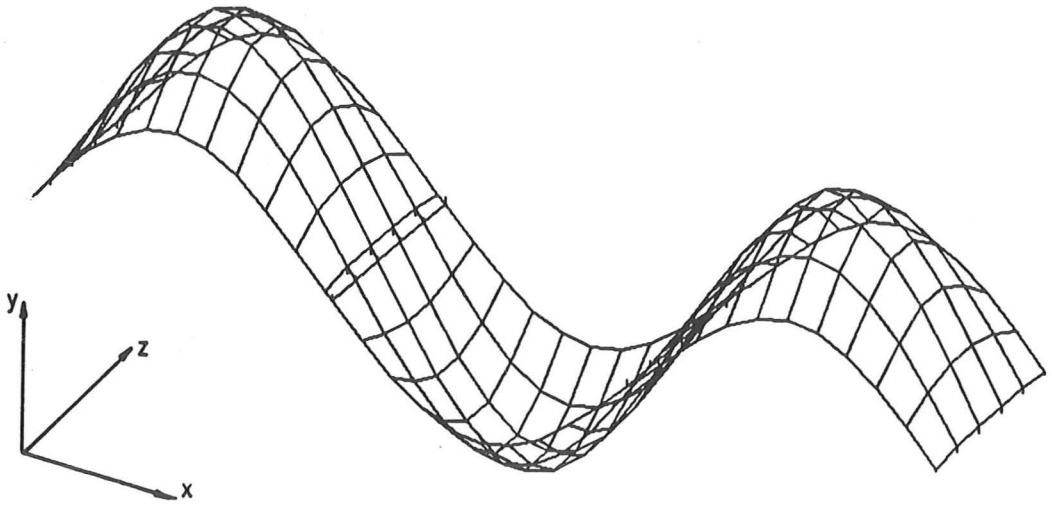

(a) Mode 1: $f_{fe} = 5.8$ Hz

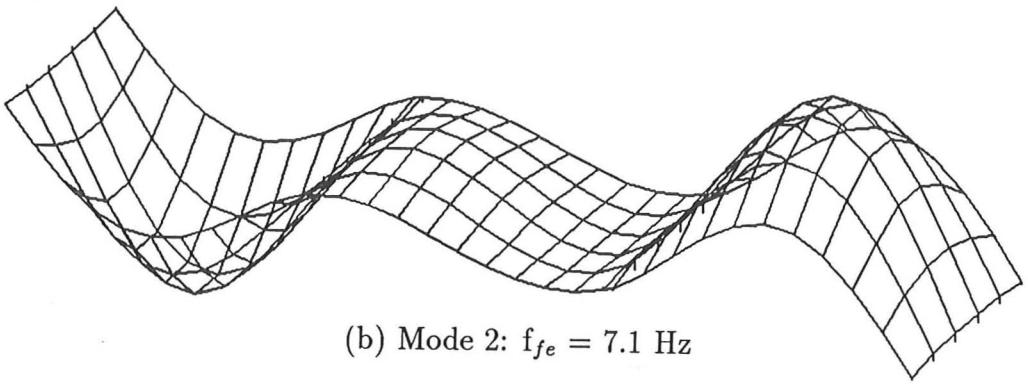

(b) Mode 2: $f_{fe} = 7.1$ Hz

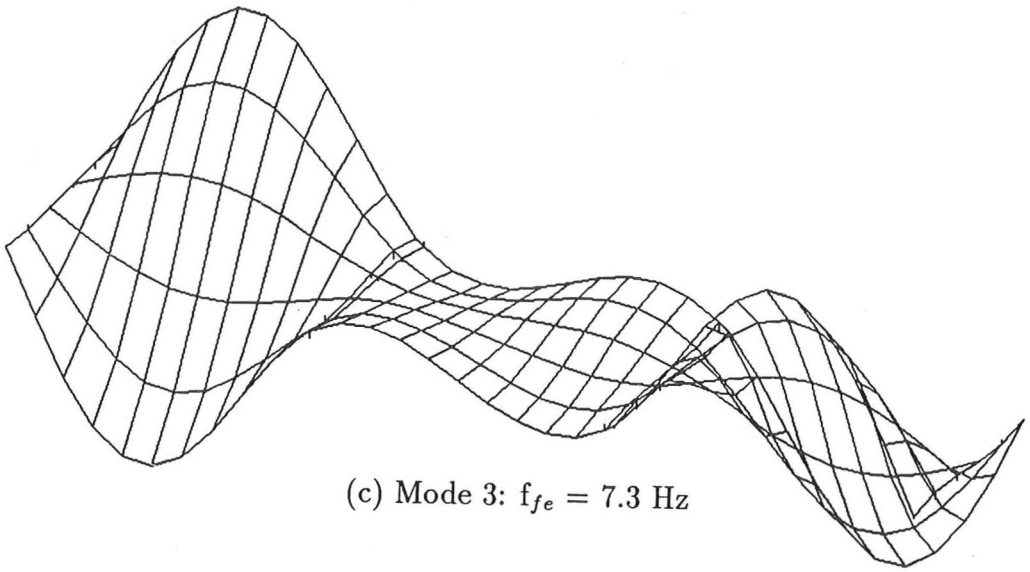

(c) Mode 3: $f_{fe} = 7.3$ Hz

Figure 5.7: Lower Earley bridge - First three modes from two-dimensional finite element bridge model

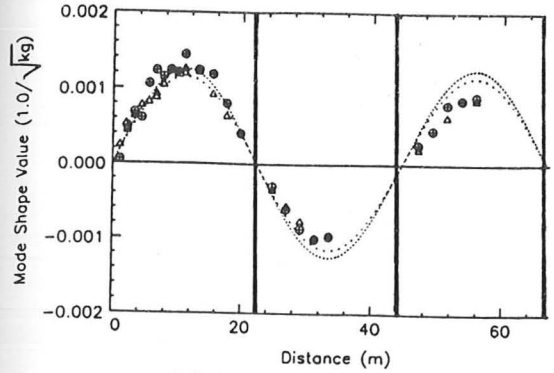

(a) Mode 1 : f_m = 5.7 Hz

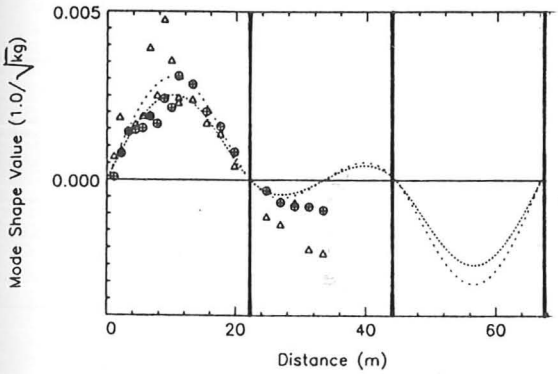

(b) Mode 2 : f_m = 6.9 Hz

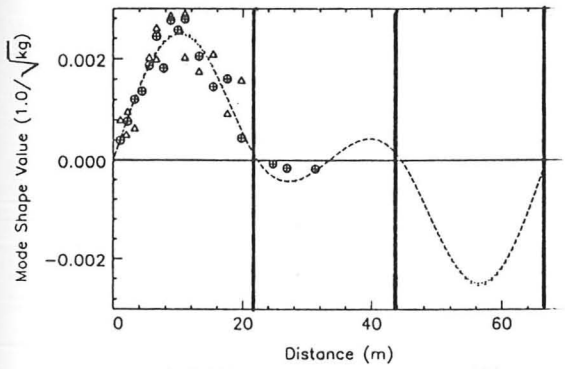

(c) Mode 3 : f_m = 7.4 Hz

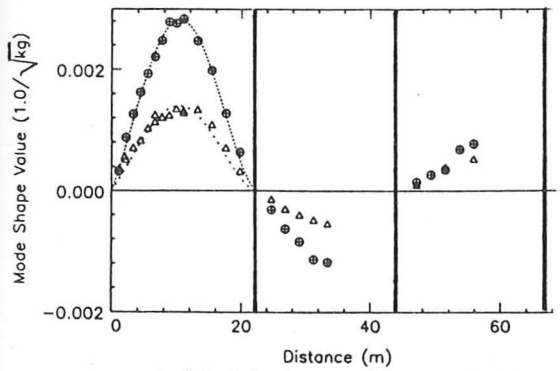

(d) Mode 4 : f_m = 9.7 Hz

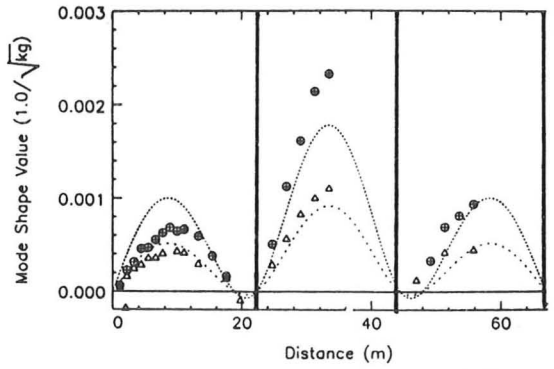

(e) Mode 5 : f_m = 11.3 Hz

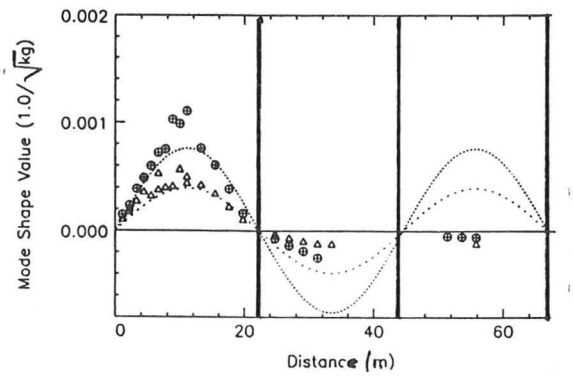

(f) Mode 6 : f_m = 13.3 Hz

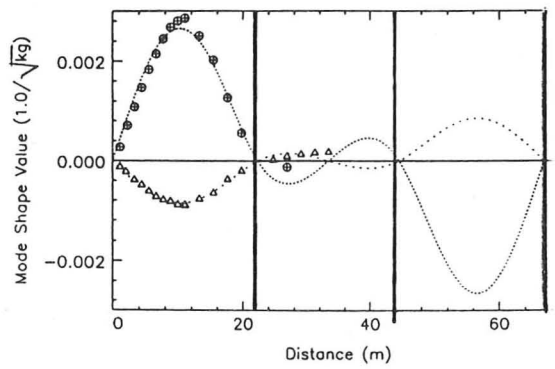

(g) Mode 7 : f_m = 18.0 Hz

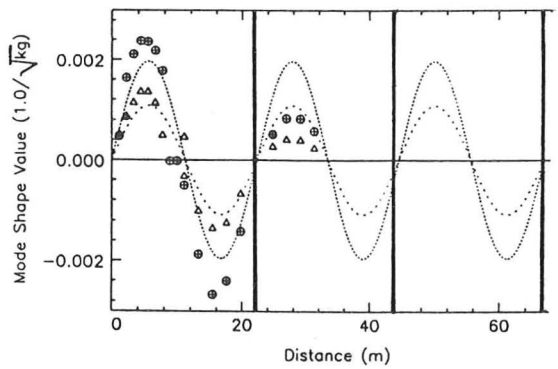

(h) Mode 8 : f_m = 24.4 Hz

Figure 5.8: Lower Earley bridge - Fitted mode shapes
Vertical lines indicate the positions of the supports
Measured : Centre-line track ⊕ Curbside track △
Fit : Centre-line track ----------
Curbside track - - - - - - - - - -

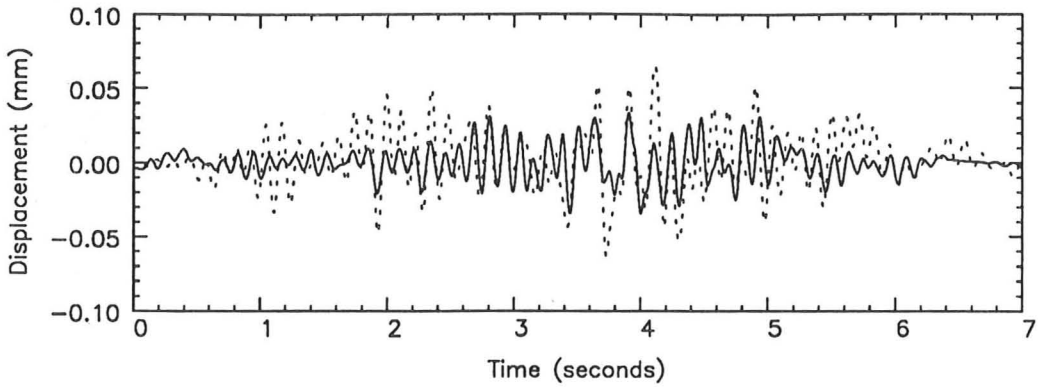

(a) Measurement position 1 (midspan)

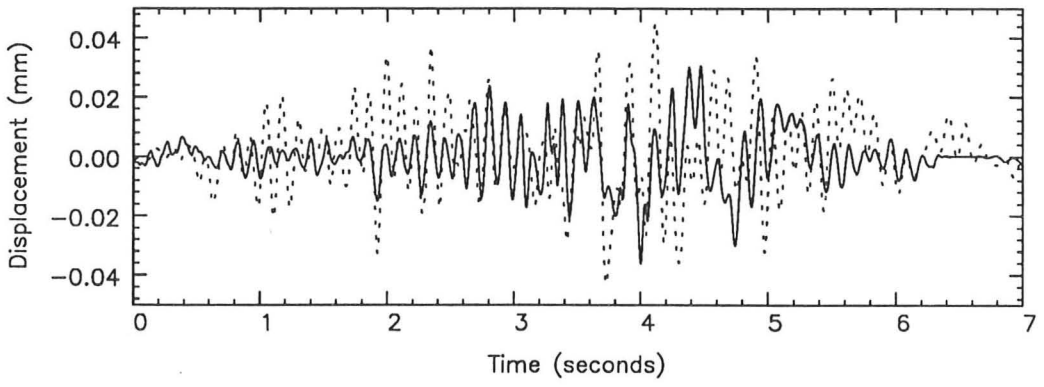

(b) Measurement position 3 (1/4 span)

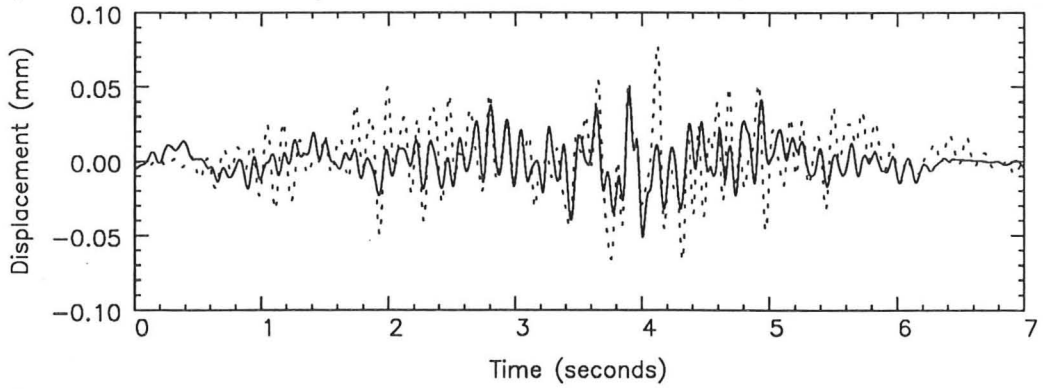

(c) Measurement position 4 (midspan, offset)

Figure 5.9: Drift Road bridge - Validation results (time domain)
Speed 50 km/h Direction : South-east to north-west
Measured ————————
Predicted . . . . . .

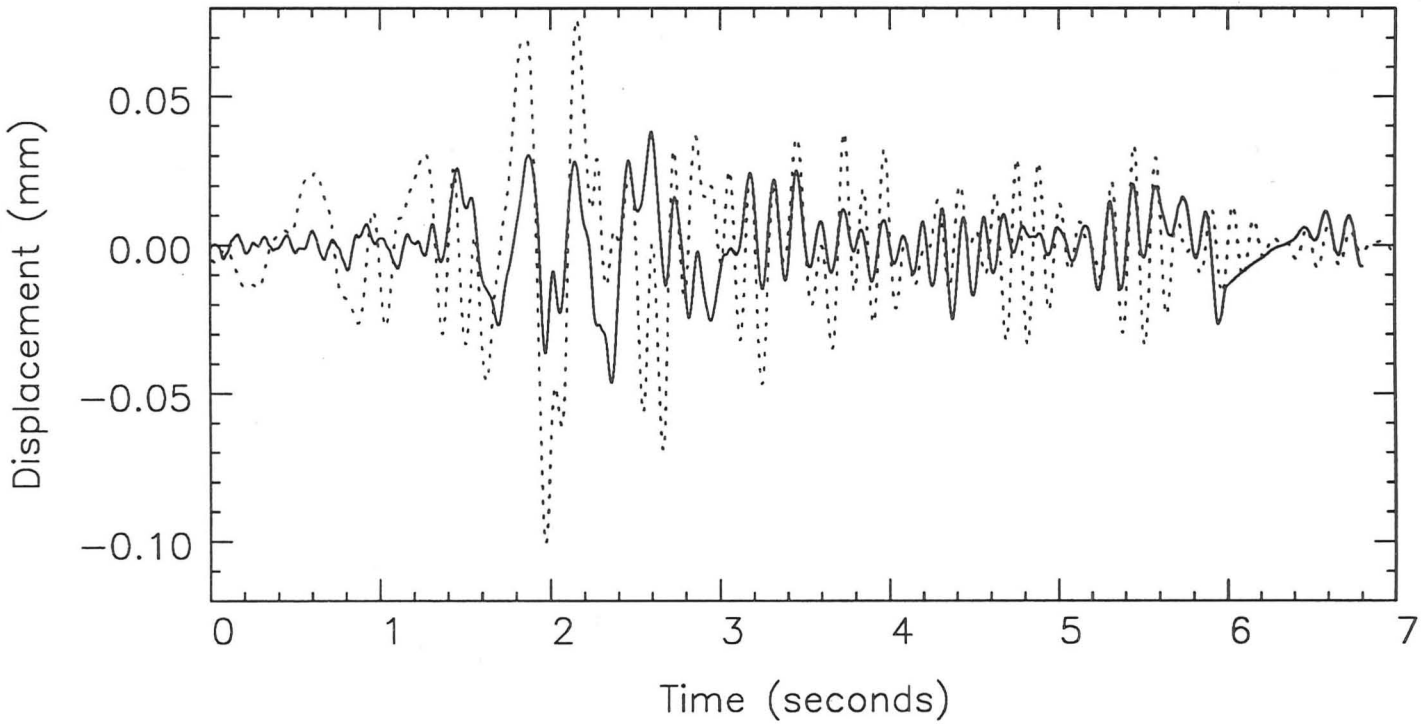

Figure 5.10: Drift Road bridge - Validation results (time domain)
Measurement position 1 (midspan)
Speed 50 km/h Direction : North-west to south-east
Measured ————————
Predicted - - - - - - - - -

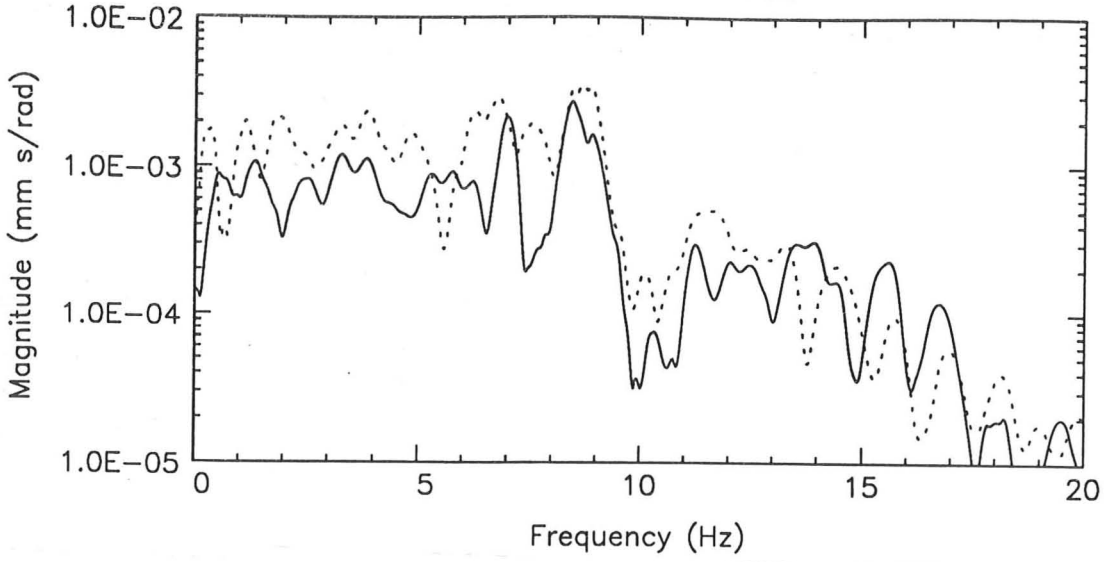

(a) Measurement position 1 (midspan)

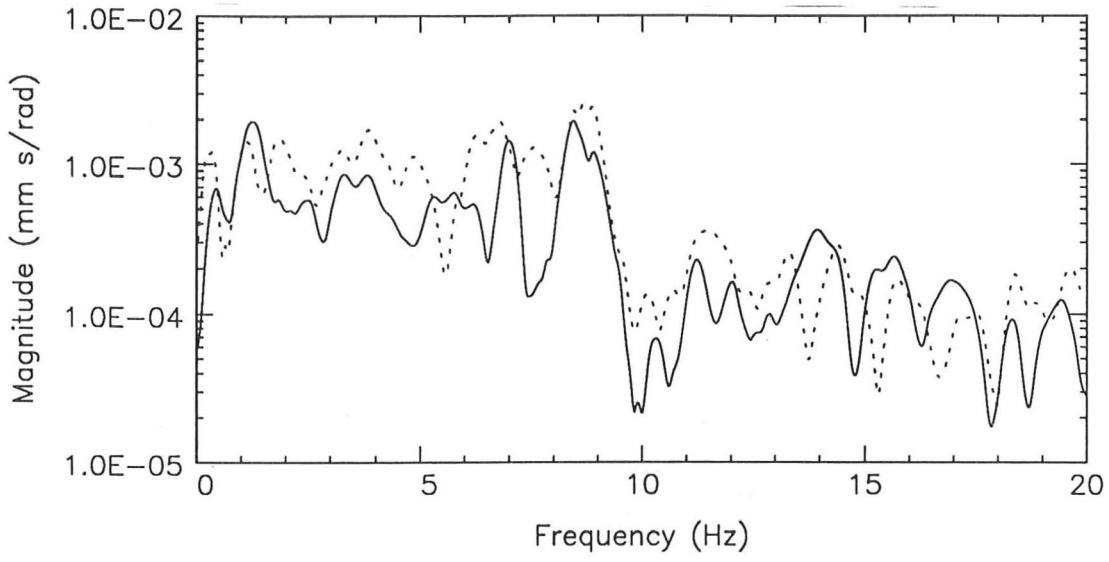

(b) Measurement position 3 (1/4 span)

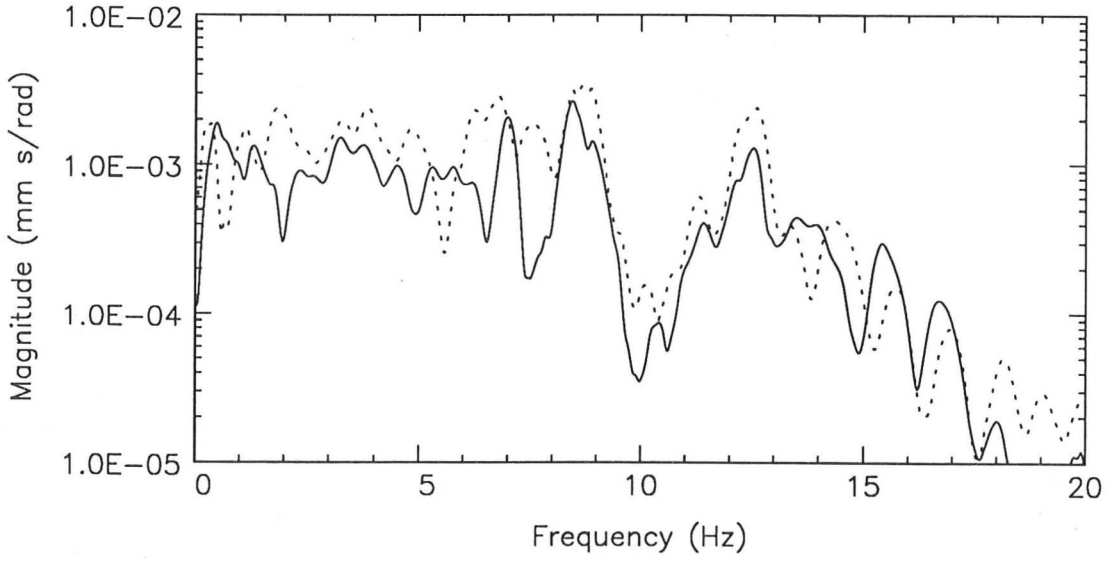

(c) Measurement position 4 (midspan, offset)

Figure 5.11: Drift Road bridge - Validation results (frequency domain)
Speed 50 km/h Direction : South-east to north-west
Measured ————————
Predicted - - - - - - - - - -

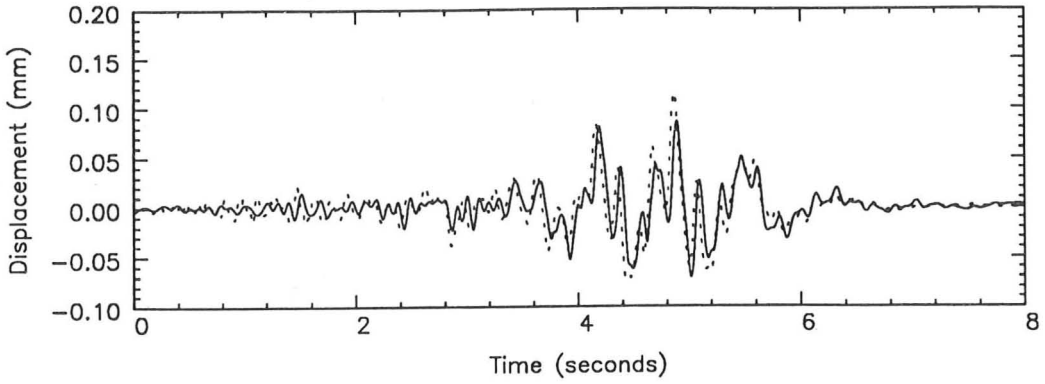

(a) Measurement position 1 (midspan)

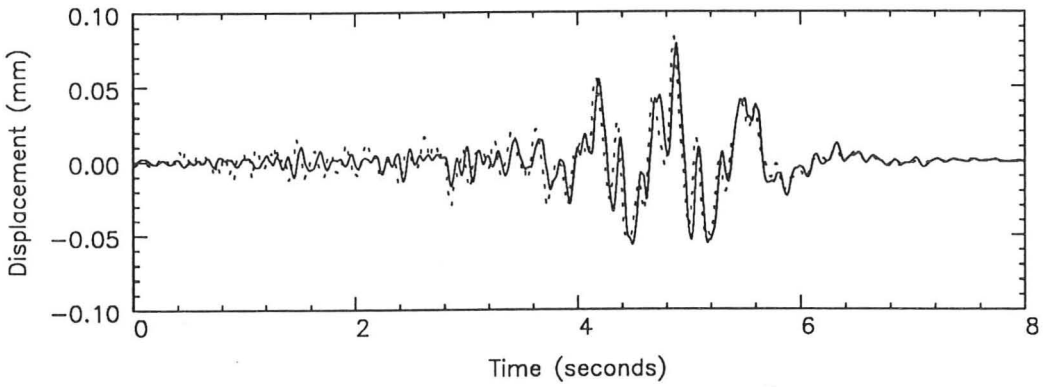

(b) Measurement position 3 (1/4 span)

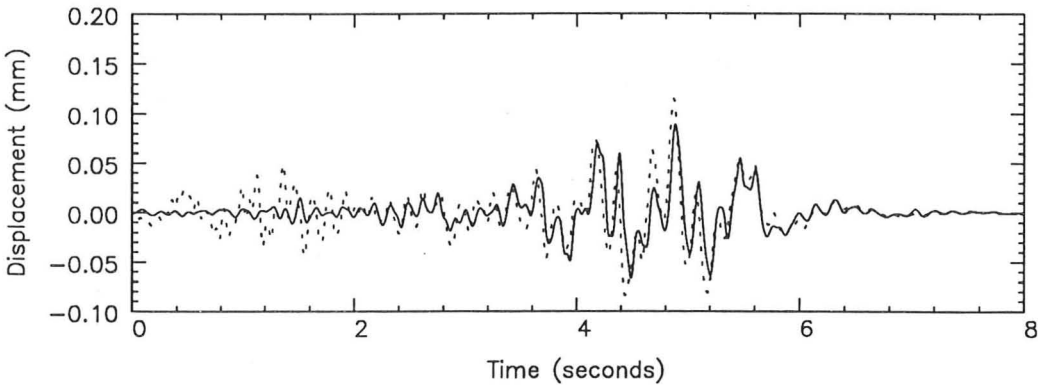

(c) Measurement position 4 (midspan, offset)

Figure 5.12: Lower Earley bridge - Validation results (time domain)
Speed 50 km/h Direction : South to north
Measured ————————
Predicted . . . . . .

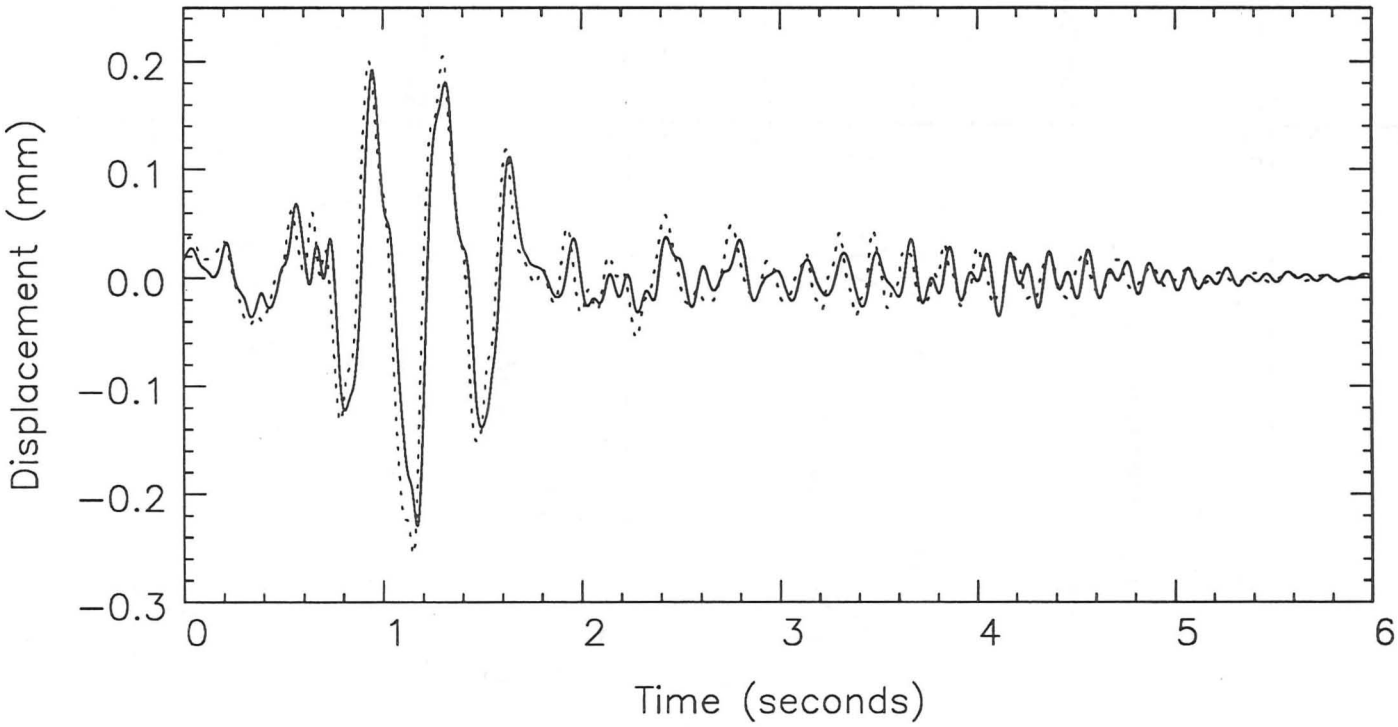

Figure 5.13: Lower Earley bridge - Validation results (time domain)
Measurement position 1 (midspan)
Speed 65 km/h Direction : North to south
Measured ————————
Predicted - - - - - - - - - -

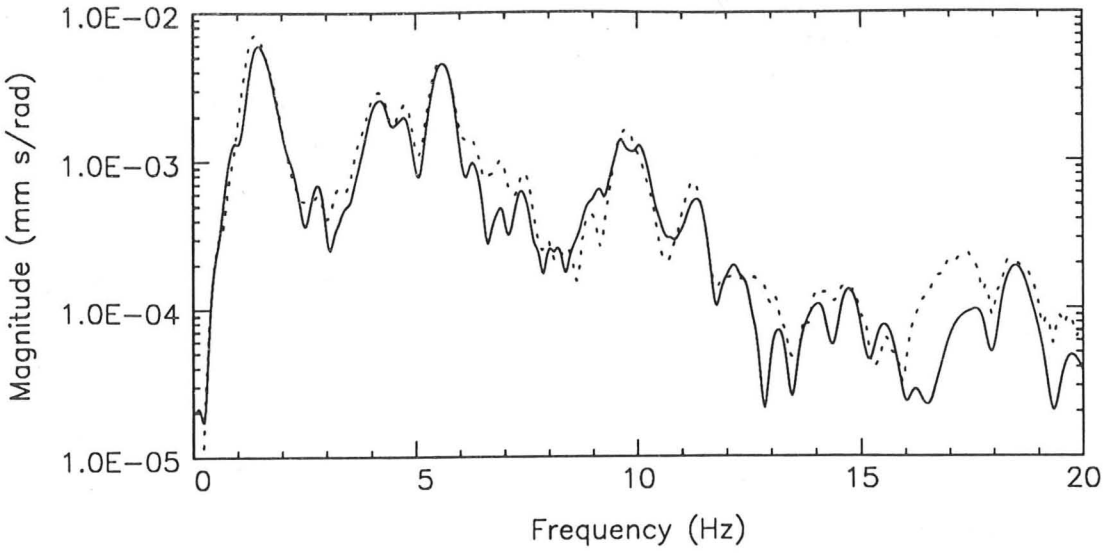

(a) Measurement position 1 (midspan)

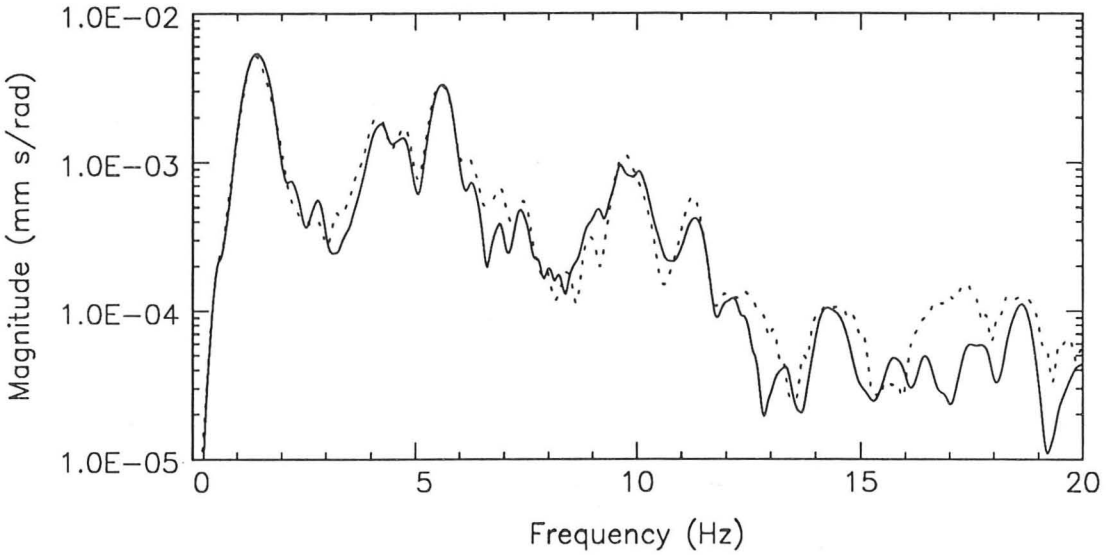

(b) Measurement position 3 (1/4 span)

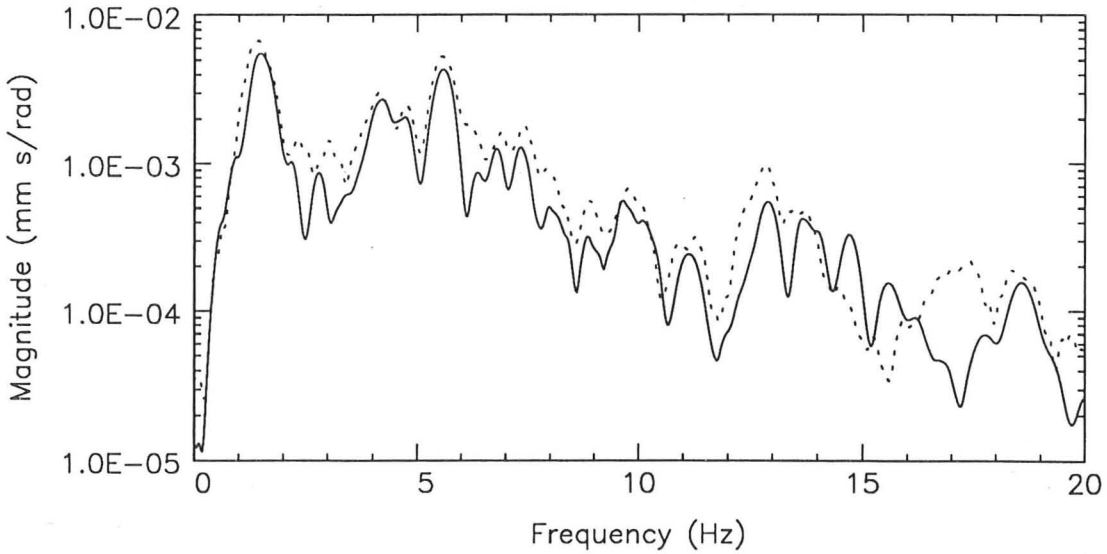

(c) Measurement position 4 (midspan, offset)

Figure 5.14: Lower Earley bridge - Validation results (frequency domain)
Speed 50 km/h Direction : South to north
Measured ————
Predicted - - - - - - - - - -

6 BRIDGE-VEHICLE INTERACTION

In chapter 2, a method was presented for calculating the dynamic response of bridges to moving loads. This method was validated experimentally by tests on two bridges, but the formulation did not include any specific reference to the interaction between vehicles and bridges. This chapter details the procedure used to combine vehicle models with the convolution method. A parametric study for analysing the importance of bridge-vehicle interaction will be presented, but first some background information about vehicle dynamics and bridge-vehicle interaction will be discussed.

6.1 Background

6.1.1 Vehicle Dynamics

One of the most important aspects in the study of bridge-vehicle systems is modelling the applied loads. This is a difficult task because realistic vehicle models are required.

The simplest model is a constant force traversing a bridge at a constant speed [52, 92, 93]. This is not representative of a vehicle, but closed-form bridge response solu-

6 BRIDGE-VEHICLE INTERACTION

In chapter 2, a method was presented for calculating the dynamic response of bridges to moving loads. This method was validated experimentally by tests on two bridges, but the formulation did not include any specific reference to the interaction between vehicles and bridges. This chapter details the procedure used to combine vehicle models with the convolution method. A parametric study for analysing the importance of bridge-vehicle interaction will be presented, but first some background information about vehicle dynamics and bridge-vehicle interaction will be discussed.

6.1 Background

6.1.1 Vehicle Dynamics

One of the most important aspects in the study of bridge-vehicle systems is modelling the applied loads. This is a difficult task because realistic vehicle models are required.

The simplest model is a constant force traversing a bridge at a constant speed [52, 92, 93]. This is not representative of a vehicle, but closed-form bridge response solu-

tions can be determined analytically and used to check more realistic bridge-vehicle models. Some improvement can be made by considering an unsprung mass moving across the bridge [52, 100], but some sort of sprung mass system is necessary to model vehicle suspension systems. The simplest of these is a single degree of freedom system with mass, damping and stiffness [6, 38, 45, 56, 57, 66, 100]. Some authors have included an extra degree of freedom to model the higher frequency wheel-hop suspension modes [94]. Finally, multiple axle vehicles with linear suspensions have been considered by some authors [23, 42, 43, 44, 48, 54, 81].

In recent years, more realistic vehicle models have been developed for calculating heavy vehicle ride and dynamic wheel loads. Many of the models can simulate vehicles with any number of axles and non-linear suspension and tyre elements. There have been some tentative attempts to apply more realistic vehicle models to bridge vibration problems [51, 68, 87], but much more work is needed.

Cebon [17] developed a computer program to implement one of these models. This program has been validated extensively by comparison with two independent sets of measurements on instrumented vehicles [17, 27, 26] and will be used in this dissertation to generate vehicle wheel loads.

The combination of a realistic vehicle model with a validated bridge response model should enable the effects of different vehicles and suspensions on bridge response to be studied more accurately.

6.1.2 Bridge-Vehicle Interaction

Most authors have deemed dynamic bridge-vehicle interaction to be important [6, 25, 37, 44, 52, 54, 55, 56, 66, 72, 87, 91, 94], although some have ignored it [45, 52, 83]. There has been little systematic study about when the interaction is important, and when the two systems can be considered to be essentially uncoupled.

Walker and Veletsos [95] considered a simply-supported bridge and calculated bridge responses caused by a moving constant force and a moving sprung mass. They compared the two responses by computing the maximum dynamic increments for

each case, and related the importance of interaction to the frequency ratio, γ, defined as

$$\gamma = \frac{\omega_v}{\omega^{(1)}} \tag{6.1}$$

where ω_v is the natural frequency of the vehicle and $\omega^{(1)}$ is the first natural frequency of the bridge. Bridge-vehicle interaction was deemed unimportant if γ was less than 0.3 and greater than about 1.0 [95]. This criterion seems quite reasonable, but Walker and Veletsos did not quantify the errors incurred by neglecting bridge-vehicle interaction.

Chiu, Smith, and Wormley [24] conducted a parametric study similar to that of Walker and Veletsos for an elevated guide-way traversed by a high-speed vehicle. They found that interaction was unimportant for mass ratios below $\frac{1}{8}$, or for low frequency ratios. Their interaction criteria were based only on maximum guideway deflections and vehicle accelerations. They were not concerned with time histories of displacements. In addition, most of their results were calculated for speed ratios far in excess of those attained on highway bridges. Their criteria are consistent with those of Walker and Veletsos, but do not provide enough detail for low speeds.

Finally, Ting and Genin [90] outlined interaction criteria based on the quantity $2\epsilon\ddot{Z}$ where ϵ is the mass ratio as defined by Walker and Veletsos, and $\ddot{Z}$ is the the second time derivative of the vehicle displacement normalized by the maximum static deflection of the bridge. They concluded that interaction can be ignored if $2\epsilon\ddot{Z} \ll 1$. Although this may be valid, it is vague and based on vehicle acceleration which is unknown for highway bridges. This guideline is more applicable to elevated guideways where vehicle acceleration can be estimated in the design process.

The author has not found sufficient detail in interaction criteria proposed by others, and has not discovered any published research that quantifies the errors involved in neglecting the bridge-vehicle interaction. Therefore, this chapter will present a method of solving the bridge-vehicle interaction problem, examine interaction criteria, and present guidelines for estimating errors incurred by ignoring interaction.

6.2 Treatment of Dynamic Bridge-Vehicle Interaction

For the purposes of this study, the bridge-vehicle interaction was incorporated iteratively. The procedure was as follows:

(i) An initial set of vehicle wheel loads was used as the input to the bridge calculation program. These initial vehicle loads were usually obtained by calculating the vehicle response to a specified bridge surface profile.

(ii) The displacement response of the bridge was calculated under each tyre of the vehicle.

(iii) The bridge displacement response was added to the surface profile and used as the input to the vehicle model. New wheel loads were predicted.

(iv) The displacement response, $y(t)$, from the loads in (iii) was computed by the procedure of (ii). In order to facilitate convergence, successive displacement responses were often averaged

$$y_j(t) = \frac{y(t) + y_{j-1}(t)}{2} \tag{6.2}$$

where $y_j(t)$ is the j^{th} estimate for the bridge displacement response.

(v) Steps (iii) and (iv) were repeated until convergence was obtained. Convergence was deemed to have occurred when the following criterion was satisfied:

$$\frac{|y(t) - y_{j-1}(t)|}{\max(|y(t)|)} \leq \text{Tolerance} \quad \text{for} \quad 0 \leq t \leq T_{vp}. \tag{6.3}$$

where T_{vp} is the time for the vehicle to pass completely over the bridge.

Similar iterative methods have been used by other authors. In fact, Hawk and Ghali [44] outlined an almost identical convergence procedure which they termed the 'iterative dynamic substructuring method (IDSM).' In addition, they compared their method with solutions obtained by Runge-Kutta Nystrom numerical integration and found good agreement.

This iterative method is essentially a perturbation method because the dynamic solution is assumed to oscillate about the quasi-static solution. Since this is the case for vehicle-induced vibrations of highway bridges, perturbation methods are usually satisfactory. Nevertheless, the method is not guaranteed to converge. Convergence was not found to be a problem, except for vehicles with large wheel forces at frequencies greater than about 10Hz. Since most vehicles generate dynamic wheel loads with energy concentrated in the 1.5-4.5Hz frequency range [19], this limitation was not serious.

The next two subsections describe the implementation of the iterative procedure. In the first subsection, the iterative procedure is applied to simple vehicle models while in the latter the importance of the dynamic bridge-vehicle interaction is discussed.

6.2.1 Convergence with Simple Vehicle Models

Two different vehicle models were selected to test the convergence of the iterative procedure. The first was a two degree of freedom, '1/4 car' model as shown in figure 6.1. The vehicle parameters for a highly idealized 40 tonne vehicle are:

m_t = 4 tonne $\qquad$ m_s = 36 tonne $\quad$ (total weight = 392kN)

k_t = 7.2x10^7 Nm^{-1} $\qquad$ k_s =1.8x10^7 Nm^{-1}
$\omega_v^{(1)}$ = 20 rad/s $\qquad$ $\zeta_v^{(1)}$ = 0.07

c_t = 14.4x10^4 kgs^{-1} $\qquad$ c_s = 14.4x10^4 kgs^{-1}
$\omega_v^{(2)}$ = 150 rad/s $\qquad$ $\zeta_v^{(2)}$ = 0.24

where $\omega_v^{(j)}$ is the j^{th} natural frequency of the vehicle (j = 1,2),

$\zeta_v^{(j)}$ is the j^{th} modal damping ratio of the vehicle,

m_t is the tyre mass,

k_t is the tyre stiffness,

c_t is the tyre damping constant,

m_s is the body sprung mass,

k_s is the suspension stiffness,

and c_s is the suspension damping constant.

For the second convergence test a two axle vehicle model was used. Figure 6.2 illustrates the layout of the vehicle. It had four degrees of freedom: two tyre displacements, sprung mass displacement, and sprung mass pitch rotation. The mass, stiffness, and damping properties were:

$$m_t^{(1)} = m_t^{(2)} = 2 \text{ tonne} \qquad m_s = 36 \text{ tonne}$$
$$I_v = 144\text{x}10^3 \text{ kgm}^2 \qquad \text{a} = 1.0 \text{ m}$$

$$k_t^{(1)} = k_t^{(2)} = 3.6\text{x}10^7 \text{ Nm}^{-1} \qquad k_s = k_s = 0.9\text{x}10^7 \text{ Nm}^{-1}$$
$$c_t^{(1)} = c_t^{(2)} = 7.2\text{x}10^4 \text{ kgs}^{-1} \qquad c_s = 7.2\text{x}10^4 \text{ kgs}^{-1}$$

resulting in:

$$\omega_v^{(1)} = 10 \text{ rad/s} \quad \zeta_v^{(1)} = 0.03 \quad \omega_v^{(2)} = 20 \text{ rad/s} \quad \zeta_v^{(2)} = 0.07$$
$$\omega_v^{(3)} = 150 \text{ rad/s} \quad \zeta_v^{(3)} = 0.24 \quad \omega_v^{(4)} = 150 \text{ rad/s} \quad \zeta_v^{(4)} = 0.24$$

where I_v is the body pitch inertia, and 'a' is the axle spacing.

For the examples in this section, the non-dimensional speed parameter, α, is introduced, and defined as follows:

$$\alpha = \frac{\pi V}{\omega^{(1)} L} \tag{6.4}$$

where V is the vehicle speed and L is the length of the bridge.

The bridge used in the examples in the rest of this chapter was the simply-supported Pirton Lane bridge tested by TRRL [33, 63, 99]. This bridge had a 40m span and a first natural frequency of 20rad/s. Other parameters of the bridge were given in section 2.2.5. The method was verified at two different speeds, $V_1 = 25$m/s and $V_2 = 50$m/s, resulting in speed parameters as follows:

$$\alpha_1 = \frac{\pi V_1}{\omega^{(1)} L} = 0.1 \qquad \alpha_2 = \frac{\pi V_2}{\omega^{(1)} L} = 0.2$$

The results of the iterative procedure are shown in figures 6.3 to 6.5. Figure 6.3 illustrates the convergence of the method by plotting the final three iterations. Two curves are shown on each plot of figures 6.4 and 6.5. The first curve is the predicted bridge response from equivalent static loads moving over the bridge. The other curve

is the result when the bridge and vehicle models are combined at the specified speeds. The tolerance on convergence in all cases was 1% and the number of iterations required to achieve this tolerance was

Vehicle Model	Speed Parameter (α)	Iterations
'1/4 car'	0.1	5
'1/4 car'	0.2	4
'1/2 car'	0.1	5
'1/2 car'	0.2	4

It is evident that the iterative method works well and does not require excessive computation time.

6.3 Importance of Interaction: Parameter Study

This section will examine the importance of bridge-vehicle interaction, and present guidelines for estimating when interaction can be ignored.

A parametric study was performed. The vehicle model was a single degree of freedom oscillator and the bridge was simply-supported with properties as described in section 2.2.5. Six non-dimensional parameters were defined as shown in the following table.

Parameter	Symbol	Definition	Parameter Range
Speed	α	$\frac{\pi V}{\omega^{(1)} L}$	0.05 - 0.20
Frequency ratio	γ	$\frac{\omega_v}{\omega^{(1)}}$	0.5 - 2.0
Modal mass ratio	κ	$\frac{2m_v}{mL}$	0.16 - 0.64
Vehicle damping ratio	ζ_v	$\frac{c}{2\sqrt{km_v}}$	0.01 - 0.20
Bridge damping ratio	ζ		0.01 - 0.05
Bump height	h_s	$\frac{H_s}{y_{st}}$	0 -10

H_s is the height of a step placed at the entry to the bridge, m is the mass per unit length of the bridge, and y_{st} is the maximum static displacement at the midspan of the bridge.

Three different ways of assessing the importance of bridge-vehicle interaction were considered. The first method was to compare dynamic wheel forces with static values. This was rejected because it does not give a direct estimate of how the interaction affects bridge response. Dynamic response increments were considered as an alternative, but they only measure maximum dynamic effects. Dynamic response increments do not show how interaction affects the overall vibration of the bridge. A third method was chosen and implemented as follows:

(i) An initial set of wheel loads was predicted using the specified bridge surface profile as the input to the vehicle model.

(ii) The initial loads were applied to the bridge to calculate the initial midspan displacement, $y_{in}(x_0, t)$, where $x_0 = L/2$.

(iii) The iterative calculation of section 6.2 was performed to calculate the midspan bridge displacement, $y(x_0, t)$.

(iv) $y(x_0, t)$ was compared with $y_{in}(x_0, t)$ by computing the error term

$$\mathcal{E}(t) = \left| \frac{y(x_0, t) - y_{in}(x_0, t)}{y_{st}} \right| \tag{6.5}$$

(v) The maximum value of $\mathcal{E}(t)$ and the standard deviation, $\sigma_{\mathcal{E}}$, were recorded. The standard deviation was calculated from $\mathcal{E}(t)$ for the time the vehicle was on the bridge.

This method considers the consequences of ignoring interaction on the calculated dynamic bridge responses. Figures 6.6 and 6.7 show normalized responses of the

bridge to a sprung mass (dotted curve) and to a constant force (solid curve). The normalization was performed by dividing the dynamic deflection response by the maximum midspan static deflection, y_{st}. The following parameters were used:

$$\gamma = 1.0 \qquad \kappa = 0.32 \qquad \zeta_v = 0.05$$
$$\zeta = 0.02 \qquad h_s = 0.$$

In figure 6.6 the speed parameter is 0.10 while in figure 6.7 the speed parameter is 0.20. Errors were calculated by the formula of equation 6.5 and the values corresponding to the two figures are as follows

α	Maximum error (%)	σ_ε(%)
0.1	11.4	5.3
0.2	21.7	9.8

From an inspection of figure 6.6, a 5% standard deviation of error seems to be a reasonable threshold for ignoring interaction. Both curves on this figure show approximately the same amount of vibration and maximum errors are only about 10%.

Several combinations of frequency ratios and speed parameters were computed and errors were calculated. Figure 6.8 shows values of maximum error and standard deviation of error. The frequency ratio was chosen for the horizontal axes while errors are plotted on the vertical axes. Error estimates for each speed parameter are connected by solid lines and the errors for the curves of figures 6.6 and 6.7 are included. The errors increase with the speed parameter. The maximum errors are approximately double the standard deviation values. The curves peak at $\gamma = 1.0$ where the natural frequencies are matched except at the slowest speed ($\alpha = 0.05$). For the slow speed, the quasi-static response dominates and so there only a small amount of energy at the bridge natural frequency to be fed back into the vehicle. This results in a lower level of interaction, regardless of the frequency ratio. Finally, when the frequency ratio, γ, is less than or equal to 0.5, the errors are small and the dependence on speed is reduced. An error standard deviation, σ_ε, of 5% is thought to be a reasonable threshold. Hence, in this case, interaction is important if $\alpha \geq 0.1$ and $\gamma \geq 0.7$. For the Pirton Lane bridge with length 40m and natural frequency of 3.2Hz, this threshold would be crossed for vehicles travelling at speeds

greater than 25m/s (90km/h) with natural frequencies in excess of 2Hz. Therefore interaction would only be significant at motorway speeds. For the Drift road and Lower Earley bridges, the main spans are approximately 20m long and the lowest natural frequencies are at 6.8 and 5.7Hz, respectively. For these two bridges, the speed threshold is once again about 25m/s, but vehicles with frequencies up to about 3Hz will cause little interaction.

Since the curves for maximum error and σ_ε are similar, only the plots for σ_ε will be presented for the rest of this study. The effect of vehicle mass on the interaction is demonstrated in figure 6.9. Curves for two values of the speed parameter, α, are shown. Larger modal mass ratios cause more interaction, and this effect is pronounced at the higher speed. At the lower speed ($\alpha = 0.05$), changes in vehicle mass result in only minor alterations in the amount of interaction.

Damping is varied for the curves in figures 6.10 and 6.11. Increased vehicle damping reduces the interaction, especially near a frequency ratio of unity. Bridge damping, however, influences the interaction over a larger frequency range, but the interaction is not very sensitive to bridge damping when vehicle damping is high (figure 6.11b).

Finally, the influence of bridge abutment roughness on the interaction is presented in figure 6.12. The vehicle was excited by a step at the entrance to the bridge. Initial excitation of the vehicle has an overwhelming influence on the amount of bridge-vehicle interaction. Increased vehicle response results in more interaction and the average errors incurred by neglecting the interaction can be almost 60%. It was noticed, however, that for a frequency ratio of 0.5 the errors averaged less than 5% for all cases.

Bridge responses corresponding to $\kappa = 0.32$, $\gamma = 1.0$, and $h_s = 10$ are plotted in figure 6.13. The solid curves were obtained by considering the interaction while the dotted lines were the responses to the initial wheel loads. The discrepancies between the estimates are large, and the vibration is much larger when the interaction is ignored. This occurs because the vehicle damping dissipates some of the energy of the bridge vibration. The third curve on the graphs was obtained by increasing

the modal damping of the bridge to 0.05 and applying the initial vehicle loads (no interaction). The approximation errors are reduced. Therefore, it may be possible to find a simple system that approximates the vibration absorbing effect of the vehicle on the bridge. Adjusting bridge damping may be one way of compensating for the absence of the vehicle when interaction is ignored. Figure 6.14 shows new error estimates for a revised bridge damping value of 0.05 for the initial bridge responses. The average errors are generally reduced, but near a frequency ratio of 1.0 the errors are still large.

This parameter study has revealed some interesting aspects of bridge-vehicle interaction. Within the normal range of parameters on highway bridges, the most important parameters are speed, frequency, and initial vehicle excitation. Large mass ratios result in significant interaction at high speeds. Bridge and vehicle damping are important when the frequency ratio is near 1.0.

For this study, interaction was deemed important if the standard deviation of the error, σ_ε, were greater than 5%. Using this criterion, dynamic interaction can be ignored if

(i) $\gamma \leq 0.5$, or

(ii) $\alpha \leq 0.1$ and $\kappa \leq 0.3$ for smooth bridge profiles.

These guidelines are valid for the parameter ranges specified in this study: $\zeta_v \geq 0.05$, $\zeta \geq 0.01$, and $\kappa \leq 0.64$.

Considering the practical application of these guidelines, heavy vehicles generate most of their wheel loads in the 1.5 to 4.5Hz frequency range so bridges with natural frequencies near 10Hz will have little interaction with most vehicles.

The second guideline applies for bridges with well maintained approaches, and light vehicles travelling at low speeds. For the Pirton Lane bridge, interaction can be ignored for vehicles up to 40 tonnes as long as they are travelling below 90km/h. This is a fairly high speed for heavy vehicles, and so the bridge-vehicle interaction can be ignored in many cases as long as the approaches are smooth. Nevertheless, more information is needed on the importance of road roughness in determining the

amount of bridge-vehicle interaction, and if any doubts exist then interaction should be considered.

The frequency criterion is similar to that suggested by Walker and Veletsos [95] although they ignored interaction for $\gamma \leq 0.3$. This study has verified some of their work, but also expanded it by estimating the errors involved in neglecting the interaction and by considering the influence of damping and initial vehicle excitation.

6.4 Conclusions

The convolution method of chapter 2 was extended to calculate the response of a dynamically coupled bridge-vehicle system using any vehicle model. An iterative procedure for the bridge-vehicle system was presented and was shown to converge for two different vehicle models.

The iterative method was applied to a parametric study of the importance of bridge-vehicle interaction. The errors involved in ignoring interaction were quantified. Criteria to assess whether or not interaction is important were developed. Interaction was shown to be unimportant for bridges with first natural frequencies more than double vehicle body bounce frequencies. Furthermore, bridges with smooth approaches were shown to have little interaction with light vehicles travelling at slow speeds.

In the next chapter, the iterative method will be applied to the problem of assessing the effects of heavy vehicle suspension design on bridge dynamic responses.

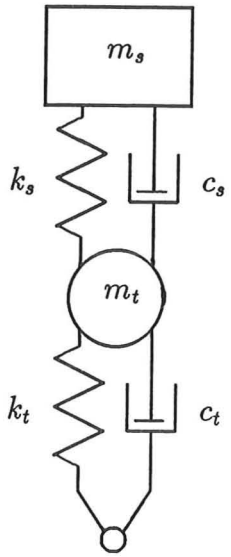

Figure 6.1: Two degree of freedom ('1/4 car') vehicle model

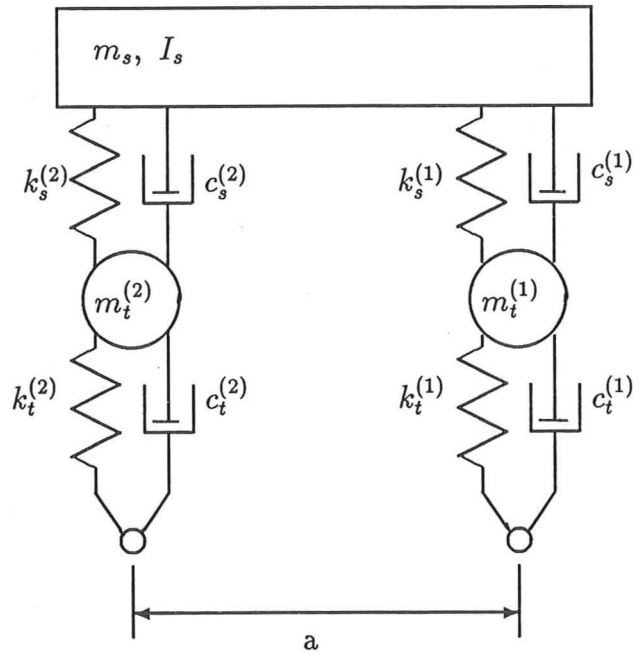

Figure 6.2: Two axle (4 degree of freedom, '1/2 car') vehicle model

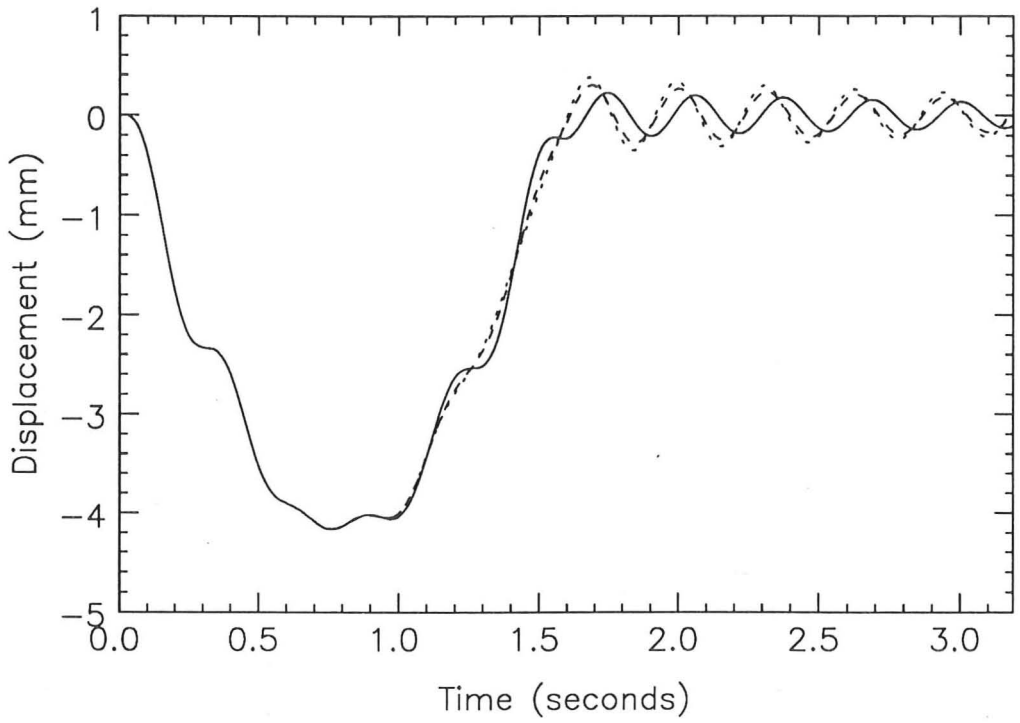

Figure 6.3: Midspan bridge deflection versus time
'1/4 car' model; $V = 25\text{m/s}$
Iteration 3 ————————
Iteration 4 . . . . . .
Iteration 5 _ _ _ _ _ _ _

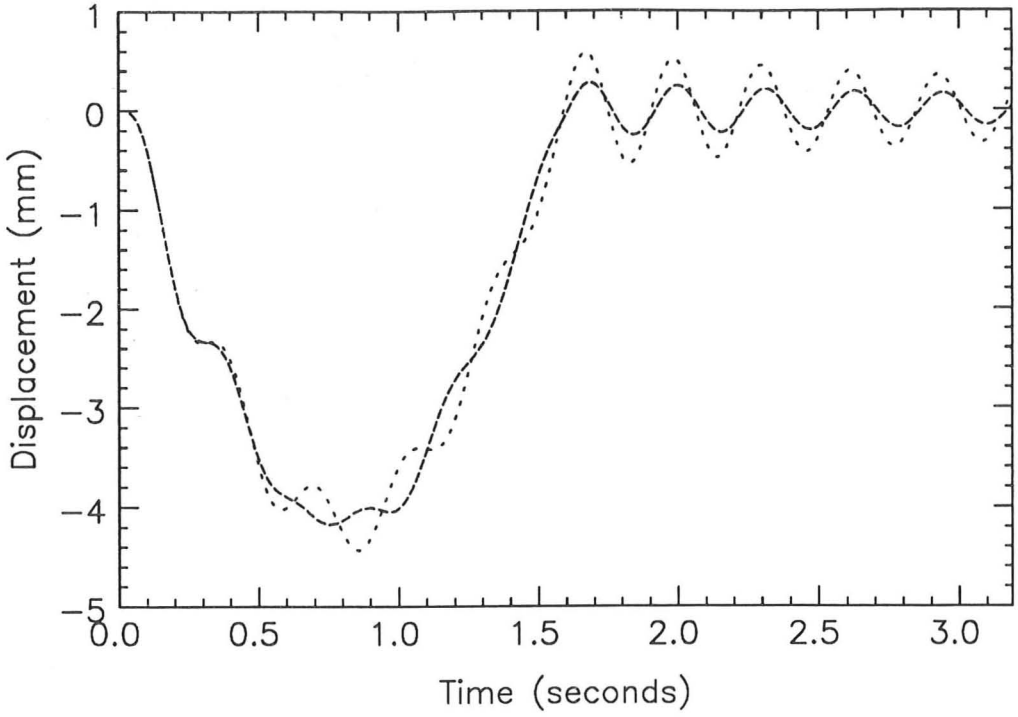

(a) $V = 25$ m/s; $\alpha = 0.1$

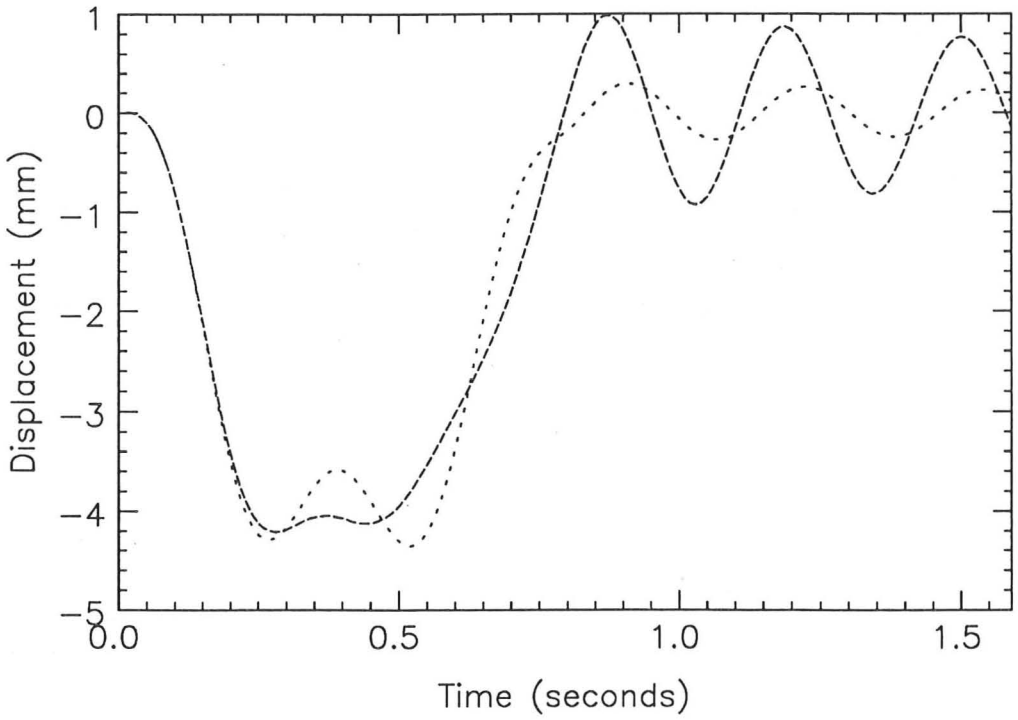

(b) $V = 50$ m/s; $\alpha = 0.2$

Figure 6.4: Midspan bridge deflection versus time
Single constant force . . . . . .
'1/4 car' vehicle _ _ _ _ _ _ _

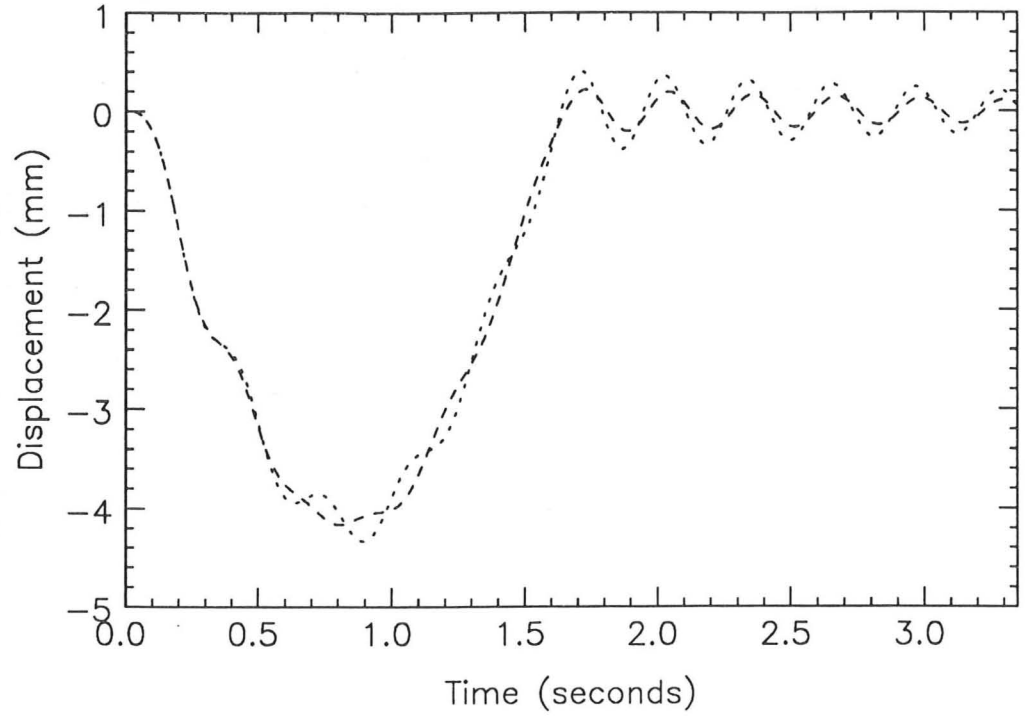

(a) $V = 25$ m/s; $\alpha = 0.1$

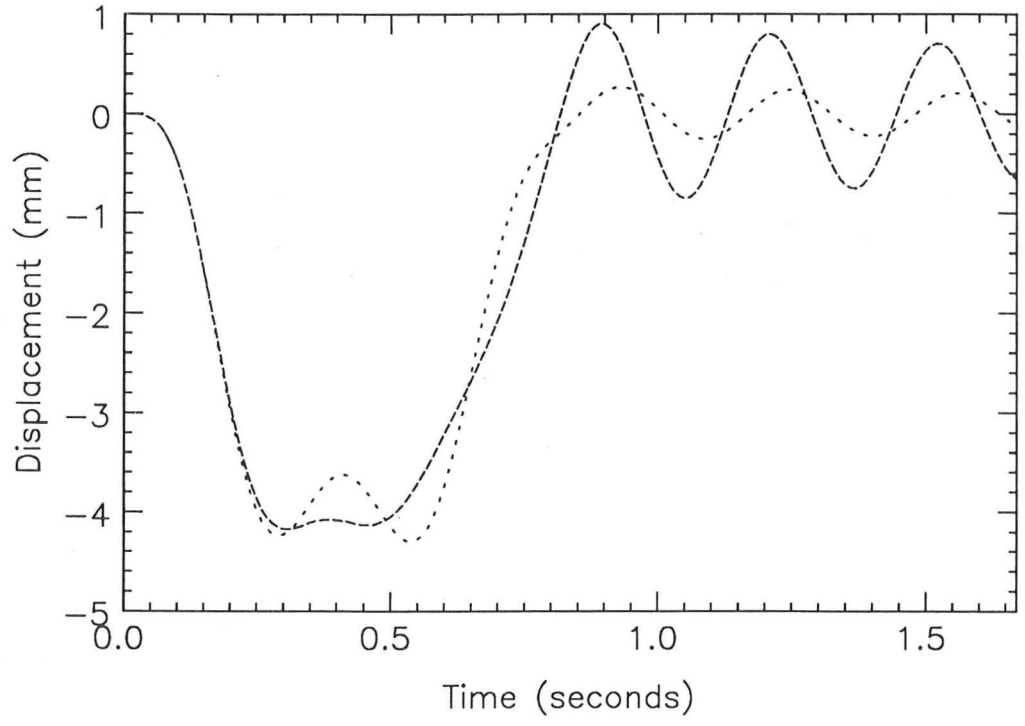

(b) $V = 50$ m/s; $\alpha = 0.2$

Figure 6.5: Midspan bridge deflection versus time
Two constant forces - - - - - - - - - -
'1/2 car' vehicle _ _ _ _ _ _ _

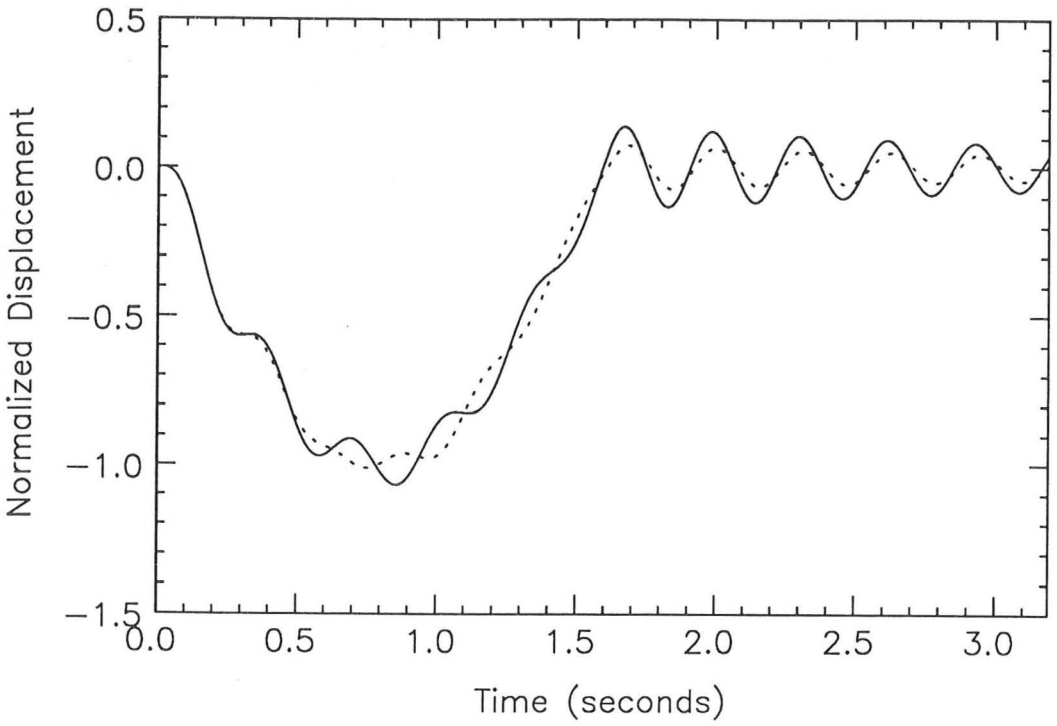

Figure 6.6: Midspan bridge deflection - interaction study
Constant force _____
Vehicle - - - - - - - - - -
$\alpha = 0.10$, $\kappa = 0.32$, $\zeta_v = 0.05$, $\zeta = 0.02$, $h_s = 0$

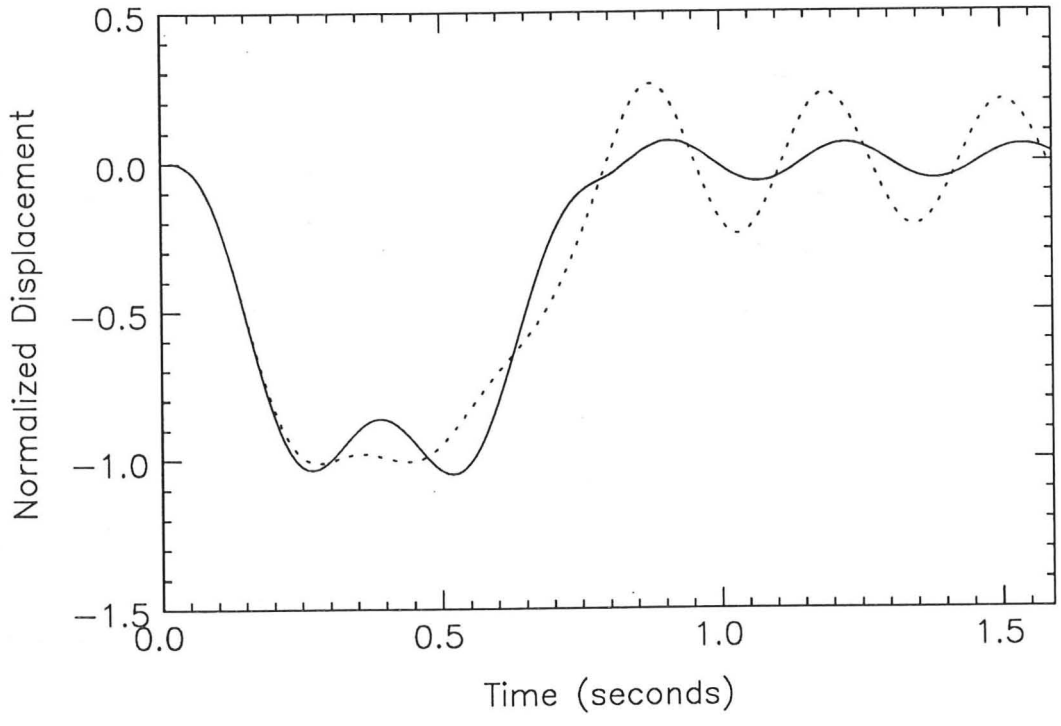

Figure 6.7: Midspan bridge deflection - interaction study
Constant force _____
Vehicle - - - - - - - - - -
$\alpha = 0.20$, $\kappa = 0.32$, $\zeta_v = 0.05$, $\zeta = 0.02$, $h_s = 0$

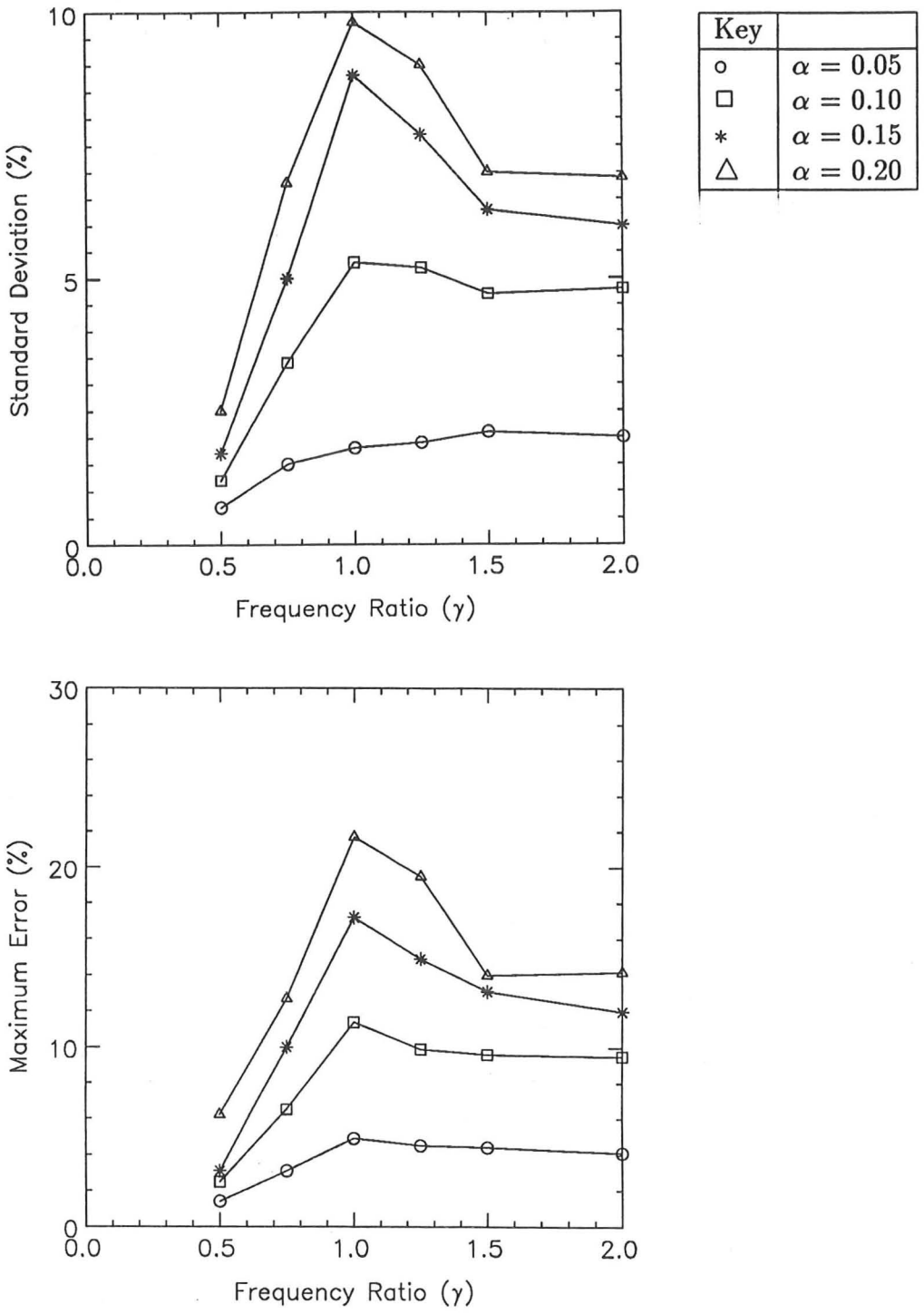

Figure 6.8: Error involved in ignoring bridge-vehicle interaction
Effect of speed parameter
$\kappa = 0.32$, $\zeta_v = 0.05$, $\zeta = 0.02$, $h_s = 0$

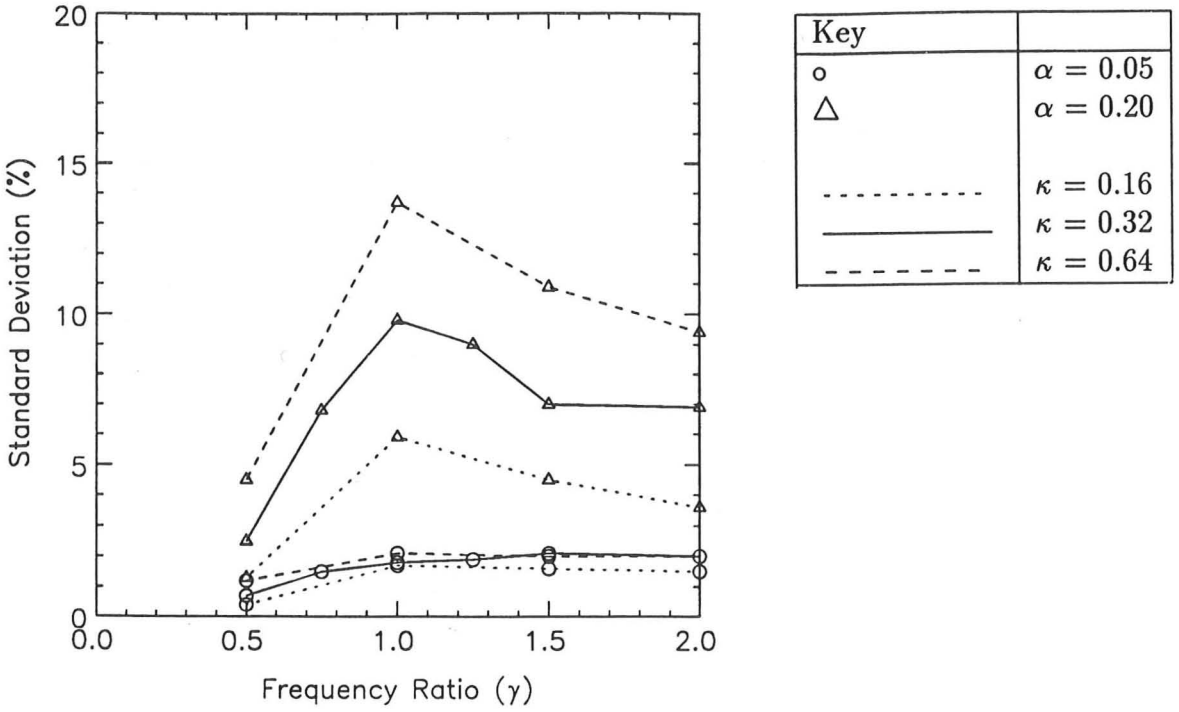

Figure 6.9: Error involved in ignoring bridge-vehicle interaction
Effect of mass ratio, κ
$\zeta_v = 0.05$, $\zeta = 0.02$, $h_s = 0$

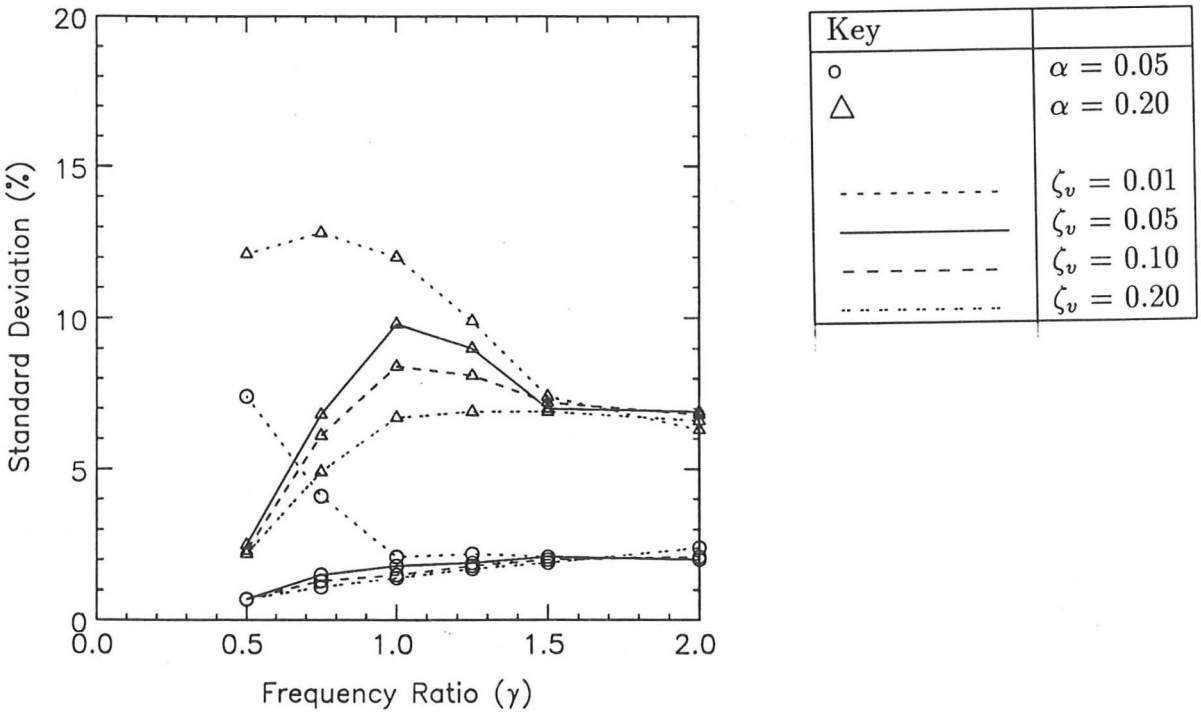

Figure 6.10: Error involved in ignoring bridge-vehicle interaction
Effect of vehicle damping, ζ_v
$\kappa = 0.32$, $\zeta = 0.02$, $h_s = 0$

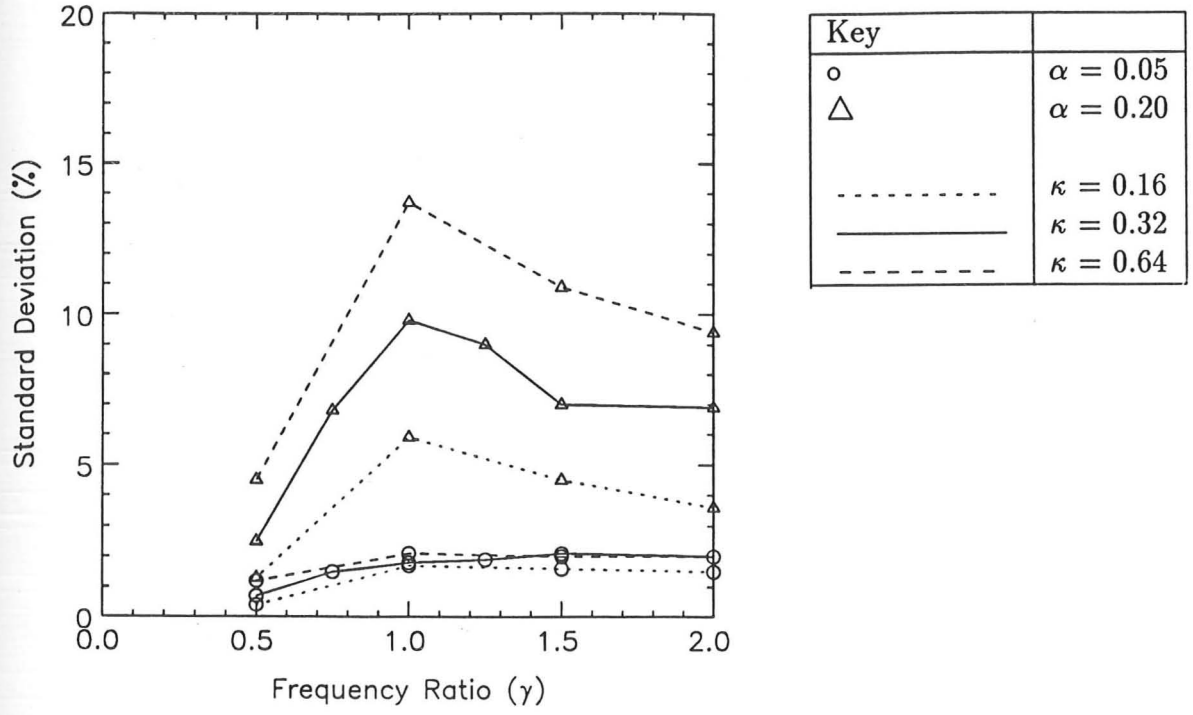

Figure 6.9: Error involved in ignoring bridge-vehicle interaction
Effect of mass ratio, κ
$\zeta_v = 0.05$, $\zeta = 0.02$, $h_s = 0$

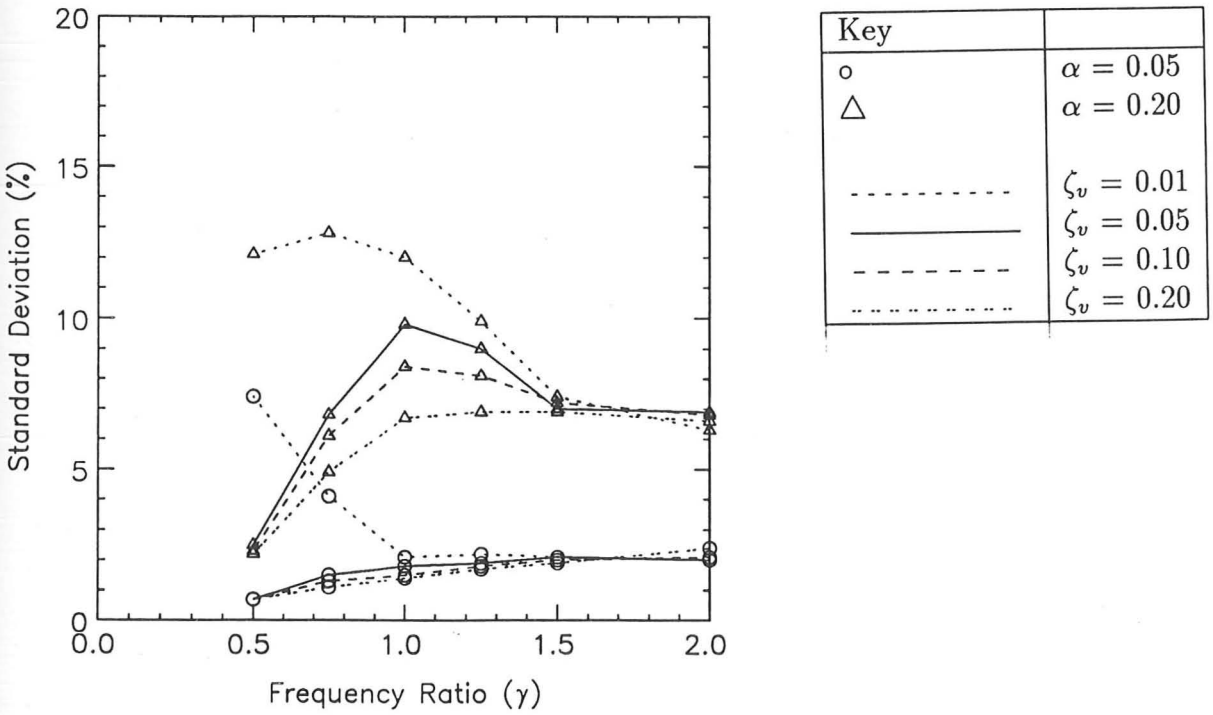

Figure 6.10: Error involved in ignoring bridge-vehicle interaction
Effect of vehicle damping, ζ_v
$\kappa = 0.32$, $\zeta = 0.02$, $h_s = 0$

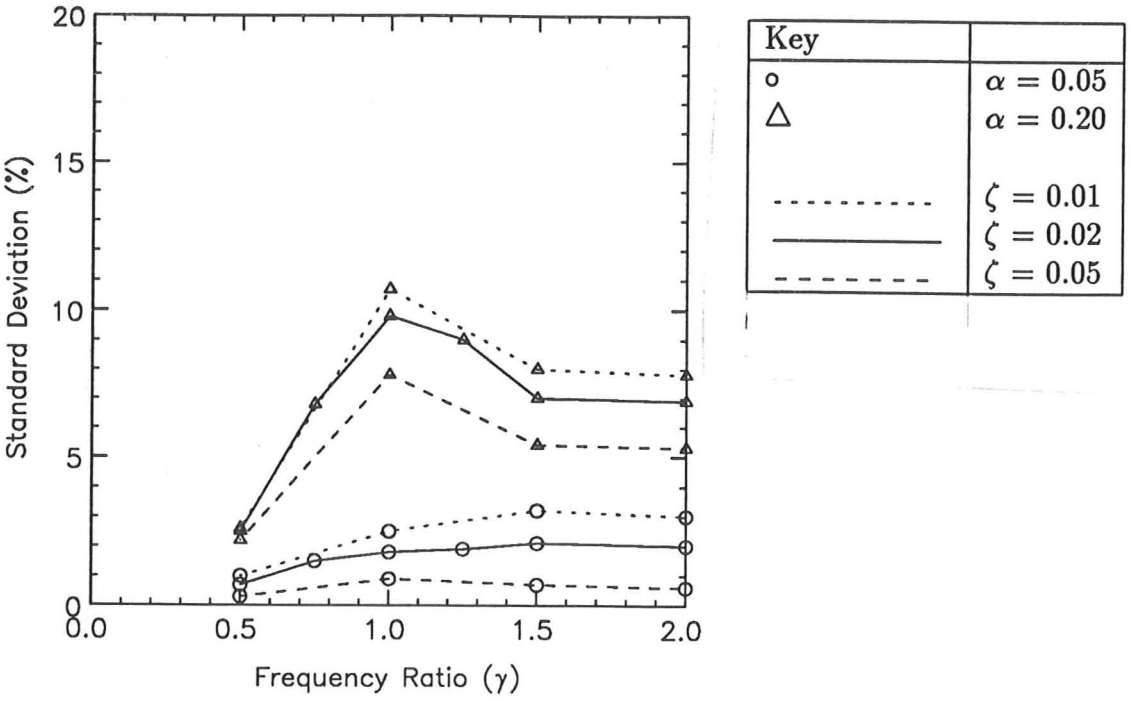

(a) $\zeta_v = 0.05$

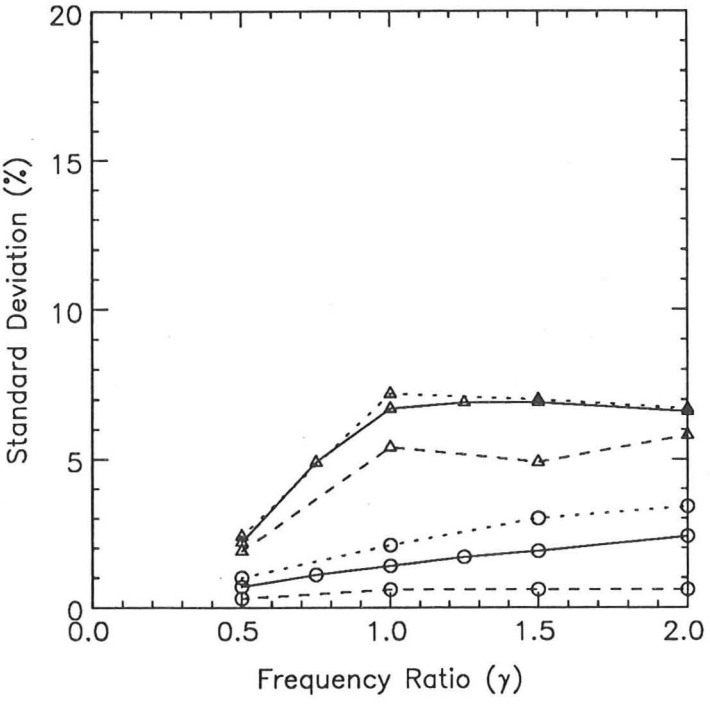

(b) $\zeta_v = 0.20$

Figure 6.11: Error involved in ignoring bridge-vehicle interaction
Effect of bridge damping, ζ
$\kappa = 0.32$, $h_s = 0$

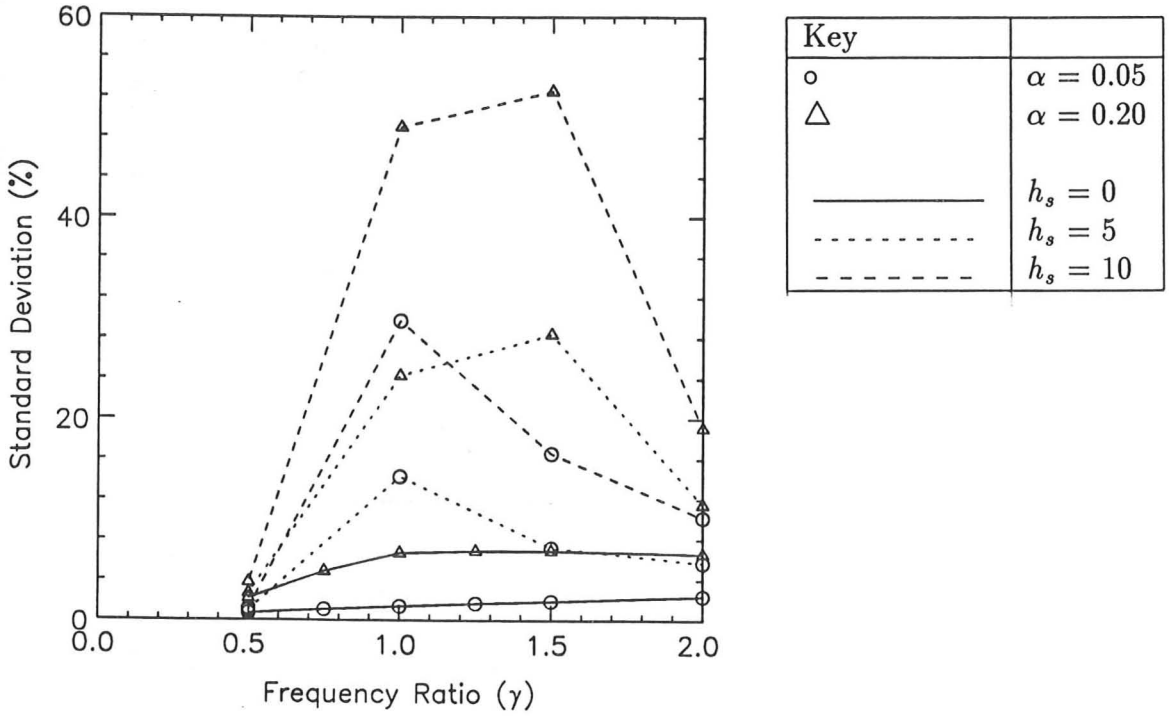

Figure 6.12: Error involved in ignoring bridge-vehicle interaction
Effect of step at bridge entrance, h_s
$\kappa = 0.32$, $\zeta_v = 0.20$, $\zeta = 0.02$

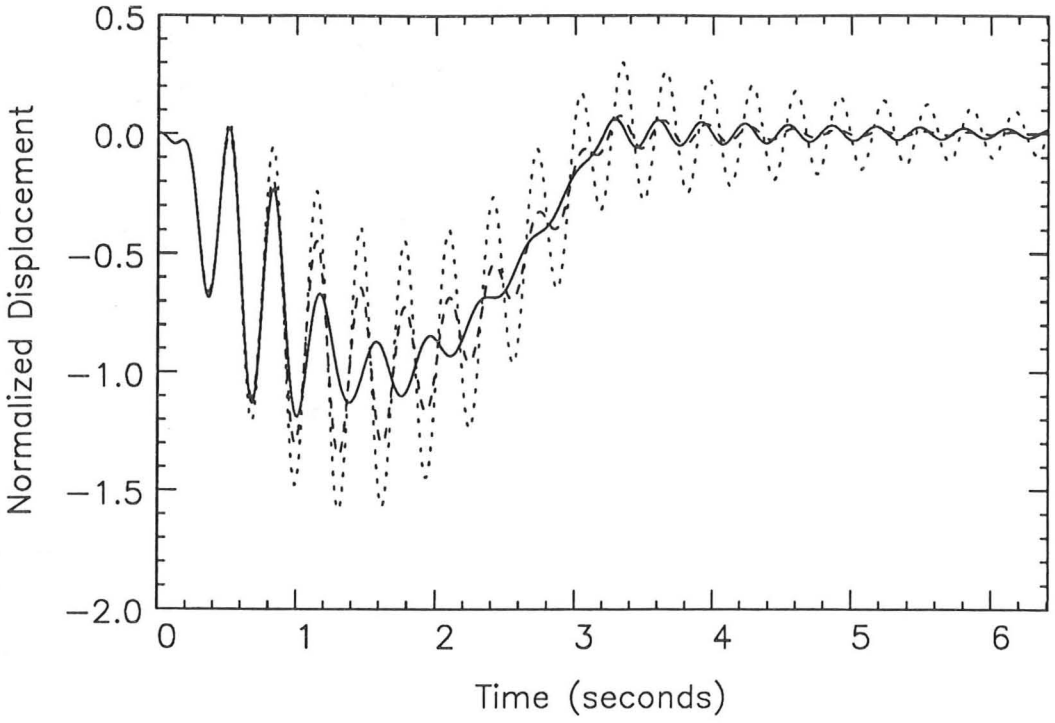

(a) $\alpha = 0.05$

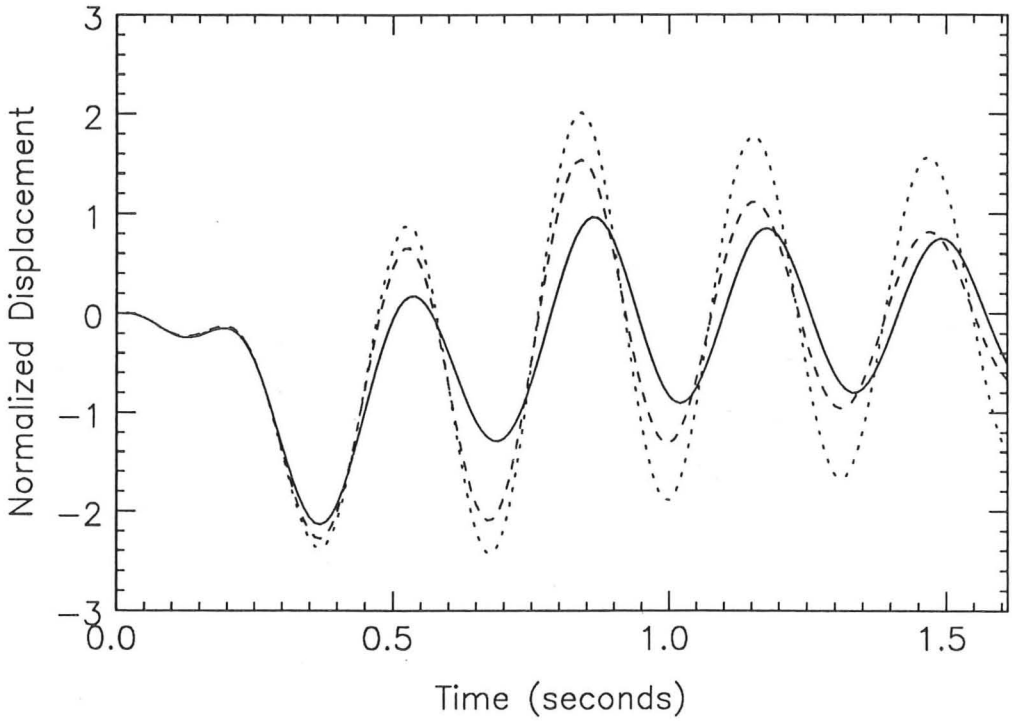

(b) $\alpha = 0.20$

Figure 6.13: Midspan bridge displacement
Iterative solution ($\zeta = 0.02$) ————————
Initial response ($\zeta = 0.02$) - - - - - - - - - -
Initial response ($\zeta = 0.05$) - - - - - - - -
$\kappa = 0.32$, $\zeta_v = 0.20$, $\gamma = 1.0$, $h_s = 10$

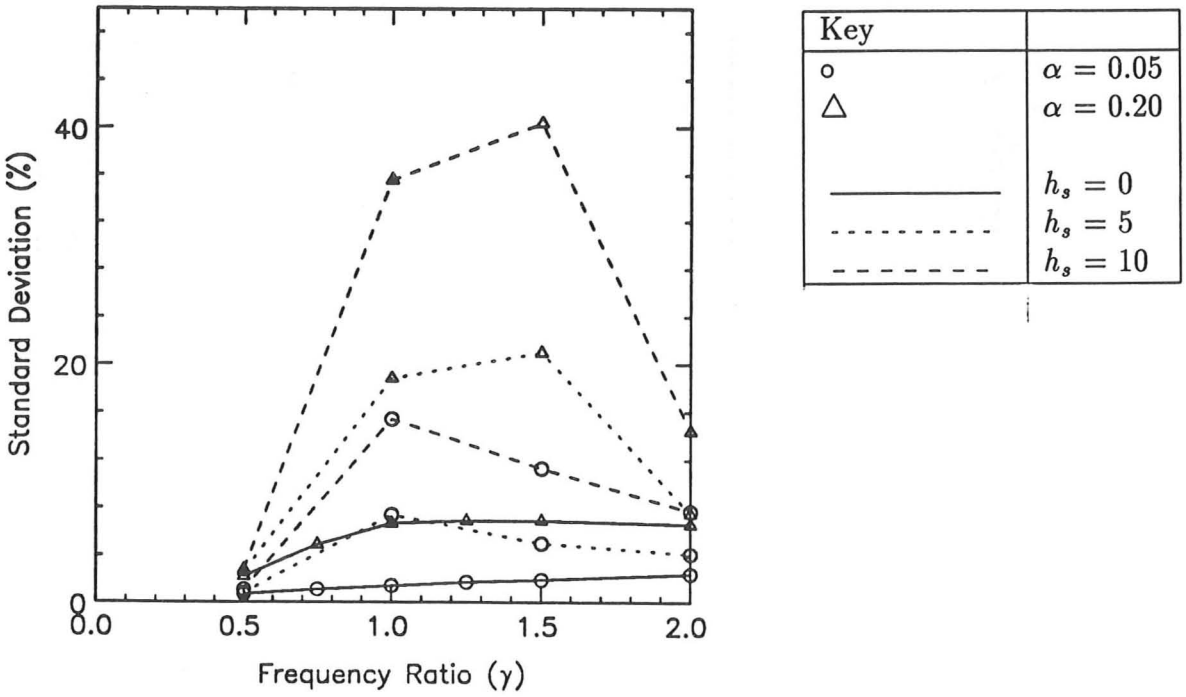

Figure 6.14: Error involved in ignoring bridge-vehicle interaction
Effect of step at bridge entrance, h_s
Bridge damping for no interaction, $\zeta = 0.05$
Bridge damping with interaction, $\zeta = 0.02$
$\kappa = 0.32$, $\zeta_v = 0.20$

EFFECTS OF VEHICLE SUSPENSION DESIGN ON BRIDGE DYNAMICS

7

This chapter considers the effects of leaf-spring and air-spring vehicle suspensions on bridge dynamic response.

7.1 General Parameters

7.1.1 Vehicle Models

Over the last few years, Cebon [17] and Cole [26] have developed a vehicle model which is representative of a typical, four axle, 32.5 tonne articulated vehicle in the U.K. Their model has 11 degrees of freedom as shown in figure 7.1. Non-linear suspension elements model the action of the leaf-springs and a schematic plot of the leaf-spring behaviour is shown on the figure. The model was validated [26, 27] by an extensive programme of field tests on the Transport and Road Research Laboratory test track, and the calculated dynamic wheel forces were found to agree very accurately with experimental measurements. This vehicle model was used, in this study, to investigate the effects of typical leaf-sprung vehicles on bridges.

In order to compare the effects of vehicle suspension design on bridge vibrations,

the model was modified to represent a vehicle with an air suspension. The leaf-spring elements on the drive axle and the two trailer axles were replaced with models of air springs. The suspension on the steer axle was the same for both vehicle models. The levelling beam on the trailer axles was discarded for the second vehicle model because air-springs in tandem suspensions are usually dynamically independent. The air suspension was of the popular trailing-arm type and the air-springs were modelled with the following equation [18]

$$F_{air} = F_{stat}\left[1 - \frac{A_x x}{V_0}\right]^{-\gamma_h} \tag{7.1}$$

where F_{air} is the air-spring force,

F_{stat} is the static force,

A_x is the cross-sectional area (0.045m^2),

V_0 is the static volume (0.020m^3),

x is the air-spring deflection,

and γ_h is the specified heat ratio (1.38).

The trailing arm lever ratio was 0.4.

Each vehicle model was two-dimensional, and represented only half of a typical vehicle. Cole [26, 27] showed that this is a reasonable approximation for predicting wheel loads. Nevertheless, the total mass of the vehicle is important for predicting the dynamic response of bridges. Therefore, the wheel loads from the two-dimensional vehicle models were doubled to simulate the passage of a fully laden vehicle over the bridges.

7.1.2 Bridge Models

Three bridges were chosen for the purposes of this parameter study. Two of the bridges were based on the validated models of the Drift Road and Lower Earley bridges. The third bridge was the simply-supported Pirton Lane bridge tested by TRRL [33, 63, 99] and described in section 2.2.5.

To simplify the calculations, the vehicles were assumed to have zero width and to apply dynamic wheels along the centre-line of the bridges. Bridge displacement responses were calculated at the midspan and quarter span of each bridge. Therefore,

only the flexural modes were included in the computations for the Drift Road bridge (see section 5.1.2), and only the mode shapes along the centre-line wheel path were included in the Lower Earley bridge model (see section 5.1.3).

7.1.3 Road Profiles

Two different road profiles were considered. For most of the results in this study, the surface profile was assumed to be smooth except for a 20mm step up at the entrance to each bridge. This step modelled differential settling of the abutments, or poorly maintained expansion joints. This author has not found any measurements of surface roughness on bridges in the U.K., but Honda and Kobori [47] measured the surface profile at expansion joints of approximately 400 bridges in Japan, and found three quarters of the bridges had a maximum roughness amplitude between 10 and 25mm.

For some trials, a pseudo random surface profile was used. This alternative profile was generated by applying the inverse DFT to a roughness spectrum as described by Cebon and Newland [17, 20]. Honda, Kajikawa, and Kobori [46, 47] measured the roughness on several hundred bridges in Japan and calculated roughness spectra. They found most bridges had medium to good surface profiles and could be classified by the same standards as used for roads in general.

The roughness spectrum used to calculate the pseudo random surface profile was chosen to be typical of a 'good' road surface in the U.K. according to the two index spectral description used by Cebon [17] and proposed by Anon [3]. Figure 7.2 shows the actual profile used. Position zero on the plot is the entrance to the bridge. The maximum roughness amplitude is approximately 10mm which is large in compared with dynamic deflections of bridges (usually less than 5mm). However, the measurements by Honda and Kobori [47] indicate that short wavelength roughness can have deviations from the average profile as large as 60mm.

7.1.4 Speed

Six different vehicle speeds were chosen for this study: 10, 15, 20, 25, 30, and 40m/s. Speeds of 25 and 30m/s are typical of motorways. Although 40m/s is faster than the legal maximum in the U.K., it provides information on the dynamic effects at higher speeds.

7.2 Results

Bridge responses were calculated for most combinations of the parameters outlined in the previous section. All three bridges were combined with both vehicles at all six speeds for the first road profile (20mm step) while for the pseudo random roughness profile only speeds of 15m/s and 40m/s were considered.

7.2.1 Bridge Responses

Figures 7.3 to 7.8 show bridge responses at three different speeds. The horizontal axis on all the plots is the position of the steer axle of the vehicle, with the entrance to the bridge defined as position zero. The solid curves were obtained for a speed of 1m/s and represent the quasi-static bridge responses. The dotted and dashed curves show midspan bridge displacements for speeds of 15 and 40m/s, respectively. The top plots of on the six figures illustrate the effects of the leaf-sprung vehicle while the responses to the air suspended vehicle are contained in the lower plots. Figures 7.3 to 7.5 shows bridge responses using the step road profile while figures 7.6 to 7.8 contain responses calculated with the pseudo random road profile.

For the Drift Road and Lower Earley bridges the responses are relatively small, but the responses increase with speed. On the other hand, the Pirton Lane bridge shows much larger responses which also increase with speed. The Pirton Lane bridge has a lower first natural frequency (3.2Hz) than either the Drift Road (6.8Hz) or Lower Earley (5.7Hz) bridges. Therefore, larger responses are expected on the Pirton Lane bridge because the bridge natural frequency is closer to the natural frequencies

of the vehicles.

In contrast to the plots for the leaf-sprung vehicle, the lower three plots of figures 7.3 to 7.5 show the dynamic bridge responses obtained for the air-sprung vehicle. The dynamic responses are much smaller and are actually quite close to the static bridge responses except for the highest speed on the Pirton Lane bridge. This indicates little interaction between these three bridges and the air-sprung vehicle.

The air-sprung vehicle reduces dynamic response for two reasons. Firstly, the air-sprung vehicle has lower natural frequencies than the leaf-sprung vehicle and part of the reason it does not excite the Pirton Lane bridge as much is that frequency matching does not occur. The responses are reduced on the other two bridges because the air-sprung suspension applies smaller dynamic loads.

Figures 7.6 to 7.8 illustrate midspan bridge responses calculated with the pseudo random roughness surface profile. For the leaf-sprung vehicle, the dynamic responses of the Lower Earley and Pirton Lane bridges are qualitatively similar to the responses to the step. The dynamic responses of the Drift Road bridge (figure 7.6) are much larger than for the step profile. This increased response occurs because the Drift Road bridge has a short side span leading up to the instrumented span. The mode shape values on the shorter span are relatively small (see section 5.1.2) and with a step at the bridge entrance, the largest vehicle loads occur on the shorter span. Therefore, the dynamic responses are noticeably larger with the rough surface profile because it excites the vehicle throughout the passage over the bridge. The other two bridges exhibit slightly larger dynamic responses throughout the whole vehicle passage time because of continual excitation of the vehicle by the rough surface.

To compare the two vehicle suspensions, consider the lower three plots of figures 7.6 to 7.8. The dynamic responses of all three bridges to the air suspended vehicle are again considerably less than for the leaf-spring vehicle. The reduction in response is most noticeable on the Pirton Lane bridge (figure 7.8) which exhibited the largest responses with the leaf-sprung vehicle. The air-spring suspension effectively acts as a dynamic vibration absorber and reduces the bridge vibrations.

Air-spring vehicle suspensions cause lower dynamic responses on bridges because

they have natural frequencies (usually below 2Hz) which are lower than first natural frequencies of most highway bridges, and also because they apply smaller dynamic loads to the bridges. In addition, they are more heavily damped than leaf-spring suspensions and this tends to reduce dynamics.

7.2.2 Dynamic Response Increments

In order to quantify the comparison between the two different suspensions, dynamic response increments were calculated (see section 3.1.3).

The pseudo random profile was not included in this quantitative analysis because the use of a particular pseudo random profile would bias the results in ways that may not be representative of a typical bridge. A quantitative analysis considering such roughness would require simulation of the response of the bridges to many such profiles to obtain a proper statistical representation. Time constraints prevented this.

The maximum bridge displacement response increment for each parameter combination with the step surface profile was computed and the results are shown in figure 7.9. In the examination of these plots, three major features were noticed

Frequency: The Pirton Lane bridge has the largest dynamic increments at all speeds for both vehicles. This bridge has a natural frequency at 3.2Hz which is close to the dynamic wheel load frequencies generated by the vehicles. Therefore, matching of the bridge and vehicle frequencies increases the dynamic response of the bridge. This agrees with other research [8, 14]. The other two bridges show similar increments to each other because they have higher first natural frequencies (5.7 and 6.8Hz).

Suspensions: The simulated responses to the air suspended vehicle are significantly less than for the steel suspensions. The maximum dynamic response increments for the air suspension are below 10%

while those for the steel suspension are as high as 50%. The air suspension applies lower dynamic wheel loads to the bridges and also has more damping. These two factors combine to reduce the bridge dynamic responses to the air suspended vehicle.

Speed: Peaks at certain speeds are evident on all the dynamic response increment plots. These peaks are caused by a combination of factors including the vehicle speed, axle spacing, and natural frequencies of both the bridge and the vehicle. The largest increments occur when these factors combine to produce a maximum of the dynamic bridge response in phase with the maximum quasi-static bridge response. This effect is evident on the upper plot of figure 7.4. At a speed of 15m/s the dynamic response is in phase with the quasi-static and results in a relatively large dynamic response increment. On the other hand, the dynamic response at 40m/s is out of phase with the quasi-static response and a much lower dynamic increment is the result.

Although maximum dynamic increments are a conventional measure of bridge vibration, are widely quoted in the literature (see section 3.1.3) , and also correspond closely with conventional practices for design against bridge dynamics (Appendix A), these plots show some of their deficiencies as a measure of dynamic response. Consider the increment plots for the Lower Earley bridge. At a speed of 40m/s, the dynamic increment for the steel suspension is almost zero, but approximately 6% for the air suspension. From this information, it might be concluded that there is no dynamic bridge response with the steel suspension and more with the air suspension. An examination of the response plots for this case (figure 7.4), however, reveals the opposite. The dynamic response is actually significantly larger with the leaf-sprung vehicle than with the air-sprung vehicle, but the bridge response caused by the leaf-spring suspension has a local minimum at the position of maximum static response. This results in the maximum dynamic response being less than the maximum static

response. The dynamics may still be important for design against fatigue where stress cycles and not maximum levels are important. Therefore, better measures of the importance of dynamic response need to be developed. Some possibilities include the average (rms) deviation of the dynamic response from the quasi-static response, the ratio of the magnitude of the largest dynamic cycle to the maximum static deflection, or a more complicated formula based on a fatigue damage calculation. Even so, the maximum dynamic response increment provides a useful measure for estimating maximum responses and designing against overloads.

7.3 Conclusions

This study has shown that the air-sprung vehicle produced smaller theoretical dynamic responses than the leaf-sprung vehicle on all three bridges. The largest dynamic responses were observed for the bridge with a 3.2Hz natural frequency.

Air-sprung vehicles cause lower dynamic responses on bridges because they have lower natural frequencies than most highway bridges, because they apply smaller dynamic loads to the bridges, and also because they are more heavily damped than leaf-spring suspensions. Based on the theoretical analysis performed here, there is tentative evidence to suggest that air-sprung vehicles could be allowed to carry larger loads than vehicles with leaf-spring suspensions.

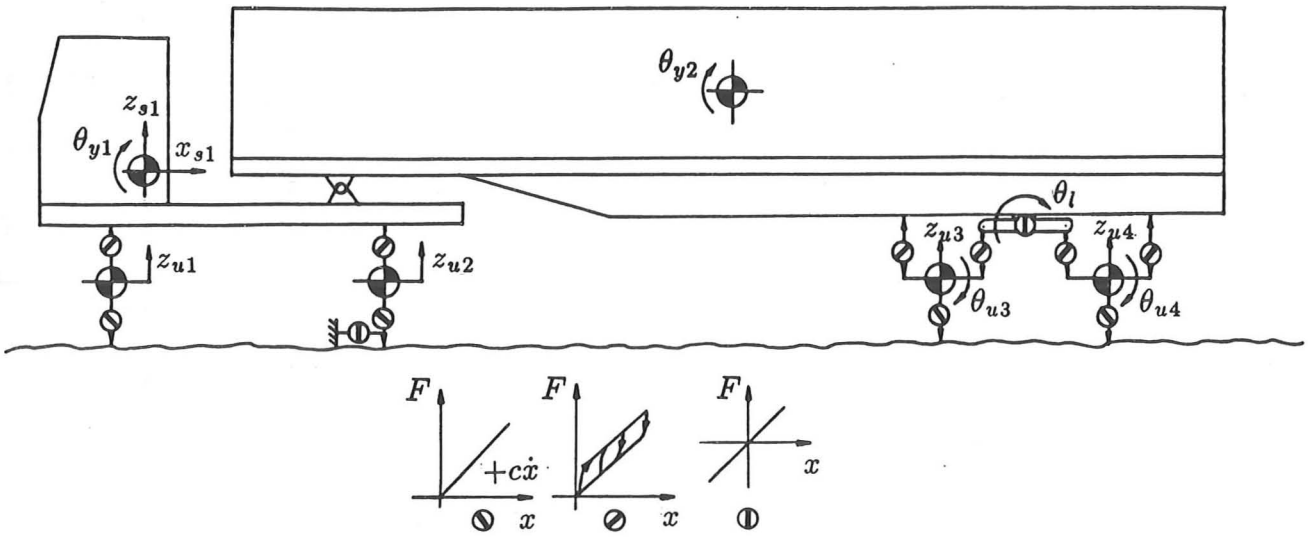

Figure 7.1: 11 degree of freedom, two-dimensional tractor and trailer vehicle model with leaf-spring suspensions. (After Cole [17])

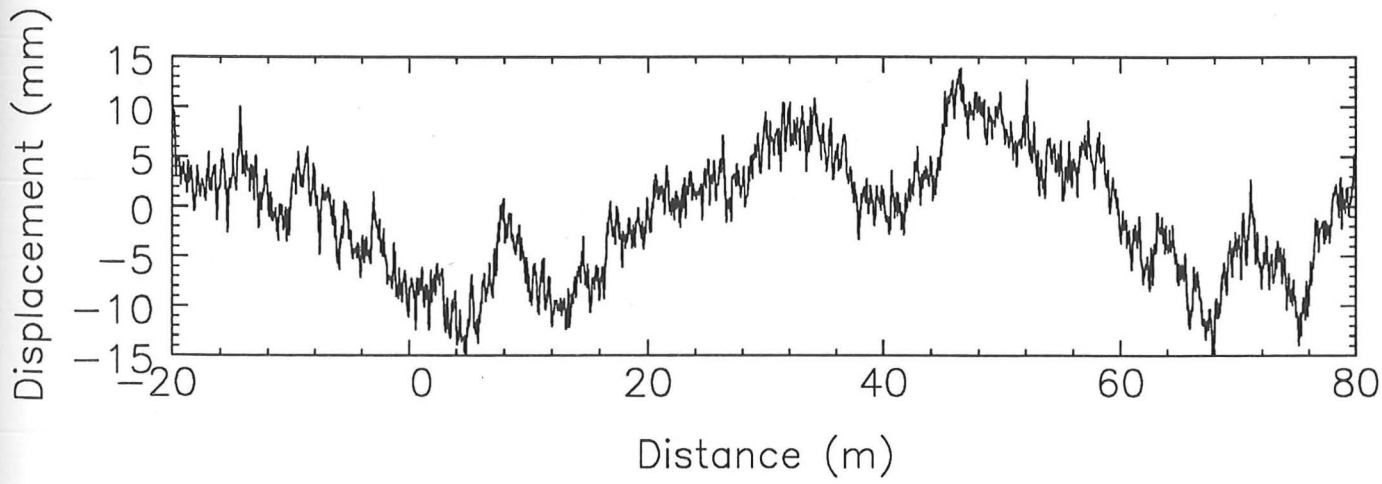

Figure 7.2: Pseudo random bridge surface roughness corresponding to a good road. The bridge entrance is located at position zero.

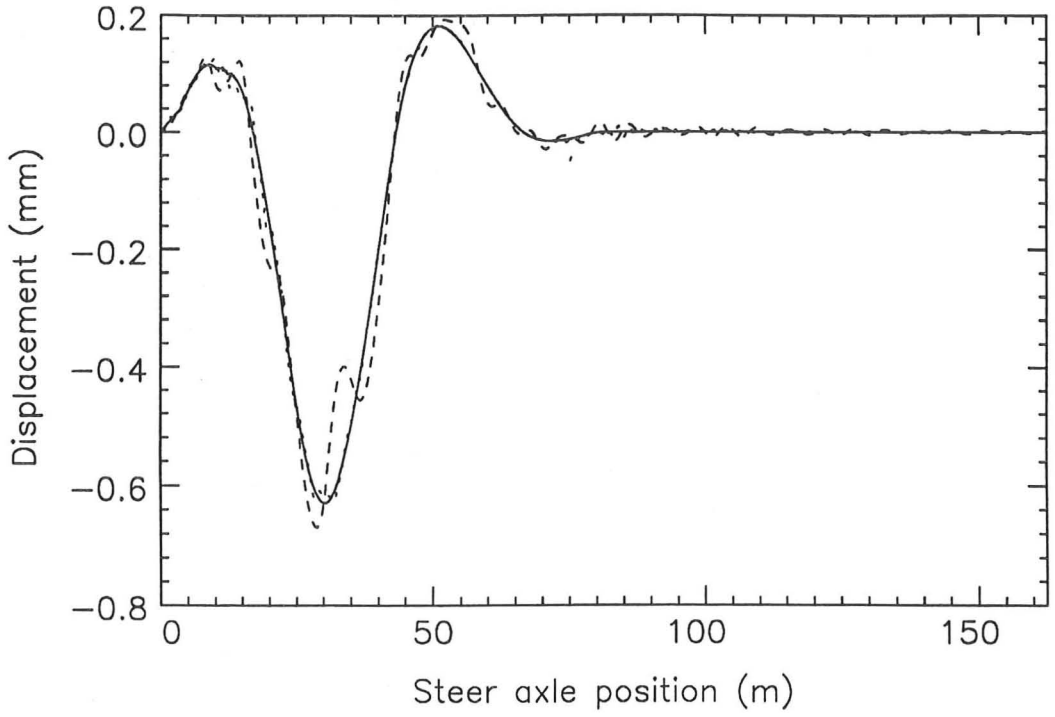

(a) Response to vehicle with leaf-springs

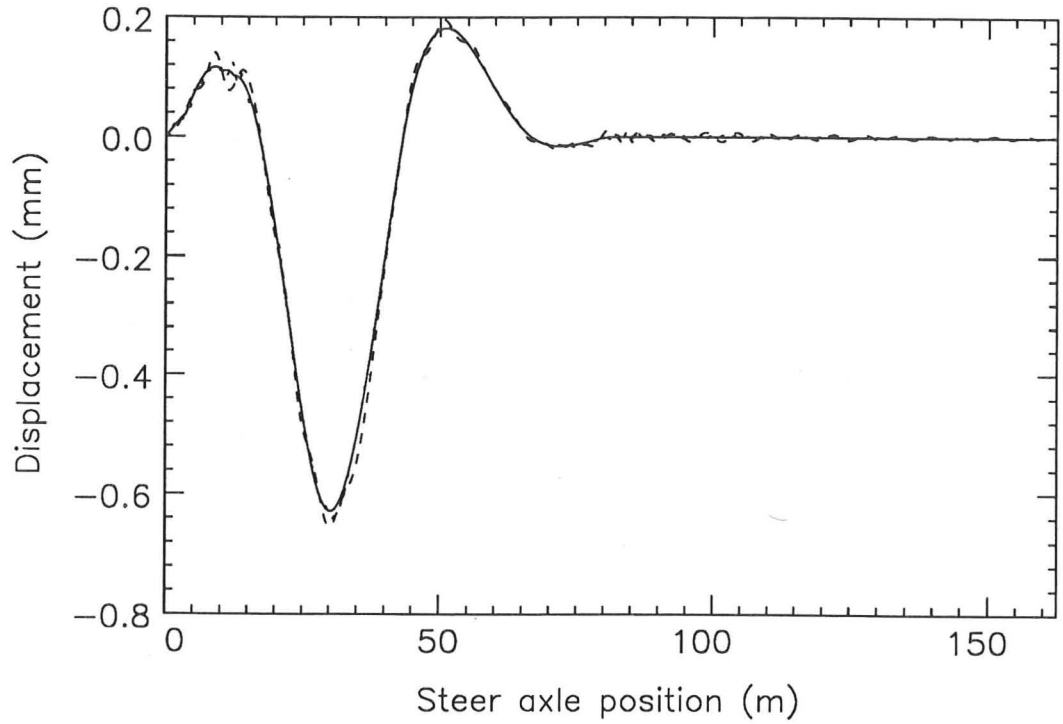

(b) Response to vehicle with air-springs

Figure 7.3: Drift Road bridge - Midspan displacements at three speeds.
20mm step at bridge entrance
1m/s (quasi-static) ————
15m/s - - - - - - - - - 40m/s - - - - - - -

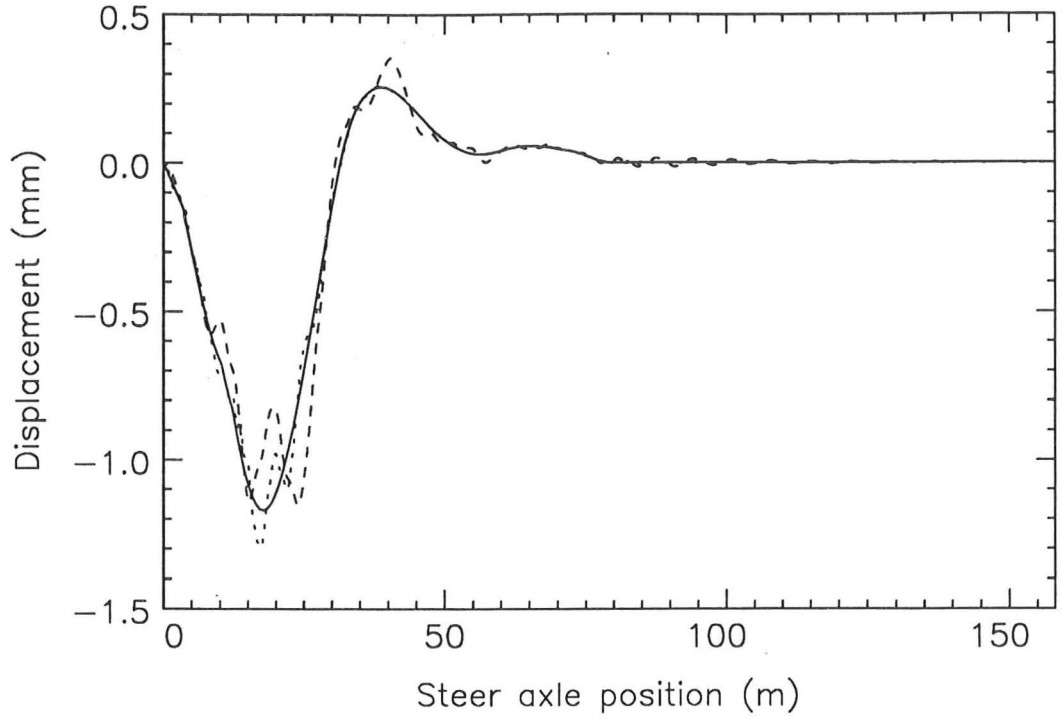

(a) Response to vehicle with leaf-springs

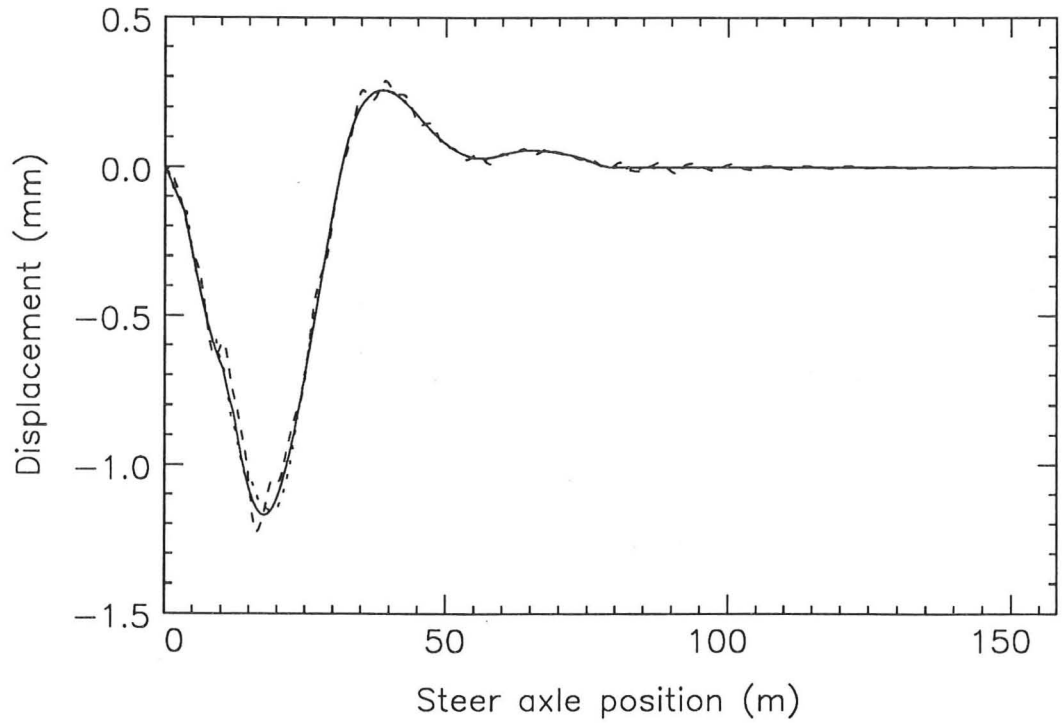

(b) Response to vehicle with air-springs

Figure 7.4: Lower Earley bridge - Midspan displacements at three speeds.
20mm step at bridge entrance
1m/s (quasi-static) ————————
15m/s - - - - - - - - - - 40m/s - - - - - - -

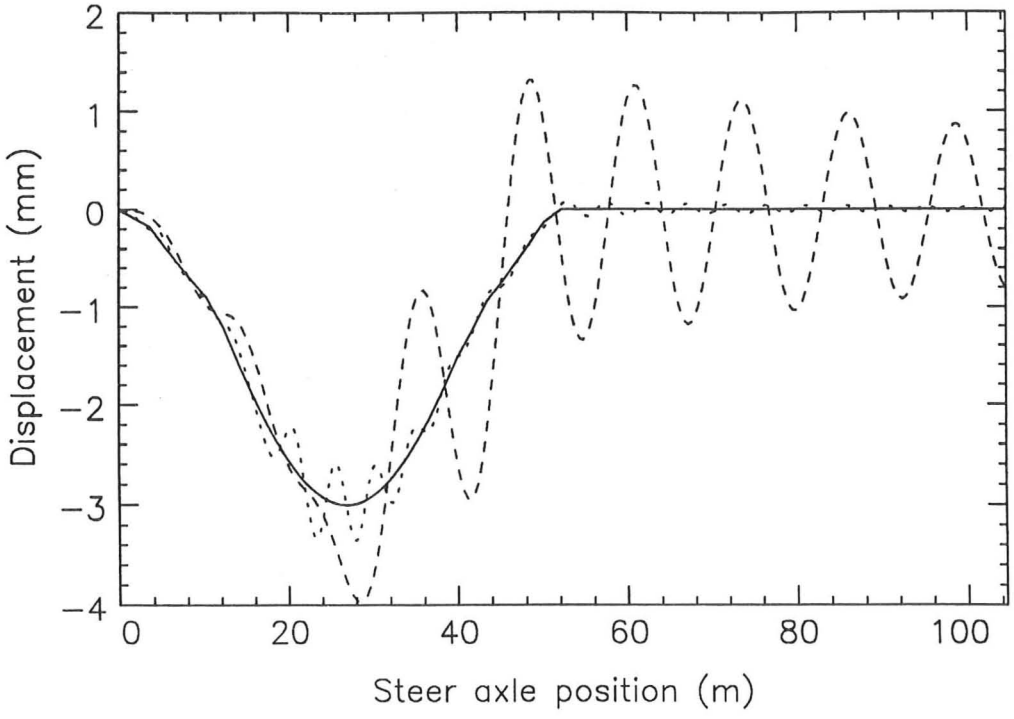

(a) Response to vehicle with leaf-springs

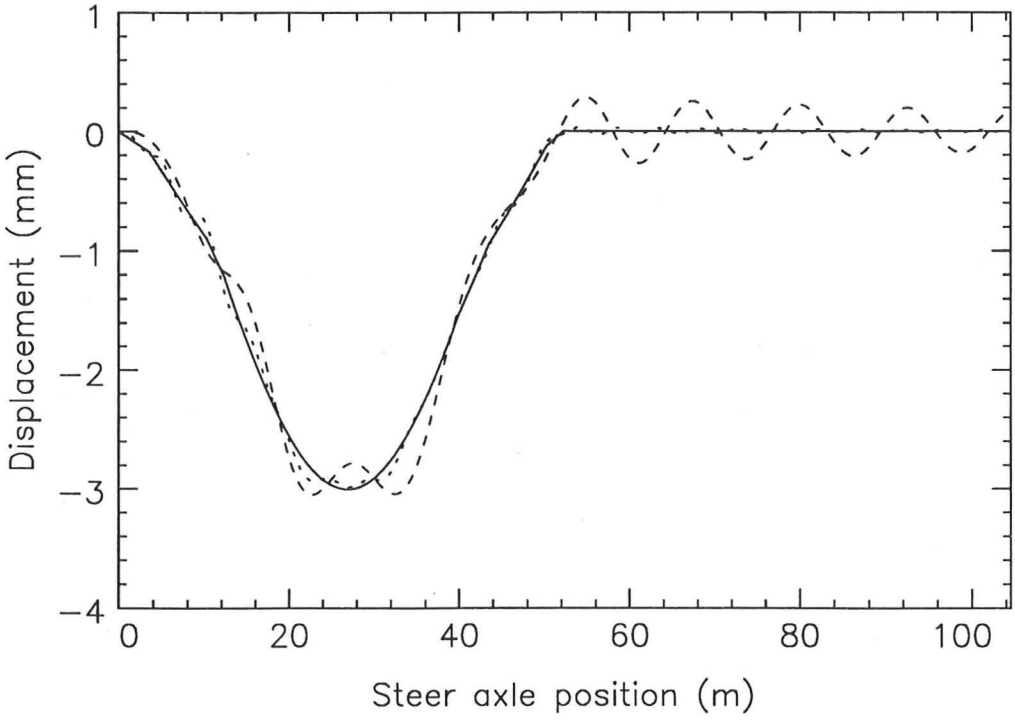

(b) Response to vehicle with air-springs

Figure 7.5: Pirton Lane bridge - Midspan displacements at three speeds.
20mm step at bridge entrance
1m/s (quasi-static) ————————
15m/s - - - - - - - - - - 40m/s - - - - - - -

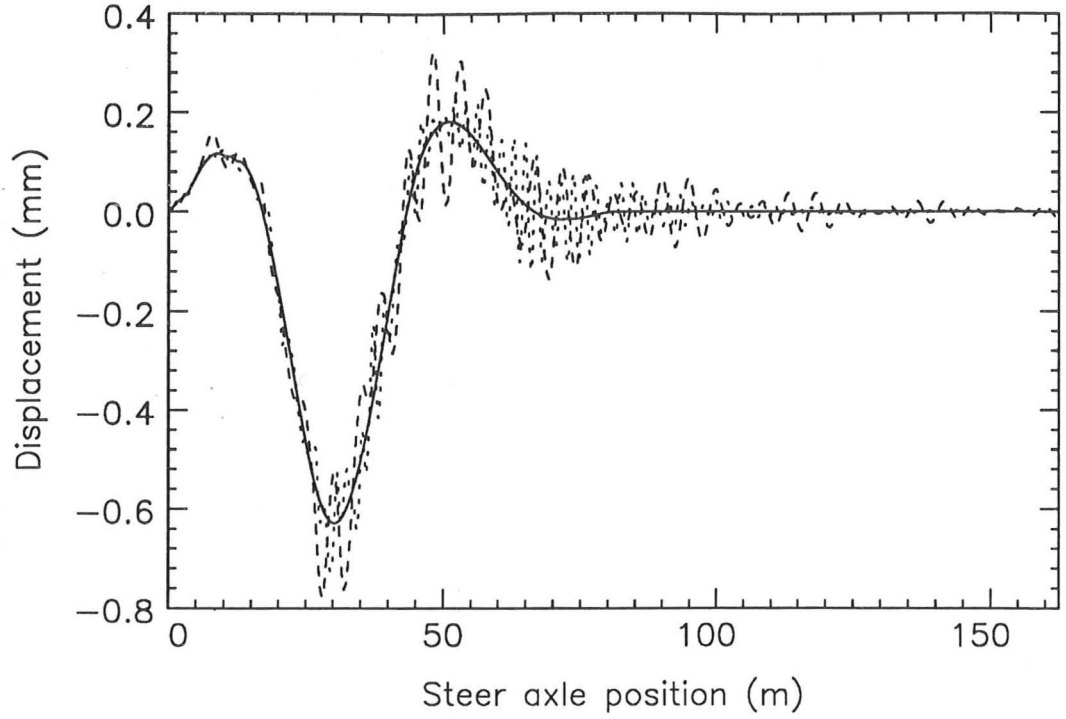

(a) Response to vehicle with leaf-springs

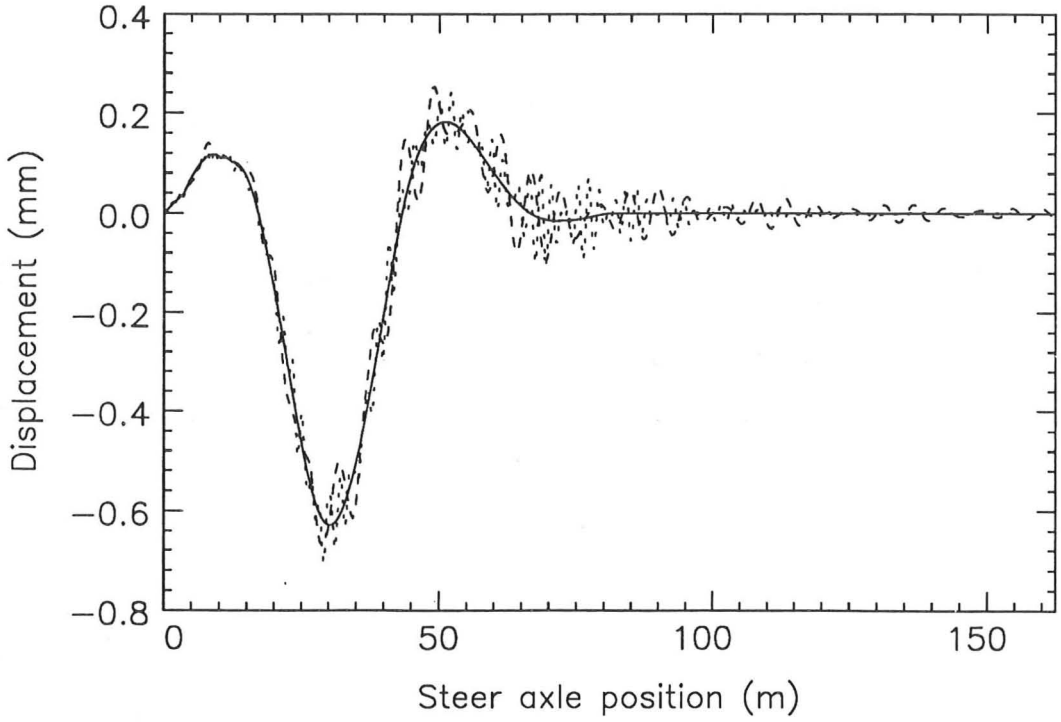

(b) Response to vehicle with air-springs

Figure 7.6: Drift Road bridge - Midspan displacements at three speeds.
Pseudo random surface profile
1m/s (quasi-static) ————————
15m/s - - - - - - - - - - 40m/s - - - - - - -

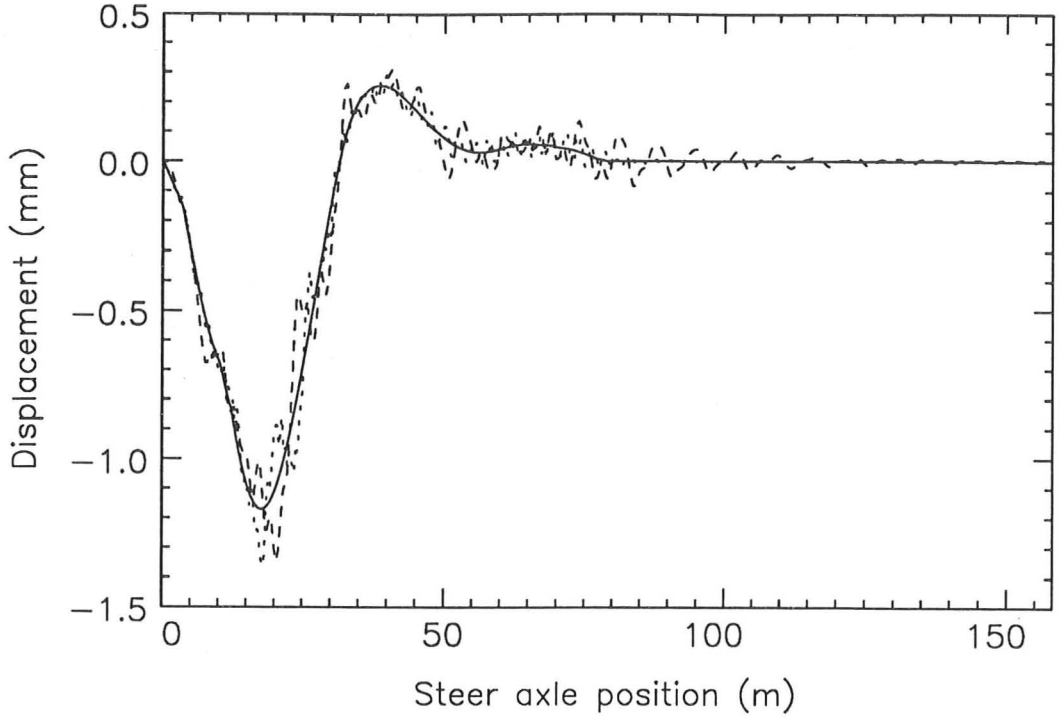

(a) Response to vehicle with leaf-springs

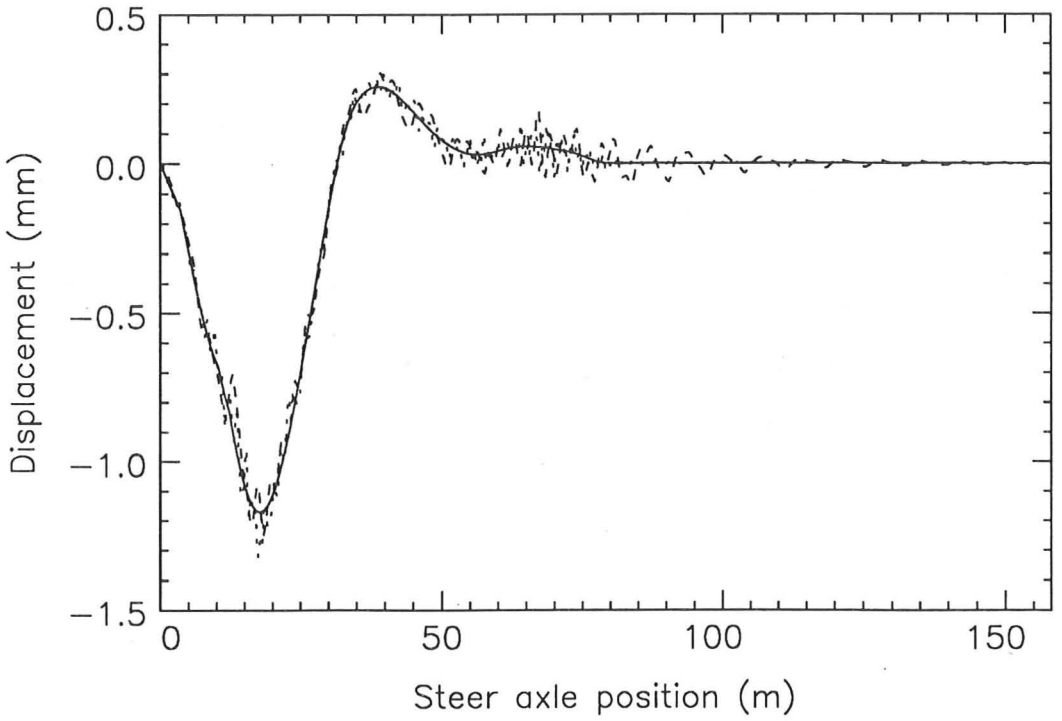

(b) Response to vehicle with air-springs

Figure 7.7: Lower Earley bridge - Midspan displacements at three speeds.
Pseudo random surface profile
1m/s (quasi-static) ————————
15m/s . . . . . 40m/s - - - - - - -

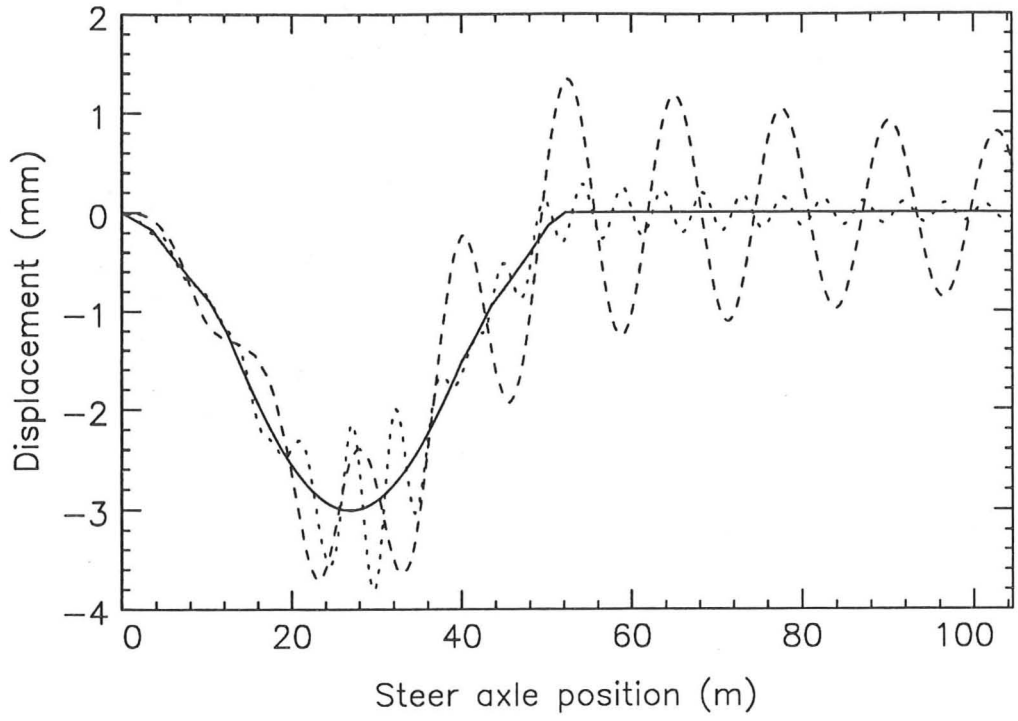

(a) Response to vehicle with leaf-springs

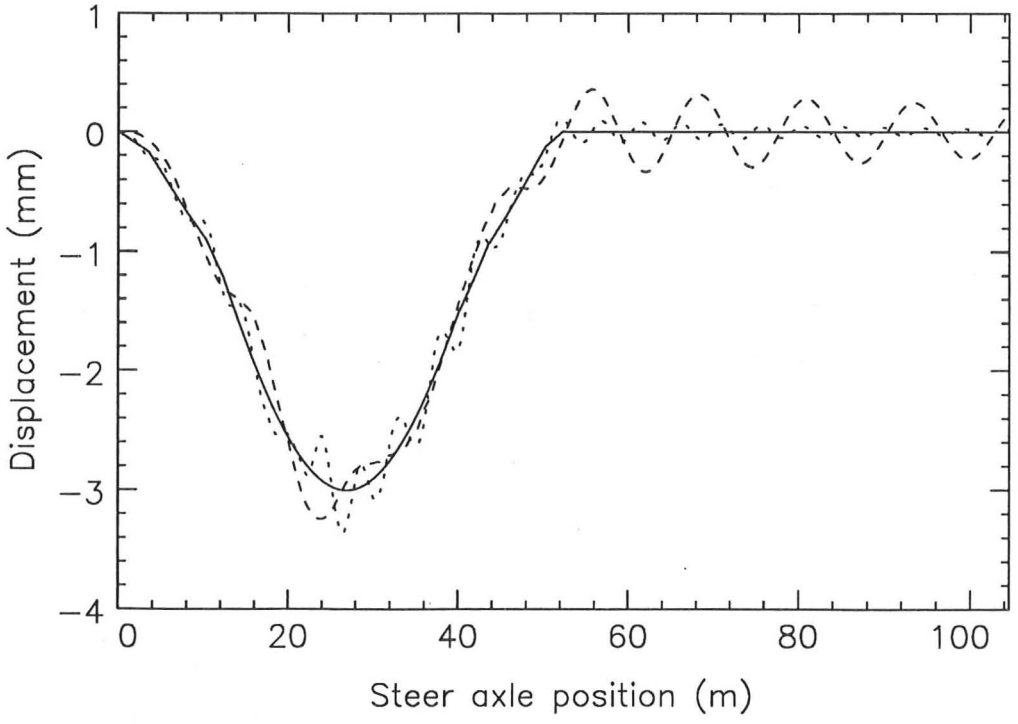

(b) Response to vehicle with air-springs

Figure 7.8: Pirton Lane bridge - Midspan displacements at three speeds.
Pseudo random surface profile
1m/s (quasi-static) ————————
15m/s . . . . . 40m/s - - - - - - -

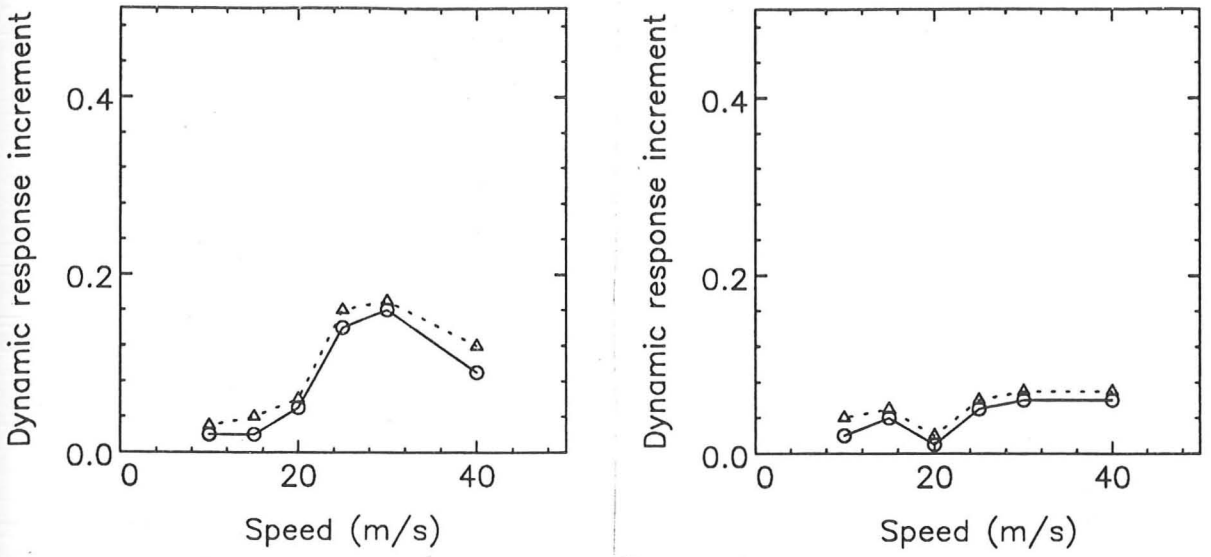

(a) Drift Road (leaf-spring)

(b) Drift Road (air-spring)

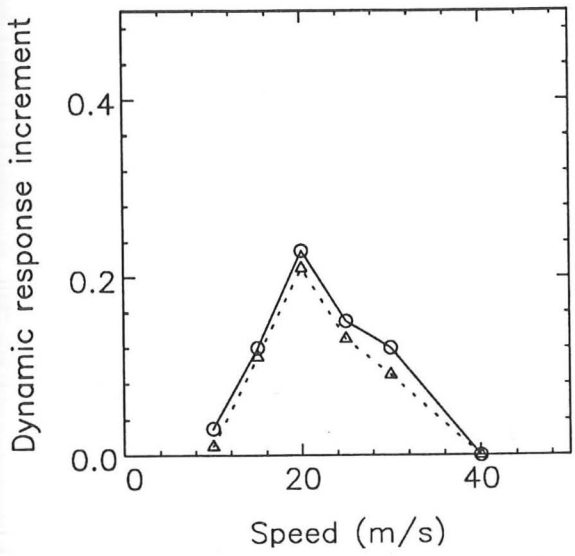

(c) Lower Earley (leaf-spring)

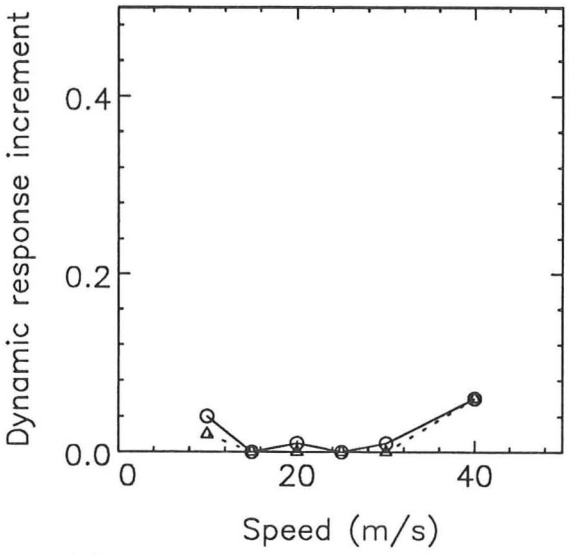

(d) Lower Earley (air-spring)

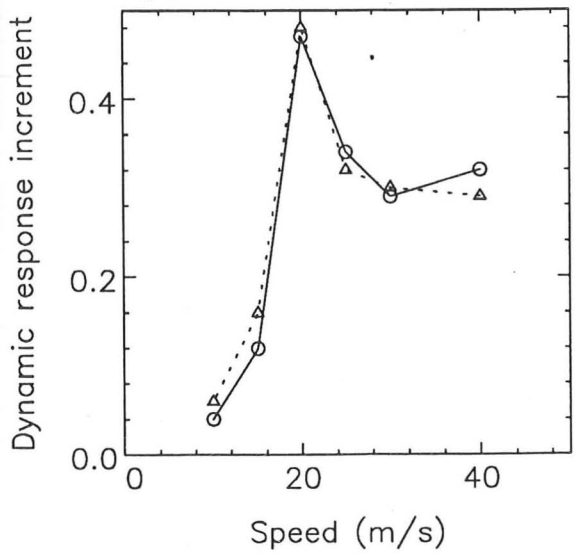

(e) Pirton Lane (leaf-spring)

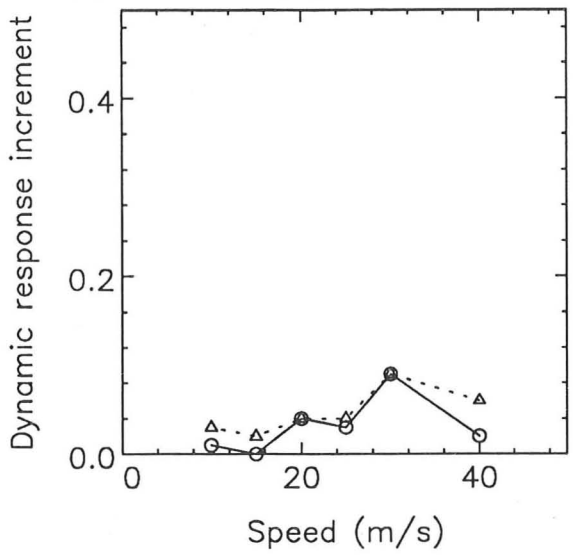

(f) Pirton Lane (air-spring)

Figure 7.9: Maximum dynamic response increments (displacement)
20mm step at bridge entrance
Response at midspan ————————
Response at 1/4 span - - - - - - - - - -

8 CONCLUSIONS AND RECOMMENDATIONS FOR FURTHER WORK

8.1 Conclusions

The dynamic response of short-span highway bridges to heavy vehicle loads has been described mathematically, and methods for solving the equations of motion have been developed and verified experimentally. The validated methods were used in two studies: to determine the importance of bridge-vehicle interaction, and to assess the effects of vehicle suspension design on bridge dynamics.

8.1.1 Vehicle-Induced Bridge Dynamics

A convolution formulation for calculating vehicle-induced bridge response was developed and discussed in chapter 2. A new technique for evaluating the convolution integral in the frequency domain by using the Fourier transform was developed. This method has several advantages including

(i) The frequency domain calculations are much faster than the equivalent time domain methods, especially if the wheel loads are known (eg. measured),

(ii) The method uses bridge vibration mode shapes which can come from many sources (eg. measurements, simple theories, finite element predictions),

(iii) The method can be used with any vehicle model.

8.1.2 Validation of Theory

The convolution method was verified theoretically by comparison with simple theories, and experimentally by tests on two typical highway bridges.

The Drift Road bridge exhibited modes characteristic of continuous beams on several rigid supports. The finite element model of the Drift Road bridge predicted the natural frequencies more accurately than the beam theory, but did not predict significantly different mode shapes. On the other hand, the Lower Earley bridge displayed two-dimensional behaviour. Nevertheless, mode shapes from beam theory were found to be good approximations for response predictions.

For the vehicle-induced responses, good agreement between prediction and measurement was observed on both bridges. The discrepancies could largely be attributed to experimental error.

8.1.3 Bridge-Vehicle Interaction

The validated convolution method was extended to include vehicle models through an iterative procedure which was shown to converge for two different vehicle models.

A parametric study was performed to assess the importance of dynamic bridge-vehicle interaction. In general, interaction can be ignored if the vehicle frequency is less than half of the first natural frequency of the bridge, or the vehicles are light and the speeds are low. Since most vehicle frequencies are in the 1.5 to 4.5Hz range, bridges with natural frequencies near 10Hz will have little interaction with most vehicles.

8.1.4 Vehicle Suspensions

A parametric study was conducted to compare the effects of air and leaf-spring vehicle suspensions on bridge dynamic response.

Air suspensions were found to cause consistently lower dynamic response increments than steel suspensions because the air-springs acted like dynamic vibration absorbers and generated lower dynamic wheel loads.

8.2 Recommendations for Further Work

8.2.1 Theory

The theory for calculating bridge response to prescribed vehicle loads is well understood and has been refined in this dissertation. Nevertheless, questions still remain about the validity of damping assumptions. More theoretical and experimental research is needed into the mechanisms of damping behaviour in bridges.

8.2.2 Validation of Theory

Validated vehicle models were used for the computations of chapter 7, but the vehicles corresponding to these models were not available for the bridge tests. In addition, the surface profile of the bridges was not measured. In order to verify the whole system, the following procedure is recommended:

(i) Measure the surface profile of the test bridge including the roughness at the expansion joints,

(ii) Conduct tests with a vehicle for which a validated model is available, and include constant speed and variable speed tests to assess the validity of response calculations. For variable speed tests, the vehicle position would have to be monitored continuously.

(iii) Measure wheel loads and bridge responses simultaneously. Both displacement and acceleration measurements of the bridge response should be made, if possible.

(iv) Predict bridge responses from measured wheel loads and from bridge-vehicle interaction calculations and compare the two predictions with the measurements.

In addition to these validation experiments, more information is needed to describe the surface roughness of bridges in the U.K. to provide a data-base for researchers and possibly bridge designers.

8.2.3 Bridge-Vehicle Interaction

The convolution integral should be implemented into the step-by-step integration of the vehicle simulation [17, 26] and evaluated in the time domain. This would provide a check on the validity of the iterative implementation of the frequency domain method, and would also enable an assessment of the relative efficiency of the two methods for bridge-vehicle interaction calculations to be made.

Further study is needed to extend the guidelines for determining the importance of bridge-vehicle interaction. The following parameters should be studied:

(i) The effects of pseudo random bridge surface roughness should be examined in a systematic manner.

(ii) The simple vehicle models should be extended to include wheel-hop and pitch modes of vibration,

(iii) The results from the simpler models should be assessed with more realistic bridge models.

8.2.4 Vehicle Design

More work is required to assess the bridge damaging effects of different heavy vehicles. In this study, vehicles with air-spring suspensions were shown theoretically to cause lower dynamic response increments than vehicles with steel suspensions. This work should be extended to other damage criteria for bridges such as fatigue life, and punching shear resistance of deck slabs. In addition, local damage to expansion joints should be considered because poor expansion joints can cause large dynamic loads and thus exacerbate other dynamic effects.

Some of the parameters that should be investigated more fully are:

(i) the bridge surface profile,

(ii) vehicle tyre, suspension, and inertia parameters,

(iii) bridges known to exhibit large dynamic responses.

Finally, research should be conducted to understand the speed peaks in the dynamic increment plots. These speed peaks are related to several parameters including the vehicle speed, bridge and vehicle natural frequencies, vehicle axle spacing, and surface profile. The phenomenon should be investigated with simple vehicle models to try to isolate the effects of the various parameters.

8.2.5 Bridge Design

No attempt was made in this dissertation to evaluate the provisions of current bridge design codes, but the tools for such an investigation have been developed. Any research into design codes should first question the validity of a dynamic load allowance based on static loads. Unfortunately, more rational design procedures may not be as easy to develop or to implement. An assessment of bridge codes would involve selecting a design vehicle and calculating dynamic bridge responses for different cases. The resulting responses would then be compared against static design procedures by comparing dynamic increments, fatigue life, and maximum

wheel loads. More rational design procedures could then be developed by observing the deficiencies inherent in the existing procedures.

8.3 Review of objectives

The main objectives of this study have been achieved. A new method for calculating vehicle-induced bridge dynamics was developed and validated experimentally. The third objective, to identify the importance of bridge-vehicle interaction, has been completed for the case of a single degree of freedom vehicle moving over a bridge. Guidelines for determining the importance of the interaction were developed. Finally, the effects of two different vehicle suspensions on bridge responses were compared and steel suspensions were found to cause larger bridge dynamic responses than air suspensions.

This dissertation has highlighted the importance of vehicle-induced bridge vibrations. Further changes to vehicle or bridge design practices should incorporate present knowledge of bridge-vehicle dynamic interaction.

Bridge Design Codes: A Review

A

This appendix reviews bridge design procedures for accounting for vehicle-induced bridge vibration. Three different design codes are compared: British Standard 5400 (U.K.) [10], AASHTO[1] (U.S.A.) [2], and the OHBDC[2] (Ontario, Canada) [75]. The AASHTO code is reviewed because its design process is used in several other countries and is somewhat of a standard while the OHBDC is important because of its progressive attitude towards bridge design.

A.1 Comparison

All three codes share the same basic philosophy in that they specify (directly or indirectly) a 'dynamic load allowance' or 'impact factor' to account for dynamic effects. The term 'dynamic load allowance' was introduced by the OHBDC, and is preferred over 'impact factor' because impact between vehicles and bridges seldom occurs except in the case of collisions! The dynamic load allowance (DLA) is defined

[1] American Association of State Highway and Transportation Officials

[2] Ontario Highway Bridge Design Code

implicitly as follows

$$\text{Dynamic design load} = (1 + DLA)\ \text{Static design load.} \tag{A.1}$$

Therefore the dynamic load allowance is analogous to the dynamic load increment, DI_l defined in section 3.1.2. The following table illustrates the way in which this dynamic load allowance is applied in the three codes

Design code	Dynamic load allowance
BS 5400 (U.K.)	0.25 for one axle as part of the uniformly distributed loading (type HA)
BD 21/84 (U.K.) [29] (Assessment only)	0.80 for the heaviest axle of a single heavy goods vehicle for short-span bridges
AASHTO (U.S.A.)	$DLA = \frac{15.24}{L+38} \leq 0.30$ where L is the loaded length of the bridge in metres
OHBDC (Ontario)	$0.20 \leq DLA \leq 0.40$ and varies with the first natural frequency of the bridge as shown in figure A.1

In the U.K., the dynamic load allowance of BS 5400 is not applied by the designer, but is included implicitly in the formulation of the live load specifications. Furthermore, the increment of 0.80 (BD 21/84 [29]) is only used for assessment of existing bridges and not for design of new ones. This large factor was based on measurements of wheel loads on bridges by Page [76]. He measured maximum dynamic loads that were almost double the static values (see section 3.1.2) and the assessment code reflects these large measured increments. BS 5400 includes a separate dynamic load allowance for fatigue design. Figure A.2 shows that this allowance is applied by increasing the influence line for static stress near a discontinuity in the road surface

profile. The static influence line is increased by 25% at the discontinuity and then decreased to the original level over a distance of 5 metres.

An important difference between the British code and the two North American codes is that the HA loading of BS 5400 is an uniformly distributed lane load while the other two codes specify design vehicles in addition to a lane load. The HB loading of BS 5400 is a design vehicle, but it is meant to represent exceptionally large loads (electrical transformers, generators, military vehicles, etc.), and not heavy goods vehicles. In addition, the HB loading does not include any dynamic allowance. Nevertheless, design vehicles are considered for fatigue design under BS 5400.

The design provisions for dynamic wheel loads in Ontario are more detailed. Five different criteria are specified for obtaining dynamic load allowances.

(i) use tests or dynamic analyses to estimate dynamic effects,

(ii) for a single axle or wheel load use an allowance of 0.4,

(iii) for two or more axles with bridge lengths greater than 22m then calculate allowances based on figure A.1,

(iv) use an allowance of 0.1 for the uniformly distributed lane load,

(v) otherwise use an allowance of 0.3.

The linking of the dynamic load allowance in the Ontario code to the first natural frequency of the bridge (see figure A.1) represented a fundamental change in design philosophy. For the first time, the dynamic load allowance was based on a criterion that has a direct connection with the dynamic nature of the bridge-vehicle interaction. The dynamic load allowance is largest in the 2 to 5Hz frequency region where heavy vehicles generate most of their dynamic wheel loads. Furthermore, the values of the dynamic load allowance were based on dynamic response increment measurements (see section 3.1.3)

This new design philosophy has been recognized by many researchers as a more rational method of design and similar design practices have recently been introduced in Switzerland [14].

A.2 Summary

Design of bridges to withstand dynamic wheel loads has long been an empirical procedure. The dynamic load allowances were often based on bridge span (eg. AASHTO), or were simply constant factors for all bridges as is the practice in the U.K., and did not bear any relation to the dynamics of the bridge-vehicle interaction. The dynamic load allowance of the Ontario code was the first to be based on bridge natural frequencies. This is thought to be a good way forward for design against vehicle-induced bridge vibrations.

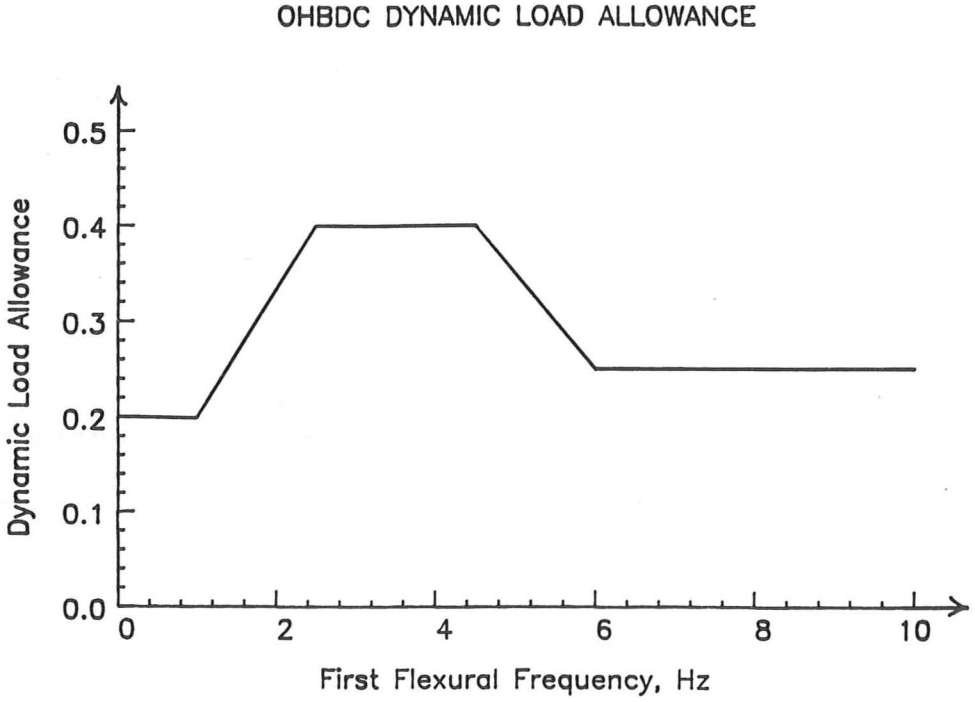

Figure A.1: Dynamic load allowance for the OHBDC

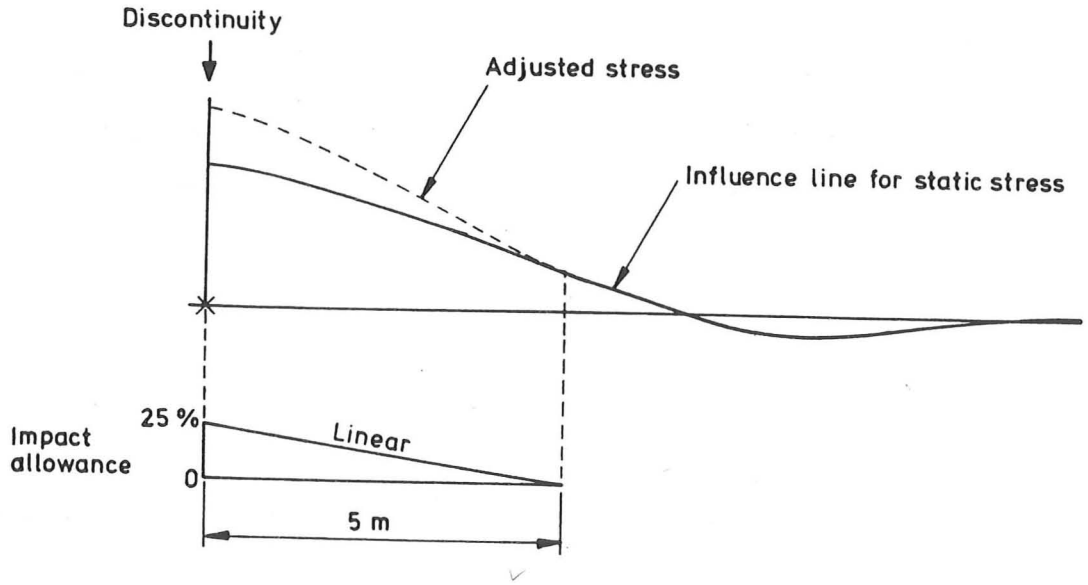

Figure A.2: Dynamic allowance for fatigue design in BS 5400

B

Self-adjoint operators

This appendix explains the concept of self-adjoint operators as introduced in chapter 2, and illustrates how the assumption that the linear differential operator, $\mathcal{L}\{\cdot\}$, is self-adjoint leads to the fact that the modes satisfy the orthogonality conditions of section 2.2.1.

B.1 Theory

Consider the following differential equation for an undamped bridge model

$$m(\mathbf{x})\frac{\partial^2 y}{\partial t^2}(\mathbf{x},t) \; + \; \mathcal{L}\{y(\mathbf{x},t)\} = 0. \tag{B.1}$$

where $m(\mathbf{x})$ is the mass per unit surface area, and $y(\mathbf{x},t)$ is the transverse deflection of the bridge. A modal solution of this differential equation in the following form is sought

$$y(\mathbf{x},t) = \sum_{n=1}^{\infty} \phi^{(n)}(\mathbf{x}) q_n(t) \tag{B.2}$$

where the $\phi^{(n)}(\mathbf{x})$ are the mode shapes and the $q_n(t)$ are the normal coordinates. It will be shown that if $\mathcal{L}\{\cdot\}$ is self-adjoint then the following two orthogonality

conditions hold

$$\int_R m(\mathbf{x})\phi^{(j)}(\mathbf{x})\phi^{(n)}(\mathbf{x})\,d\mathbf{x} = \delta_{jn} \qquad j,n = 1,2,3,\ldots,\infty \quad \text{(B.3)}$$

$$\int_R \mathcal{L}\left\{\phi^{(j)}(\mathbf{x})\right\}\phi^{(n)}(\mathbf{x})\,d\mathbf{x} = {\omega^{(n)}}^2\delta_{jn} \qquad j,n = 1,2,3,\ldots,\infty \quad \text{(B.4)}$$

where $\omega^{(n)}$ is the n^{th} natural frequency (rad/s),

$\zeta^{(n)}$ is the n^{th} modal damping ratio,

R is the surface area of the bridge,

and δ_{jn} is unity if $j = n$ and zero otherwise.

The first step is to define an inner product for functions of the spatial derivatives as

$$\langle u(\mathbf{x}), v(\mathbf{x})\rangle = \int_R u(\mathbf{x})v(\mathbf{x})\,d\mathbf{x} \quad \text{(B.5)}$$

where $\langle u(\mathbf{x}), v(\mathbf{x})\rangle$ denotes the inner product of the function $u(\mathbf{x})$ with $v(\mathbf{x})$. An operator, $\mathcal{L}\{\cdot\}$, is self-adjoint with respect to the inner product if it satisfies the following relationship

$$\langle \mathcal{L}\{u(\mathbf{x})\}, v(\mathbf{x})\rangle = \langle u(\mathbf{x}), \mathcal{L}\{v(\mathbf{x})\}\rangle \quad \text{(B.6)}$$

i.e.

$$\int_R \mathcal{L}\{u(\mathbf{x})\}\,v(\mathbf{x})\,d\mathbf{x} = \int_R u(\mathbf{x})\mathcal{L}\{v(\mathbf{x})\}\,d\mathbf{x}. \quad \text{(B.7)}$$

For the rest of this discussion, the linear differential operator, $\mathcal{L}\{\cdot\}$, will be assumed to self-adjoint with respect to the inner product of equation B.5. If the modal expansion of equation B.2 satisfies the differential equation, then so must any single mode solution, $y_n(\mathbf{x}, t)$,

$$y_n(\mathbf{x}, t) = \phi^{(n)}(\mathbf{x})q_n(t). \quad \text{(B.8)}$$

Substituting this single mode solution into equation B.1 and separating variables gives

$$\frac{\frac{d^2q_n}{dt^2}(t)}{q_n(t)} = \frac{-1}{m(\mathbf{x})}\frac{\mathcal{L}\left\{\phi^{(n)}(\mathbf{x})\right\}}{\phi^{(n)}(\mathbf{x})} = -\lambda_n \quad \text{(B.9)}$$

where λ_n is a constant.

Now assume that there are two distinct solutions for λ_n, say λ_p and λ_q, then

$$\mathcal{L}\left\{\phi^{(p)}(\mathbf{x})\right\} = m(\mathbf{x})\,\lambda_p\,\phi^{(p)}(\mathbf{x}) \tag{B.10}$$

and

$$\mathcal{L}\left\{\phi^{(q)}(\mathbf{x})\right\} = m(\mathbf{x})\,\lambda_q\,\phi^{(q)}(\mathbf{x}). \tag{B.11}$$

Taking inner products of these two equations with $\phi^{(q)}(\mathbf{x})$ and $\phi^{(p)}(\mathbf{x})$ respectively gives

$$\langle\phi^{(q)}(\mathbf{x}),\, \mathcal{L}\left\{\phi^{(p)}(\mathbf{x})\right\}\rangle = \langle\phi^{(q)}(\mathbf{x}),\; m(\mathbf{x})\,\lambda_p\,\phi^{(p)}(\mathbf{x})\rangle \tag{B.12}$$

and

$$\langle\mathcal{L}\left\{\phi^{(q)}(\mathbf{x})\right\},\, \phi^{(p)}(\mathbf{x})\rangle = \langle m(\mathbf{x})\,\lambda_q\,\phi^{(q)}(\mathbf{x}),\; \phi^{(p)}(\mathbf{x})\rangle. \tag{B.13}$$

Subtracting equation B.13 from B.12, and noticing that the definition of a self-adjoint operator means that the left hand sides of these two equations are equal, results in

$$\lambda_p\,\langle\phi^{(q)}(\mathbf{x}),\; m(\mathbf{x})\,\phi^{(p)}(\mathbf{x})\rangle - \lambda_q\,\langle m(\mathbf{x})\,\phi^{(q)}(\mathbf{x}),\; \phi^{(p)}(\mathbf{x})\rangle = 0. \tag{B.14}$$

For the inner product defined as an integral (equation B.5) the following relationship holds

$$\langle\phi^{(q)}(\mathbf{x}),\; m(\mathbf{x})\,\phi^{(p)}(\mathbf{x})\rangle = \langle m(\mathbf{x})\,\phi^{(q)}(\mathbf{x}),\; \phi^{(p)}(\mathbf{x})\rangle \tag{B.15}$$

and so

$$(\lambda_p - \lambda_q)\,\langle\phi^{(q)}(\mathbf{x}),\; m(\mathbf{x})\,\phi^{(p)}(\mathbf{x})\rangle = 0. \tag{B.16}$$

Since λ_p and λ_q are distinct, the conclusion is that

$$\langle\phi^{(q)}(\mathbf{x}),\; m(\mathbf{x})\,\phi^{(p)}(\mathbf{x})\rangle = 0 \qquad \text{if } p \neq q \tag{B.17}$$

and therefore that the $\phi^{(n)}(\mathbf{x})$ form an orthogonal set. By suitable scaling, they can be made to satisfy

$$\langle \phi^{(n)}(\mathbf{x}),\ m(\mathbf{x})\,\phi^{(n)}(\mathbf{x})\rangle = 1 \qquad \text{for all } n. \tag{B.18}$$

Therefore the $\phi^{(n)}(\mathbf{x})$ form an orthonormal set of functions which satisfy the first orthogonality condition. In order to show that the second orthogonality condition holds, the first orthogonality condition is substituted into the inner product of equation B.12 to obtain

$$\langle \phi^{(j)}(\mathbf{x}),\ \mathcal{L}\left\{\phi^{(n)}(\mathbf{x})\right\}\rangle = \lambda_n \delta_{jn}. \tag{B.19}$$

All that remains is to show that λ_n is equal to ${\omega^{(n)}}^2$. Consider the differential equation for the normal coordinations

$$\frac{d^2 q_n}{dt^2}(t) + \lambda_n q_n(t) = 0 \tag{B.20}$$

which has solutions of the form

$$q_n(t) = C_1 \cos(\omega^{(n)} t) \ + \ C_2 \sin(\omega^{(n)} t) \tag{B.21}$$

where ${\omega^{(n)}}^2 = \lambda_n$ and C_1, C_2 are constants dependent on the initial or boundary conditions. Therefore equation B.19 can be written as

$$\langle \phi^{(j)}(\mathbf{x}),\ \mathcal{L}\left\{\phi^{(n)}(\mathbf{x})\right\}\rangle = {\omega^{(n)}}^2 \delta_{jn} \tag{B.22}$$

and the second orthogonality condition has been shown to follow from the first.

B.2 Example

To demonstrate that the assumption of self-adjoint operators is valid for bridge vibration problems, consider the differential equation for a simply-supported Euler-Bernoulli beam

$$m\frac{\partial^2 y}{\partial t^2}(\mathbf{x}, t) \ + \ EI\frac{\partial^4 y}{\partial x^4}(\mathbf{x}, t) = 0. \tag{B.23}$$

with boundary conditions

$$\begin{aligned} y(0,t) = \quad & y(L,t) \quad = 0 \\ \frac{\partial^2 y}{\partial x^2}(0,t) = \quad & \frac{\partial^2 y}{\partial x^2}(L,t) \quad = 0 \end{aligned} \tag{B.24}$$

where L is the length of the beam, m is the mass per unit length, EI is the stiffness, and the linear differential operator, $\mathcal{L}\{\cdot\}$, is the fourth derivative with respect to x. Consider the inner product as follows

$$\langle u(x), v(x) \rangle = \int_0^L u(x)v(x)\,dx \tag{B.25}$$

and compute the following

$$\langle \mathcal{L}\{u(x)\}, v(x) \rangle = \int_0^L \frac{d^4u}{dx^4}(x)v(x)\,dx. \tag{B.26}$$

Integrating by parts twice, and applying the boundary conditions gives

$$\langle \mathcal{L}\{u(x)\}, v(x) \rangle = \left[\frac{d^3u}{dx^3}(x)v(x)\right]_0^L - \int_0^L \frac{d^3u}{dx^3}(x)\frac{dv}{dx}(x)\,dx \tag{B.27}$$

$$= -\left[\frac{d^2u}{dx^2}(x)\frac{dv}{dx}(x)\right]_0^L + \int_0^L \frac{d^2u}{dx^2}(x)\frac{d^2v}{dx^2}(x)\,dx \tag{B.28}$$

$$= \int_0^L \frac{d^2u}{dx^2}(x)\frac{d^2v}{dx^2}(x)\,dx. \tag{B.29}$$

because all of the boundary terms vanish. The last expression is symmetric in u and v and so by applying a similar procedure it can be deduced that

$$\langle u(x), \mathcal{L}\{v(x)\} \rangle = \int_0^L \frac{d^2u}{dx^2}(x)\frac{d^2v}{dx^2}(x)\,dx. \tag{B.30}$$

Therefore the differential operator for the simply-supported beam vibration problem is self-adjoint. The integration by parts illustrates that this differential operator will not be self-adjoint for all beam problems and depends on the boundary conditions. This fact should be taken into account when attempting modal expansions for problems with unusual boundary conditions such as moving supports. For support conditions typical of vehicle-induced bridge vibration problems, however, the differential operator will almost always be self-adjoint.

The Effects of Double Impulses with the Instrumented Hammer

C

This appendix analyses the effects of multiple hammer impulses on the data analysis. Special consideration is given to the calculation of transfer functions.

C.1 Frequency domain analysis

The transfer functions of chapter 4 were calculated by dividing the Fourier transform of the response by the transform of the input as follows

$$H(\omega) = \frac{Y(\omega)}{F(\omega)} \tag{C.1}$$

where $H(\omega)$ is the transfer function at frequency ω,

$Y(\omega)$ is the Fourier transform of the response,

and $F(\omega)$ is the Fourier transform of the input.

This procedure is valid as long as the transform of the input is not zero.

Consider a force input composed of two distinct impulses, P_0 and P_1, applied to the bridge

$$f(t) = \delta(t)P_0 + \delta(t - t_1)P_1 \tag{C.2}$$

$$= P_0(\delta(t) + \delta(t - t_1)\eta), \tag{C.3}$$

where η is the ratio of the magnitude of the second impulse to the first, and the impulses are applied at times zero and t_1 respectively.

To illustrate the effect of the double hit in the frequency domain, the Fourier transform of $f(t)$ is computed as

$$F(\omega) = \frac{1}{2\pi}\int_{-\infty}^{\infty} f(t)e^{-i\omega t}\,dt \tag{C.4}$$

$$F(\omega) = \frac{P_0}{2\pi}\left(1+\eta e^{-i\omega t_1}\right). \tag{C.5}$$

Figure C.1 shows the magnitude of a Fourier transform of a double impulse calculated from equation C.5. The mean value of the transform is proportional to the magnitude of the first impulse and the amplitude of the superimposed oscillations is proportional to the magnitude of the second impulse. The oscillations have a period of $\frac{1}{t_1}$. Therefore, zeros of $F(\omega)$ can occur only if the two impulses have identical magnitudes. This conclusion can also be shown algebraically by setting

$$F(\omega) = 0 = \frac{P_0}{2\pi}\left(1+\eta e^{-i\omega t_1}\right) \tag{C.6}$$

which has solutions when $\omega t_1 = j\pi$ where $j = 1, 2, 3, \ldots, \infty$, and $\eta = 1$.

Therefore, transfer functions can be calculated from equation C.1 as long as the impulses are not of similar magnitude. In this study, the magnitude of second impulse was less than 20% of the first. Therefore, repeated impacts of the impulse hammer did not adversely affect the data analysis. One exception occurs when the second impulse effectively cancels the response caused by the first (which requires precise magnitude and phase). This cancellation would be immediately evident when the responses were measured and was not a problem for the tests in this study.

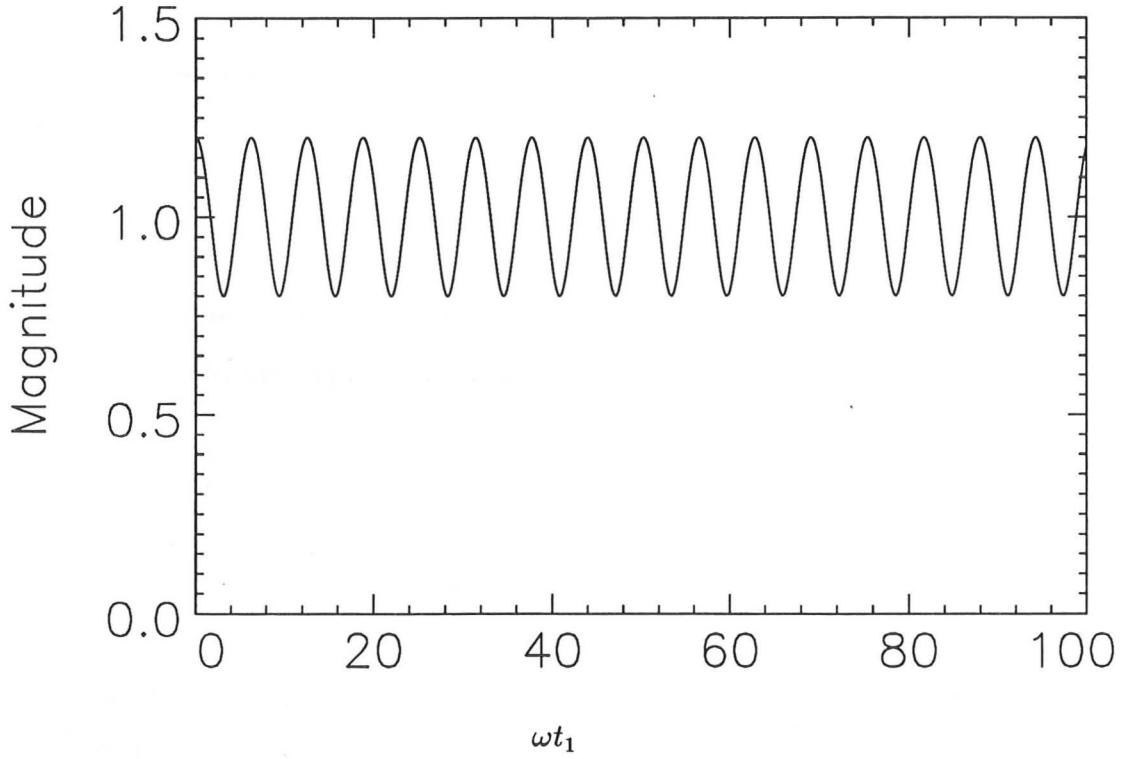

Figure C.1: Fourier transform of a double impulse showing the oscillations caused by the second impulse
$P_0 = 2\pi$, $\eta = 0.2$

Bibliography

[1] 'More bridge cash for 40 t lorries'. New Civil Engineer, 8 June 1989. p.14.

[2] American Association of State Highway and Transportation Officials. *Standard Specifications for Highway Bridges*, 12th ed. Washington, D. C., 1977.

[3] Anon. 'Proposals for generalised road inputs to vehicles'. ISO/TC 108/WG9 Draft Number 3e, May 1972.

[4] ASCE Committee on Loads and Forces on Bridges of the Committee on Bridges of the Structural Division . 'Recommended design loads for bridges'. *ASCE Journal of the Structural Division 110*, ST1 (January 1984), 190–191.

[5] Bendat, J., and Piersol, A. *Random Data: Analysis and Measurement Procedures.* Wiley-Interscience, London, 1971.

[6] Biggs, J. M., Suer, H. S., and Louw, J. M. 'Vibration of simple-span highway bridges'. *Transactions of the ASCE* (1957), 291–318.

[7] Billing, J., and Green, R. 'Design provisions for dynamic loading of highway bridges'. *TRB Second Bridge Engineering Conference, Transportation Research Record 950* (September 1984), 94–103.

[8] Billing, J. R. 'Dynamic loading and testing of bridges in Ontario'. *Canadian Journal of Civil Engineering 11* (1984), 833–843.

[9] Blanchard, J., Davies, B. L., and Smith, J. W. 'Design criteria and analysis for dynamic loading of footbridges', Symposium on dynamic behaviour of bridges. TRRL Supplementary Report 275, Transport and Road Research Laboratory, Crowthorne, England, May 1977.

[10] British Standards Institution. *Steel, concrete and composite bridges. BS 5400 Part 2: Specification for loads, 1978, Part 10: Code of practice for fatigue, 1980.* London, England.

[11] Cantieni, R. 'Dynamic load tests on highway bridges in Switzerland: 60 years experience of EMPA'. Tech. Rep. 211, Swiss Federal Laboratories for Materials Testing and Research, Dubendorf, Switzerland, 1983.

[12] CANTIENI, R. 'A laser system for the measurement of displacements of structures under static and dynamic loading'. In *Industrial Applications of Lasers*, H. Koebner, Ed. John Wiley & Sons Ltd, 1984, ch. 11, pp. 231–235.

[13] CANTIENI, R. 'Dynamic load testing of highway bridges'. In *IABSE Proceedings P-75/84* (August 1984), pp. 57–72.

[14] CANTIENI, R. 'Dynamic load testing of a two-lane highway bridge'. In *International Conference on Traffic Effects on Structures and the Environment"* (Strbske Pleso, Czecheslovakia, December 1987).

[15] CANTIENI, R. 'Dynamische belastungsversuche an der bergspurbrucke Deibuel'. Tech. Rep. 116/4, EMPA, Switzerland, December 1988.

[16] CANTIENI, R. Draft paper for OECD Working Group IR2 on 'Dynamic loading of pavements', September 1990.

[17] CEBON, D. *The Dynamic Interaction between Wheeled Vehicles and Road Surfaces.* PhD thesis, Cambridge University Engineering Department, June 1985.

[18] CEBON, D. 'A theoretical investigation into the vibration and roll-over of the "FRED" semitrailer'. British Aerospace plc, November 1987.

[19] CEBON, D. 'Vehicle-generated road damage: A review'. *Vehicle System Dynamics 18* (1989), 107–150.

[20] CEBON, D., AND NEWLAND, D. E. 'The artificial generation of road surface topography by the inverse FFT method'. In *Proceedings of the Eighth IAVSD Symposium on the Dynamics of Vehicles on Roads and on Tracks* (MIT, Cambridge, Mass., August 1983), Swets and Zeitlinger.

[21] CHAN, T. H. T., AND O'CONNOR, C. 'Vehicle model for highway bridge impact'. *Journal of Structural Engineering 116*, 7 (July 1990), 1772–1793.

[22] CHAN, T. H. T., AND O'CONNOR, C. 'Wheel loads from highway bridge strains: Field studies'. *Journal of Structural Engineering 116*, 7 (July 1990), 1751–1771.

[23] CHAUDHURI, S. K., AND SHORE, S. 'Dynamic analysis of horizontally curved I-girder bridges'. *ASCE Journal of the Structural Division 103*, ST8 (Aug 1977), 1589–1604.

[24] CHIU, W. S., SMITH, R. G., AND WORMLEY, D. N. 'Influence of vehicle and distributed guideway parameters on high speed vehicle-guideway dynamic interactions'. *ASME Journal of Dynamic Systems, Measurement, and Control* (March 1971), 25–34.

[25] CHU, K., GARG, V. K., AND DHAR, C. L. 'Railway bridge impact : Simplified train and bridge model'. *ASCE Journal of the Structural Division 105*, ST9 (September 1979), 1823–1844.

[26] COLE, D. *Measurement and Analysis of Dynamic Tyre Forces Generated by Lorries.* PhD thesis, Cambridge University Engineering Department, October 1990.

[27] COLE, D., AND CEBON, D. 'Simulation and measurement of dynamic tyre forces'. In *Proceedings of the 2nd International Conference on Heavy Vehicle Weights and Dimensions* (Kelowna, British Columbia, June 1989).

[28] CSAGOLY, P. F., CAMPBELL, T., AND AGARWAL, A. C. 'Bridge vibration study'. Tech. Rep. RR181, Ministry of Transportation and Communications, Downsview, Ontario, September 1972.

[29] DEPARTMENT OF TRANSPORT. *The Assessment of Highway Bridges and Structures,* Departmental Note BD 21/84, March 1984.

[30] EWINS, D. *Modal Testing: Theory and Practice.* Research Studies Press Ltd., England, 1984.

[31] EWINS, D., AND GLEESON, P. 'A method for modal identification of lightly damped structures'. *Journal of Sound and Vibration 84*, 1 (1982), 57–79.

[32] EYRE, R., AND SMITH, I. J. 'Wind and traffic induced dynamic behaviour of some steel box girder bridges', Symposium on dynamic behaviour of bridges. TRRL Supplementary Report 275, Transport and Road Research Laboratory, Crowthorne, England, May 1977.

[33] EYRE, R., AND TILLY, G. P. 'Damping measurements on steel and composite bridges', Symposium on dynamic behaviour of bridges. TRRL Supplementary Report 275, Transport and Road Research Laboratory, Crowthorne, England, May 1977.

[34] FRYBA, L. *Vibration of solids and structures under moving loads.* Noordoff International Publishing, Groningen, The Netherlands, 1972.

[35] FRYBA, L. 'Non-stationary response of a beam to a moving random force'. *Journal of Sound and Vibration 46*, 3 (1976), 323–338.

[36] FRYBA, L. 'Dynamic interaction of vehicles with tracks and roads'. *Vehicle System Dynamics 16* (1987), 129–138.

[37] GENIN, J., GINSBERG, J. H., AND TING, E. C. 'A complete formulation of inertial effects in the guideway-vehicle interaction problem'. *Journal of Sound and Vibration 38*, 1 (1975), 15–26.

[38] GENIN, J., TING, E. C., AND VAFA, Z. 'Curved bridge response to a moving vehicle'. *Journal of Sound and Vibration 81*, 4 (1982), 469–475.

[39] GOLD, B., AND RADER, C. *Digital Processing of Signals.* McGraw-Hill Inc., London, 1984.

[40] GRACE, N. F., AND KENNEDY, J. B. 'Dynamic response of two-span continuous composite bridges'. *Canadian Journal of Civil Engineering 15* (1988), 579–588.

[41] GREEN, R. 'Dynamic response of bridge superstructures - Ontario observations', Symposium on dynamic behaviour of bridges. TRRL Supplementary Report 275, Transport and Road Research Laboratory, Crowthorne, England, May 1977.

[42] GUPTA, R. K. 'Dynamic loading of highway bridges'. *ASCE Journal of the Engineering Mechanics Division 106*, EM2 (April 1980), 377–394.

[43] GUPTA, R. K., AND TRAILL-NASH, R. W. 'Vehicle braking on highway bridges'. *ASCE Journal of the Engineering Mechanics Division 106*, EM4 (Aug 1980), 641–658.

[44] HAWK, H., AND GHALI, A. 'Dynamic response of bridges to multiple truck loading'. *Canadian Journal of Civil Engineering 8* (1981), 392–401.

[45] HINO, J., YOSHIMURA, T., KONISHI, K., AND ANANTHANARAYANA, N. 'A finite element method prediction of the vibration of a bridge subjected to a moving vehicle load'. *Journal of Sound and Vibration 96*, 1 (1984), 45–53.

[46] HONDA, H., KAJIKAWA, Y., AND KOBORI, T. 'Spectra of road surface roughness on bridges'. *ASCE Journal of the Structural Division 108*, ST9 (September 1982), 1956–1966.

[47] HONDA, H., AND KOBORI, T. 'Numerical data base on roadway roughness of highway bridges and roughness characteristics'. *Proceedings of JSCE 398*, I-10 (October 1986), 385–394.

[48] HONDA, H., KOBORI, T., AND YAMADA, Y. 'Some considerations on impact of multispan continuous highway bridges'. *Transactions of JSCE 15* (1983), 52–55.

[49] HUNT, H. *Measurement and Modelling of Traffic-Induced Ground Vibration.* PhD thesis, Cambridge University Engineering Department, July 1988.

[50] HUSBAND & CO. 'EEC vehicles: Lorries and the environment, Report on study into the effects of heavy vehicles on bridges'. Department of Transport, March 1980.

[51] HWANG, E.-S. *Dynamic Loads for Girder Bridges.* PhD thesis, The University of Michigan Civil Engineering Department, 1990.

[52] INBANATHAN, M. J., AND WIELAND, M. 'Bridge vibrations due to vehicle moving over rough surface'. *ASCE Journal of Structural Engineering 113*, 9 (September 1987), 1994–2008.

[53] INGLIS, C. *A Mathematical Treatise on Vibrations in Railway Bridges.* Cambridge University Press, Cambridge, 1934.

[54] KISHAN, H., AND TRAILL-NASH, R. W. 'Calculation of response and loading of highway bridges from modal coordinates'. *International Association for Bridge and Structural Engineering 33*, II (1973), 113–130.

[55] KOBORI, T., CHIKATA, Y., KIDO, T., AND ASAI, T. 'Dynamic response of the isotropic slab bridge under traffic jam'. *Memoirs of the Faculty of Technology of Kanazawa University 18*, 2 (October 1985), 1–9.

[56] KOMATSU, S., AND KAWATANI, M. 'Nonstationary random response of highway bridges under moving vehicles'. *Technology Reports of the Osaka University 32*, 1648 (March 1982), 151–158.

[57] KULKARNI, G. G., AND NG, S. F. 'Dynamic analysis of two dimensional simply supported orthotropic bridge decks'. *Canadian Journal of Civil Engineering 5* (1978), 58–69.

[58] KUMARASENA, T., SCANLAN, R. H., AND MORRIS, R. 'Deer Isle bridge: Field and computed vibrations'. *Journal of Structural Engineering 115*, 9 (September 1989), 2313–2328.

[59] KURIHARA, M., AND SHIMOGO, T. 'Stability of a simply-supported beam subjected to randomly spaced moving loads'. *ASME Journal of Mechanical Design 100* (July 1978), 507–513.

[60] LEE, D. 'Comparative maintenance costs of different bridge types'. In *Bridge Management: Inspection, Maintenance, Assessment, and Repair* (London, England, 1990), J. Harding, G. Parke, and M. Ryall, Eds., Elsevier Applied Science, pp. 145–154.

[61] LEE, P., HO, D., AND CHUNG, H. W. 'Static and dynamic tests of concrete bridge'. *ASCE Journal of Structural Engineering 113*, 1 (January 1987), 61–73.

[62] LEONARD, D. 'Dynamic tests on highway bridges - test procedures and equipment'. TRRL Laboratory Report 654, Transport and Road Research Laboratory, Crowthorne, England, January 1974.

[63] LEONARD, D. 'Damping and frequency measurements on eight box girder bridges'. TRRL Laboratory Report 682, Transport and Road Research Laboratory, Crowthorne, England, 1975.

[64] MAGUIRE, AND SEVERN. 'Assessing the dynamic properties of prototype structures by hammer testing'. *Proceedings of the Institution of Civil Engineers, Part 2 83* (December 1987), 769–784.

[65] MITCHELL, C., AND GYENES, L. 'Dynamic pavement loads measured for a variety of truck suspensions'. In *Proceedings of the 2nd International Conference on Heavy Vehicle Weights and Dimensions* (Kelowna, British Columbia, June 1989).

[66] MOODY, J. R., AND MANSELL, D. S. 'Dynamics interaction of bridge bearings, superstructure and loads'. In *Australasian Conference on the Mechanics of Structures and Materials* (1980), pp. 80–84.

[67] MOSS, P. J., CARR, A. J., AND PARDOEN, G. C. 'The vibrational behaviour of three composite beam-slab bridges'. *Engineering Structures 4* (October 1982), 277–288.

[68] MULCAHY, N. L., PULMANO, V. A., AND TRAILL-NASH, R. W. 'Vehicle properties for bridge loading studies'. *Proceedings of the International Association of Bridge and Sructural Engineering* (1983), 153–167.

[69] NEWLAND, D. *An Introduction to Random Vibration and Spectral Analysis*, 2nd ed. Longman, England, 1984.

[70] NEWLAND, D. *Mechanical Vibration Analysis and Computation.* Longman, England, 1989.

[71] NG, S., AND KAUL, V. 'Free vibration analysis of continuous orthotropic bridge decks'. *Journal of Sound and Vibration 119*, 1 (1987), 29–38.

[72] O'CONNOR, C., AND CHAN, T. H. 'Dynamic wheel loads from bridge strains'. *ASCE Journal of Structural Engineering 114*, 8 (August 1988), 1703–1723.

[73] O'CONNOR, C., AND CHAN, T. H. 'Wheel loads from bridge strains: Laboratory studies'. *ASCE Journal of Structural Engineering 114*, 8 (August 1988), 1724–1740.

[74] O'CONNOR, C., AND PRITCHARD, R. W. 'Impact studies on a small composite girder bridge'. *ASCE Journal of Structural Engineering 111*, 3 (March 1985), 641–653.

[75] ONTARIO MINISTRY OF TRANSPORTATION AND COMMUNICATIONS. *Ontario Highway Bridge Design Code.* Downsview, Ontario, 1983.

[76] PAGE, J. 'Dynamic wheel load measurements on motorway bridges'. TRRL Laboratory Report 722, Transport and Road Research Laboratory, Crowthorne, England, 1976.

[77] PENDERED, J., AND BISHOP, R. 'The determination of modal shapes in resonance testing'. *Journal of Mechanical Engineering Science 5*, 4 (1963), 379–385.

[78] PRAKASH RAO, D., TAMHANKAR, M., AND SHARMA, S. 'Literature survey on in situ testing of concrete bridges'. *Materiaux et Constructions 16*, 96 (1983), 457–466.

[79] RAYLEIGH, J. *Theory of Sound.* Dover Publications, New York, 1945.

[80] RICHARDSON, H. H., AND WORMLEY, D. N. 'Transportation vehicle/beam-elevated guideway dynamic interactions : A state-of-the-art review'. *ASME Journal of Dynamic Systems, Measurement, and Control* (June 1974), 169–179.

[81] SCHILLING, C. G. 'Impact factors for fatigue design'. *ASCE Journal of the Structural Division 108*, ST9 (September 1982), 2034–2044.

[82] SCHILLING, C. G. 'Stress cycles for fatigue design of steel bridges'. *ASCE Journal of Structural Engineering 110*, 6 (June 1984), 1222–1234.

[83] SHEPHERD, R., AND AVES, R. J. 'Impact factors for simple concrete bridges'. *Proceedings of the Institution of Civil Engineers, Part 2 55* (March 1973), 191–210.

[84] SHEPHERD, R., BROWN, H., AND WOOD, J. H. 'Dynamic investigations of the Mohaka river bridge'. *Proceedings of the Institution of Civil Engineers, Part 1 66* (August 1979), 457–469.

[85] STOCKHAM, JNR., T. 'High-speed convolution and correlation with applications to digital filtering'. In *Digital Processing of Signals*, B. Gold and C. Rader, Eds. McGraw-Hill Inc., London, England, 1984.

[86] STOKES, G. 'Discussion of a differential equation relating to the breaking of railway bridges'. *Transactions of the Cambridge Philosophical Society 8* (1849), 707–735.

[87] SWANNELL, P., AND MILLER, C. W. 'Theoretical and experimental studies of a bridge-vehicle system'. *Proceedings of the Institution of Civil Engineers, Part 2 83* (September 87), 613–615.

[88] SWEATMAN, P. 'A study of dynamic wheel forces in axle group suspensions of heavy vehicles'. Special Report SR No. 27, Australian Road Research Board, June 1983.

[89] TILLY, G. P. 'Damping of highway bridges : a review', Symposium on dynamic behaviour of bridges. TRRL Supplementary Report 275, Transport and Road Research Laboratory, Crowthorne, England, May 1977.

[90] TING, E. C., AND GENIN, J. 'Dynamics of bridge structures'. *Solid Mechanics Archives 5*, 3 (August 1980), 217–252.

[91] TING, E. C., GENIN, J., AND GINSBERG, J. H. 'A general algorithm for moving mass problems'. *Journal of Sound and Vibration 33*, 1 (1974), 49–58.

[92] TUNG, C. C. 'Random response of highway bridge to vehicle loads'. *ASCE Journal of Engineering Mechanics Division 93*, 5 (Oct 1967), 79–94.

[93] TUNG, C. C. 'Response of highway bridges to renewal traffic loads'. *ASCE Journal of Engineering Mechanics Division 95*, EM1 (February 1969), 41–57.

[94] VELETSOS, A., AND HUANG, T. 'Analysis of dynamic response of highway bridges'. *ASCE Journal of Engineering Mechanics Division 96*, EM5 (Oct 1970), 593–620.

[95] WALKER, W., AND VELETSOS, A. 'Response of simple-span highway bridges to moving vehicle loads'. Bulletin 486, University of Illinois, Engineering Experiment Station, Urbana, Illinois, 1966.

[96] WARD, H. S. 'Traffic generated vibrations and bridge integrity'. *ASCE Journal of Structural Engineering 110*, 10 (Oct 1984), 2487–2498.

[97] WHEELER, J. 'Bridge loading: Research needed (Discussion)'. *ASCE Journal of Structural Engineering 110*, 1 (January 1984), 190–191.

[98] WILLIS, R. 'Appendix report of the commissioners appointed to inquire into the application of iron to railway structures'. H. M. S. O., London, England, 1849.

[99] WILLS, J. 'Correlation of calculated and measured dynamic behaviour of bridges', Symposium on dynamic behaviour of bridges. TRRL Supplementary Report 275, Transport and Road Research Laboratory, Crowthorne, England, May 1977.

[100] WILSON, J. F. 'Model experiments for span-vehicle dynamics'. *ASCE Journal of the Engineering Mechanics Division 103*, EM4 (Aug 1977), 701–715.

[101] WIRIYACHAI, A., CHU, K., AND GARG, V. K. 'Bridge impact due to wheel and track irregularities'. *ASCE Journal of Engineering Mechanics Division 108*, EM4 (Aug 1982), 648–666.

[102] YOUNG, W. *Roark's Formulas for Stress and Strain*, 6th ed. McGraw-Hill Book Company, London, England, 1989.

[103] ZWERNEMAN, F. J., AND FRANK, K. H. 'Fatigue damage under variable amplitude loads'. *Journal of Structural Engineering 114*, 1 (January 1988), 67–83.